



UNIVERSITY OF  
BIRMINGHAM

DESIGN AND DEVELOPMENT OF A MEDICAL DEVICE FOR  
TREATMENT OF PROXIMAL INTERPHALANGEAL JOINT  
CONTRACTURE

by

**MAY MAHMOUD AHMED ABDO YOUSSEF**

A thesis submitted to  
University of Birmingham  
for the degree of  
DOCTOR OF PHILOSOPHY

School of Mechanical Engineering  
University of Birmingham  
December 2015

UNIVERSITY OF  
BIRMINGHAM

**University of Birmingham Research Archive**

**e-theses repository**

This unpublished thesis/dissertation is copyright of the author and/or third parties. The intellectual property rights of the author or third parties in respect of this work are as defined by The Copyright Designs and Patents Act 1988 or as modified by any successor legislation.

Any use made of information contained in this thesis/dissertation must be in accordance with that legislation and must be properly acknowledged. Further distribution or reproduction in any format is prohibited without the permission of the copyright holder.

## **ABSTRACT**

The proximal Interphalangeal (PIP) joint is vital for hand function. It is frequently affected by contractures as a result of injury or disease. Dynamic external fixators are one of the useful treatment methods of these contractures, enabling the ability to exercise adjacent joints during healing. The aim of this study was a development of the Compass hinge device to present a new design device for the digit PIP joint.

A failed Compass hinge external fixator has been analysed. The device consists of polymer parts manufactured from polyetherimide (PEI). Finite element analysis (FEA) was used to investigate the principal stresses in the device under different loading conditions. Scanning electron microscopy (SEM) was used to investigate the fracture surfaces. The FEA showed that the maximum principal stress was greater than the fatigue strength of PEI. The SEM fractographs confirm that failure was by brittle fatigue.

A new finger fixator named the PIP joint protractor hinge device comprises 17 parts which are assembled together. The proposed device materials consist of Poly-ether -ether-ketone (PEEK) and stainless steel 316LS. The design was subjected to FEA and a working model was manufactured and subjected to cyclic mechanical testing. The FEA showed that the maximum stress was 242.9 MPa and this was less than the yield strength and the fatigue endurance limits for the selected materials. Mechanical testing showed that testing reached run-out of 170,000 cycles with no cracks or damage visible in the device parts.

## **ACKNOWLEDEMENTS**

There are so many people to acknowledge in this thesis, without who I could not have achieved what I have.

I should begin with my academic supervisor, Prof. Duncan Shepherd without his support, knowledge, guidance and advice I could not have completed this thesis.

I would like to thank Mr. Garth Titley for his believe in this project and support throughout my PhD.

My thanks are also due to Mr Simon Rowan for his technical support which made the experimental aspects of this thesis possible.

From the bottom of my heart, I would like to thank my mother, my father and my brother who have always supported me in so many ways, they always believe in me and been there whenever I have needed them. Their being let me strong, compassionate and motivated.

My fiancé has been there for me through the stress of my PhD and our engagement and never once doubted me or shown me anything but support and motivation. Thank you for your unconditional love, strength, kindness and never giving up.

Finally, I would like to thank the Egyptian government for the provision of the financial support that made this research work possible.

# Table of Contents

<b>ABSTRACT.....</b>	<b>i</b>
<b>LIST OF FIGURES .....</b>	<b>vii</b>
<b>LIST OF TABLES.....</b>	<b>xiii</b>
<b>CHAPTER 1.....</b>	<b>1</b>
<b>1 INTRODUCTION .....</b>	<b>2</b>
<b>CHAPTER 2.....</b>	<b>4</b>
<b>2 BACKGROUND .....</b>	<b>5</b>
2.1 Chapter overview .....	5
2.2 The human hand anatomy .....	5
2.3 Hand biomechanics.....	7
2.4 Proximal interphalangeal (PIP) joint .....	14
2.4.1 Anatomy.....	14
2.4.2 Contractures .....	15
2.5 Dupuytren’s disease.....	16
2.5.1 Clinical Presentation .....	21
2.5.2 Treatment .....	23
2.6 External finger fixators .....	23
2.7 Medical device design process .....	40
2.8 Summary.....	44
<b>CHAPTER 3.....</b>	<b>45</b>
<b>3 ENGINEERING ANALYSIS OF A FAILED COMPASS HINGE.....</b>	<b>46</b>
3.1 Chapter overview .....	46

3.2	Compass hinge device .....	46
3.2.1	Introduction.....	46
3.2.2	Components and surgical technique .....	47
3.2.3	Review of clinical studies .....	49
3.2.4	Model .....	55
3.2.5	Results.....	62
3.3	Scanning electron microscopy .....	68
3.3.1	Results.....	71
3.4	Discussion.....	73
3.5	Summary.....	75
<b>CHAPTER 4</b>	<b>.....</b>	<b>77</b>
<b>4</b>	<b>NEW DEVICE DESIGN.....</b>	<b>78</b>
4.1	Chapter overview .....	78
4.2	Introduction.....	78
4.3	Design requirements .....	79
4.4	Concept designs .....	81
4.4.1	Design strategy .....	81
4.4.2	Concept Design 1 – (Screw drive hinge movement) .....	83
4.4.3	Concept Design 2 – (Worm and worm wheel hinge movement) .....	94
4.5	Detailed design .....	100
4.5.1	Materials .....	101
4.5.2	The PIP joint protractor hinge device .....	104
	Table 4-2. Gear general nomenclature and design formula (Designatronics, 1999). 113	
4.6	Discussion.....	139
4.7	Summary.....	142
<b>CHAPTER 5</b>	<b>.....</b>	<b>143</b>
<b>5</b>	<b>ENGINEERING ANALYSIS OF THE NEW DEVICE DESIGN.....</b>	<b>144</b>
5.1	Chapter overview .....	144
5.2	Finite element analysis.....	144
5.2.1	Results.....	147
5.3	Risk analysis .....	152

5.3.1	Undertaking risk analysis.....	152
5.3.2	Risk analysis of the PIP joint protractor hinge device.....	154
5.3.3	Design description and characteristics.....	154
5.3.4	Identification of hazards and estimation of risks .....	154
5.4	Manufacturing.....	158
5.4.1	Techniques .....	158
5.4.2	Models .....	161
5.5	Mechanical testing .....	170
5.5.1	Testing equipment.....	170
5.5.2	Testing setup .....	171
5.5.3	Methods .....	173
5.5.4	Results.....	173
5.6	Discussion.....	175
5.7	Summary.....	178
<b>CHAPTER 6.....</b>		<b>180</b>
<b>6</b>	<b>OVERALL DISCUSSION AND CONCLUSIONS .....</b>	<b>181</b>
6.1	Chapter overview .....	181
6.2	Project objectives.....	181
6.3	Discussion.....	182
6.3.1	Analysis of failed Compass hinge device .....	183
6.3.2	The PIP joint protractor hinge device design.....	184
6.3.3	Finite element modelling .....	185
6.3.4	Prototyping.....	186
6.3.5	Mechanical testing .....	188
6.4	The PIP joint protractor hinge surgical technique .....	189
6.4.1	Further development .....	190
6.5	Comparison of the new proposed device with other external finger fixators ....	193
6.6	Conclusions.....	197
<b>APPENDICES.....</b>		<b>198</b>
<b>Appendix A.....</b>		<b>199</b>
<b>Appendix B .....</b>		<b>201</b>

<b>Appendix C.....</b>	<b>215</b>
<b>Appendix D.....</b>	<b>225</b>
<b>Appendix E .....</b>	<b>226</b>
<b>Appendix F .....</b>	<b>228</b>
<b>REFERENCES.....</b>	<b>229</b>

# LIST OF FIGURES

<b>Figure 2-1.</b> Hand bones and joints diagram (Tate, 2011). .....	6
<b>Figure 2-2.</b> The different couplings of fingers (a) poke; (b) 90-degree distal pad pull; (c) 180-degree distal pad press; (d) lateral pinch; (e) palmar pinch; (f) three-jaw chuck pinch; (g) power grasp (author's own drawing, adapted from Astin and Nussbaum, 2003). .....	9
<b>Figure 2-3.</b> Schematic drawing of proximal interphalangeal (PIP) joint (Ng and Oliver, 2009). .....	14
<b>Figure 2-4.</b> Grades of Dupuytren's disease (Murphey <i>et al.</i> , 2009). .....	18
<b>Figure 2-5.</b> (a) Normal digital fascia and (b) Dupuytren's disease diseased fascia ( <a href="http://bonefix.co.nz">http://bonefix.co.nz</a> ) .....	19
<b>Figure 2-6.</b> The presence of Dupuytren's disease of a PIP joint (Lahiri <i>et al.</i> , 2007). .....	22
<b>Figure 2-7.</b> The Hueston's tabletop test finger joint contractures diagnosis ( <a href="http://dupuytren.biz/dupuytren_1.html">http://dupuytren.biz/dupuytren_1.html</a> ). .....	22
<b>Figure 2-8.</b> Mini external fixator (Houshian and Schröder, 2004) .....	24
<b>Figure 2-9.</b> Hoffmann II Micro External Fixation System (Asche <i>et al.</i> , 2009). .....	25
<b>Figure 2-10.</b> Mini external fixator (pins and elastic bands) (White <i>et al.</i> , 2012). .....	26
<b>Figure 2-11.</b> Pins and dental rubber bands fixator (Ruland <i>et al.</i> , 2008). .....	26
<b>Figure 2-12.</b> A Digit Widget device (Slater <i>et al.</i> , 2003). .....	27
<b>Figure 2-13.</b> The different types of treatment techniques (a) Robertson Banjo splint; (b) Extension-block splinting; (c) The Suzuki frame; (d) Allison device; (e) The force couple splint; (f) The Schenk device facilitating mobilization; (g) The Hynes and Giddings device (author's own drawing, adapted from Ng and Oliver, 2009). .....	28
<b>Figure 2-14.</b> The Stockport serpentine spring system "S-Quattro" a flexible mini external fixator (Bostock <i>et al.</i> , 1993 <sup>a</sup> ). .....	29
<b>Figure 2-15.</b> JESS (Joshi external stabilising system) device (Salafia and Chauhan, 1997). .....	30
<b>Figure 2-16.</b> The Continuous Extension Technique (TEC) device (Citron and Messina, 1998). .....	31
<b>Figure 2-17.</b> Verona device (Citron and Messina, 1998). .....	32

<b>Figure 2-18.</b> PIPSTER (Proximal Interphalangeal Skeletal Traction Extender) device (Hodgkinson, 1994). .....	32
<b>Figure 2-19.</b> Small dynamic external finger fixator (Inanami <i>et al.</i> , 1993).....	33
<b>Figure 2-20.</b> Multiplanar distractor (Kasabian <i>et al.</i> , 1998). .....	34
<b>Figure 2-21.</b> The medical device design process flowchart (Aitchison <i>et al.</i> , 2009). .....	43
<b>Figure 3-1.</b> Compass hinge external fixator.....	47
<b>Figure 3-2.</b> Surgical technique for the Compass hinge fixator (a) axis K-wire insertion (b) proximal and distal K-wires insertion (c) dorsal view for the implanted fixator .....	48
<b>Figure 3-3.</b> Compass hinge device supported on patient finger (a) Position A and (b) Position B (adapted from (Lahiri <i>et al.</i> , 2007)). .....	49
<b>Figure 3-4.</b> Mechanical failure at distal arcuate hinge (adapted from (Lahiri <i>et al.</i> , 2007)). .....	50
<b>Figure 3-5.</b> Pin-track infections (adapted from (Lahiri <i>et al.</i> , 2007)). .....	50
<b>Figure 3-6.</b> Compass hinge disassembled components.....	56
<b>Figure 3-7.</b> An example of measurements made on the distal arcuate hinge member. ....	56
<b>Figure 3-8.</b> Solid model of the distal arcuate hinge member.....	57
<b>Figure 3-9.</b> Solid model of the proximal and distal arcuate hinge assembled members. ...	57
<b>Figure 3-10.</b> Meshed finite element model I with the load and constrains applied.....	59
<b>Figure 3-11.</b> Four different positions of engagement with the worm gear (a) position 1 (15-30°); (b) position 2 (30-45°); (c) position 3 (65-80°); (d) position 4 (90-105°).....	60
<b>Figure 3-12.</b> Meshed finite element model II with the load and constrains applied.....	61
<b>Figure 3-13.</b> Two different positions of engagement with the worm gear (a) position 1 (15 - 30°) (b) position 4 (90-105°). .....	62
<b>Figure 3-14.</b> Distribution of maximum Principal stress for model I for four different positions of gear teeth fixed at (a) position 1 (15-30°); (b) position 2 (30-45°); (c) position 3 (65-80°); (d) position 4 (90-105°).....	64
<b>Figure 3-15.</b> Maximum principal stress against force for the gear teeth fixed at 15 - 30°. 65	
<b>Figure 3-16.</b> Maximum principal stress distribution around the distraction screw hole. ...	65

<b>Figure 3-17.</b> Finite element analysis stress distribution results for Model II for position 1 gear teeth fixed at (15 - 30°). .....	67
<b>Figure 3-18.</b> Maximum principal stress distribution around the left distraction screw hole. ....	67
<b>Figure 3-19.</b> Fracture surfaces examined using scanning electron microscopy. ....	68
<b>Figure 3-20.</b> Emscope SC500 sputter coater.....	69
<b>Figure 3-21.</b> Fracture surface samples (a) before (b) after gold spray coating. ....	69
<b>Figure 3-22.</b> Joel JSM-6060 LV microscope with computer.....	70
<b>Figure 3-23.</b> SEM fractography images of the distal block fracture surfaces (a) fracture surface 1 (b) fracture surface 2 (c) fracture surface 3.....	72
<b>Figure 4-1.</b> 3D assembly design of the screw drive hinge movement concept design 1 ....	83
<b>Figure 4-2.</b> 3D design of the proximal protractor part design -1.....	84
<b>Figure 4-3.</b> 3D design of the proximal protractor part design -1, idea1. ....	85
<b>Figure 4-4.</b> 3D design of the distal protractor part design -1, idea2. ....	87
<b>Figure 4-5.</b> Distribution of stresses for the distal protractor part design -1, idea2. ....	88
<b>Figure 4-6.</b> 3D design of the distal protractor part design -1, idea3. ....	89
<b>Figure 4-7.</b> Distribution of stresses for the distal protractor part design -1, idea3. ....	90
<b>Figure 4-8.</b> 3D design of the distal protractor part design -1, idea4. ....	91
<b>Figure 4-9.</b> Distribution of stresses for the distal protractor part design -1, idea4. ....	91
<b>Figure 4-10.</b> 3D design of the distal protractor part design -1, idea5. ....	92
<b>Figure 4-11.</b> Distribution of stresses for the distal protractor part design -1, idea5. ....	93
<b>Figure 4-12.</b> 3D assembly design of the worm and worm wheel hinge movement concept design 2.....	94
<b>Figure 4-13.</b> 3D design of the distal protractor part design -2, idea1. ....	95
<b>Figure 4-14.</b> 3D assembly design of the proximal and distal protractor parts design -2, idea1.....	96

<b>Figure 4-15.</b> 3D assembly design of the proximal and distal protractor parts design -2, idea2.....	97
<b>Figure 4-16.</b> 3D design of concept selection 2, idea2.....	101
<b>Figure 4-17.</b> 3D exploded view of the assembly of the PIP joint protractor hinge. ....	105
<b>Figure 4-18.</b> 3D design assembly of the PIP joint protractor hinge final design.....	105
<b>Figure 4-19.</b> 3D design of the proximal protractor hinge part.....	107
<b>Figure 4-20.</b> Drawing of the proximal protractor hinge part. ....	108
<b>Figure 4-21.</b> 3D design of the distal protractor part.....	109
<b>Figure 4-22.</b> Drawing of the distal protractor hinge part. ....	110
<b>Figure 4-23.</b> The pressure angle at mating gear teeth (Designatronics, 1999) .....	112
<b>Figure 4-24.</b> Involute curve derivation of the worm wheel tooth .....	115
<b>Figure 4-25.</b> The gear involute (Buckingham, 1949). ....	116
<b>Figure 4-26.</b> The gear tooth profile (Buckingham, 1949).....	118
<b>Figure 4-27.</b> Engineering drawing of the worm wheel tooth profile. ....	120
<b>Figure 4-28.</b> 3D design of the worm wheel part. ....	121
<b>Figure 4-29.</b> Drawing of the worm wheel part. ....	122
<b>Figure 4-30.</b> 3D design of the worm gear part.....	123
<b>Figure 4-31.</b> Engineering drawing of the worm part. ....	124
<b>Figure 4-32.</b> 3D design of the rod part.....	125
<b>Figure 4-33.</b> Drawing of the rod part. ....	126
<b>Figure 4-34.</b> 3D design of the solid clamping blocks. ....	128
<b>Figure 4-35.</b> 3D design of the slotted clamping blocks. ....	128
<b>Figure 4-36.</b> Drawing of the solid clamping block part.....	129
<b>Figure 4-37.</b> Drawing of the slotted clamping block part.....	130
<b>Figure 4-38.</b> 3D design of the assembly of the screw 1 (left) and nut 2 (right).....	131

<b>Figure 4-39.</b> Drawing of the screw 1 part. ....	132
<b>Figure 4-40.</b> Drawing of the nut 2 part. ....	133
<b>Figure 4-41.</b> The screw. ....	134
<b>Figure 4-42.</b> Drawing of the screw. ....	135
<b>Figure 4-43.</b> A guide Jig for inserting the K-Wires (a) Isometric view and (b) Rear view of the proposed design. ....	137
<b>Figure 4-44.</b> A 3D assembling design of the Jig with the PIP joint protractor hinge device. ....	137
<b>Figure 4-45.</b> Drawing of the jig. ....	138
<b>Figure 4-46.</b> 3D design of the Compass hinge device (left) and the PIP joint protractor hinge device (right). ....	141
<b>Figure 5-1.</b> Meshed finite element model with the load of 210 N applied and constraints applied at position 1 with the gear teeth fixed at 15 - 30°. ....	145
<b>Figure 5-2.</b> Two different positions of engagement with the worm gear (a) position 1 gear teeth fixed at 15 - 30° (b) position 2 gear teeth fixed at 90 - 105°. ....	146
<b>Figure 5-3.</b> Distribution of stresses in the model for position 1 gear teeth fixed at 15 - 30°. ....	148
<b>Figure 5-4.</b> Distribution of stresses in the model for position 2 gear teeth fixed at 90 - 105°. ....	148
<b>Figure 5-5.</b> FEA Iso Clipping at 110 MPa with the gear teeth fixed at 15 - 30°. ....	150
<b>Figure 5-6.</b> FEA Iso Clipping at 65 MPa with the gear teeth fixed at 15 - 30°. ....	151
<b>Figure 5-7.</b> FEA Iso Clipping at 65 MPa with gear teeth fixed at 90 - 105°. ....	152
<b>Figure 5-8.</b> Rapid prototyping model of the PIP joint protractor hinge device. ....	162
<b>Figure 5-9.</b> Disassembled rapid prototyping model of the PIP joint protractor hinge device. ....	162
<b>Figure 5-10.</b> Worm and worm wheel teeth meshing. ....	167
<b>Figure 5-11.</b> External dynamic protractor hinge fixator working model. ....	169
<b>Figure 5-12.</b> A manufactured worm gear by stainless steel 17-4PH composition, Solid Concepts Inc. ....	169

<b>Figure 5-13.</b> The mechanical test model.....	169
<b>Figure 5-14.</b> The Bose ElectroForce® 3330 Series II Test Instrument. ....	171
<b>Figure 5-15.</b> The designed mechanical test rig. ....	172
<b>Figure 5-16.</b> The device model after the cyclic bending mechanical test.....	174
<b>Figure 5-17.</b> Applying cyclic load on the new designed device using a Bose ElectroForce® 3330 Series II Test Instrument .....	175
<b>Figure 5-18.</b> The maximum stress location for both models of the Compass hinge device (left) and the PIP joint protractor hinge device (right) at position 1 with the gear teeth fixed at 15 - 30° with a load of 210 N.....	176
<b>Figure 6-1.</b> A new feature design for the proximal protractor hinge part.....	190

# LIST OF TABLES

<b>Table 2-1.</b> Finger couplings and grip strength summary. ....	10
<b>Table 2-2.</b> Pulp pinch strength average maximum (N) .....	11
<b>Table 2-3.</b> Classification of Dupuytren’s disease according to Tubiana (1986).....	18
<b>Table 2-4.</b> Summary of the main features of the different PIP joint fixators.....	36
<b>Table 3-1.</b> The previous clinical studies summary.....	51
<b>Table 4-1.</b> Pugh matrix to concept design selection. ....	98
<b>Table 4-2.</b> Gear general nomenclature and design formula (Designatronics, 1999). ....	113
<b>Table 4-3.</b> The Formulas of gear tooth profile (Buckingham, 1949).....	117
<b>Table 4-4.</b> The protractor hinge device size guide. ....	140
<b>Table 5-1.</b> Rating of occurrence, severity and detection for potential hazards.....	153
<b>Table 5-2.</b> Results of risk analysis. ....	155
<b>Table 5-3.</b> Comparison between the designed and measured dimensions. ....	164
<b>Table 6-1.</b> A predicted timeline of the design process required for the PIP joint protractor hinge device. ....	192

# CHAPTER 1

## INTRODUCTION

# 1 INTRODUCTION

Flexion contracture of the proximal Interphalangeal (PIP) joint is a common clinical problem that can occur as a result of injury or disease, such as Dupuytren's disease. Movement of this joint is responsible for 85% of the total motion of the digit and severe flexion deformity can lead to marked loss of global hand function that hinders activities of daily living (Houshian *et al.*, 2013). PIP external dynamic fixators are medical devices that are used for patients with the case of contractures of a skeletal PIP joint such as Dupuytren's disease and unstable fracture subluxation of the PIP joint. One type of fixator is the Compass proximal interphalangeal (PIP) joint hinge (Smith & Nephew, Memphis, TN, USA) (Hotchkiss *et al.*, 1994) and this device has been used by Mr. Garth Titley (Consultant Plastics and Burns Surgeon at the Queen Elizabeth Hospital, Birmingham). He has found the device to fail following attachment to patients and believed that an improved design would have many clinical benefits.

The aim of this thesis was to investigate, design and develop a new fixator, based on analysis of a failed Compass hinge device. The specific objectives were to:

- Determine the main cause of Compass hinge failure;
- Generate a new design of fixator device;
- Evaluate the proposed design using finite element analysis;
- Manufacture a prototype model of the new designed fixator;
- Mechanically test the prototype.

Chapter 2 presents the background information. The chapter begins with a description and explanation of the anatomical and biomechanical terms used for the human fingers. Dupuytren's disease and its treatment methods then follow. The chapter continues by describing the different dynamic external fixators available for the human hand with the advantages and disadvantages associated with their use. The design process for a new medical device is explained in detail in this chapter.

Chapter 3 starts by introducing the Compass hinge device, followed by an engineering analysis of a failed device. The predicted stress levels and distributions in the Compass hinge device, subjected to bending loads, were investigated using Finite Element Analysis and Scanning Electron Microscopy. The chapter concludes with recommendations for an improved design.

Chapter 4 describes the development of a new fixator to treat PIP joint contractures. In this chapter the development and evaluation of various concept designs are presented and discussed. The final design is presented.

In Chapter 5, the prototype device and the engineering analysis for the final design are presented. The new design is verified by Finite Element Analysis and the working prototype is mechanically tested.

Chapter 6 presents the overall discussion of the study and the thesis is summarised by presenting the general conclusions with regards to the original aim of the research.

# CHAPTER 2

## BACKGROUND

## **2 BACKGROUND**

### **2.1 Chapter overview**

This chapter aims to provide the general information required to understand the subsequent chapters. Section 2.2 presents the human hand anatomy. The biomechanics of the hand is described in § 2.3. The proximal interphalangeal joint anatomy and contractures are provided in § 2.4. Dupuytren's disease and its treatment methods are presented in § 2.5, followed by a description of the different dynamic external fixators available to treat proximal interphalangeal (PIP) joint contractures in § 2.6. Section 2.7 presents a brief description of the process used for the design of medical devices. Detailed background information on each specific part of the study is given in the relevant chapter.

### **2.2 The human hand anatomy**

The human hand consists of five digits, with four fingers and a thumb. The fingers comprise three intercalated bony segments: the proximal, intermediate and distal phalanges. The thumb lacks the intermediate phalanx and is made up of only the proximal and distal phalanges (Bundhoo and Park, 2005).

The bones of the hand, naturally group themselves into the carpus; the base of the hand is formed by eight carpal bones. The carpal bones are united into two rows of bones. The

proximal row contains (from lateral to medial) the scaphoid, lunate, triquetrum, and pisiform bones. The scaphoid, lunate, and triquetrum bones contribute to the formation of the radiocarpal joint. The distal row of carpal bones contains (from medial to lateral) the hamate, capitate, trapezoid, and trapezium bones. The anterior hamate has a prominent bony hook (Taylor and Schwarz, 1955). The proximal and distal carpal rows articulate with each other at the midcarpal joint. The five metacarpal bones form the palm of the hand. The metacarpal bones are numbered 1–5, starting with the thumb side. The first metacarpal bone is freely mobile, but the other bones are united as a group. The digits are also numbered 1–5, with the thumb being number 1. The fingers and thumb contain a total of 14 phalanges (phalanx bones) (Betts *et al.*, 2013). A diagram of the hand bones and joints are illustrated in Figure 2-1 (Tate, 2011).

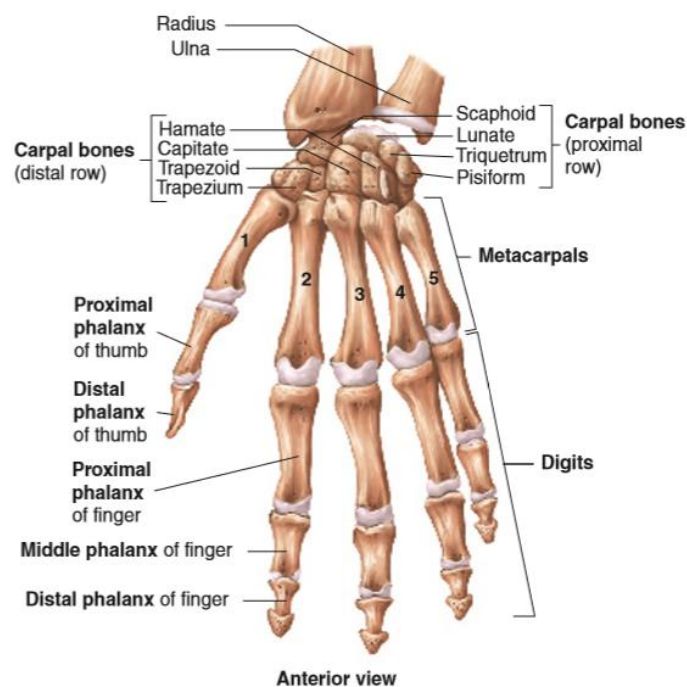


**Figure 2-1.** Hand bones and joints diagram (Tate, 2011).

The joints between the metacarpals and the proximal phalange are “condyloid” synovial joints, which allow movement in two planes due to the shape of the bones against each other. These are the metacarpal (MCP) joints (Joyce, 2004). The fingers can flex and straighten or abduct and adduct; move apart and together sideways, spreading the fingers. This provides the mobility and versatility of the hand. The interphalangeal joints, those between each phalanx and the next are simple hinge shaped joints, which allow only flexion and extension (Abrahams *et al.*, 2003) with a normal range of motion being 0°/100° extension/flexion (Reese and Bandy, 2013). The index finger is found to have the greatest range of extension/flexion amongst the five fingers: 90° at the MCP joint, 100° to 110° at the PIP joint and 80° at the distal interphalangeal (DIP) joint. In addition, adduction and abduction angles of 20° have been measured in the MCP joint of the fingers (Bundhoo and Park, 2005).

## 2.3 Hand biomechanics

The hand is one of the most important parts of the human body. It is the structure that allows for a number of tasks: adaptation, exploration, prehension, perception and manipulation. The prehensile movements of the human hand can be divided into power grip and precision grip (Napier, 1956).

A thorough understanding of the biomechanical principles of the human hand is useful for medical device design engineers. Medical device design ought to account either the forces which will be exerted by the human due to daily tasks or the direction of these forces to avoid any possible failure of the devices. Failure to consider biomechanics in design can result in non-physiological loads being applied to the device.

To verify the proposed design, the digit maximum exerted load for the healthy human will be considered as the first study parameter. Load direction is measured as the second parameter. Finally, the finger joint angles during exerting this load are the third parameter in this study for designing a new external medical fixator. This is to confirm that the new device design is a safe design from an engineering point of view.

Astin and Nussbaum (2003) compiled and examined the maximum forces exerted by the fingers in a variety of couplings to both enhance and supplement available data across 100 subjects. The seven couplings investigated in this research were divided into prehensile (wrapping around with the whole hand and the power grasp) and non-prehensile couplings (lateral pinch, palmar pinch, three-jaw chuck pinch, poke, 90-degree distal pad pull and 180-degree distal pad press) (Figure 2-2).

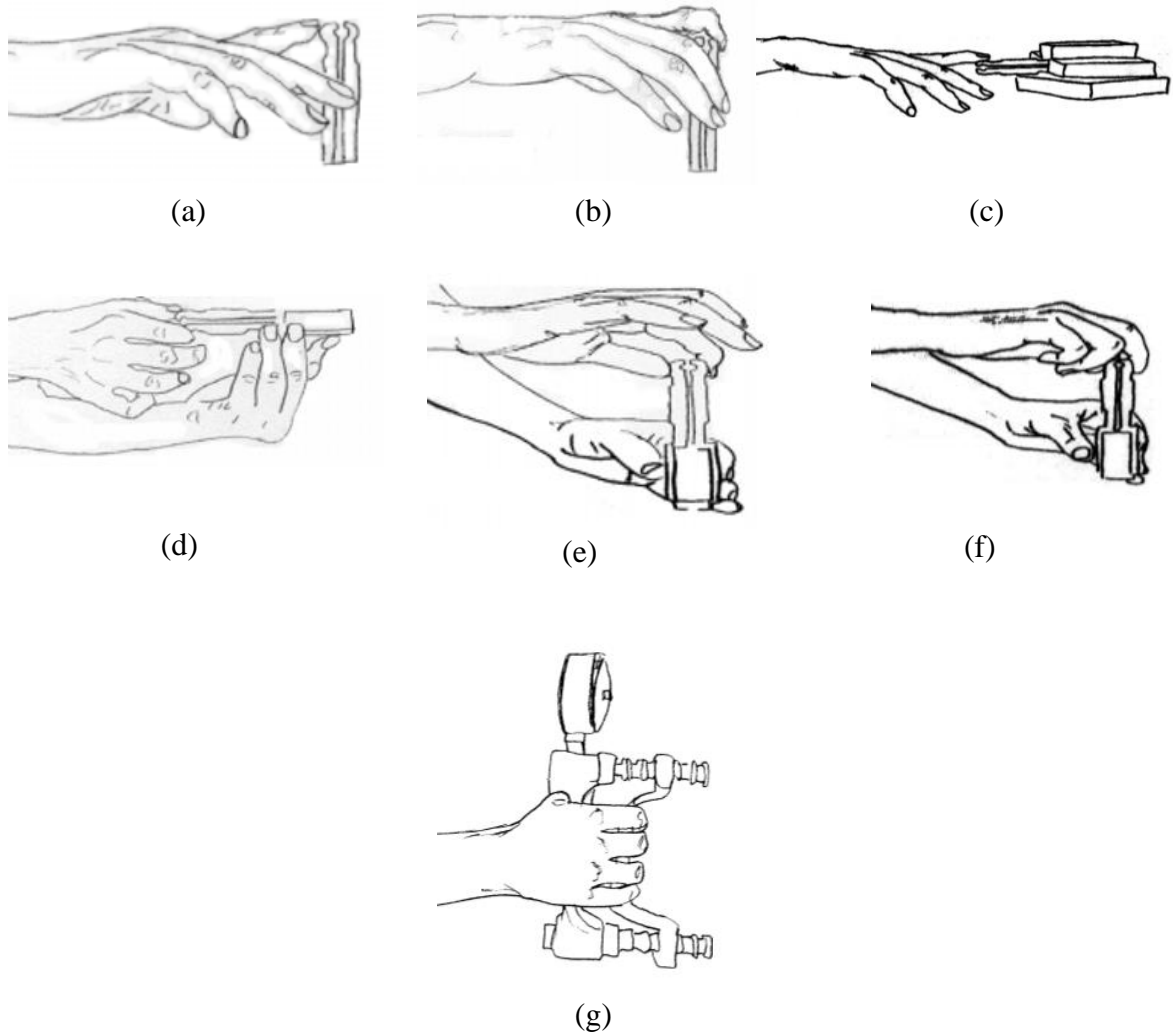


**Figure 2-2.** The different couplings of fingers (a) poke; (b) 90-degree distal pad pull; (c) 180-degree distal pad press; (d) lateral pinch; (e) palmar pinch; (f) three-jaw chuck pinch; (g) power grasp (author's own drawing, adapted from Astin and Nussbaum, 2003).

A summary of the strength and variability in each of the finger couplings and for simple grips are given in table 2-1.

**Table 2-1.** Finger couplings and grip strength summary.

<b>Coupling</b>	<b>Mean (N)</b>	<b>Standard deviation (N)</b>	<b>Relevant coupling to the current study</b>
Poke	46.0	17.8	Not relevant (axial force not a parameter)
Press	43.1	18.4	✓
Pull	60.1	25.2	✓
Lateral	80.9	28.2	✓
Chuck	79.8	29.0	✓
Palmar	54.2	18.8	✓
Grip	370.7	117.7	✓

Swanson *et al.* (1974) recorded the strength of the normal hand as applied in basic hand patterns: grip, chuck pinch (three-digit pinch), pulp (fingertip) pinch with separate fingers, and lateral pinch. Measurements were reported as an average maximum strength grip force of 466.8 N for males, and 241.2 N for females. The average maximum strength of a chuck pinch force was 77.5 N for males, and 51 N for females and an average maximum strength lateral pinch force of 73.5 N for males, and 48 N for females. The average maximum strength of pulp pinch measured force compared with the average maximum strength of pulp pinch in the study of Walker and Erkman (1977) is shown in (Table 2-2). An *et al.* (1978) also measured the pulp pinch strengths but for two fingers only (index and long) for 18 males and 22 females. They reported that the strengths of the two fingers were equal and the

strength was the same for tip and pulp pinch actions. The average maximum strength was 63 N (SD=14 N) for male subjects and female subjects had 46 N (SD=10 N).

**Table 2-2.** Pulp pinch strength average maximum (N)

Hand patterns	Digit	Swanson <i>et al.</i> (1974)		Walker and Erkman (1977)	
		Male	Female	Male	Female
Pulp pinch	index	52	35.3	74	56 (index digit only)
	middle	55	37.2	65	
	ring	37.2	24.5	47	
	small	22.5	16.6	37	

Berme *et al.* (1977) measured the strength of four normal female subjects pinching a 45 mm diameter cylinder, and reported a mean strength of only 19 N. Weightman and Amis (1982) showed that the maximal isometric pinch mean strength external force was 35 N of the index finger by squeezing a strain-gauged instrument for eleven female subjects.

The tip, key, and palmar pinch grip strength were measured for a sample of 310 male and 328 female adults, ages 20 to 94 years using a dynamometer. The results showed that the maximum grip strength was 463.9 N, tip pinch was 75.6 N, key pinch 108.9 N and palmar pinch was 104.1 N (Mathiowetz *et al.*, 1985). In pinch strength, men were 40 percent stronger than women, but in grip strength men were twice as strong (Walker *et al.*, 1978). Radwin *et al.* (1992) used a small conductive polymer force sensor to measure the individual finger forces exerted during submaximal static pinch. Sensors were attached to the distal

phalangeal pads. The average maximum five finger pinch strength for the study subjects was 100 N (SD=26 N) where the average finger strength was 61 N (SD=15 N) for index, 58 N (SD=21 N) for middle, 36 N (SD=13 N) for ring and 28 N (SD=11 N) for small. Lee and Rim (1990) developed a biomechanical model to predict maximum isometric, finger-grip forces for plane motion of the middle finger for different cylinder sizes. The maximum force of 210 N occurred at the joint angles of  $-40^{\circ}$  at the wrist,  $80^{\circ}$  at the MCP joint, and  $70^{\circ}$  at the PIP joint.

The cylindrical type finger-force measuring system with a five-axis force/moment sensor was designed and manufactured using digital signal processing (DSP), which can measure the grasping finger-force (Kim *et al.*, 2010). It was found that the average force of men's right hands was about 218 N, and that of the left hands was 199 N.

A three-dimensional static biomechanical model was presented by Vigouroux *et al.* (2006) to estimate finger muscle tendon, pulley forces and external fingertip during the "slope" and the "crimp" grip. The results of the model showed that the mean external fingertip force was 95.6 N (SD=26.4 N) in the crimp grip and 97 N (SD=21.8 N) in the slope grip. Schweizer (2001) investigated bowstringing and forces during crimp grip position. Two devices were built to measure the force and the distance of bowstringing and one device to measure forces at the fingertip. All measurements of 16 fingers (only middle and ring fingers) of 4 subjects (one woman and three men) were made *in vivo*. The maximum forces at one fingertip were determined in two positions; parallel slope grip (maximum force at fingertip for middle and ring while all other fingers were acting at the horizontal grip) and isolated crimp grip (the long finger had contact with the grip, the other fingers being in a

flexed and unloaded position). The maximum force at one fingertip (middle and ring) while all other long fingers were acting at the same horizontal grip (parallel grip) and at the same finger was performed while only this finger had contact with the grip, the other long fingers being in a flexed and unloaded position (isolated grip) were determined. The maximum forces at one fingertip for an isolated crimp grip was 96 N (SD=21 N), parallel crimp grip was 82 N (SD=19 N), isolated slope grip was 116 N (SD=30 N) and for parallel slope grip was 78 N (SD=22 N). The maximum crimp grip fingertip forces were 100 N (SD=46 N) for index, 90 N (SD=35 N) for long and 45 N (SD=24 N) for ring in a study by Marco *et al.* (1998) where the force at the fingertip (external force) of a closed traumatic rupture of the flexor tendon pulleys in rock climbers were measured. The individual fingers were tested separately under simulated *in vivo* loading conditions. Olandersson *et al.* (2005) developed an extension finger force measurement device, and investigated the intra individual repeatability. The design of the measuring device allows single finger force and whole hand measurements. The results are shown that the average whole hand force is 170 N (SD=10 N) and for individual fingers; 30.2 N (SD=3.30 N) for the index, 33.9 N (SD=3.63 N) for long, 28.3 N (SD=3.05 N) ring and the little is 19.5 N (SD=2.24 N).

The conclusions of the previous studies of the human hand biomechanics are as follows:

- The different types of the hand tasks aspect (prehensile and non-prehensile) and the ergonomic aspect (gender, age and which hand is dominant) were the main causes for the variety of the force magnitudes. All previous studies take into account these two aspects during their studies,

- The middle digit exerted the maximum finger-grip force of 210 N (Lee and Rim, 1990) and this magnitude force will be used as a loading condition in the finite element analysis sections to analysis the existing device (Compass hinge) and to verify the new proposed design (chapters 3 and 5, respectively in this study).
- The range of forces which can be exerted by the healthy human hand was from 10 N to 210 N by the little and middle fingers, respectively.
- Prehensile coupling as a grip action had a larger magnitude force than non-prehensile couplings for single and multi-digits tasks (poke, press, pull, lateral, chuck and palmar). The magnitude force of the poke task will be excluded from this current study as the axial force is not a parameter for the external fixator device.

## 2.4 Proximal interphalangeal (PIP) joint

### 2.4.1 Anatomy

The PIP joint is a pure hinge joint in function (Figure 2-3). Its stability results from the articular congruence and the surrounding soft-tissue structures (Ng and Oliver, 2009).

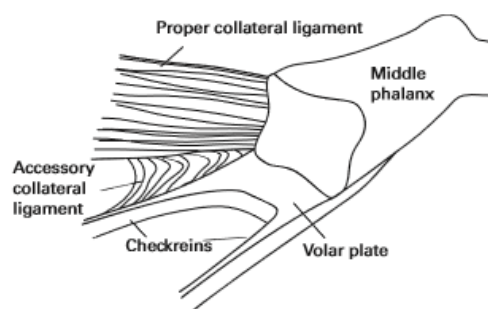


**Figure 2-3.** Schematic drawing of proximal interphalangeal (PIP) joint (Ng and Oliver, 2009).

Ligaments are tough bands of tissue that connect bones or joints together. In the PIP joint, the strongest ligament is the volar plate which connects the proximal phalanx to the middle phalanx on the palm side of the joint. There is also a collateral ligament on each side of the PIP joint which tightens when the joint is bent sideways and keeps the joint stable from side to side (Bailie *et al.*, 1996). The collateral ligament consists of the collateral ligament proper (taut in flexion) and an accessory collateral ligament (taut in extension). The volar plate is a thick fibrocartilaginous structure that constitutes the palmar aspect of the PIP joint capsule. Distally, it is attached to the volar lip of the base of the middle phalanx. Proximally, the attachment of the volar plate to the proximal phalanx is more elastic and is U-shaped due to two lateral bands, known as the checkrein ligaments. Dorsally, the PIP joint is stabilized by the dorsal extensor apparatus, which consists of a central slip that inserts on the dorsal tubercle of the middle phalanx and lateral slips that are connected by retinacular ligaments (Clavero *et al.*, 2002).

### **2.4.2 Contractures**

Contractures of the PIP joints are vexing problems for patient and surgeon alike. Pain, stiffness, degenerative arthritis and chronic instability are common outcomes of PIP joint contractures (Feldscher and Blank, 2002).

Most PIP joint injuries are caused by high velocity, such as in sports injuries. The low-velocity injuries are less common and are usually caused by twisting; this often causes

disruption of the thin volar plate origin. The simple injury classification for PIP joints according to Freiberg (2007) are:

- Dislocations (volar, dorsal);
- Subluxations (volar, dorsal, ulnar, radial);
- Avulsion or ‘chip’ fractures (associated with ligamentous injuries);
- Intra-articular fractures or fracture dislocations:
  - Unipolar:
    - proximal phalanx: one condyle, two condyles or comminuted;
    - middle phalanx: comminuted
  - Bipolar: complete joint destruction.

Salafia and Chauhan (1997) classified the PIP contracture considering the treatment strategies to be as follows: (1) mild; the PIP can be extended by stretching the skin, (2) moderate; maximum extension 50°-60° and surgical intervention is required, and (3) severe; the PIP contracture 90° or more correction is possible only by surgical methods.

## 2.5 Dupuytren’s disease

Palmar fibromatosis was originally described in 1831 by the French physician Dupuytren and is often referred to as Dupuytren’s disease or contracture. It is the most common of the superficial fibromatosis, affecting 1%–2% of the general population. The disease most commonly occurs in patients over 65 years of age, with a frequency of 20% in this age group. Men are three to four times more likely to be affected by the disease than women, and lesions are bilateral in 40%–60% of patients (Murphey *et al.*, 2009). Dupuytren contracture depends on genetic (family

history) and environmental factors namely; alcohol consumption, tobacco exposure and, possibly, manual activities (athletes specially rock climbers), diabetes, smoking, human immunodeficiency virus (HIV) infection and seizures have been suggested as associated factors (Balakrishnan *et al.*, 2008; Riester *et al.*, 2014). Palmar fibromatosis is confined to Caucasians of north western European origin (Gudmundsson *et al.*, 1999). Dupuytren's disease develops in both hands regardless of hand dominance. The ring and small finger are the predominately affected digits which are followed by the index, middle fingers and the thumb. Both severity and the impact of the disease are different for every individual, but Dupuytren's disease is considered more aggressive in younger people when it occurs (Mafi *et al.*, 2012).

Dupuytren's disease is a benign condition that can present with varying severity. It results in abnormal "scar-like" tissue in the palmar fascia leading to irreversible, permanent, and progressive contracture of the injured digits. The decision to carry out surgical correction is dependent on the surgeon's evaluation of clinical severity of the disease, where a goniometer is used to measure the severity of the flexion deformity (Hindocha *et al.*, 2007). The propagation of Dupuytren's disease was summarized by Murphey *et al.* (2009) in three grades (Figure 2-4):

- Grade 1 - presents as a thickened nodule and a band in the palmar aponeurosis that may progress to skin tethering, puckering, or pitting;
- Grade 2 - presents as a peritendinous band that limits extension of the affected finger;
- Grade 3 - presents as flexion contracture.

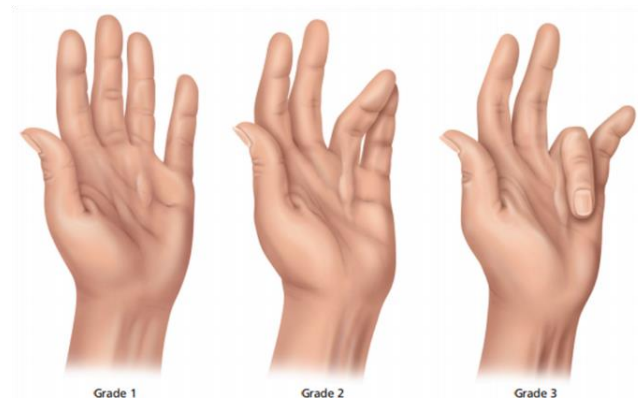


**Figure 2-4.** Grades of Dupuytren's disease (Murphey *et al.*, 2009).

Tubiana (1986) classified Dupuytren's disease into four grades (Table 2-3) according to the range of PIP flexion angle where grade III and IV are the most serious cases (Citron and Messina, 1998).

**Table 2-3.** Classification of Dupuytren's disease according to Tubiana (1986)

Grade	Total fixed deformity (degrees)
I	0 to 45
II	45 to 90
III	90 to 135
IV	Over 135

Dupuytren's disease can be explained in terms of a distortion of the normal palmar fascia. The anatomical diagram for the normal elements of the digital fascia and the diseased fascia of Dupuytren's disease (Figure 2-5).

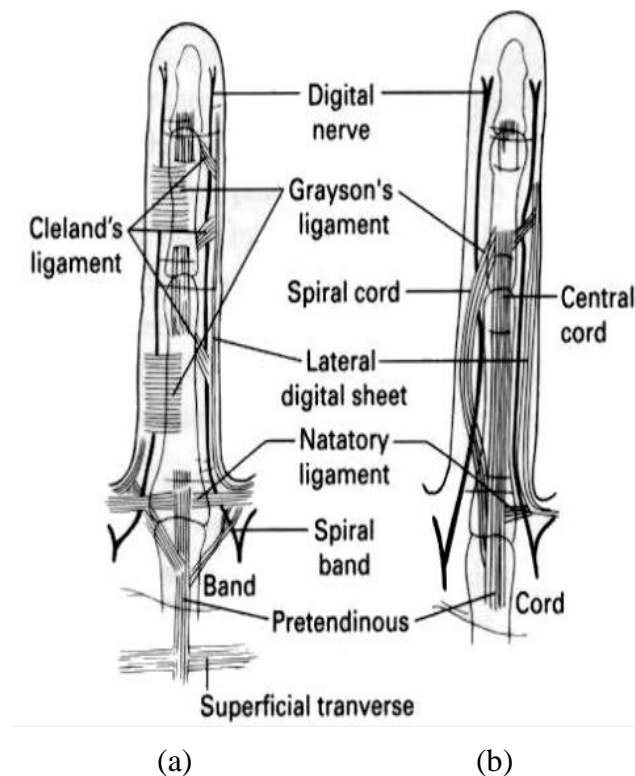


**Figure 2-5.** (a) Normal digital fascia and (b) Dupuytren's disease diseased fascia (<http://bonefix.co.nz>)

In the normal hand, the palmar aponeurosis runs longitudinally from the wrist, crosses over the superficial transverse palmar ligament, and splits into pretendinous bands to each digit. The insertion of the pretendinous bands to the skin distal to the distal palmar crease is by means of a bifurcate insertion into the side of the finger dorsal to the neurovascular bundle. A natatory ligament runs transversely across each web space distal to the MCP joint, giving fibers that blend with each lateral digital sheet and to the superficial aspect of the flexor tendon sheath. The superficial transverse ligament lies deep to the pretendinous bands, proximal to the MCP joints and the natatory ligament (Trojian and Chu, 2007).

Diseased bands were referred to as cords. The bands and cords are characterized as follows:

- The pretendinous cord is formed from pretendinous bands.
- The spiral cord is made up of the pretendinous band, spiral band, lateral digital sheet, and Grayson ligament; this cord takes an encircling path around the neurovascular bundle that often occurs in the ring and small fingers. The spiral cord runs dorsal to the neurovascular bundle proximally and volar to it distally.
- The lateral cord is formed from the lateral digital band and is rarely observed, except on the ulnar aspect of the small finger.
- The central cord has no defined fascial precursor; it is the most common cause of proximal PIP contracture.
- The natatory cord contributes to web space contractures and passes superficially to the neurovascular bundles (McFarlane, 1984).

Skin pitting is a result of involvement of small vertical fibers (Grapow fibers) that connect the dermis to the palmar fascia. Nodules develop from the superficial fibers of the palmo-digital fascia, adhere to the overlying skin, and usually precede cords. The affected bands of the digital fascia are referred to as cords. Contraction of cords results in predictable deformity as they cross joints—the pretendinous cord causes flexion contracture at the metacarpophalangeal joint. The lateral digital sheet becomes the lateral cord and causes flexion of the proximal interphalangeal joint through its attachment to the Grayson's ligament. The spiral cord is responsible for both proximal interphalangeal joint contracture and superficial displacement of the neurovascular bundle, making it more susceptible to accidental division at surgery (Townley *et al.*, 2006).

### 2.5.1 Clinical Presentation

In its early stages, Dupuytren disease can be difficult to diagnose where skin changes are the earliest manifestation. Changes on the dorsum of the hand consist of either garrod nodes or knuckle pads (common) which are fibrosing lesions over the proximal interphalangeal joints (Rayan, 2007). Dupuytren's disease can be notable from other causes of hand contracture because it begins as a nodule and slowly progresses to contracture of the fingers. During the physical examination, the following features should be noted by physicians:

- the site of the nodule (tender/non-tender) and the presence of contractures;
- bands;
- skin pitting, tenderness, and dimpling in the palm and digits.

If contractures are present, the angles should be distinguished at the PIP and MCP joints where patients can do that by themselves. A functional history and rate of progression also should be noted (Trojian and Chu, 2007). Figure 2-6 shows a patient with Dupuytren's disease (Lahiri *et al.*, 2007). The typical findings are the presence of a nodule followed by the formation of a cord. The contracture usually starts in the palm and then progresses distally. The palmar skin and underlying tissue thicken, and the subcutaneous fat becomes more fibrotic, leading to the skin becoming more attached to the underlying fascial structures. Skin pits are usually seen in the palm distal to the distal palmar crease. They result from the contraction of the longitudinal fibers of the palmar aponeurosis that insert into the dermis. (Shaw *et al.*, 2007).

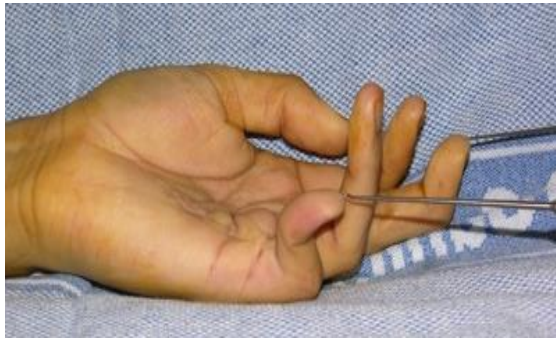


**Figure 2-6.** The presence of Dupuytren's disease of a PIP joint (Lahiri *et al.*, 2007).

The Hueston's tabletop test is a useful, quick and simple test to diagnose the disease. The patient is asked to put his hand and fingers prone on a table (Figure 2-7). The test is positive when the hand will not go flat and surgery or other treatment may be indicated. Additionally, finger joints may become fixed and rigid. If the hand lies completely flat on the table, the test is considered negative (Bayat and McGrouther, 2006).



**Figure 2-7.** The Hueston's tabletop test finger joint contractures diagnosis ([http://dupuytren.biz/dupuytren\\_1.html](http://dupuytren.biz/dupuytren_1.html)).

### 2.5.2 Treatment

The treatment for Dupuytren's disease is to correct the deformities which are causing functional limitations for the patient. The treatment of the disease was subdivided by Jose and Bainbridge (2010) into: non-surgical treatments and surgical treatment; needle aponeurotomy, segmental fasciectomy, limited fasciectomy, dermofasciectomy, other surgical treatments (skeletal distraction, arthrodeses, and amputation). Surgical release or excision of the affected palmodigital tissue is the mainstay of treatment, however, symptoms often recur. Although surgeons apply the long-term safety and recurrence rate of the nonsurgical correction procedure, it needs further assessment (Shih and Bayat, 2010). Surgical intervention is usually considered when there is a MCP contracture of at least 30 degrees or any degree of PIP joint contracture (Shaw *et al.*, 2007). Preoperative and postoperative skeletal traction with an external fixation device has been utilized to improve correction of severe contractures of the PIP joint.

## 2.6 External finger fixators

The treatment of PIP joint contractures by external fixators is a useful method enabling the ability to exercise adjacent joints during healing (Halliwell, 1998). Distractors were first used in 1897 by Clayton (USA) and they have gone through various modifications (Salafia and Chauhan, 1997). The main feature of external fixators is their ability to stretch finger tissues. Each device has a specific mechanical mechanism that allows the passive motion of the injured digit. Different material combinations have been used in the manufacture of PIP joint fixators. Typical fixators are either manufactured totally from a metal, or a combination

of a metal and a polymer. The metal is generally medical grade stainless steel or medical grade aluminum alloy. The polymers as polyetherimide (PEI) and rubber.

In 1938 Hoffman introduced his mini-hand fixator, used mainly in cases of fractures, and this was modified by Mantero (Italy) in 1976 (Salafia and Chauhan, 1997). The fixator was manufactured from aluminum alloy and stainless steel. It consists of 6 components: proximal and distal blocks, two 2 mm threaded pins, a lengthening bar and a distraction nut, as shown in Figure 2-8. Houshian and Schrøder were interested in using this type of fixator and they stated that the fixator was easy to apply and effective in reducing contractures of the PIP joint by soft tissue distraction. The complications included superficial pin-track infection in 17% of cases and 30% of patients had slight pain at the beginning of distraction (Houshian and Schrøder, 2004; Houshian *et al.*, 2007).

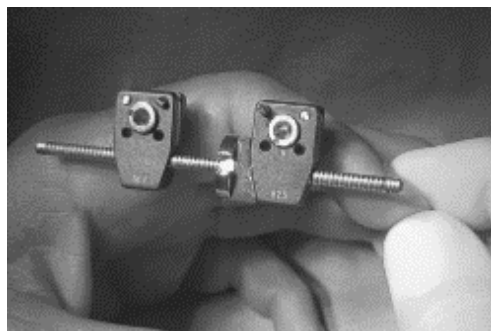


**Figure 2-8.** Mini external fixator (Houshian and Schrøder, 2004)

In the late 1990s, a group of renowned design surgeons and Stryker engineers developed the innovative Hoffmann II Micro External Fixation System (Figure 2-9). The Hoffmann II fixator is manufactured from stainless steel and carbon composite materials to provide an optimal low profile high resistance features, and was designed to answer the growing needs of small bone injuries by ensuring ease of use, versatility and patient comfort (Asche *et al.*, 2009).



**Figure 2-9.** Hoffmann II Micro External Fixation System (Asche *et al.*, 2009).

Ruland *et al.* (2008) and White *et al.* (2012) applied the design mini fixator idea of 1.4 – 1.6 mm diameter K-wires and rubber bands (Figure 2-10 and Figure 2-11). The difference between these two studies was the position of the inserted pins in the finger phalanx. The pins were implemented dorsally during treatment of severe Dupuytren's contracture of the PIP joint in 38 fingers (27 patients) between 1999 and 2004 (White *et al.*, 2012). On the other hand, Ruland *et al.* (2008) inserted the pins laterally in the injured digit to correct 34 PIP joint contractures. Both studies reported that the pin and bands idea achieved fair results towards their patients especially in the study of White *et al.* (2012) where the fixator can be

attached to any digit, because of its size and position. The common complication was pin site infections and more complications were listed by White *et al.* (2012) as: loose pins, osteoarthritis at the PIP joint, reflex sympathetic dystrophy, and disease recurrence needing PIPJ fusion.



**Figure 2-10.** Mini external fixator (pins and elastic bands) (White *et al.*, 2012).



**Figure 2-11.** Pins and dental rubber bands fixator (Ruland *et al.*, 2008).

The dorsal aspect of pin implementation in the involved finger was also presented and described by Slater *et al.* (2003), who believed in the advantage of this technique where the device can be applied to more than one digit simultaneously. Their new device, A Digit Widget device (Figure 2-12) employs the principle that a gentle extension torque, applied continuously, simulates the growth and elongation of contracted soft tissues. No complications were reported in their study.



**Figure 2-12.** A Digit Widget device (Slater *et al.*, 2003).

Different types of treatment techniques was presented in 2009 by Ng and Oliver and reviewed by the British Editorial Society of Bone and Joint Surgery Journal (Ng and Oliver, 2009). Devices (Figure 2-13) included the dynamic traction device, the Robertson Banjo splint 1946, extension-block splinting 1972, the Suzuki frame 1994, the Allison device 1996, the force couple splint 2000, the Schenk device facilitating mobilisation 2000 and the Hynes and Giddings device 2001. The review study concluded that the surgical treatment of fractures of the PIP joint is still mainly based on the experience and personal preference of individual surgeons. For the dorsal fracture-dislocation with a volar lip, if the volar fragment is less than 30% of the articular surface the extension-block splinting with a wire was a favorable technique. For those with more extensive articular involvement or with complex

unstable fractures, including Pilon fracture, the ‘S’ Quattro is the preferred fixator because of its relative ease of application.

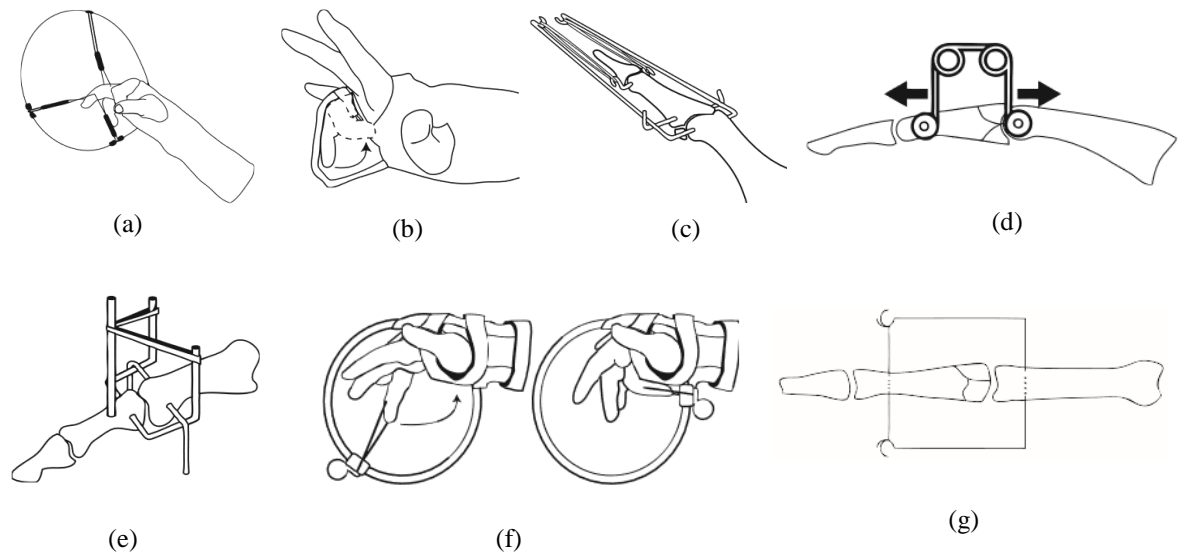


**Figure 2-13.** The different types of treatment techniques (a) Robertson Banjo splint; (b) Extension-block splinting; (c) The Suzuki frame; (d) Allison device; (e) The force couple splint; (f) The Schenk device facilitating mobilization; (g) The Hynes and Giddings device (author’s own drawing, adapted from Ng and Oliver, 2009).

The device was devised by Fahmy in 1990 (Fahmy, 1990) and designed to treat comminuted unstable intra-articular phalangeal fractures. It contains a unique, dual, parallel, but opposing action, spring column system. It consists of two modified unthreaded notched K-wires and two serpentine springs (Figure 2-14) (Bostock *et al.*, 1993<sup>a</sup>). The advantages of the S-Quattro are: low mass; a reduced operative time; distraction of joints in different degrees of flexion, extension and radial-ulnar deviation; allowing movement in intra-articular fractures; its use in some compound fractures and in cases of mal-union (Bhamra *et al.*, 2012). The S-Quattro

was used in 224 cases (Fahmy, 1990; Fahmy and Harvey, 1992; Bostock *et al.*, 1993<sup>b</sup>; Mullet *et al.*, 1999; Khan and Fahmy, 2006<sup>a</sup>; Khan and Fahmy, 2006<sup>b</sup>; Byrne *et al.*, 2008) with good overall results. Some complications were reported in a few cases such as devices dislodging, pin site infections and pin loosening.

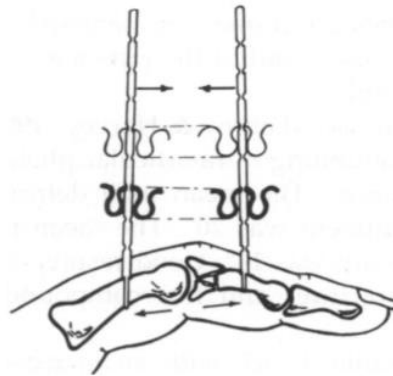


**Figure 2-14.** The Stockport serpentine spring system “S-Quattro” a flexible mini external fixator (Bostock *et al.*, 1993<sup>a</sup>).

The Joshi external stabilising system (JESS) is considered one of the most comprehensively used systems where many previous clinical studies from 1991 to 2013 have referred to it (Figure 2-15). A wide range of complex problems in the management of fracture of the humerus and hand were corrected using the JESS fixator. In 1991 Dr Joshi (Bombay, India) introduced the external fixator JESS which is economical, reliable, reusable and low mass. This system has a high safety profile and unparalleled ease of implantation. It can be applied easily by any surgeon with minimal instrumentation (Ghosh *et al.*, 2013). It uses transfixing K-wires which are bridged together via ‘link joints’. JESS allows frames of varying rigidity to be readily constructed depending upon the clinical need. Malleable connecting rods obviate the need for complex joints with multiplanar freedom. The construction of standard

hand positioning frames allows proper positioning of crushed hands. Subsequent mobilization of the hand with the help of slings and rubber bands is also possible. With the addition of hinges and distractors the system is able to cope with complex problems as well such as stiff contracted joints and clubfoot (Joshi, 1997). The JESS device was applied for correction of PIP Joint contracture deformities in 68 fingers between 1991 and 1997 by Salafia and Chauhan (1997). The study results were compared with other distractors at that time which were made in the USA and Europe and it was concluded that the JESS was easy to apply, economical, reliable, re-usable and will be accepted by the patient. The device complications included mechanical malalignment of the K-wire and infection. In another study, 25 patients with hand injuries, fractures and a mangled hand used the JESS device and it was evaluated by x-ray (Sathishchandra *et al.*, 2011). The study reported that all cases recovered from the injuries with rod migration and rotational instability the complications.

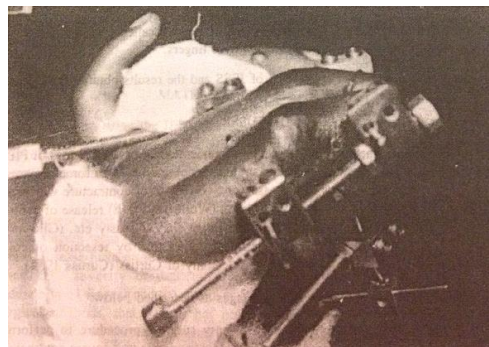


**Figure 2-15.** JESS (Joshi external stabilising system) device (Salafia and Chauhan, 1997).

In 1998 a comparison study was undertaken between one of the most widely used devices for a continuous elongation treatment for severe Duputren's disease, The Continuous

Extension Technique (TEC) device (Figure 2-16) and a new designed device by Neil Citron, the Verona device (Figure 2-17). The TEC device was constructed in 1986 by A. Messina (Messina and Messina, 1993). The TEC was used widely between 1991 and 1996. Citron and Messina (1998) used the TEC and the Verona for the preoperative correction of the deformities of severe Dupuytren's disease in 13 patients (18 fingers) with 7 cases using the Verona and 11 cases using the TEC. The conclusions of the study were that the TEC is a large device which can apply longitudinal traction to several fingers simultaneously and to the various joints in that finger independently with the possibility of varying the direction of traction from a straight pull. The Verona fixator is less bulky and it can apply an angular corrective force as well as distraction if required. It can be used on only one joint at a time and was employed only for the PIP joint.

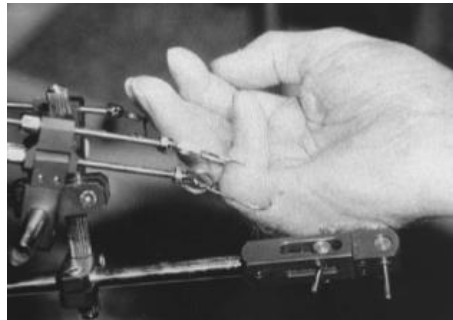


**Figure 2-16.** The Continuous Extension Technique (TEC) device (Citron and Messina, 1998).



**Figure 2-17.** Verona device (Citron and Messina, 1998).

The PIPSTER (Proximal Interphalangeal Skeletal Traction Extender) device (Figure 2-18) was designed by Hodgkinson in 1994 (Hodgkinson, 1994) in order to develop the TEC. The PIPSTER is described as a very simple device and small in size in which two fixation points are separated as a nut is turned. One of them is transversely across the base of the proximal phalanx and the other across the head of the middle phalanx. A silicone gel spacer separates the device from the skin of the finger. The PIPSTER device was applied in five patients with seven affected fingers and two complications were found to occur with a skin ulcer in the web of the K-wires.

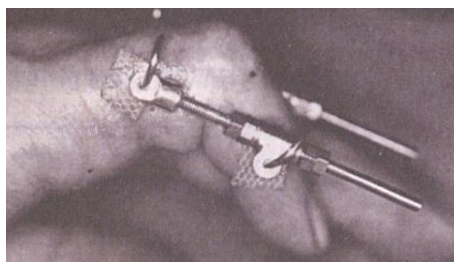


**Figure 2-18.** PIPSTER (Proximal Interphalangeal Skeletal Traction Extender) device (Hodgkinson, 1994).

Between 1993 and 1998 two more external fixators were designed and presented. By 1993 a small dynamic external finger fixator (Inanami *et al.*, 1993) was designed to maintain the reduced position of the dislocated PIP joint (Figure 2-19). In 1998 the “Multiplanar” distractor (Figure 2-20) was designed for three-dimensional distraction of the mandible by Kasabian *et al.* (1998). Inanami *et al.* (1993) fixator consists of a pair of rhomboid apparatuses that have two pulleys at both ends and a pair of arm apparatuses that have one pulley in the middle. The Multiplanar was placed in the proximal phalanx and two pins were placed in the middle phalanx and the angle of distracter performed by simple rotation of a screw on the device. The small fixator was attached to 7 male patients (5 ring and 2 index digits) and the Multiplanar was attached only in one patient. All patients were satisfied with the final results of the treatment in both studies. In only one case did a patient suffer from pain (Inanami *et al.*, 1993) with no complications reported by Kasabian *et al.* (1998).

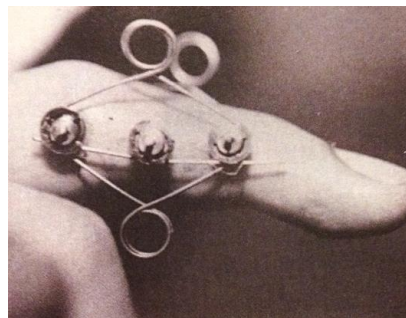


**Figure 2-19.** Small dynamic external finger fixator (Inanami *et al.*, 1993).

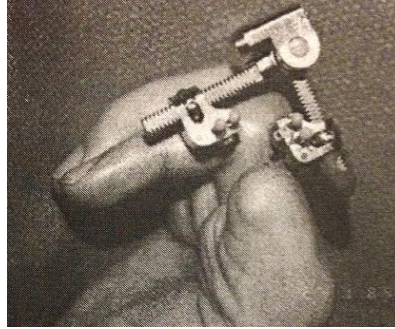


**Figure 2-20.** Multiplanar distractor (Kasabian *et al.*, 1998).

A unique unilateral external device was designed by Hotchkiss *et al.* (1994), which is the Compass PIP joint hinge. The Compass hinge differs from other devices in that there is easier access for fasciectomy, less technically demanding fasciectomy, the device corrects contracture prior to fasciectomy and maintains an active and passive range of movement. In contrast to the other distraction devices, only the Compass hinge allows and maintains active extension. Mechanical failures are the most common problems associated with the use of the Compass device (Bonaspetti *et al.*, 1999; Bain *et al.*, 1998; Houshian *et al.*, 2002; Feldscher and Blank, 2002; Lahiri *et al.*, 2007; Youssef *et al.*, 2015). Full details about the Compass hinge will be addressed in the next chapter.

By the end of this section, there are some design considerations that can be picked from the background study of the different PIP joint fixators and these key points helped in generating some of the new design device requirements (see chapter 4 in this study). These considerations can be summarized as:

- There were two possible fixation positions for the fixators in the digits, laterally and dorsally. But the surgeon feedback from Mr. Titley confirmed that the lateral position is most sufficient than dorsal one,
- The fixator's mechanical working mechanisms are classified mainly into two; lock mechanism (screw and nut) and gear mechanism (worm and worm wheel) supporting in the fixators widely used. They will be the basis of the two concept designs for the mechanisms of the new device design.
- A low profile fixator was recommended from the previous studies and had a positive feedback from surgeons and patients as well. They can be attached to the central digits easily and the patients feel comfort due to the small space between the fingers,
- Surgeons considered the polymer in the device as important as it is light weight and natural in color so it close to the skin color. That makes patients motivated to implant it in their injured digits.

Table 2-4 shows a summary from the available data about the main features of the different external fixators used to treat PIP joint contractures.

**Table 2-4.** Summary of the main features of the different PIP joint fixators.

<b>Fixator</b>	<b>Number of patients/ digits</b>	<b>Working mechanism</b>	<b>Device implanted position</b>	<b>Size</b>	<b>Weight</b>	<b>Material</b>	<b>Applicability / usability</b>	<b>Complications (fractures, infections, and loosening)</b>	<b>References</b>
Mini external fixator	42 patients	Lock mechanism (screw and nut)	Lateral side	Not available data	Not available data	Aluminum alloy and stainless steel	Easy to apply	Pin-track infection, pain	Houshian and Schrøder, 2004; Houshian <i>et al.</i> , 2007.

Hoffmann II Micro External Fixation	Not available data	Lock mechanism (screw and nut)	Lateral side	Low profile	Not available data	Stainless steel and carbon composite materials	Ease of use	Not available data	Asche <i>et al.</i> , 2009.
Pins and elastic bands	38 digits	Pins and elastic bands	Dorsal side	Small size	Low mass	Stainless steel and rubber	Not available data	Pin site infections, loose pins.	White <i>et al.</i> , 2012.
Pins and dental rubber bands fixator	34 digits	Pins and rubber bands	Lateral side	Small size	Light weight	Stainless steel and rubber	Not available data	Pin site infections.	Ruland <i>et al.</i> , 2008

S-Quattro fixator	224 patients	Unthreaded notched K- wires and two serpentine springs	Lateral side	Small	Low mass	Stainless steel	Easy to apply	Devices dislodging, pin site infections, pin loosening.	Fahmy, 1990; Fahmy and Harvey, 1992; Bostock <i>et al.</i> , 1993 <sup>b</sup> ; Mullet <i>et al.</i> , 1999; Khan and Fahmy, 2006 <sup>a</sup> ; Khan and Fahmy, 2006 <sup>b</sup> ; Byrne <i>et al.</i> , 2008.
JESS device	93 digits	Lock mechanism	Lateral side	High safety profile	Low mass	Not available data	Reusable, applied easily	Mechanical malalignment of the K-wire, infection.	Joshi, 1997; Salafia and Chauhan, 1997

		(screw and nut)							; Ghosh <i>et al.</i> , 2013; Sathishchandra <i>et al.</i> , 2011.
TEC device	11 digits	Lock mechanism (screw and nut)	Lateral side	Large device	Heavy	Not available data	Not easy to use	No complications recorded due to the use of TEC device.	Messina and Messina, 1993.
Verona device	7 digits	Worm and worm wheel mechanism	Lateral side	Less bulky	Not available data	Not available data	Easy to use, easy to apply	No complications recorded due to the use of Verona device.	Citron and Messina, 1998.
PIPSTER device	7 digits	Lock mechanism	Lateral side	Small in size	Not available data	Not available data	Easy to apply	Skin ulcer in the web of the K-wires	Hodgkinson, 1994.

		(screw and nut)							
--	--	--------------------	--	--	--	--	--	--	--

## 2.7 Medical device design process

The design process for implantable orthopedic medical devices can be divided into six stages (Aitchison *et al.*, 2009): market research, design specification, development of concept designs, detail design, manufacturing and sales. The detailed structure to the design process, shown in Figure 2-21, presents the sequence of procedures which should be followed to implement a new device design into the market.

In order to ensure the safety of patients and healthcare workers, the design process of medical devices is highly regulated. The design of the device has to meet certain requirements directed by legislations such as the Medical Device Directive for Europe and the Food and Drug Administration for the USA. A Design History File which describes the design history of the product should keep the record of the design process, which needs to be maintained after the product is released to include any subsequent modifications.

For the design aspects, where the conceptual design creates many solutions to meet the design requirements. A conceptual idea is chosen and developed until a detail design has been produced.

The design is verified using finite element analysis which is a method that has been used widely to analyse medical devices. A major advantage of this method is allowing the different designs to be assessed and optimized without the need to build unnecessary and expensive prototypes. Finite element model parameters can be changed repeatedly and

quickly to evaluate the effect and influence of each single component before the final design is manufactured.

An important step in the design of a medical device is to carry out a risk assessment. Any risk associated with the device must be eliminated or reduced as far as possible so that the safety of patients and healthcare workers is not compromised. Since June 1998 it has been law that no new medical device can be sold in the European Union without the device being European Conformity (CE) marked. Every medical device prior to approval with CE marking needs to have completed a risk analysis procedure. It is a legal procedure which is very useful to evaluate the design during the development stages. To gain a CE mark a medical device must comply with the Medical Device Directive (MDD) (1993). The MDD (1993) has been developed as a means to regulate medical devices in Europe (Crisp, 1996). This regulation covers any instruments, apparatus, appliance, material or other article intended for use or in the human body.

The MDD is now well established and is used by medical device manufacturers as a benchmark for the minimum standard of quality required (EN14971; MDD). During manufacture faults can occur and these faults are described by the MDD as risks. A risk is the probability of a hazard causing harm to a patient or healthcare worker. Therefore, the device also requires documented evidence that the device is fit for the purpose for which it was intended and that packaging, sterilization, transportation and storage must not adversely affect it.

A repeatable and reliable manufacturing process should be chosen before transferring the final design to the production stage and the final design is verified using validation processes (e.g. mechanical testing) to ensure that the medical device meets the user requirements and

the intended use. All documents and training associated with the device should all be stored in the Design History File. Finally, there is the launch of the new device in the market and post-market surveillance.

A design review is required, at each stage of the design process, to formally document complete and systematic examination of a design (Aitchison *et al.*, 2009).

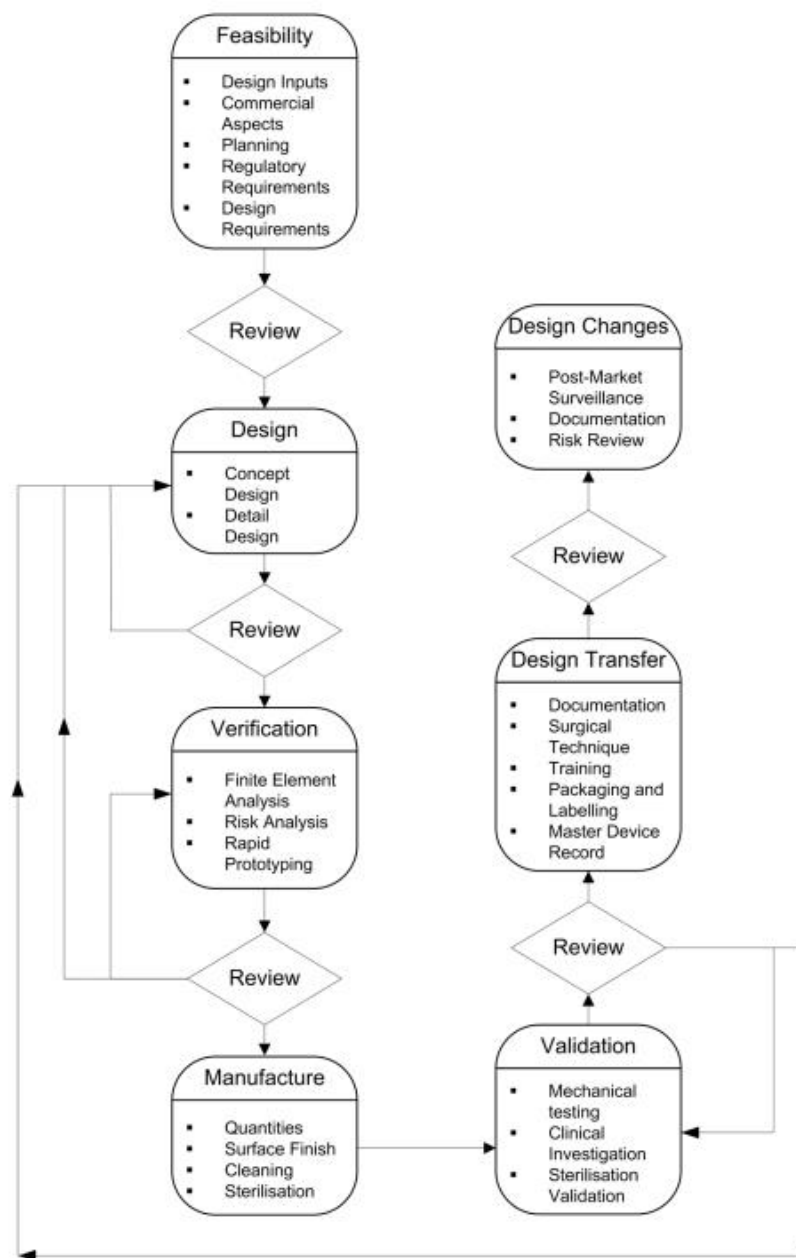


**Figure 2-21.** The medical device design process flowchart (Aitchison *et al.*, 2009).

## 2.8 Summary

Contracture of the proximal interphalangeal (PIP) joint is a common clinical problem and a number of skeletal fixation devices have been used to correct flexion contractures of the PIP joint. The TEC, PIPSTER, JESS, Verona, Multiplaner distractor, S Quattro, Ortho fix, Digit Widget device and Compass hinge device are examples of the fixators. Of these devices, the Compass hinge has received the most investigation regarding its effect on contractures associated with Dupuytren's disease. The Compass hinge is characterised by allowing active extension movement. Mechanical failures and pin infection are the most common problems associated with the use of the Compass device. A complete engineering analysis for a failed Compass hinge device was required to understand the main causes of mechanical failure and this will be presented in the next chapter.

CHAPTER 3  
ENGINEERING ANALYSIS OF A FAILED  
COMPASS HINGE

## **3 ENGINEERING ANALYSIS OF A FAILED COMPASS HINGE**

### **3.1 Chapter overview**

This chapter aims to provide an engineering analysis of a failed Compass hinge device. Section 3.2 introduces the Compass hinge device. The engineering analysis of a failed device is presented in § 3.3. The chapter concludes with recommendations for an improved design which is described in § 3.4. A peer reviewed journal paper based on this chapter has been published (Youssef *et al.*, 2015).

### **3.2 Compass hinge device**

#### **3.2.1 Introduction**

The Compass hinge (Smith & Nephew, Memphis, TN, USA) is an example of a dynamic external fixation device (Figure 3-1) which is used by surgeons for correcting the PIP joint for conditions such as fractures and diseases. Dupuytren's disease is one of the diseases which the Compass hinge is commonly used to treat it. (Krakauer and Stern, 1996; Bain *et al.*, 1998; Houshian *et al.*, 2002; Feldscher and Blank, 2002). The Compass hinge is used to

stretch tissues prior to corrective surgery (Bonaspetti *et al.*, 1999). The Compass hinge fixator is a unilateral external hinge that attaches with skeletal fixation to either side of the joint with stainless steel Kirschner wires (K-wires) (Feldscher and Blank, 2002).

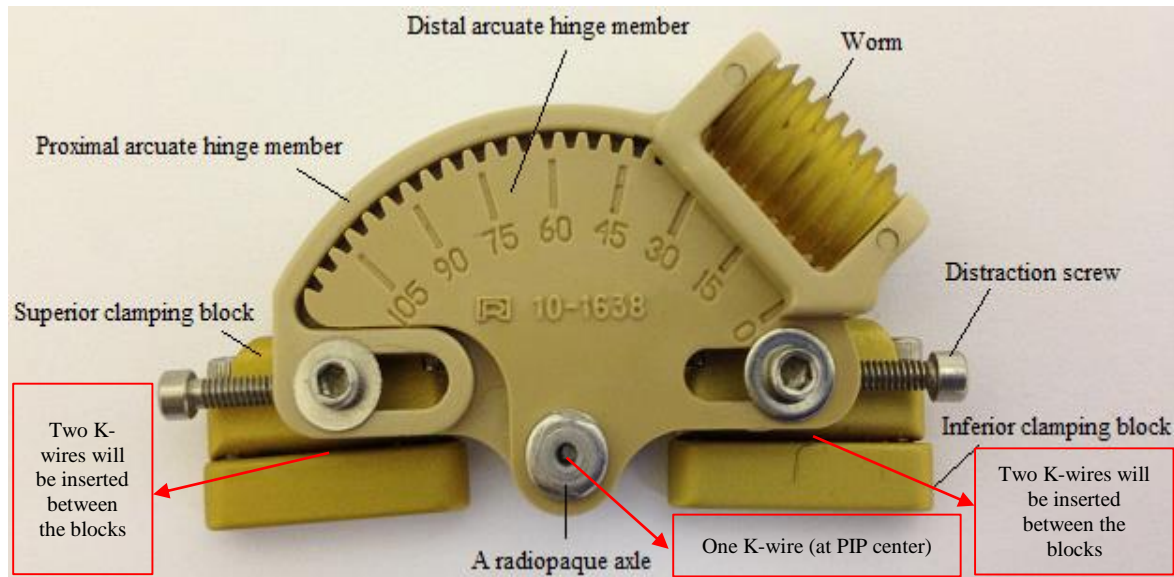


**Figure 3-1.** Compass hinge external fixator.

### 3.2.2 Components and surgical technique

The Compass hinge consists of eight main parts: proximal arcuate hinge member; distal arcuate hinge member; worm gear; 2 superior clamping blocks; 2 inferior clamping blocks; a radiopaque axle (Hotchkiss *et al.*, 1994). The device is surgically attached under fluoroscopic guidance (Krakauer and Stern, 1996). The first step is placement of a K-wire through the approximate axis of rotation of the PIP joint; this becomes the mechanical axis of the Compass hinge. Two K-wires are then inserted into both the proximal and middle phalanges and the proximal and distal clamping blocks are clamped around the two K-wires.

These K-wires should be placed parallel to the first inserted K-wire. The original K-wire, which marks the axis of rotation, is then removed at the end of the procedure (Figure 3-2). Distraction may be applied by tightening a screw in the distal block. The device is equipped with a worm gear (Houshian *et al.*, 2002). When the worm gear is disengaged, active movement of the finger is possible by the patient (Bain *et al.*, 1998). With the gear engaged only passive motion is possible. The Compass hinge differs from other devices in that it can provide distraction, stabilisation and controlled passive mobilisation, whilst allowing disengagement for active motion (Krakauer and Stern, 1996).

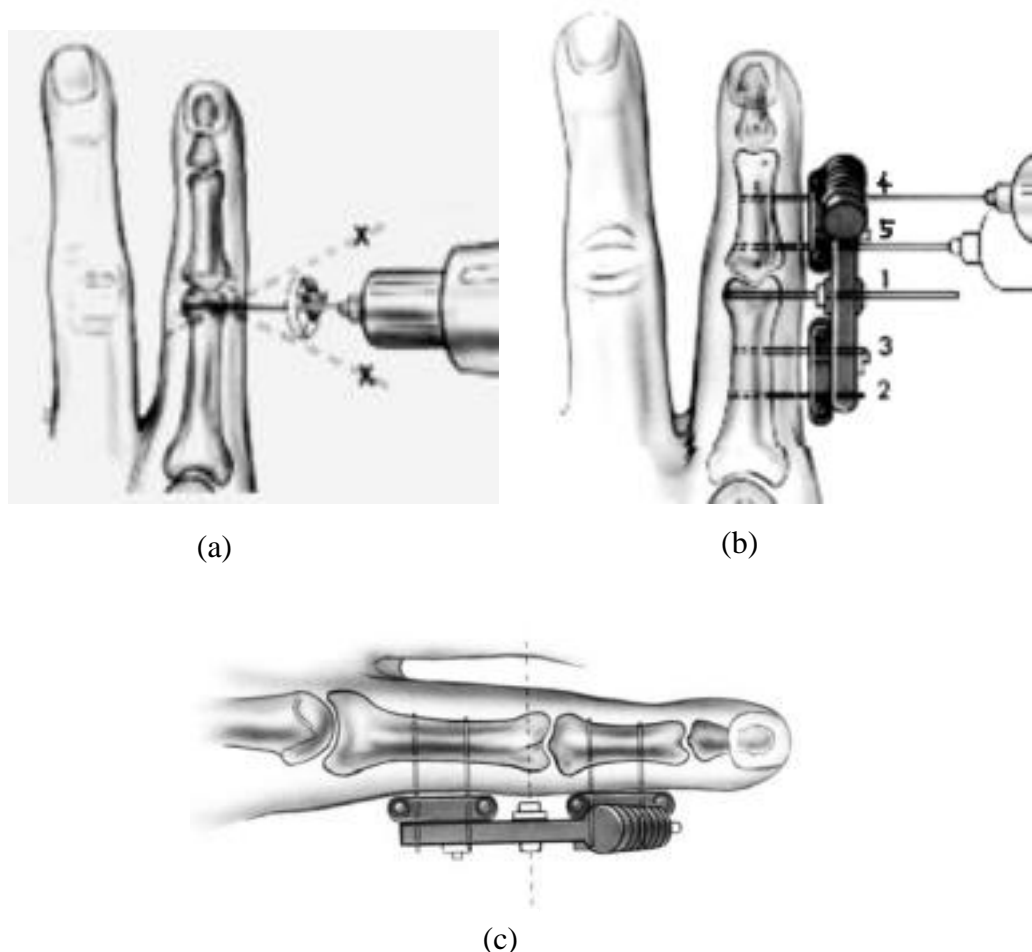


**Figure 3-2.** Surgical technique for the Compass hinge fixator (a) axis K-wire insertion (b) proximal and distal K-wires insertion (c) dorsal view for the implanted fixator (author's own drawing, adapted from Hotchkiss *et al.*, 1994).

The Compass hinge device can be attached to the fingers in two positions depending on which finger is injured in which hand (Figure 3-3). Position A is where the distal arcuate hinge member is supported in the middle phalanx of the patient injured finger and the proximal arcuate hinge member in the proximal phalanx. Position B is where the proximal arcuate hinge member is supported in the middle phalanx and the distal arcuate hinge member in the proximal phalanx (Lahiri *et al.*, 2007).

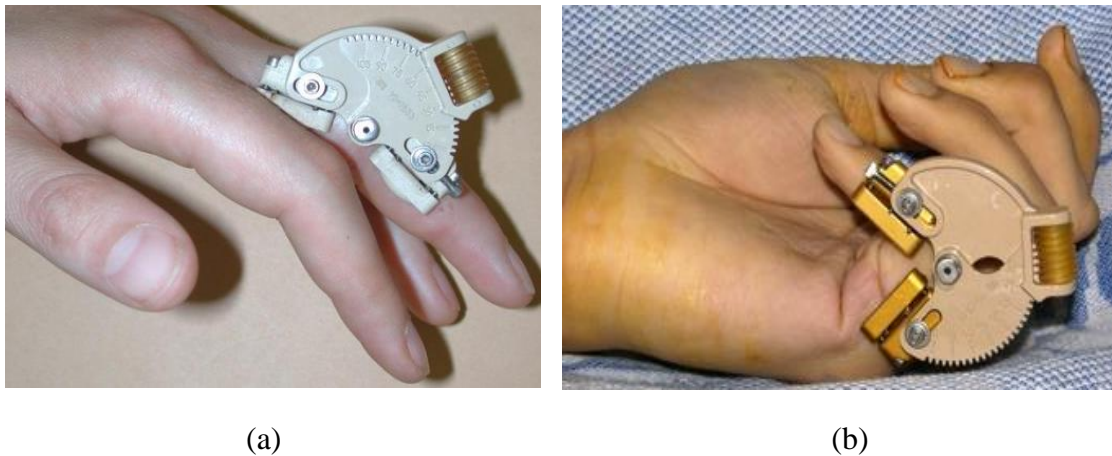


**Figure 3-3.** Compass hinge device supported on patient finger (a) Position A and (b) Position B (adapted from (Lahiri *et al.*, 2007)).

Previous clinical case studies have reported different time periods for use of the Compass hinge device for each patient depending on the severity of injury; the maximum period the device was attached to a patient was 64 days (Bain *et al.*, 1998). Pin-track infections and mechanical failures (Krakauer and Stern, 1996; Bain *et al.*, 1998; Bonaspetti *et al.*, 1999; Houshian *et al.*, 2002; Feldscher and Blank, 2002; Lahiri *et al.*, 2007) are the most common problems associated with the use of the device (Figure 3-4 and Figure 3-5).



**Figure 3-4.** Mechanical failure at distal arcuate hinge (adapted from (Lahiri *et al.*, 2007)).



**Figure 3-5.** Pin-track infections (adapted from (Lahiri *et al.*, 2007)).

The Compass hinge device was applied between 1994 and 2007 in 88 patients with PIP joint contractures; fracture dislocations, dorsal dislocation, fracture subluxation and Dupuytren's disease affected 54 border digits (index and small) and 43 central digits (middle and ring). The compliance of the patients was high and they responded well to the fixator. The overall results of the device were acceptable for surgeons. The advantages of the devices were reported as: low profile; easy to apply; easy to use; allows for active and passive mobility. Table 3-1 is a summary of the previous clinical studies where the Compass hinge device was used in them.

**Table 3-1.** The previous clinical studies summary

<b>Year of study</b>	<b>PIP contractures</b>	<b>Number of Patients</b>	<b>Injured digits</b>	<b>Complications</b>	<b>References</b>
1993 -1994	Fractures of the PIP joint	20	3 index 3 middle 4 ring 10 small	mild pain was rated in 4 cases and moderate to severe in 2 cases, recurrent subluxation in 3 cases, fixator reduction was lost in 1 case, 2 cases of pin track infection, and the device worked its way off the digit in 1 case.	Krakauer and Stern,1996
1994 -1996	Fracture dislocations of the PIP, a dorsal dislocation of the PIP joint, a PIP	20	3 index 11 ring 1 middle 5 little	four pin-track infections and two fractured pin blocks	Bain <i>et al.</i> , 1998

	joint contracture, fractures of the base of the middle phalanx, a fracture of the head of the proximal phalanx, swan-neck deformities after longstanding avulsions of the volar plate				
1999	Dupuytren's disease	6	6 small	one case the clamp broke and was replaced; another patient had skin infection in his palm which was treated with antibiotics for 10 days	Bonasperti <i>et al.</i> , 1999

1997 - 2000	Device developed after tendon surgery, severe hand injuries, replantation surgery, Dupuytren surgery , dislocation of PIP joint and fracture surgery	21	2 index 6 middle 7 ring 12 little	pin-track infections occurred in 11 cases and 2 cases of them led to pin loosening, aseptic pin loosening occurred in 2 cases and the pin support block of the Compass hinge broke in 5 cases (in 2 cases it happened twice)	Houshian <i>et al.</i> , 2002
2002	A chronic PIP joint fracture dislocation	1	1 ring 1 small	frame cracked after 35 days from use	Feldscher and Blank, 2002

2007	Dupuytren's, flexion contractures, fracture subluxation	20	12 border digits, 10 central digits	the distal arcuate hinge polymer part fractured in all cases, Pin-tract infection in 7 patients	Lahiri <i>et al.</i> , 2007
------	---------------------------------------------------------------------	----	----------------------------------------------	----------------------------------------------------------------------------------------------------	-----------------------------

From the previous clinical studies using the Compass hinge device it was concluded that the device was applied to 88 patients with 97 digits where some patients had more than one injured digit with PIP joint contractures. Fracture happened in 22 devices; 14 in the device frame and 8 in the clamping blocks. There has been no recorded causes of these failures. Pin track infection occurred in 25 cases; surgeons confirmed that infection might happen due to the different response from the human body with the K-wire and also patients should keep the area around the inserted K-wires clean as possible to avoid any infection.

### **3.2.4 Model**

A Compass hinge device was provided by Mr. Garth Titley (Consultant Plastics and Burns Surgeon at the Queen Elizabeth Hospital, Birmingham). The device was disassembled (Figure 3-6) by using a standard hexagonal head driver and the dimensions of its parts were measured using a digital vernier caliper (Hilka Tools (UK) Ltd, Surrey, UK). Figure 3-7 shows an example of these measurements. The width was in a range from 49.5 to 58.5 mm, height was 35 mm and thickness was 11.5 mm. The Compass hinge had a range of motion from 0° extension to 105° flexion as written on the device frame. Its mass was 15 g (with a standard deviation of 0.02 g) that was measured using a digital laboratory scale (GA200D, OHAUS®, European Instruments Ltd, Oxford, UK). The gear part nomenclature (module, worm gear teeth pitch and the outer diameter) in the device was measured using the gear tooth pitch gauge. From the measured dimensions two solid models of the Compass hinge device were created using SolidWorks 2011® premium 2011x 64 Edition © 1995-2010 (Dassault Systèmes SolidWorks Corporation, Waltham, USA).

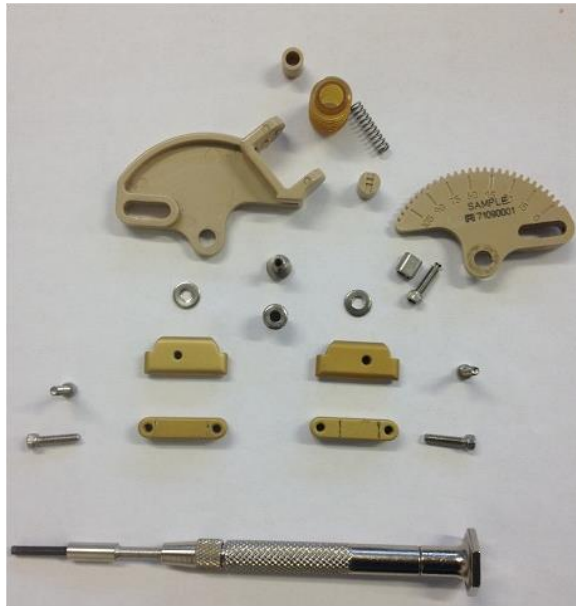


**Figure 3-6.** Compass hinge disassembled components.

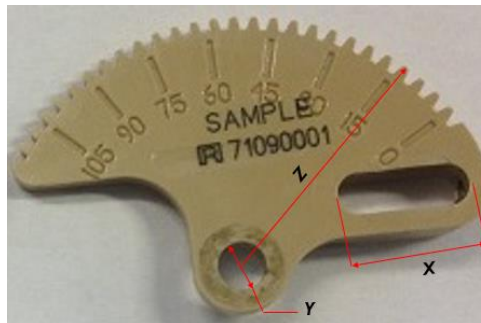


**Figure 3-7.** An example of measurements made on the distal arcuate hinge member.

The first model (Model I) consisted of the distal arcuate hinge member and this was used to model the Compass hinge on the middle phalanx (Figure 3-8). The second model (Model II) consisted of the assembly of the proximal arcuate hinge member and the distal arcuate hinge member which were used to model the Compass hinge on the proximal and middle phalanges (Figure 3-9). For both models SolidWorks Simulation (SolidWorks 2011®

premium 2011x 64 Edition © 1995-2010 (Dassault Systèmes SolidWorks Corporation, Waltham, USA) was used for the finite element analysis.

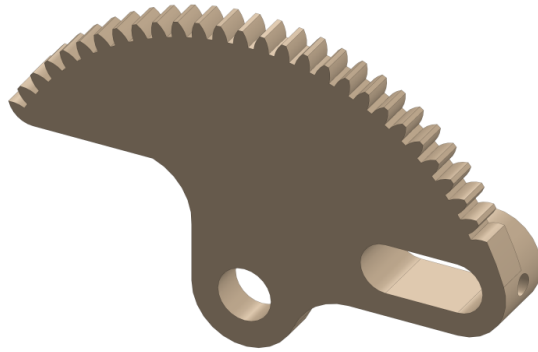


**Figure 3-8.** Solid model of the distal arcuate hinge member.

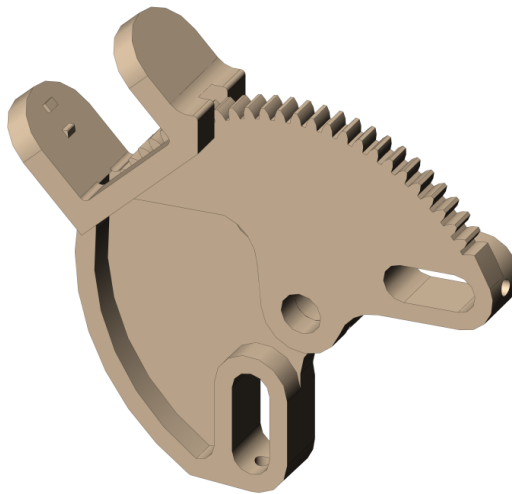


**Figure 3-9.** Solid model of the proximal and distal arcuate hinge assembled members.

The proximal and distal arcuate hinge members are manufactured from the material Ultem® which is a polyetherimide with a Young's modulus of 3.3 GPa and a Poisson's ratio of 0.44 (Kirby, 1992). Model I was meshed with a total of 75,023 parabolic tetrahedral elements (it

is second-order element which is defined by four corner nodes, six mid-side nodes, and six edges). They represent curved boundaries which means more accurate and better mathematical approximations of the results. This number was determined following mesh convergence testing and the convergence criteria was the peak stress. The parts material to be an input to the SolidWorks simulation model was selected from the data base library list which was installed in the SolidWorks program.

Constraints were then applied to the model as follows (Figure 3-10):

- The pivoting joint hole was constrained to allow only rotation;
- Four gear teeth were fixed in all directions to simulate the gear teeth in engagement with the worm gear;
- A range of forces from 10 N to 210 N were applied to the model to simulate the likely forces a patient could apply to the device, based on values of force previously determined from the literature (see chapter 2 section 2.3). Forces were applied either vertically downwards or upwards through the threaded hole of the distraction screw or perpendicular to the middle phalanx of the finger.

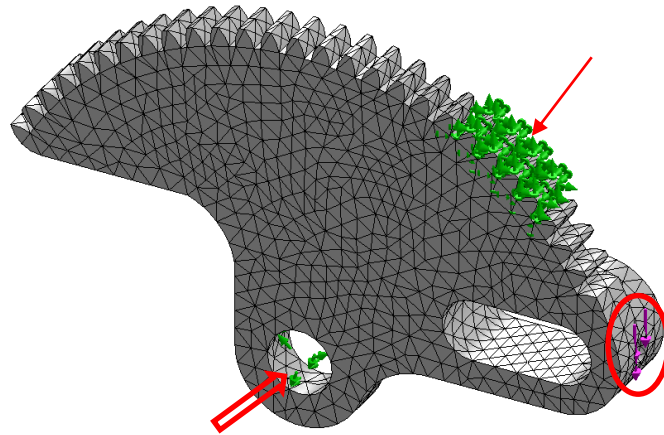


**Figure 3-10.** Meshed finite element model I with the load and constraints applied.

Four different positions of engagement with the worm gear were investigated: position (1) teeth between 15 and 30°; position (2) 30-45°; position (3) 65-80°; position (4) 90-105° (Figure 3-11).

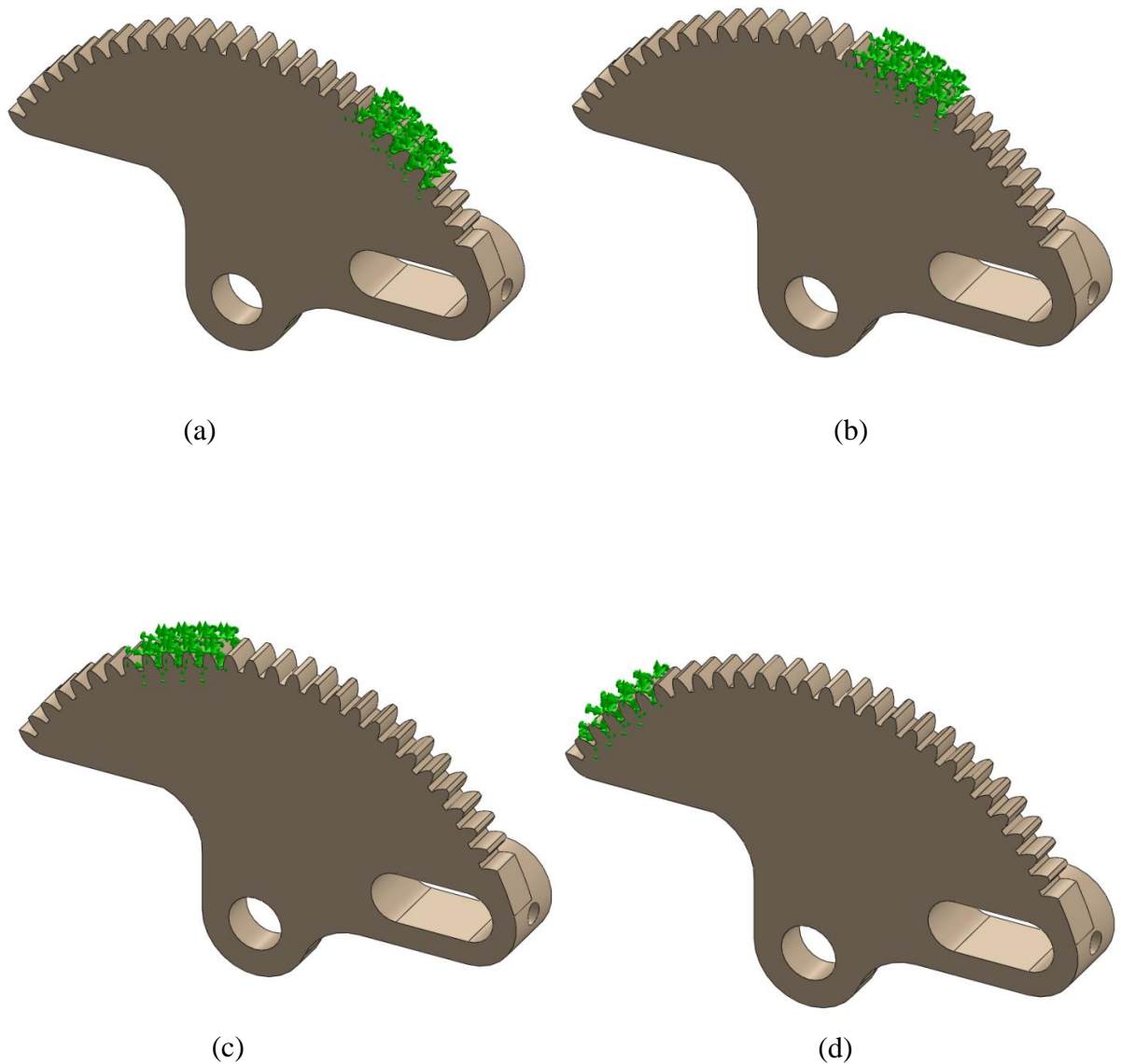
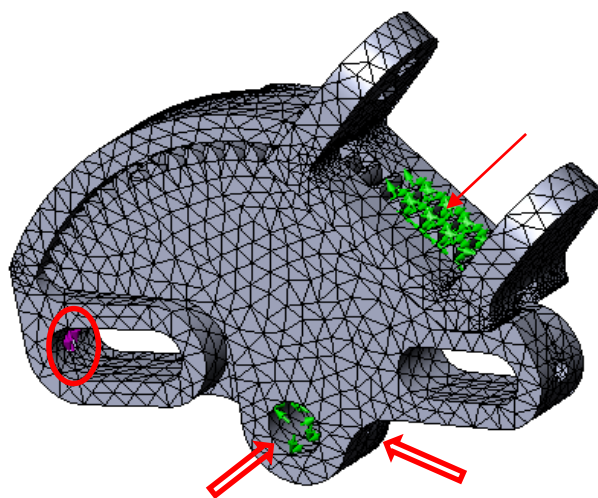


**Figure 3-11.** Four different positions of engagement with the worm gear (a) position 1 (15-30°); (b) position 2 (30-45°); (c) position 3 (65-80°); (d) position 4 (90-105°)

Maximum normal stress theory was selected for analysing the stresses in the distal arcuate hinge member rather than Von Mises stress theory due to the constraints were applied in the PEI material parts (Collins, 1993; Woods and Nimmer, 2001; Hamrock *et al.*, 2007).

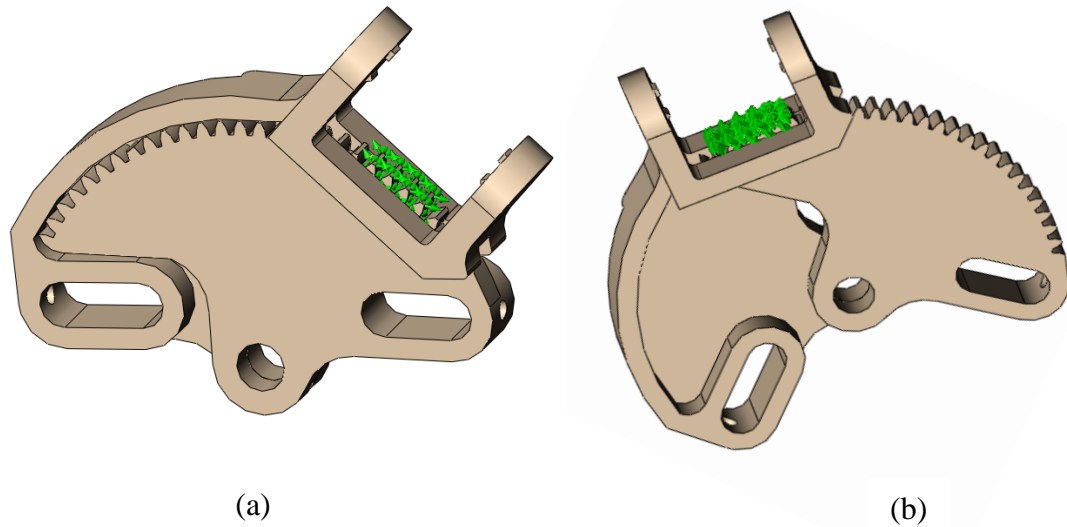
Model II was meshed with a total of 30,000 tetrahedral elements, which depended on the gear teeth fixation positions. Constraints were applied to the model as follows (Figure 3-12):

- The pivoting joint hole of the proximal arcuate hinge part was constrained to allow only rotation;
- A fixed geometry constraint was selected to the pivoting hole of the distal arcuate hinge member;
- Four gear teeth were fixed in all directions to simulate the gear teeth in engagement with the worm gear;
- Forces were applied to the model either vertically downwards through the threaded hole of the proximal arcuate hinge member distraction screw or perpendicular to the middle phalanx of the finger.



**Figure 3-12.** Meshed finite element model II with the load and constraints applied.

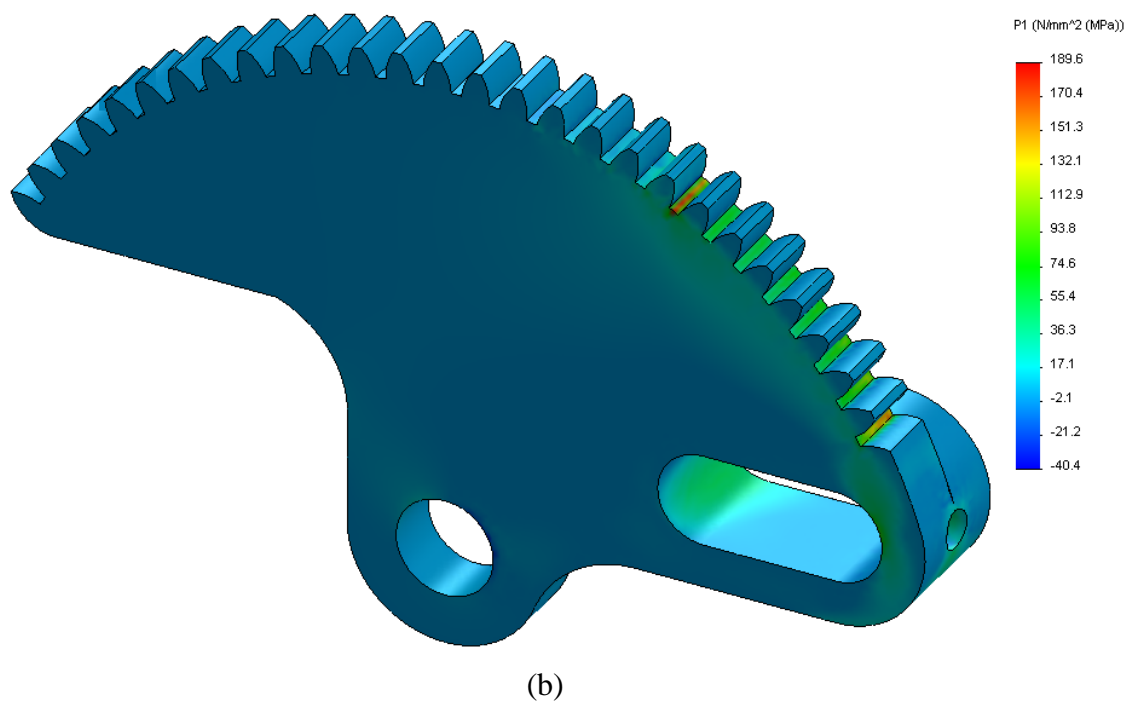
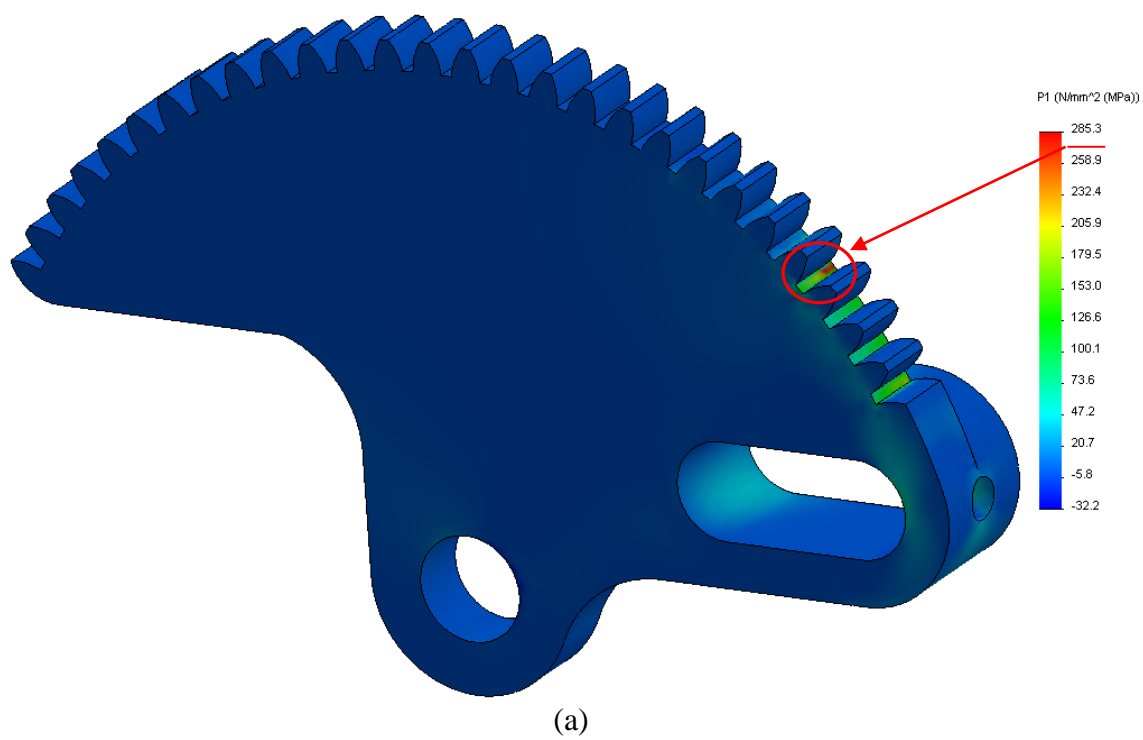
The model was analysed with the gear teeth engaged in just two of the positions used for Model I, as there has been no recorded failure case at the proximal arcuate hinge member: position (1) teeth between 15 and 30° and position (4) 90-105° (Figure 3-13).



**Figure 3-13.** Two different positions of engagement with the worm gear (a) position 1 (15 - 30°) (b) position 4 (90-105°).

### 3.2.5 Results

The results from the simulation analysis for Model I showed that stress patterns were similar for all four positions of the fixed gear teeth. For all cases the maximum value of the principal stress was located between the gear teeth at a point of fixation and the high stresses were distributed at the right side of the distal arcuate hinge member. Figure 3-14 shows the stress distribution pattern at the four different fixation positions at a load of 210 N. The maximum principal stress was 285.3 MPa in position (1) of 15 - 30°.



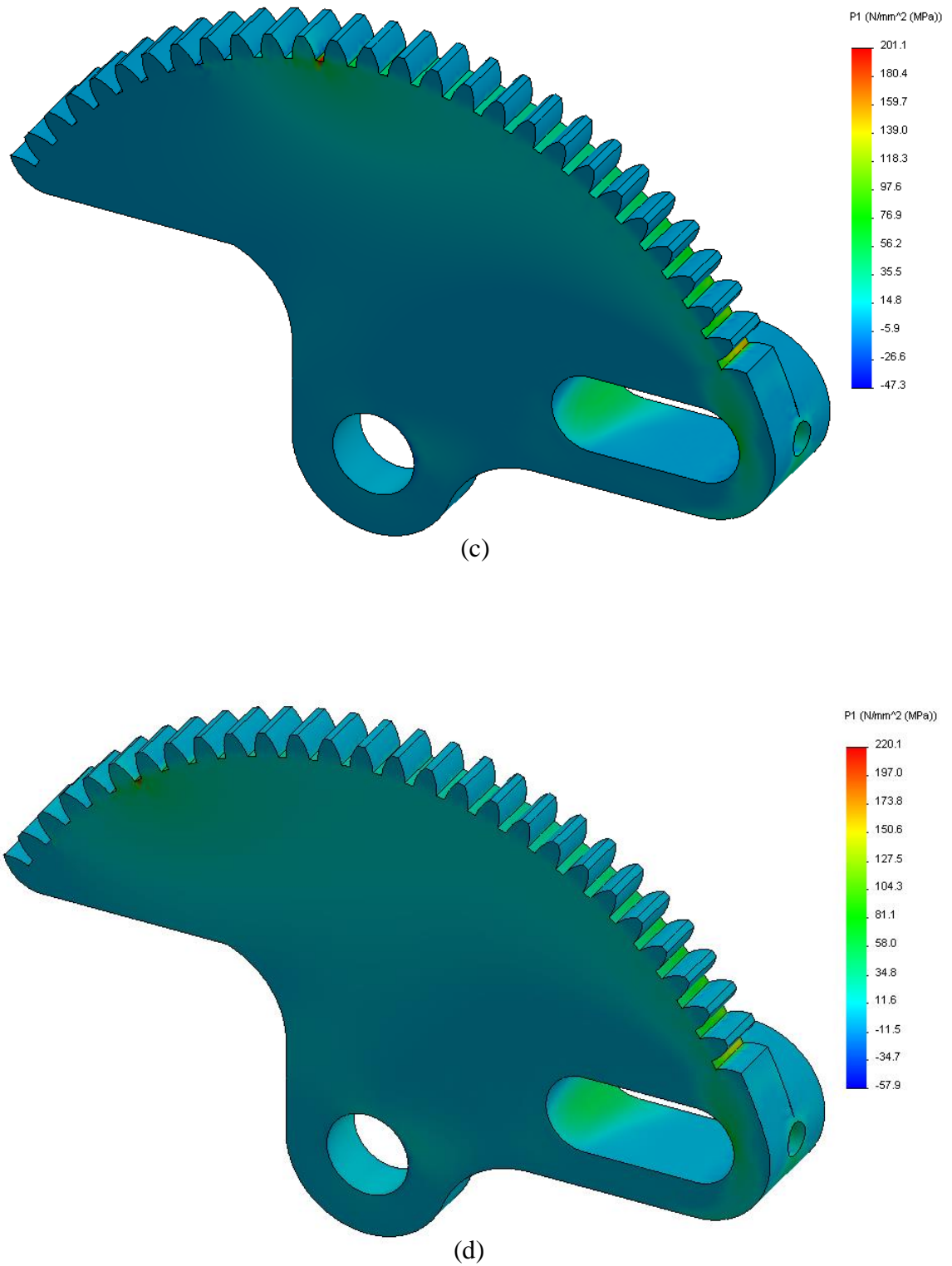


**Figure 3-14.** Distribution of maximum Principal stress for model I for four different positions of gear teeth fixed at (a) position 1 (15-30°); (b) position 2 (30-45°); (c) position 3 (65-80°); (d) position 4 (90-105°).

A linear relationship was found between the applied force in the finite element model and the corresponding maximum principal stress. This relationship was found for all four positions of the fixed gear teeth; the results for position (1) of 15 - 30° are shown in (Figure 3-15). In this position the maximum principal stress was 285.3 MPa.

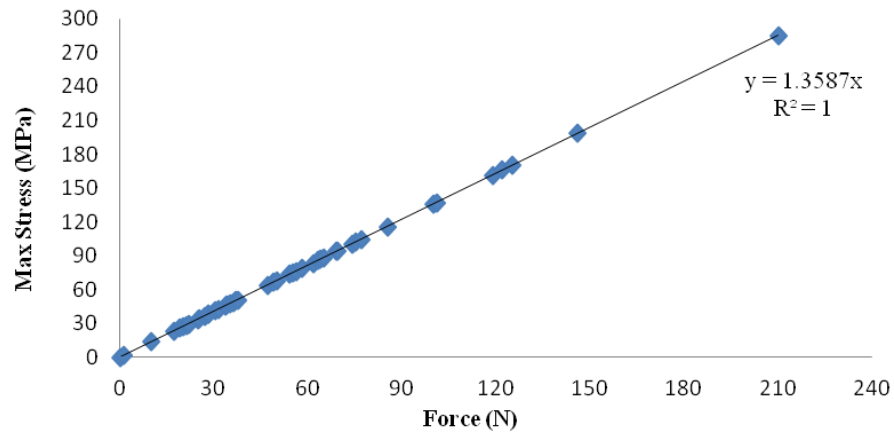


**Figure 3-15.** Maximum principal stress against force for the gear teeth fixed at 15 - 30°.

High stresses of up to 200 MPa were also found on both sides of the right threaded distraction screw hole, as shown in Figure 3-16.

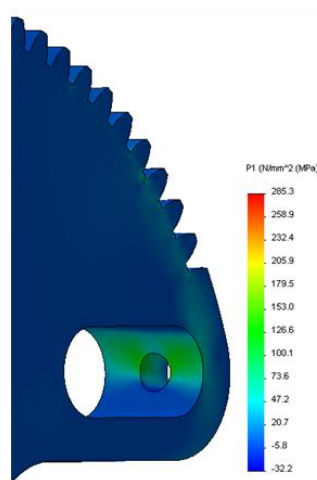
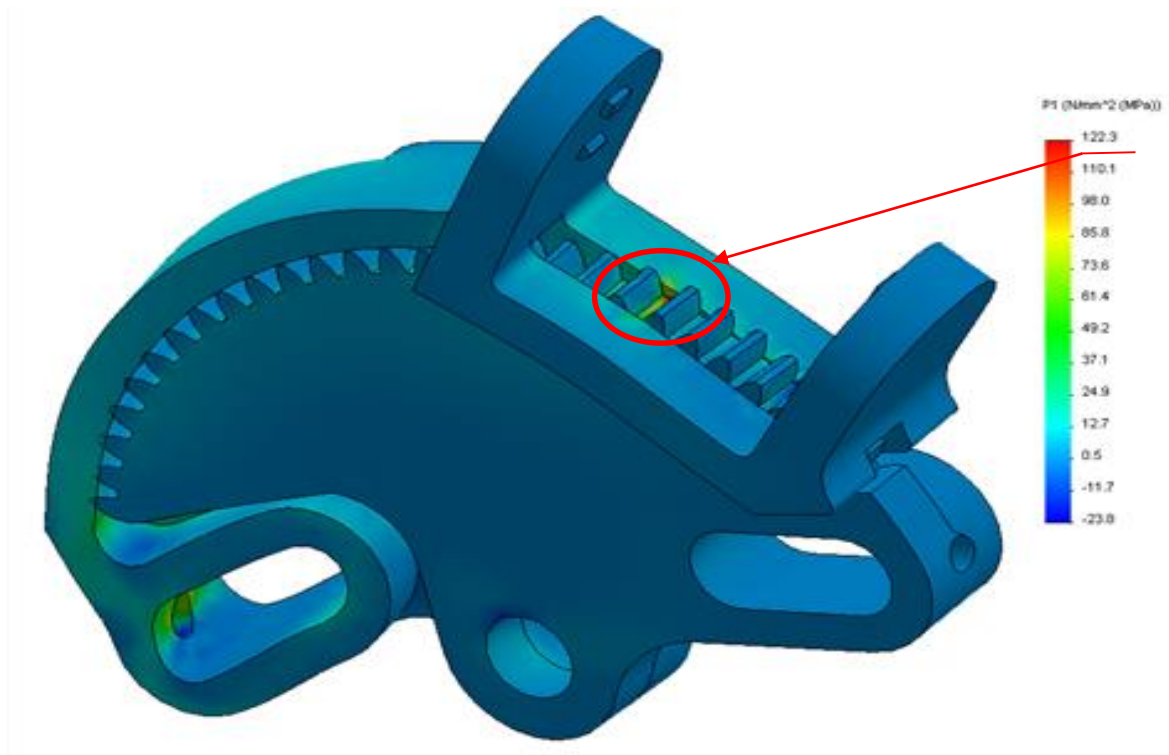


**Figure 3-16.** Maximum principal stress distribution around the distraction screw hole.

For Model II, the results from the simulation analysis showed that the stress patterns were similar for the two positions of the fixed gear teeth. For these cases the maximum value of the principal stress was located between the gear teeth at a point of fixation for the closest tooth to the applied load. Additionally, most of the high stresses were distributed at the left side of the proximal arcuate hinge member. Figure 3-17 shows the stress distribution pattern for position (1) of 15 - 30° and position (4) 90-105° at a load of 210 N. The maximum principal stress was 122.3 MPa which occurred in position (1) of 15 - 30°. High stresses of up to 90 MPa were also found on both sides of the left thread distraction screw hole as shown in Figure 3-18.



(a)

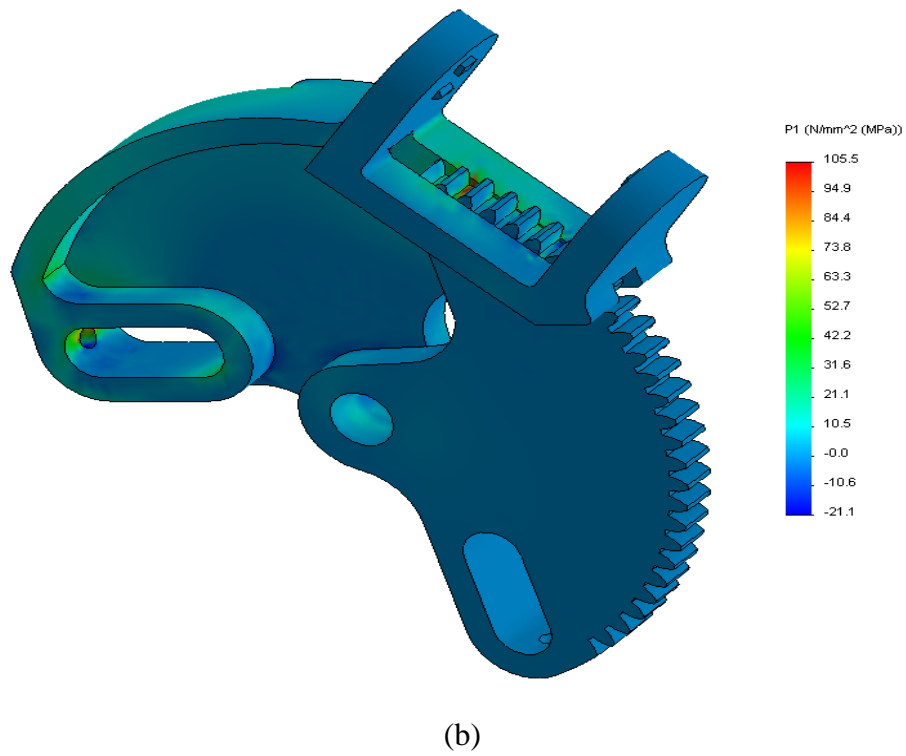


**Figure 3-17.** Finite element analysis stress distribution results for Model II for position 1 gear teeth fixed at (15 - 30°).

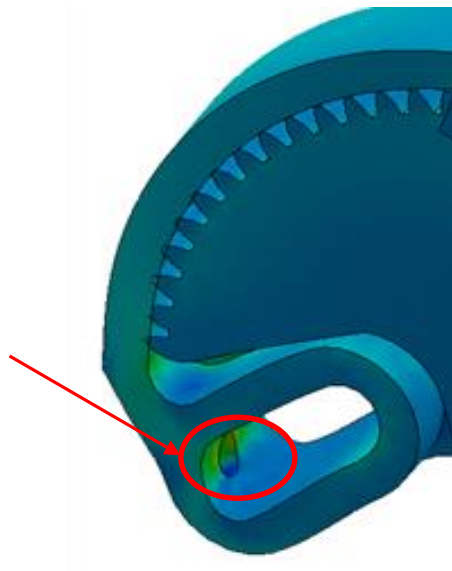


**Figure 3-18.** Maximum principal stress distribution around the left distraction screw hole.

### 3.3 Scanning electron microscopy

Scanning electron microscopy (SEM) can be very useful for many different types of material and project. It has the advantages of being able to examine fairly large samples (up to around 25 mm diameter) and has a large depth of focus (Engel *et al.*, 1981; John, 1992). SEM examination has been well documented in the use of polymers, for both characterisation and examination of damage or faults (Campbell and White, 1989). A Compass hinge that had fractured through the distal arcuate hinge member was provided by the surgeon Mr. Garth Titley and three fracture surfaces (Figure 3-19) were analysed:

- fracture surface (1) at the distraction threaded hole in the right side of the distal arcuate hinge member;
- fracture surface (2) at the detached part from the distal arcuate part;
- fracture surface (3) at the angles side in the distal arcuate hinge part.

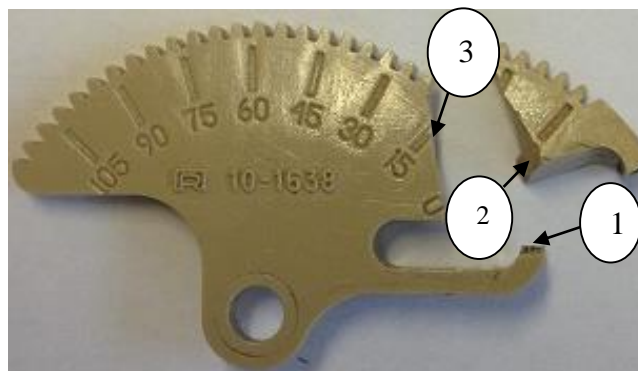


**Figure 3-19.** Fracture surfaces examined using scanning electron microscopy.

Prior to examination, the samples were cut from the fractured surfaces to size using a scalpel blade and mounted onto SEM stubs (AGAR Scientific, Standard, UK). These are metal discs measuring approximately 30 mm in diameter and 10 mm in height. The sample length and width cannot be larger than the disc and the height of the sample must be as small as possible to ensure it does not make contact with the camera in the microscope chamber. The samples were sputter coated with a thin layer of gold using a gold sputter coater (Emscope SC500; Emitech Ltd., Ashford, Kent, Great Britain) (Figure 3-20). Parts before and after coating are shown in Figure 3-21.

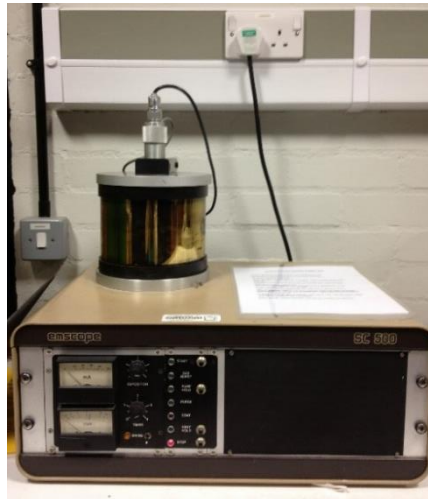
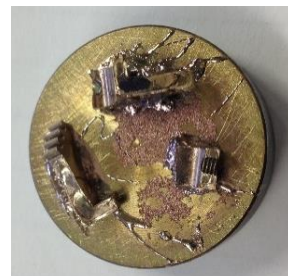


**Figure 3-20.** Emscope SC500 sputter coater.



(a)



(b)

**Figure 3-21.** Fracture surface samples (a) before (b) after gold spray coating.

SEM was performed in the School of Metallurgy and Materials (University of Birmingham) on a Joel JSM-6060 scanning electron microscope (JEOL Ltd, Tokyo, Japan), which is shown in Figure 3-22. The accelerating voltage was 10 kV and the working distance (WD) was 11 mm. The working distance is the distance between the objective lens and the specimen. A short WD results in a higher resolution and decreased depth of field, whereas a longer WD results in less resolution, but an increased depth of field. The optimum WD is 11 mm for the energy dispersive x-ray spectrometry analysis on the 6060 microscope as recommended by the University of Birmingham SEM technician.

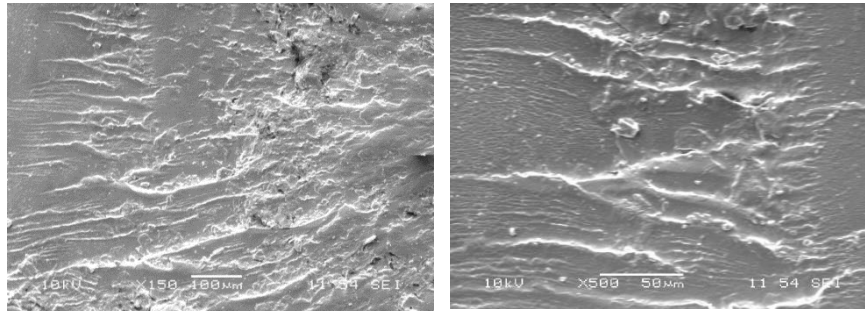


**Figure 3-22.** Joel JSM-6060 LV microscope with computer.

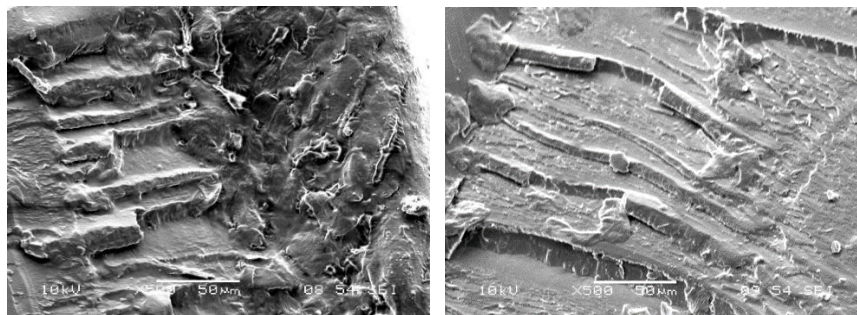
### 3.3.1 Results

The SEM images were reviewed and compared with known types of failure published in the literature. The most useful piece of literature was a journal paper entitled “SEM Analysis of Polymeric Mechanical Failures in Polyetherimide” (Zimmerman and Jones, 1994).

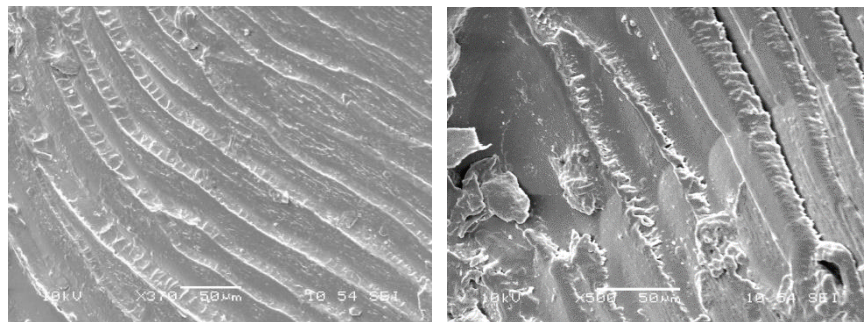
The scanning electron microscopy fractographs from the three fracture surfaces investigated from a failed Compass hinge are presented in Figure 3-23. Fracture surface 1 (Figure 3-23a) showed mirror, mist and rough regions, with brittle failure bands. This is consistent with a fracture caused by bending. Fracture surface 2 (Figure 3-23b) and fracture surface 3 (Figure 3-23c) were similar with crazes, shears bands and small indentations or voids. This failure is consistent with a brittle fracture caused by fatigue.



(a)



(b)



(c)

**Figure 3-23.** SEM fractography images of the distal block fracture surfaces (a) fracture surface 1 (b) fracture surface 2 (c) fracture surface 3.

### 3.4 Discussion

An engineering analysis of a failed Compass hinge device using FEA and SEM was undertaken to investigate the potential failure modes. The FEA for Model I which consisted of the distal arcuate hinge member shows that the highest stresses were located on the right side of the distal arcuate hinge member, usually between the gear teeth. The maximum principal stress was found to be 285.3 MPa. Model II which consisted of the assembly of the proximal arcuate hinge member and the distal arcuate hinge member showed that the highest stresses were located on the left side of the proximal arcuate hinge member, usually between the gear teeth. The maximum principal stress was found to be 122.3 MPa. These values of stress are well in excess of the fatigue strength of the polyetherimide that the parts are manufactured from which has a value of 24 MPa at 5 Hz, 20°C and  $>10^7$  cycles (Trotignon *et al.*, 1993).

Even if low forces are applied to the Compass hinge as a result of daily patient finger activities, the stresses are still likely to exceed the fatigue strength of the material. It is assumed that around 1 million finger motions per year occur (Joyce and Unsworth, 2000), so that would be an average of around 2,700 motions per day. The results also show high stress around the screw hole, which is the distal arcuate member for Model I and in the proximal arcuate member for Model II.

The SEM results were compared with published work (Zimmerman and Jones, 1994) and show that fracture surfaces 1, 2 and 3 (Figure 3-19) were caused by cyclic bending stresses. This information, together with the results of the finite element analysis for Model I confirms that the likely sequence of events for failure is as follows:

- Firstly, with the worm gear locked in position, the patient may try and move their PIP joint, thus causing high stresses between the gear teeth when in position (1) with the gear teeth between 15 and 30°;
- Then, if the loads are high enough, the stress between the gear teeth will exceed the fatigue strength of the polyetherimide material and a crack will be initiated;
- As the patient carries on loading the device the crack will propagate through the device into the slot;
- Finally, the fragment of polyetherimide will bend, fracture and detach from the device.

A number of studies have detailed failure of the polyetherimide distal arcuate hinge member (refer to section 3.2.3 in this chapter) so it does seem to be a reasonably common failure mode. On the other hand, no study has recorded any failure case at the proximal arcuate hinge member.

The difference between the failures in the two positions (A and B) (Figure 3-3) is likely due to where the stresses are distributed. In Model I the fatigue cyclic stresses were located and distributed in the same part which is the distal arcuate member; this means that cracks are likely to propagate rapidly. However, in Model II the stresses are distributed in two different areas; the distal arcuate member and in the proximal arcuate hinge member.

The results from the two models also showed that whatever the position of fixation, the high values of stresses usually appeared when the worm gear was engaged at position (1) with the teeth between 15 and 30° which means that the finger is in the fully extended position. The Compass hinge is a reliable and safe system for patients affected by Dupuytren's disease with flexion deformity. It has clinical advantages that are not available in other external distraction fixators which makes it easy to apply (Bonaspetti *et al.*, 1999), namely the ability to disengage the device to allow active flexion from an extended position. The development plan towards implementing a new design device will firstly, give consideration to other polymers that have a higher fatigue strength than polyetherimide. PEEK (Poly-ether-ether-ketone) is a potential candidate material as it is a polymer that is used increasingly in medical devices (Xin *et al.*, 2013) and it has fatigue strength at  $>10^7$  cycles and 5 Hz of around 65 MPa (Trotignon *et al.*, 1993) and a range from 99.4 to 107.4 MPa for heat treated PEEK (Xin *et al.*, 2013). Secondly, work on evolving new design features to overcome the complications in other devices will be undertaken. Finally, an evaluation of the proposed design will be undertaken using FEA and then mechanical testing to validate the design.

### 3.5 Summary

A failed Compass hinge external fixator for fingers has been analysed. The polymer parts were manufactured from a polyetherimide (PEI) and the metal parts from an aluminum alloy. The Compass hinge differs from other devices in that it can maintain an active and a passive range of movement. Pin-track infections and mechanical failures are the most common problems associated with the use of this device. Finite element analysis (FEA) was used to

investigate the principal stresses in the device under different loading conditions. Scanning electron microscopy (SEM) was used to investigate the fracture surfaces. The FEA showed that the maximum principal stress was greater than the fatigue strength of polyetherimide. The SEM fractographs confirm that failure by cyclic bending stress was the main cause of the device distal arcuate hinge member part fracture. A modified design and the use of a polymer with greater fatigue strength are considered as potential solutions to overcome this problem. The next chapter will present the design and development of a new device.

# CHAPTER 4

## NEW DEVICE DESIGN

## 4 NEW DEVICE DESIGN

### 4.1 Chapter overview

This chapter describes the design and development of a new finger fixator for treatment of PIP joint contracture. Section 4.2 presents the introduction to the design of medical devices. The new device design requirements are described in §4.3 and the different concept designs in §4.4. The detailed design and the device engineering drawings are presented in §4.5, followed by the discussion in §4.6. Section 4.7 presents a brief summary of the chapter.

### 4.2 Introduction

Dynamic external finger fixators are designed to correct and prevent finger joint contractures, improve the flexion appearance of the injured finger, restore the functional range of motion, provide stability of the joint and adequate strength to carry out daily activities (Houshian and Schrøder, 2004; Houshian *et al.*, 2007; Ng and Oliver, 2009). Ideas to improve the Compass hinge device (chapter 3 section 3.2.1) came from working on the reported complications in the previous clinical studies of the Compass hinge device (chapter 3 section 3.2.3) and other finger fixators (chapter 2 section 2.6). Towards presenting a new designed device, the detailed structure of the medical device design process which was

presented by Aitchison *et al.* (2009) was followed and each aspect of this design process (chapter 2 section 2.7) will be applied in this chapter.

### 4.3 Design requirements

For a successful design of a fixator to be used on the PIP joint it has been suggested that it should be small enough to be of use on central fingers (Hodgkinson, 1994). More considerations were adapted from the conclusions of the previous clinical studies advantages of implementing different external fixators to patients (see chapter 2 section 2.6). These considerations included easy to apply, low profile, easy to use, reliable and allows for active and passive mobility (Krakauer and Stern, 1996; Salafia and Chauhan, 1997; Bain *et al.*, 1998; Bonaspetti *et al.*, 1999; Houshian *et al.*, 2002; Feldscher and Blank, 2002; Houshian and Schrøder, 2004; Lahiri *et al.*, 2007; Houshian *et al.*, 2007; Asche *et al.*, 2009).

The standard BS EN ISO 14630 (2005) and the element of the product design specification (PDS) design core diagram presented by Pugh (1991) have been used to list the requirements of the new device. The PDS is a document that contains all the criteria relating to the product outcome. It defines the elements, factors and boundaries of the object to be designed. The PDS thus acts as the control for the total design activity (Pugh, 1991). The PDS has been formulated based on the literature review (given in chapter 2), surgeon feedback throughout the design process (Mr. Titley) and the analysis of the existing device (given in chapter 3).

The new device should have the following design requirements:

- a) Be able to withstand a dynamically applied axial force of up to 13 N (Walker and Erkman, 1975) and a quasi-static force of up to 210 N (Lee and Rim, 1990);
- b) Have a range of motion from 0° extension to 100° flexion (Reese and Bandy, 2013);
- c) Be manufactured from biocompatible materials, including a radiolucent polymer to enable the wires to be visible on radiographs;
- d) Have good fatigue resistance and be able to withstand 170,000 cycles at 2 Hz (this is based on the assumption that 1 million finger motions per year occur (Joyce and Unsworth, 2000) and the device would be attached to a patient for a maximum of 64 days (Bain *et al.*, 1998);
- e) Have a mass of less than 15 g to be comparable with the Compass hinge device;
- f) Have smaller dimensions than the Compass hinge device (the dimensions of the parts of a Compass hinge were found to be 49.5 to 58.5 mm for the width, 35 mm for the height and 11.5 mm for the thickness;
- g) Have a mechanism to allow active and passive movements;
- h) Provide a continuous movement working mechanism;
- i) Be able to fit a range of human hands based on anthropometric data (Peebles and Norris, 1998; Alexander and Viktor, 2010);
- j) Natural in color (close to skin color) to motivate patients to use it;
- k) Be simple to assemble;
- l) Manufacturing processes should be considered to do not affect the quality of the device (functionality and surface finish);
- m) Cost of the device should not exceed other market available fixators where their cost ranged from 400 to 600 British Pound Sterling.

## 4.4 Concept designs

### 4.4.1 Design strategy

The concept design stage involved generating all the possible designs that meet the product design specification. The initial drawings and a brief description of the various concept designs are presented. The process of selecting one of the concepts to develop and to be the final design will be described. The SolidWorks Computer Aided Design software 2011® premium 2011x 64 Edition © 1995-2010 (Dassault Systèmes SolidWorks Corporation, Waltham, USA) was used for the design of the new PIP joint dynamic external fixator.

In order to generate concept designs for the new device the anatomical description of the PIP joint was studied to consider the nature motion of this joint. The different available patents of the joint fixators also were studied to understand the ideas of the working mechanisms. The Compass hinge geometry, advantages and complications were considered a key points in generating the new concept designs. The steps toward generating ideas to present a new device were as follows:

- Firstly, patents of external joint fixators were studied aiming to generate ideas of working mechanical mechanisms to give the required dynamic movements (US Patent 5376091, US Patent 5100403, US Patent 0097944 A1 and US Patent 4604997). The fixation device in US Patent 0097944 A1 helped in the development of the feature of the clamping blocks which are used to support the inserted K-wires (see section 4.4.3 concept design 2). The dynamic finger support in US Patent 5376091 provided a detailed description of each device component, helping to

understand the working idea of that fixator and specifically the worm and worm wheel mechanism in it, which assisted to develop the working mechanism of the new design (see section 4.4.3 concept design 2).

- Secondly, according to the anatomical description of the PIP joint, which acts as a pure hinge in the finger (Ng and Oliver, 2009) the development process of the new device should also have this concept. The device will act as a hinge and the center of the PIP finger joint will be the pivoting point of the device.
- Finally, the device should be symmetrical so that it can be applied to any digit on the left or right hand.

The development plan was divided into three stages:

- working on the design of the proximal hinge member;
- working on the design of the distal hinge member;
- development of the clamping block parts.

There are 2 main concept designs for the device assembly which will be described in detail later, with concept design 1 being based on the screw drive working mechanism. The second concept design was based on the worm and worm wheel as the working mechanism for the device. For each concept design of the two assemblies there are a series of concept designs for the distal and proximal parts.

#### 4.4.2 Concept Design 1 – (Screw drive hinge movement)

According to the PIP joint working mechanism, a rotation movement is required in designing the new device by the surgeon. The main two parts, the proximal and the distal parts were developed to be as a protractor. Figure 4-1 is a 3D assembly of concept design 1.

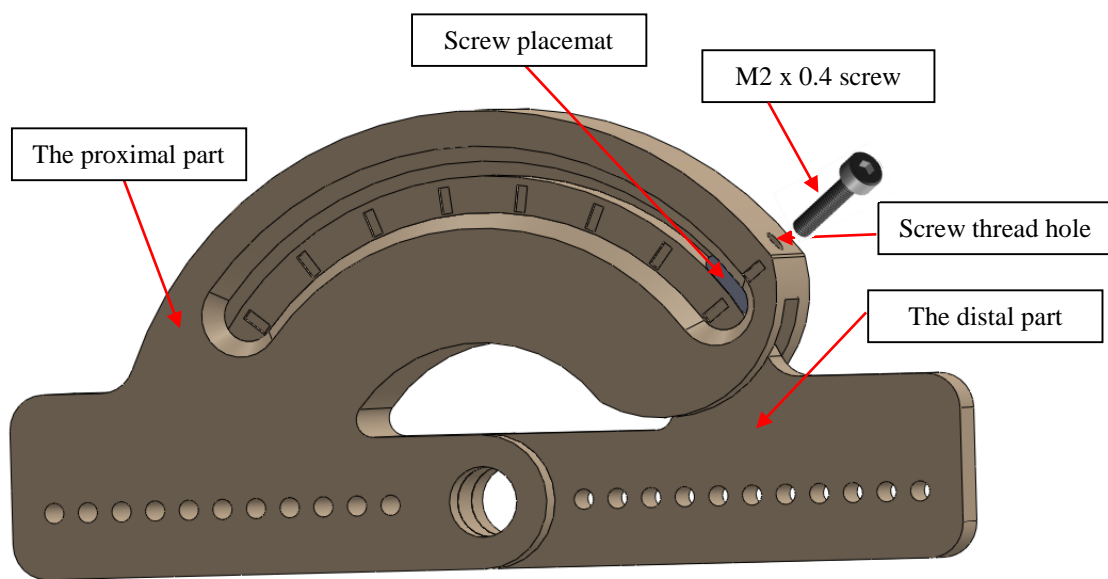


**Figure 4-1.** 3D assembly design of the screw drive hinge movement concept design 1

The proximal part (Figure 4-2) is considered the main frame of the device which has a circular middle body cavity to allow fitting of the distal part. This idea depends on the movement mechanism of the screw where a 2 mm diameter threaded hole (in the top right side of the proximal part) tapped with 1.6 mm twist drill was designed to fit with a metric standard M2 x 0.4 screw thread (Oberg, 2012). Mechanically when the screw thread was

untightened the active motions for the distal part (Figure 4-1) can occur. For keeping the distal part in a selected position the screw would be tightened.

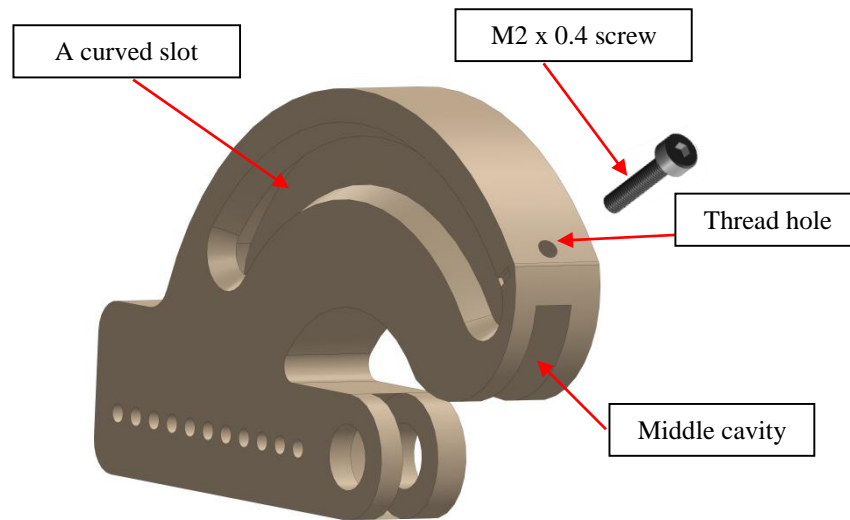


**Figure 4-2.** 3D design of the proximal protractor part design -1.

The Compass hinge proximal side clamping blocks, which clamp to the K-wires were replaced here by many small holes in the frame of the proximal part. The position of these holes is designed to be located at the same level as the lateral line of the PIP joint to work as a guide for surgeons to insert the K-wires during surgery to attach the device to the patient's fingers. These holes have a diameter of 1.4 mm and were designed to fit with the skeletal inserted K-wires diameter (1.15 mm) and the 0.25 mm difference between the diameter of the hole and the K-wire diameter, was a tolerance for each hole to allow for the drilling insertion technique of the K-wire to be used by the surgeon without damaging the device. More than 10 holes were designed along the proximal part to cover a large range of the

human digits proximal phalanges sizes (Alexander and Viktor, 2010) and for individual patient the surgeon would need to select the two most suitable holes to insert the K-wires in them. The range of movement of the PIP joint will be controlled by the angle guide on the distal part and that can be monitored during the curvature slot in the front view of the proximal part.

#### 4.4.2.1 Concept distal part idea 1

A protractor feature new distal part (Figure 4-3) was designed to insert in the middle cavity of the proximal part. The guide to the angle of the device was designed as engraved marks on the distal part at both the front and the rear. This angle guide is to help the device users attain the required PIP joint position movements which started from  $0^{\circ}$  (the PIP joint at fully extension position) to  $105^{\circ}$  (the PIP joint at the maximum flexion position).

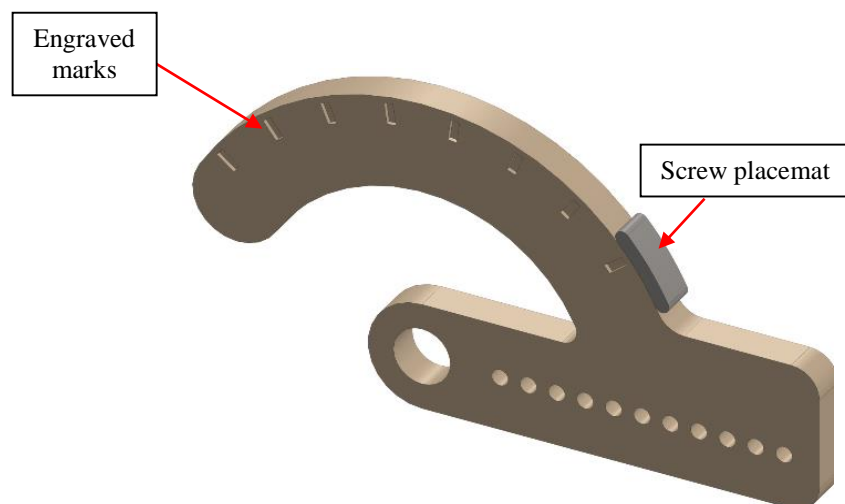


**Figure 4-3.** 3D design of the proximal protractor part design -1, idea1.

The Compass hinge distal side clamping blocks were replaced here by a series of small holes in the frame of the distal part. These 1.4 mm diameter holes were designed to fit with the skeletal inserted K-wire diameter. The numbers of holes were designed to cover a large range (from 18 mm to 26 mm) of finger middle phalanges sizes (Alexander and Viktor, 2010). For individual patients the surgeon would need to select the two most suitable holes to insert the K-wires in them according to the length of their middle phalanges which can be measured using x-ray. Wear may be a problem on the distal part during screw movement and for that reason a small metal part was added between the distal part and the screw to act as a placemat to avoid that action.

The advantages of the distal part, concept idea 1 were:

- The device consists only of 4 main assembled parts: proximal part, distal part, screw and placemat;
- A simple screw thread working mechanism was used in this design idea;
- No surgical assistant would be required for surgeons during the device attachment process where the holes will work as a guide for the K-wires.

The disadvantages were:

- The surgeon should select the most suitable holes for each patient's finger phalanx so that more time may be required during the attachment process;
- During the screw loosening action, the placemat part may be de-attached from the device;
- K-wire loosening may occur where the mechanism to clamp the wires is not sufficient to secure the wires.

#### 4.4.2.2 Concept distal part idea 2

The series of holes suggested in concept distal idea 1 (section 4.4.2.1) were merged into one slot to provide a wide range of options for the insertion of the K-wires into the finger. This idea will let the device fit with a large number of different finger middle phalange sizes (from 18 mm to 26 mm) (Alexander and Viktor, 2010) (Figure 4-4).

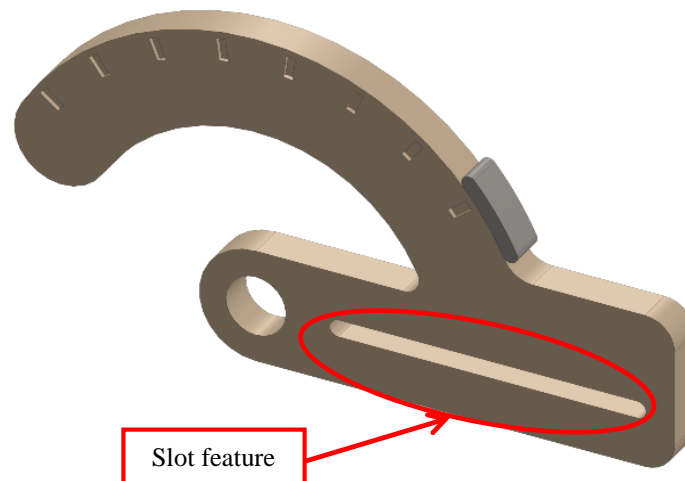


**Figure 4-4.** 3D design of the distal protractor part design -1, idea2.

From an engineering point of view because there is a long length of the slot through the distal part (Figure 4-4), a large deflection may occur under the slot during loading which makes this idea not desirable. A finite element analysis result for this idea is shown in Figure 4-5 and the maximum stress was 330.9 MPa, overall the evaluation of the design was that it was weak to resist stresses. A surgeon feedback towards this idea was negative, he not recommended slot feature idea he preferred the holes.

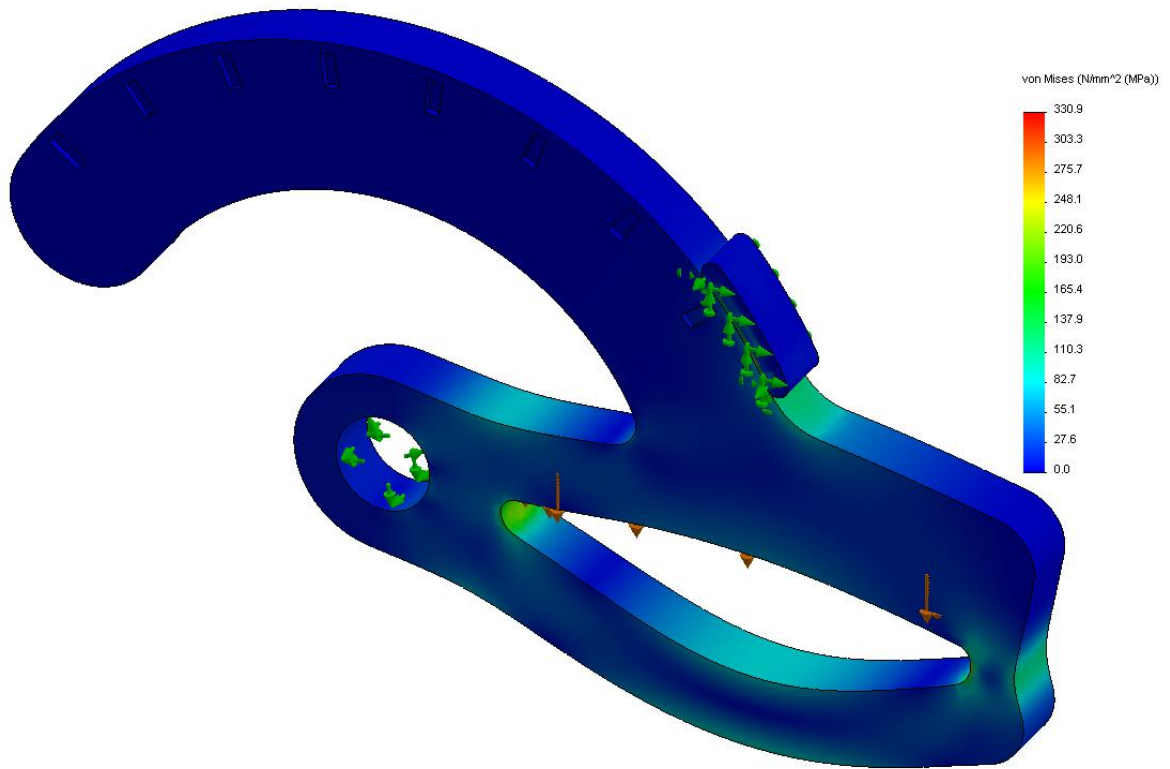


**Figure 4-5.** Distribution of stresses for the distal protractor part design -1, idea2.

#### 4.4.2.3 Concept distal part idea 3

To overcome the disadvantage of idea 2, the small holes design (concept distal idea 1, section 4.4.2.1) is a more acceptable idea than the slot design (concept distal idea 2, section 4.4.2.2) to avoid any deflection in the area underneath the slot. To make sure the distal part withstands the applied loads a slight change in dimensions from idea 1 (section 4.4.2.1) was made by increasing the length of the distal part under the holes by 2 mm (Figure 4-6).

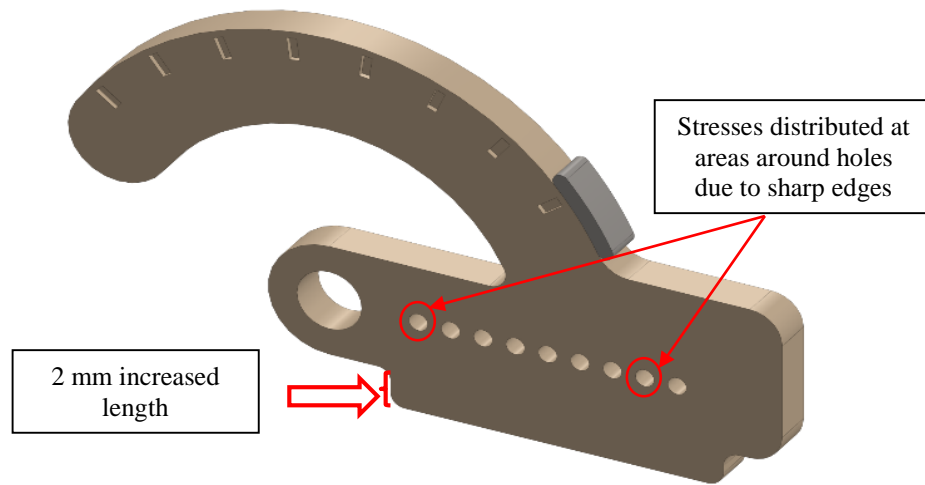


**Figure 4-6.** 3D design of the distal protractor part design -1, idea3.

The sharp end edges ( $90^\circ$ ) of the holes (zero fillets) in both sides (front and rear views) could potentially be a cause of localized stresses around the holes, which surgeons select to insert the K-wires through. A finite element analysis result for this idea is shown in Figure 4-7 and the maximum stress was 516.6 MPa. The maximum stresses were located around the holes, which the K-wires were inserted in them.

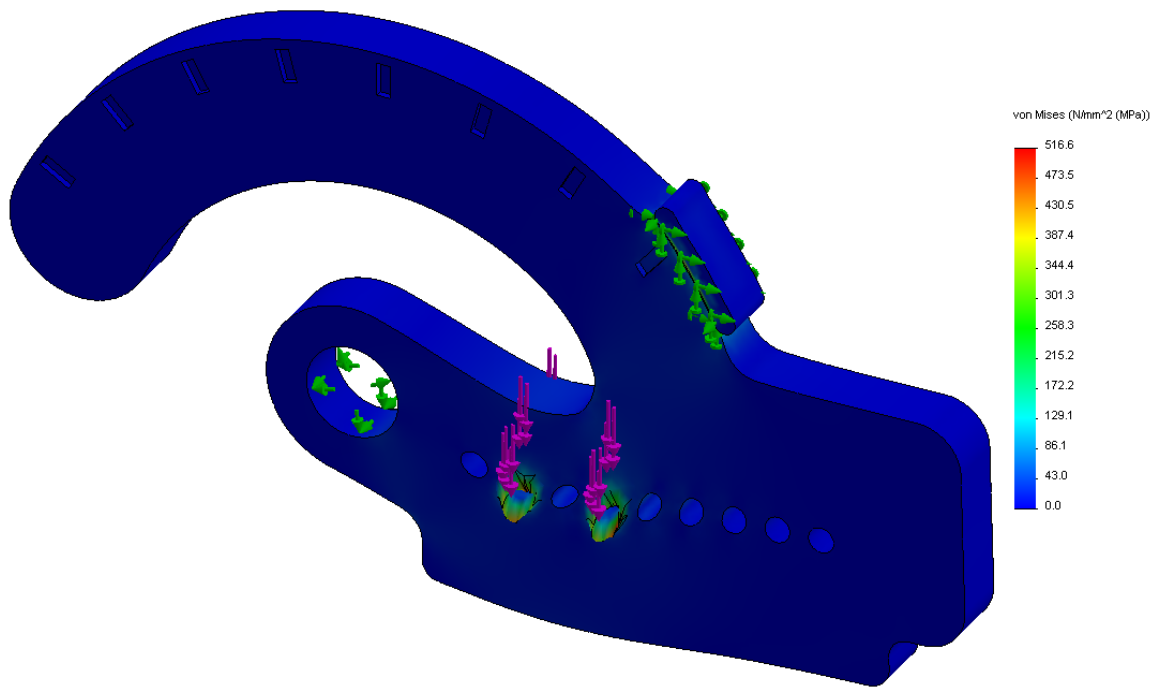


**Figure 4-7.** Distribution of stresses for the distal protractor part design -1, idea3.

#### 4.4.2.4 Concept distal part idea 4

The holes (concept distal idea 3, section 4.4.2.3) were developed to have a filleted feature so that it will help to reduce stresses around the edges of the holes due to loading through these holes (Figure 4-8). A finite element analysis result for this idea is shown in Figure 4-9 and the maximum stress was 292.9 MPa. The maximum stresses were located around the holes, which the K-wires were inserted in them.

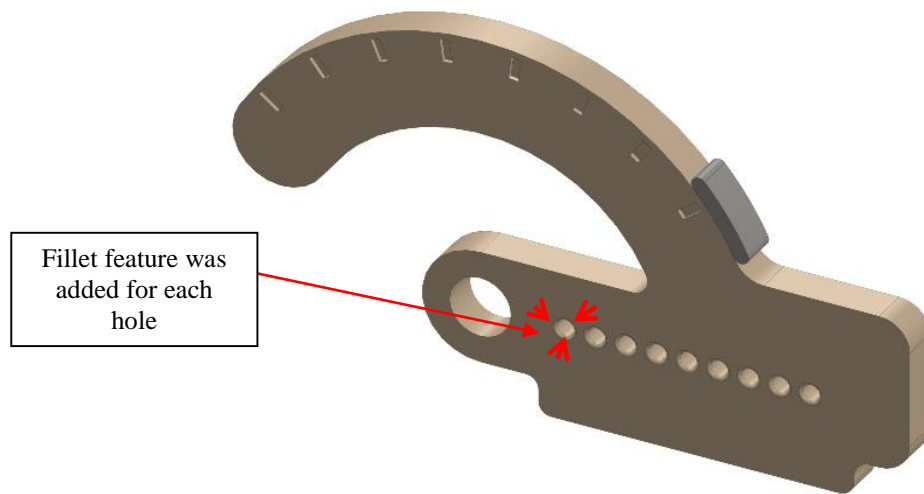


**Figure 4-8.** 3D design of the distal protractor part design -1, idea4.

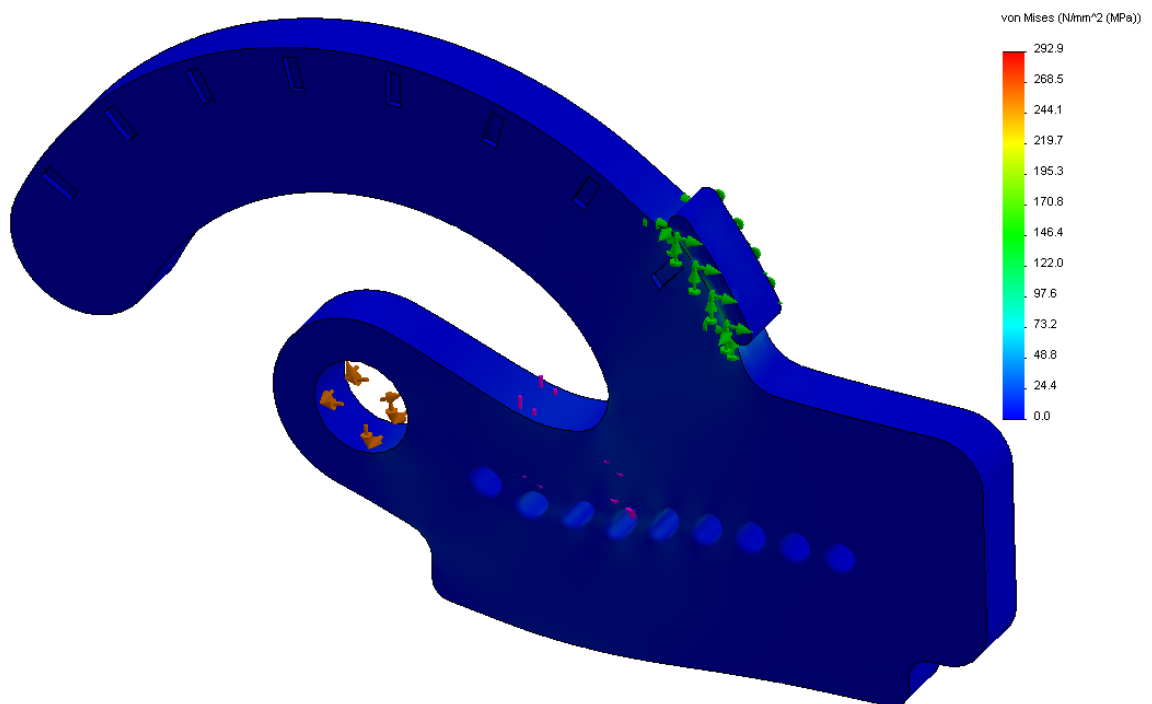


**Figure 4-9.** Distribution of stresses for the distal protractor part design -1, idea4.

#### 4.4.2.5 Concept distal part idea 5

The idea 5 mainly works on the development of the screw placemat part feature (concept distal idea 1 section 4.4.2.1). To avoid the placemat part de-attachment from the device during the device movement, a guide and guide way concept mechanism was applied to this concept idea. The curvature feature of the distal part works as a guide way to the guide placemat which was developed to be “U” shaped, moving along the distal part curve (Figure 4-10). A finite element analysis result for this idea is shown in Figure 4-11 and the maximum stress was 78.4 MPa. The maximum stresses were located around the holes, which the K-wires were inserted in them and around the both sides of the guide placemat.

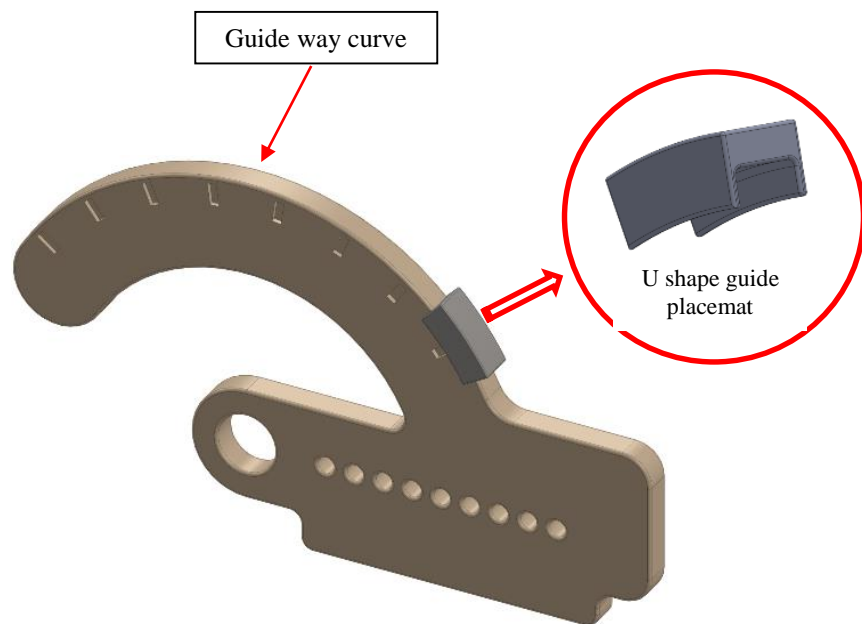


**Figure 4-10.** 3D design of the distal protractor part design -1, idea5.

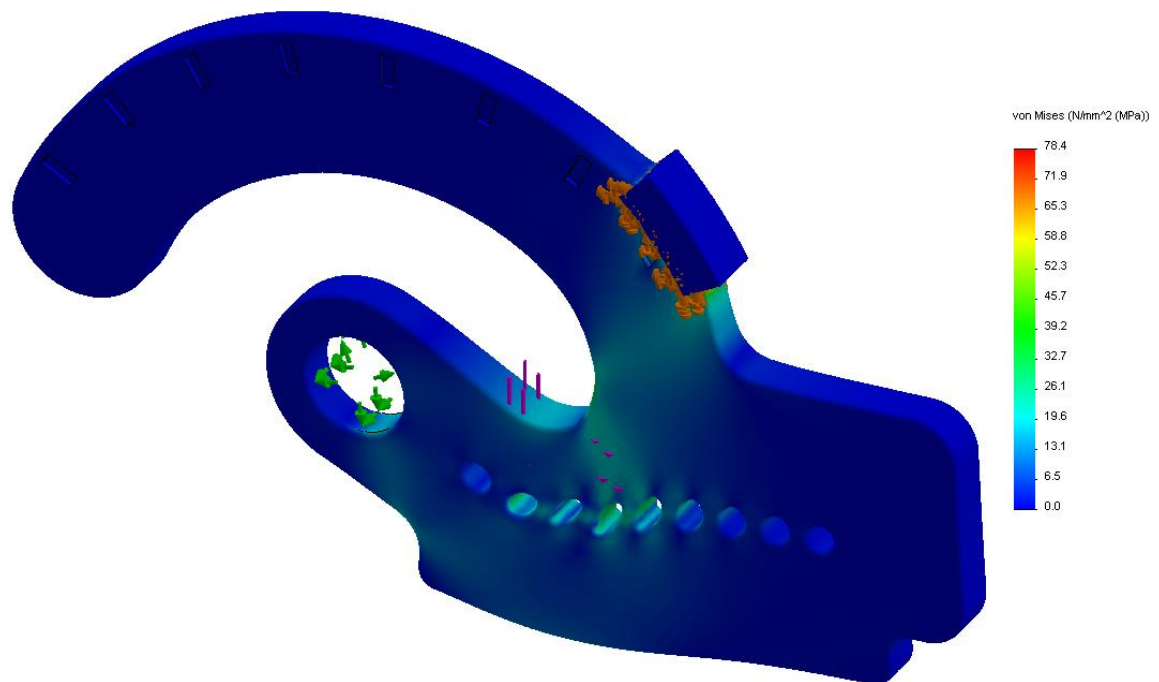


**Figure 4-11.** Distribution of stresses for the distal protractor part design -1, idea5.

The design ideas were reviewed with Mr. Garth Titley (Consultant Plastics and Burns Surgeon at the Queen Elizabeth Hospital, Birmingham) where the meetings with him provided feedback about the concept designs from a surgical point of view. Although the outside feature of the idea 5 design was acceptable to him he was concerned that there was a lack of continuous movement of the patient's PIP joint which the treatment procedure requires.

### 4.4.3 Concept Design 2 – (Worm and worm wheel hinge movement)

To provide the proposed design with a continuous movement mechanism, gears are one of the mechanisms considered to be able to do that. A worm and worm wheel for driving the distal part to the proximal part was considered as a suitable idea (Figure 4-12).

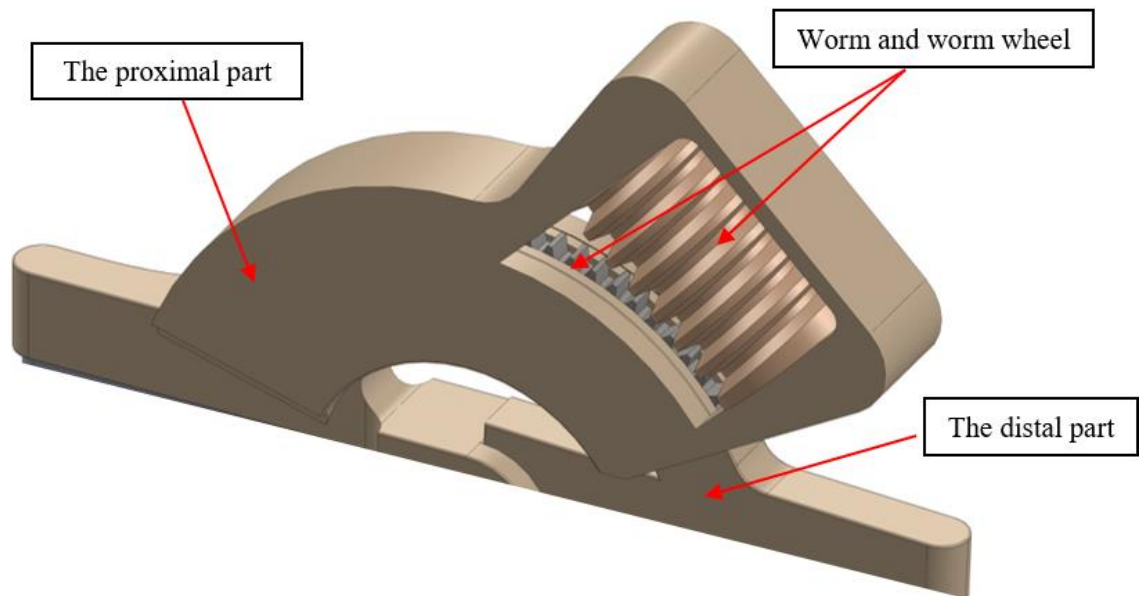


**Figure 4-12.** 3D assembly design of the worm and worm wheel hinge movement concept design 2

#### 4.4.3.1 Concept clamping block idea 1

The design works on the development of dimensions and features of the Compass hinge device worm and worm wheel parts. The aim was to reduce the stress distribution along the worm wheel part which was the main cause of failure in the Compass hinge (see chapter 3

section 3.3 and section 3.4). It was, therefore, proposed that the worm and worm wheel should be manufactured from a metal as opposed to a polymer, as with the Compass hinge. Posterior and interior Compass hinge blocks (see chapter 3 section 3.2.1) were developed to be 6 assembled blocks (four metals and two polymers) where 3 of them (2 metal and 1 polymer) were for the proximal side and others for the distal side. For each side the blocks were connected together by 2 screws (Figure 4-13).

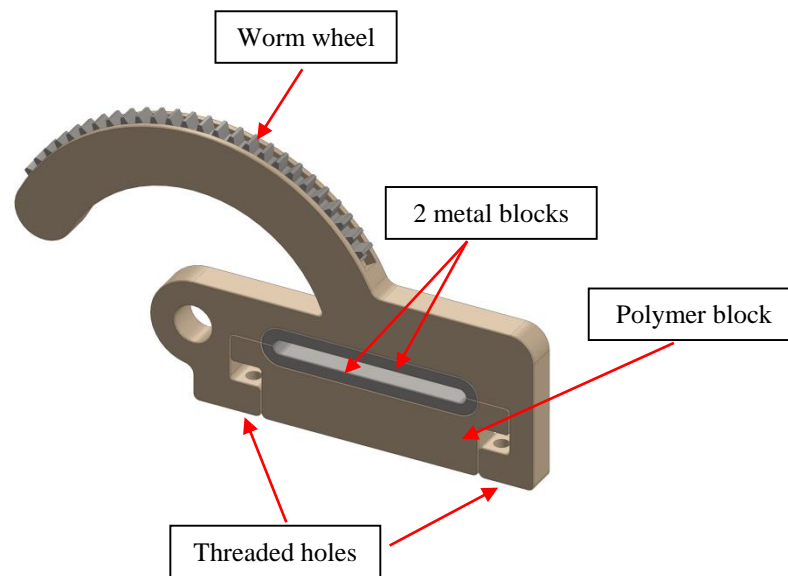


**Figure 4-13.** 3D design of the distal protractor part design -2, ideal.

The four metal blocks were responsible for clamping the inserted K-wires and they were chosen to be metal to resist stresses which will be generated in this area during exerting loads. One metal block was designed to assemble with the distal part, one with the proximal part, one with the polymer block on the distal side and the last one with another polymer block on the proximal side. A polymer was selected for the two polymer blocks for two

reasons; firstly, these blocks did not directly affect and were not close to the exerting load area, so high mechanical property materials were not required to manufacture them. Secondly, to keep the mass of the device low.

The difficulty to apply this concept design idea appeared after the assembly process was completed when allowing the distal part to rotate around the proximal part (from full extension position to any flexion angle). It was found that the distal part could not move as there was no space for this movement and the interference action would happen between the proximal and distal parts (Figure 4-14).

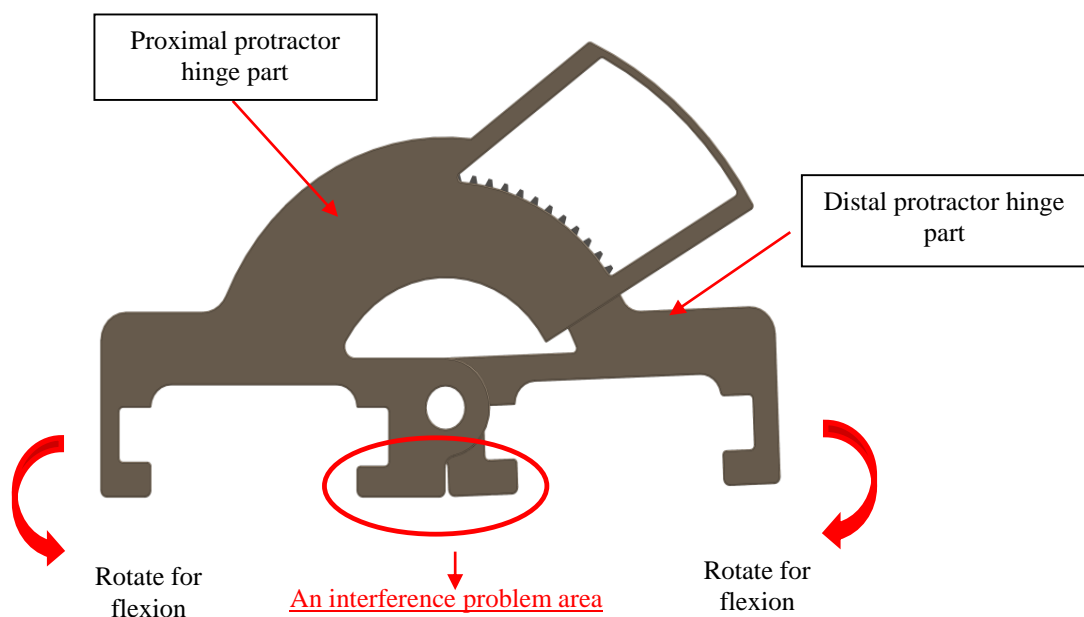


**Figure 4-14.** 3D assembly design of the proximal and distal protractor parts design -2, ideal.

#### 4.4.3.2 Concept clamping block idea 2

Four metal solid clamping blocks were designed where 2 of them were on the proximal side and the others on the distal side (Figure 4-15). These blocks will act as jaws to keep the inserted K-wires in position. A metal was selected to resist the stresses generated during active movement of the device by the patient. The four solid blocks will be inserted into the 4 fitted slots, where there is one slot in the body of the proximal protractor hinge part, one slot in the body of the distal protractor hinge part and two in the slotted polymer clamping blocks.

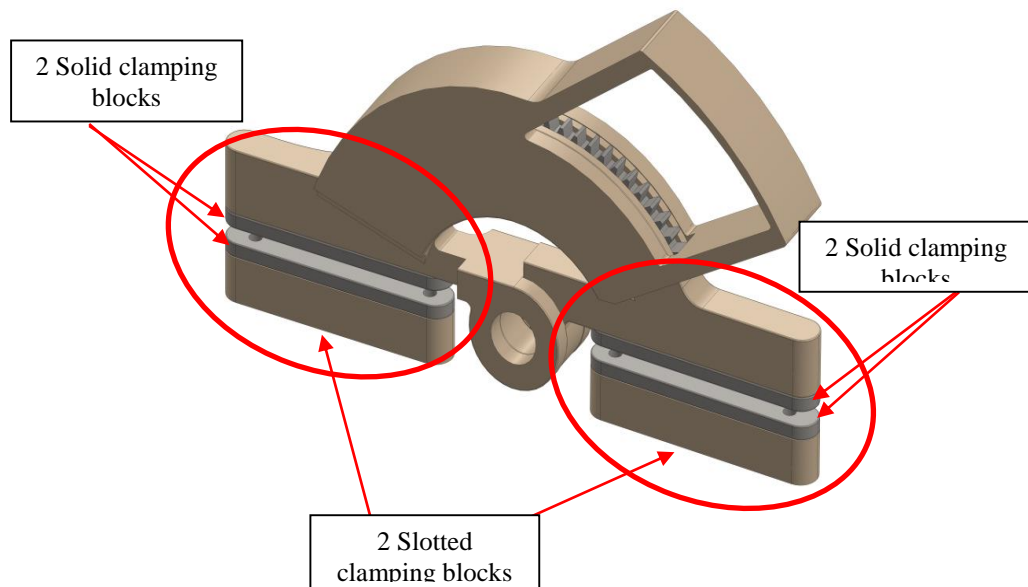


**Figure 4-15.** 3D assembly design of the proximal and distal protractor parts design -2, idea2.

Towards selecting the most describable concept design, a positive/negative score system by the Pugh matrix (Table 4-1) was used to select the concept design which will be worked on as a detailed design.

**Table 4-1.** Pugh matrix to concept design selection.

Concept design 1 – (Screw drive)								Concept design 2 – (Worm and worm wheel)	
	Baseline	Proximal part	Distal part					Clamping blocks	
			Idea 1	Idea 2	Idea 3	Idea 4	Idea 5	Idea 1	Idea 2
Easy to assemble	0	-	-	-	-	-	-	-	0
Easy to apply	0	0	0	+	0	0	0	0	+
Easy to use	0	-	-	-	-	-	-	+	+
Safe design		-	-	0	-	+	+	0	+

<b>Symmetrical features</b>	0	+	+	+	+	+	+	+	+
<b>Profile</b>	0	+	+	+	+	+	+	0	+
<b>Weight</b>	0	+	+	+	+	+	+	-	+
<b>Flexible to develop</b>	0	-	-	-	-	-	-	-	+
<b>Surgeon feedback</b>	0	-	-	-	-	-	-	-	+
<b>Reliable</b>	0	-	-	-	-	-	-	+	+
<b>Net score</b>		-3	-3	-3	-1	-3	-1	-1	+9
<b>Rank</b>		3	3	3	2	3	2	2	1
<b>Continue?</b>		No	No	No	No	No	No	No	<b>Yes</b>

## 4.5 Detailed design

During the concept design selection, concept design 2, idea 2 was chosen to be developed, as shown in Figure 4-16. This design was selected after a design review meeting with Mr. Garth Titley (Consultant Plastics and Burns Surgeon at the Queen Elizabeth Hospital, Birmingham), who provided feedback. From the surgical point of view, the device looked small in size compared to other devices, the symmetrical design enabled it to be applied to any digits on both hands and the most important advantage is that it allows both active and passive continuous motion. From an engineering point of view, the device parts which were predicted to have high stresses, referring to the previous study of the Compass hinge device (see chapter 3 section 3.3) were now designed from a metal. A metal was chosen for the areas around the applied load and the area where the working mechanism was locked (worm and worm wheel teeth were meshed together). For the other device parts, they were designed to be manufactured from a radiolucent polymer. This would enable the device to be low in mass, seen under x-ray and its working mechanism achieved the required motion without any interference between the device parts.

Concept 2, idea 2 will be worked up to a final design. Each part will be designed to optimize the size and materials, then the final geometry and materials for the whole design will be presented. The final design presented here can be used on any PIP joint on any digit.

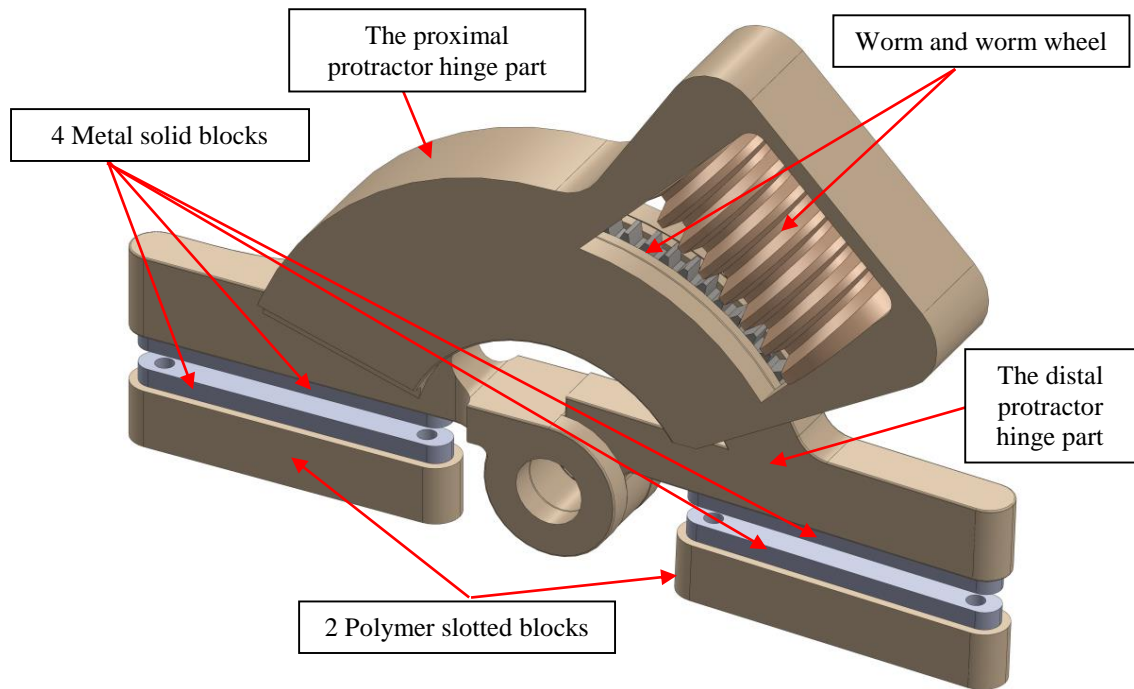


**Figure 4-16.** 3D design of concept selection 2, idea2.

### 4.5.1 Materials

The materials for the parts of the new device should provide high mechanical strength. Poly-ether-ether-ketone (PEEK) and Polyetherimide (PEI) were suggested to manufacture the new designed polymer parts where these two advanced polymers are biocompatible with high mechanical properties: PEI has a yield strength of 105 MPa and PEEK has a yield strength of 110 MPa (GE Plastics; VICTREX®). The finite element analysis results for the failed Compass hinge (see chapter 3 section 3.3) concluded that the Compass hinge fixator was affected by the cyclic bending stress due to the natural motion of the PIP joint which acts as hinge (Ng and Oliver, 2009). For that reason, PEEK was chosen for the new designed parts where its fatigue strength endurance limit (65 MPa at 5 Hz,  $>10^7$  cycles) is significantly

higher than the fatigue strength endurance limit of PEI (24 MPa at 5Hz,  $>10^7$  cycles) (Trotignon *et al.*, 1993).

PEEK was selected as the main polymer part material for the new device for its mechanical, chemical and thermal properties which helped to develop the Compass hinge device. PEEK is a highly biocompatible, non-toxic, non resorbable polymer (Cho *et al.*, 2002; Abu Bakar *et al.*, 2003). PEEK has a Young's modulus of 3.6 GPa (Chou *et al.*, 2008; Hee and Kundnani, 2010) and has good sterilization resistance (using steam, gamma irradiation and ethylene oxide processes) and can be fabricated using extrusion, injection molding, machining and 3D printing (Ferguson *et al.*, 2006; Toth *et al.*, 2006; Sagomonyants *et al.*, 2008). It is also radiolucent where this material can see under X-ray (Cho *et al.*, 2002; Ferguson *et al.*, 2006; Hee and Kundnani, 2010; Kurtz *et al.*, 2007). Recently, PEEK is the most common and favoured material for orthopedic medical devices (Kurtz, 2011). Two different grades of PEEK were considered: PEEK 90G and PEEK 450G according to the VICTREX® material properties guide sheet; 90G is a very easy flow grade for thin sections and complex parts manufactured using injection molding and 450G is a standard flow grade for general injection molding purposes. Finally, PEEK VICTREX® 90G was selected for the new designed polymer parts due to their complex features and thin wall thicknesses (0.7 mm). Each engineering drawing of the polymer parts is presented in detail (section 5.4.2) in this chapter.

A medical grade stainless steel was selected to manufacture the new parts which were selected to be metal. These parts will directly be affected with the applied load (see section 5.2.1) so the material strength for these parts should be high to be able to withstand the cyclic

stresses. Alternative materials rather than stainless steel to manufacture the new device metal parts were nonferrous alloys (such as aluminum alloys), cobalt-chromium (Co-Cr) alloys or titanium (Ti) alloys. The density of stainless steel ( $8.0 \text{ g/cm}^3$ ) is almost three times greater than the density of aluminum alloys ( $2.7 \text{ g/cm}^3$ ). Stainless steel has a high Young's modulus of 200 GPa that is approximately three times that of aluminum alloys (70 GPa) (Davis, 1994). Ti alloys and Co-Cr alloys are the most commonly used metals in total joint arthroplasty (TJA) devices and the stainless steel is used in non-active surgical medical devices (Long, 2008). Another issue that made the stainless steel the best manufacturing choice is that titanium costs five to ten times as much as stainless steel (Budinski, 1991). Co-Cr and Ti alloys are used mainly for applications where high thermal and corrosion resistance, rather than specific strength requirements, are of greater importance (Elshennawy and Weheba, 2015)

A surgical stainless steel material compliant to ASTM F138 – 13a and ASTM F899 - 12b was selected for manufacture of the designed metal parts. The 316, 420 and 440 stainless steel grades were the three options which are used in biomedical applications. Biomedical cutting instruments are often made from 440 or 420 stainless according to ASTM F899 - 12b which were high-carbon steel with a minimum chromium content of 12%. The 316L series was most suitable for the medical device parts (ASTM F138 standard). The fatigue strength of stainless steel grade 316L ranges from 180 MPa to 520 MPa at 6 Hz and  $N > 10^7$  cycle (Huang *et al.*, 2006). 316LS grade was selected to be the metal material to manufacture the new designed parts. This grade is the low carbon version of 316 stainless steel with a maximum carbon content of 0.03%, low silicon with a maximum content of 0.75%, a sulfur content of 0.010% and with a yield strength range from 190 to 690 MPa (annealed/cold

worked conditions) (ASTM F138 - UNS S31673). Finally, 316LS medical grade stainless steel, 90% cold worked condition was selected to manufacture all metal parts because its high mechanical properties where the yield strength is 946 MPa (MatWeb, material property data).

### **4.5.2 The PIP joint protractor hinge device**

The seventeen parts of the assembly are shown in the exploded view of the design (Figure 4-17) and all the parts are assembled together in Figure 4-18. The proximal protractor hinge part was designed as the housing for the distal protractor hinge part. The four polymer slotted proximal and distal blocks are assembled with the four stainless steel solid blocks and are used for securing the wires which will support the device in the human phalanges. Four hexagonal head standard screws (M2 x 0.4) are used to compress the blocks together around the K-wires. The function of the screw and nut are to hold the proximal and the distal protractor hinge parts together and allowing them to rotate.

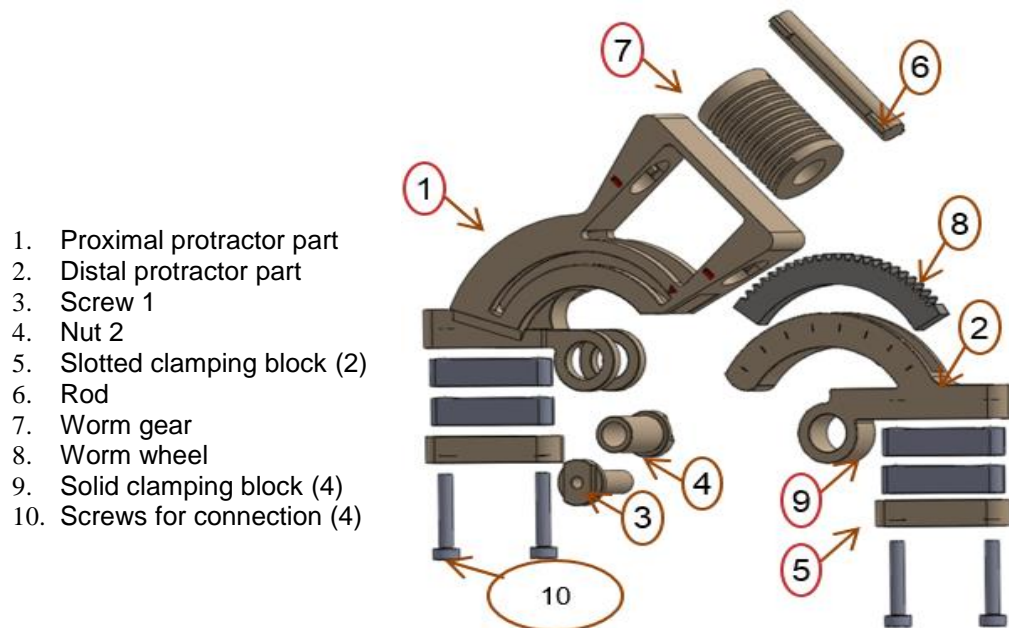


**Figure 4-17.** 3D exploded view of the assembly of the PIP joint protractor hinge.

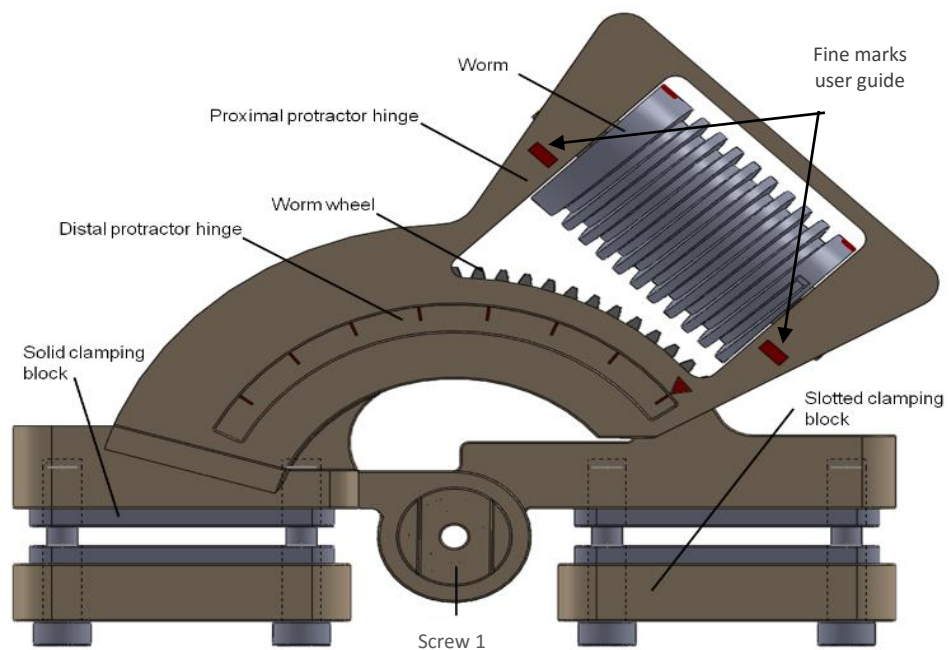


**Figure 4-18.** 3D design assembly of the PIP joint protractor hinge final design.

In the beginning, the whole concept design was divided into the individual parts that need further research for their design aspects and also separate evaluation. The complete design can be disassembled during the detailed design process into: proximal protractor hinge part, distal protractor hinge part, worm gear, worm wheel, screw 1, nut 2, rod, 2 slotted clamping blocks, and 4 solid blocks.

#### **4.5.2.1 Proximal protractor hinge part**

The proximal protractor hinge part is considered the main frame for the new device. In Figure 4-19 the 3D design of the proximal protractor hinge part is shown and the engineering drawing of the proximal protractor hinge part is shown in Figure 4-20 with the dimensions of the final design. The proximal protractor part is attached by 2 K-wires which are embedded in the skeletal elements of the digit proximal phalanx. Its key design idea is to be a house for the distal protractor hinge part; consequently the middle slot dimensions in the proximal protractor part fit the distal protractor part. Another slot (from engineering drawing bottom view, Figure 4-20) was designed to assemble with a part named solid clamping block. A worm gear will be placed on the top right designed housing and the four end small clips were provided in the side walls to keep the worm in its selected position. Four marks were engraved on the frame (two on the front frame view and two on the rear frame view) to aid the patient in how many turns should be performed. A medical grade plastic VICTREX® PEEK 90G was chosen to manufacture this part (see section 4.5.1 from this chapter). The previous engineering study of the Compass hinge which had its parts manufactured from the PEI material confirms that PEI cannot withstand the cyclic bending stresses and this causes

device failure (see chapter 3 section 3.3 and section 3.4). For that reason PEEK was chosen for the proximal protractor part.

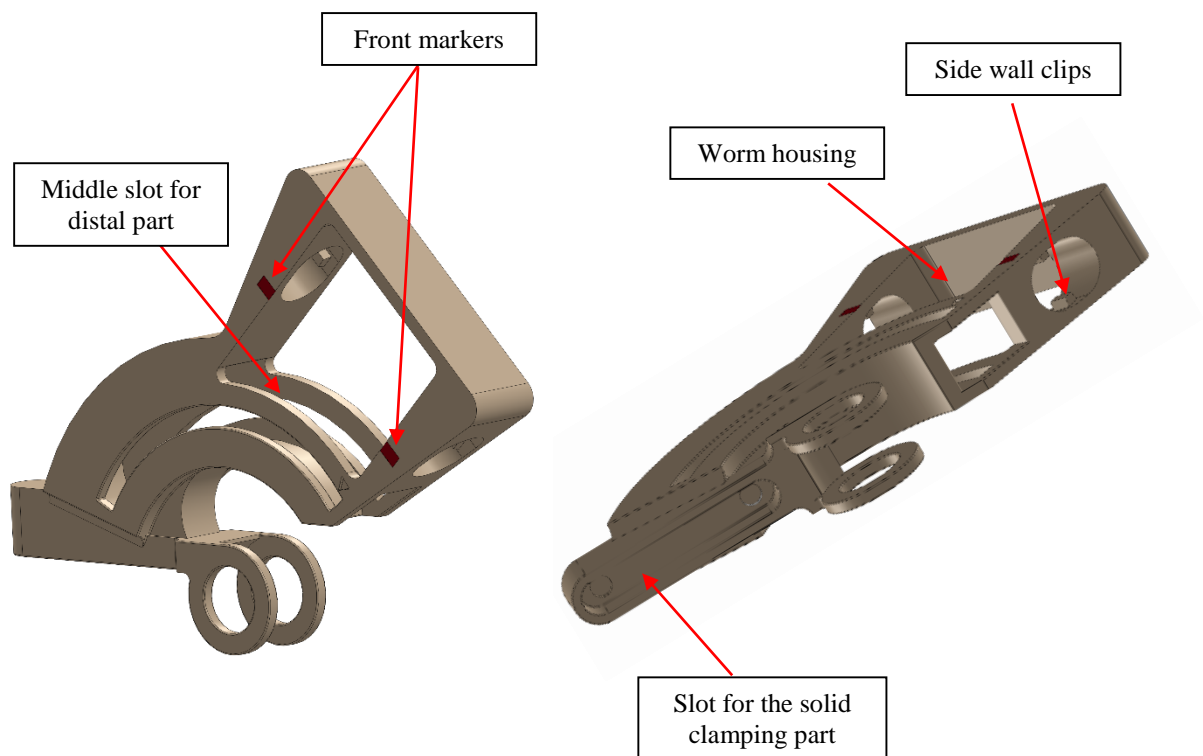


**Figure 4-19.** 3D design of the proximal protractor hinge part.



#### 4.5.2.2 Distal protractor hinge part

The distal protractor part will be inserted inside the cavity of the proximal protractor hinge part. The distal protractor hinge part is attached by 2 K-wires embedded in the skeletal distal phalanx of the finger. A semi-circular cavity on the top of the distal part body was designed so that the worm wheel component could fit inside the cavity. Also, it has a slot so that the solid clamping block can be fitted. The range of movement is guided by the engraved angles marked on both sides (front and rear) of the distal protractor hinge part. The material that has been chosen for the distal protractor hinge part is the medical grade plastic VICTREX® PEEK 90G, the same as the proximal protractor hinge part (see section 4.5.1 for this chapter). In Figure 4-21 the 3D design of the distal protractor part is presented and in Figure 4-22 the engineering drawing of the distal protractor part is shown.

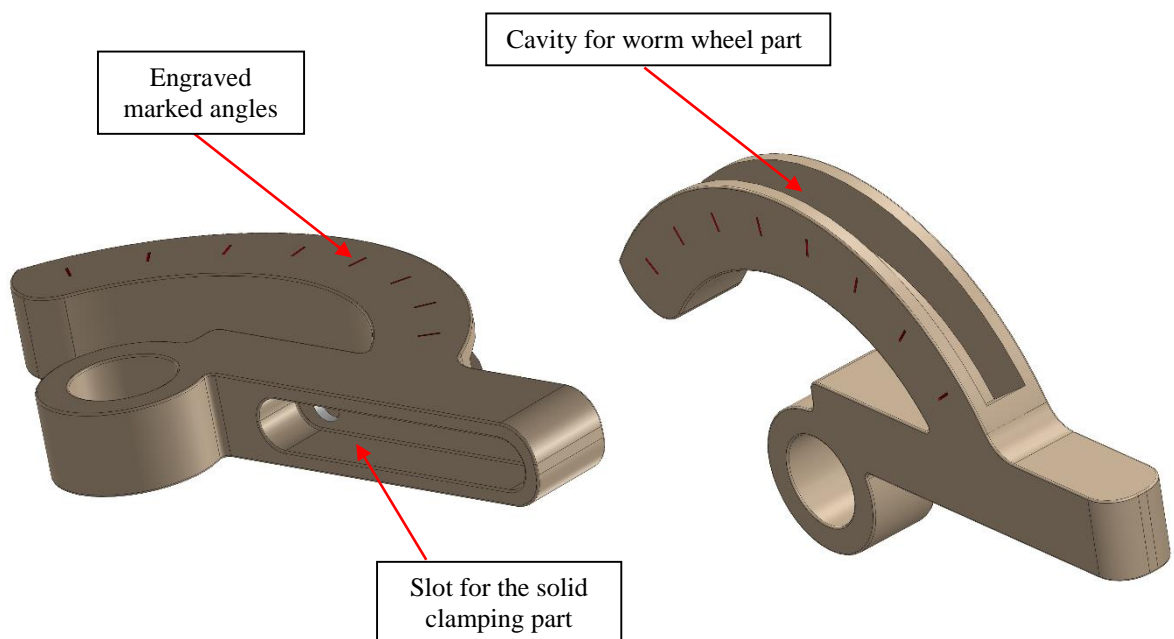


**Figure 4-21.** 3D design of the distal protractor part.

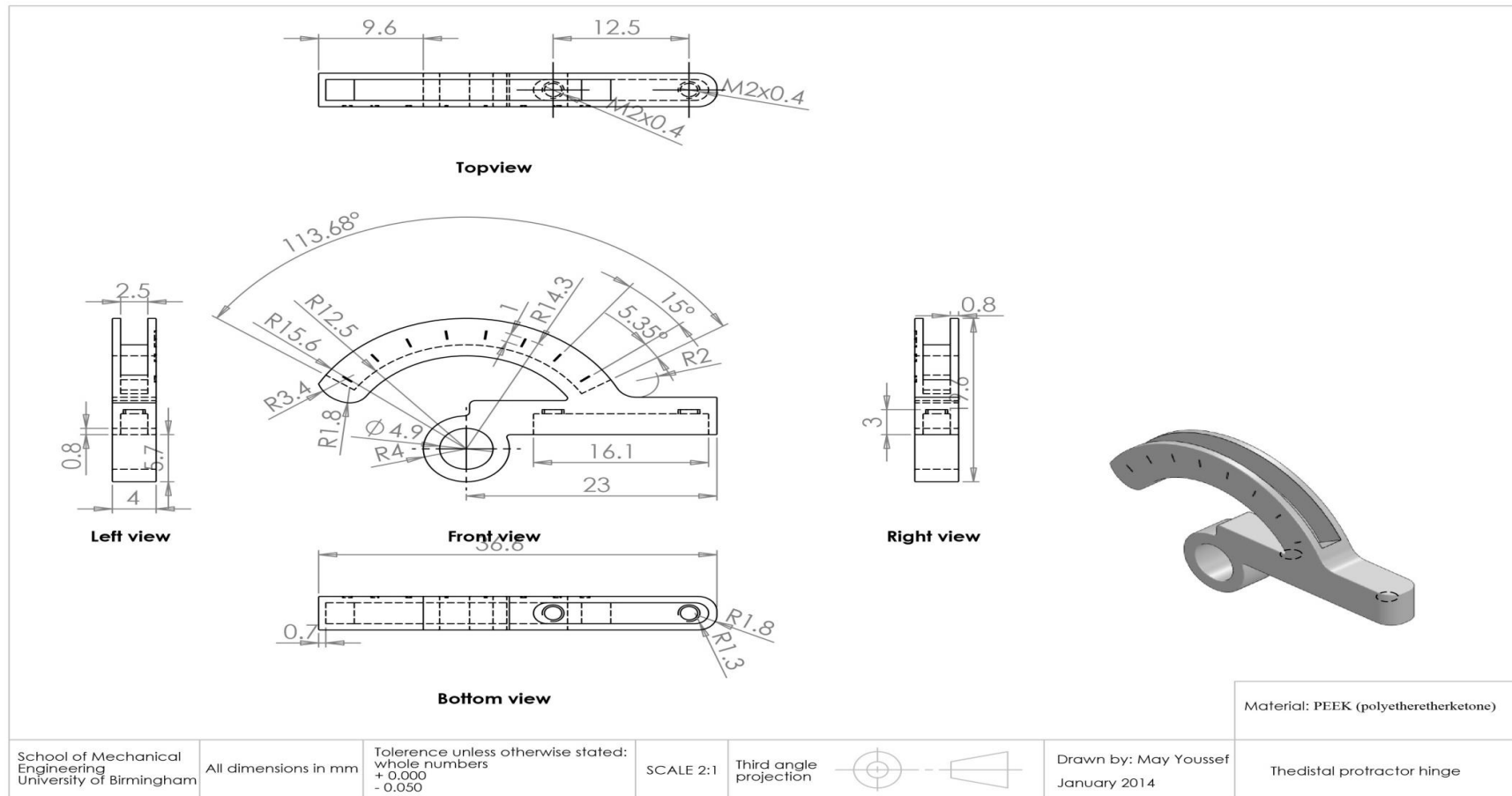
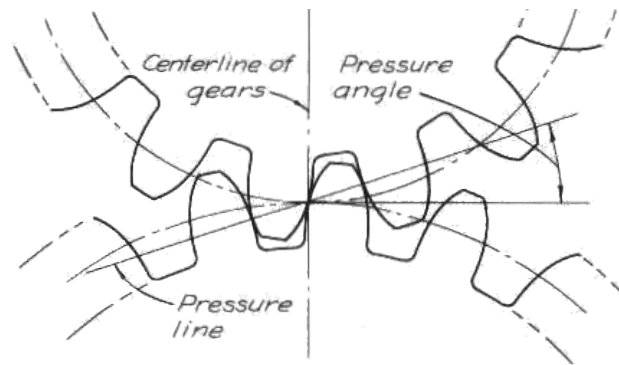


Figure 4-22. Drawing of the distal protractor hinge part.

### 4.5.2.3 Worm wheel

The worm wheel part was designed and its dimensions were calculated from the gear design formula (Designatronics, 1999). The worm wheel gear tooth nomenclature was defined from Radzevich (2012) and ANSI/AGMA 1012-G05. At the beginning, the outer circle diameter (which coincides with the tops of the teeth of a gear) was selected in the range 32 mm to 33.5 mm where the chosen gear outer diameter should be within this range to match with the overall height of the distal protractor part (section 4.5.2.2) and the proximal protractor part height (section 4.5.2.1). Then, the standard worm wheel with the outer circle diameter of 32.80 mm was selected from the catalogue (Catalogue C14) which listed the pressure angle as  $20^\circ$  (it is formed by the radial line and the line tangent to the profile at the pitch point (Figure 4-23). It describes the direction of the force created by the driving gear acting upon its mate), the module was 0.4 (is the ratio of the pitch diameter to the number of teeth in the metric system used to determine tooth size, for gears to mesh, their modules must be equal) and the number of teeth for that gear was 80. After that the worm wheel design formula (Designatronics, 1999) was used to calculate all other required data for designing the worm wheel teeth and for drawing the involute curve of the tooth. These data are summarised with each term definition and equation in table 4-2. In this gear it was found that, the root circle diameter (which coincides with the bottom of the tooth spaces) was equal to 31 mm and this was greater than the base circle diameter (the circle from which involute tooth profiles are derived) which was equal to 30.07 mm (Figure 4-24). Therefore, theoretically the involute has already started before the root circle. Thus, correction formulas were used to produce the final design (Buckingham, 1949).



**Figure 4-23.** The pressure angle at mating gear teeth (Designatronics, 1999)

**Table 4-2.** Gear general nomenclature and design formula (Designatronics, 1999).

To obtain	Term definition	From known	Use this formula
Pitch diameter (D)	The curve of intersection of a pitch surface of revolution and a plane of rotation	Module (m), teeth number(N)	$D = m N$
Addendum (a)	The radial distance between the pitch diameter and the outside diameter	Module (m)	$a = m$
Dedendum (b)	The radial distance between the pitch diameter and the root diameter	Module (m)	$b = 1.25 m$
Root diameter (D <sub>R</sub> )	Coincides with the bottoms of the tooth spaces	Pitch diameter (D), Module (m)	$D_R = D - 2.5 m$
Base circle diameter (D <sub>b</sub> )	The circle from which involute tooth profiles are derived	Pitch diameter (D), pressure angle ( $\varphi$ )	$D_b = D \cos (\varphi)$
Tooth thickness  T <sub>std</sub> (at standard pitch diameter)	Thickness of tooth	Module (m)	$T_{std} = \pi/2 m$

The following were previously decided:

$$\textbf{Module } (m) = 0.4, \textbf{ Number of Teeth } (N) = 80 \text{ and } \textbf{Pressure Angle } (\phi) = 20^\circ$$

The worm wheel design formulae, given in Table 4-1 were then used to calculate all the required dimensions:

$$\textbf{Pitch Diameter } (D) = mN = 0.4 \times 80 = 32 \text{ mm}$$

$$\textbf{Circular Pitch } (P_c) = m\pi = 0.4 \times \pi = 1.257 \text{ mm}$$

$$\textbf{Addendum } (a) = m = 0.4 \text{ mm}$$

$$\textbf{Dedendum } (b) = 1.25m = 1.25 \times 0.4 = 0.5 \text{ mm}$$

$$\textbf{Outside Diameter } (D_o) = D + 2m = m(N + 2) = 32 + 2 \times 0.4 = 32.80 \text{ mm}$$

$$\textbf{Root Diameter } (D_R) = D - 2.5m = 32 - 2.5 \times 0.4 = 31 \text{ mm}$$

$$\textbf{Base Circle Diameter } (D_b) = D \cos \phi = 32 \cos 20^\circ = 30.070 \text{ mm}$$

$$\textbf{Base Pitch } (P_b) = m \pi \cos \phi = 0.4 \times \pi \times \cos 20^\circ = 1.181 \text{ mm}$$

$$\textbf{Tooth Thickness at Standard Pitch Diameter } (T_{std}) = \pi/2 \times m = \pi/2 \times 0.4 = 0.628$$

mm

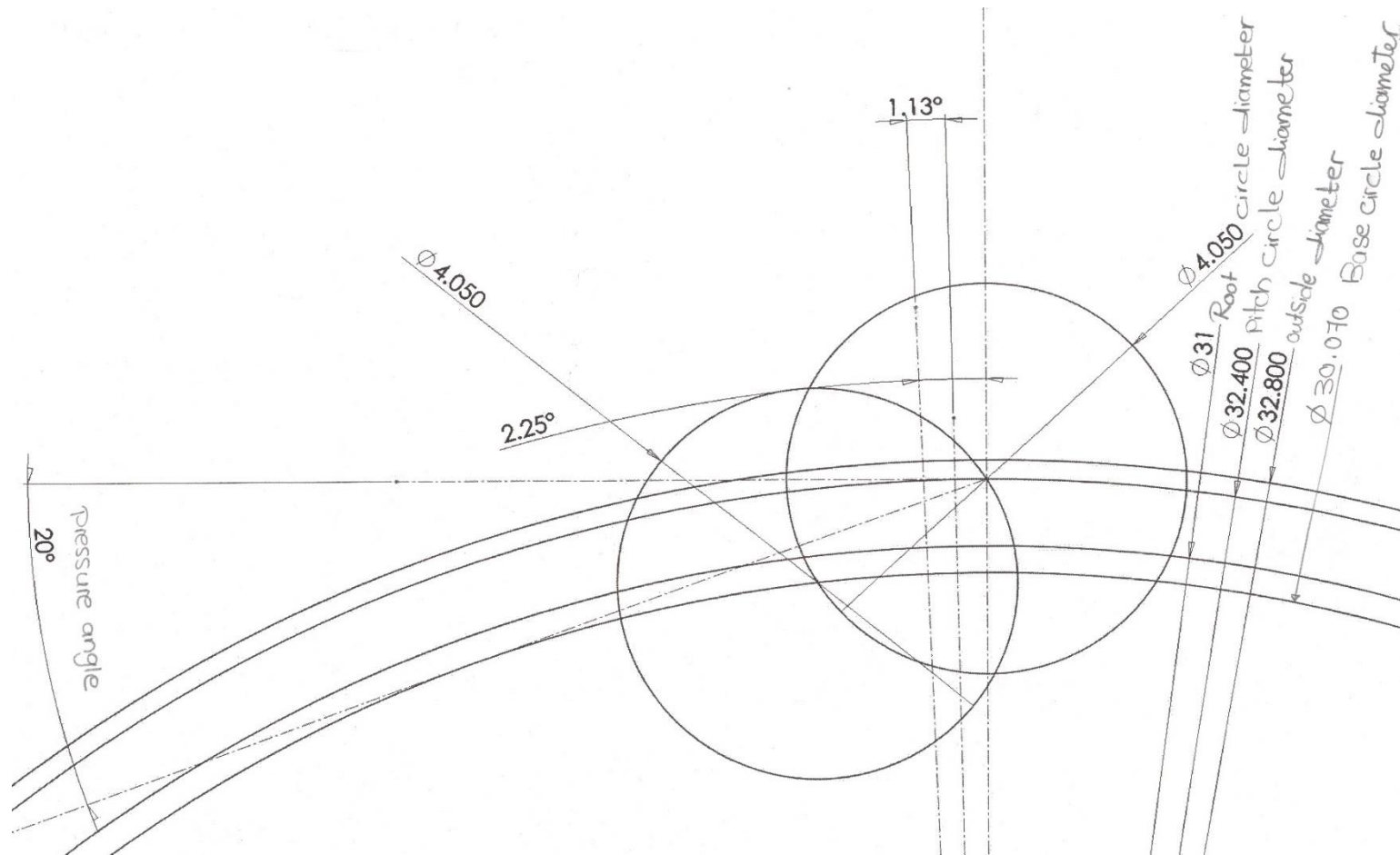


**Figure 4-24.** Involute curve derivation of the worm wheel tooth

The worm wheel gear formulae (Buckingham, 1949) were used to draw the involute curve of the gear teeth (Table 4-3) as shown in Figure 4-25 and the teeth profile as shown in Figure 4-26, where the root circle diameter was greater than the base circle diameter case. Units for these formulas in the Buckingham (1949) reference book were in English imperial measurements. The engineering drawing of the worm wheel tooth profile is shown in Figure 4-27.

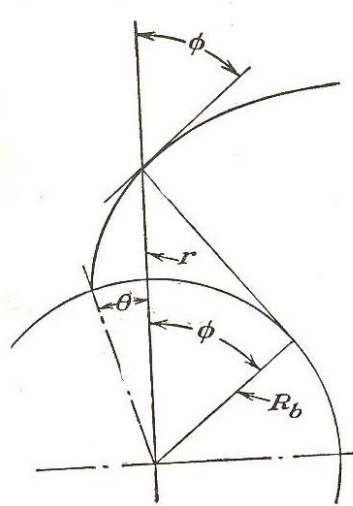


**Figure 4-25.** The gear involute (Buckingham, 1949).

**Table 4-3.** The Formulas of gear tooth profile (Buckingham, 1949).

To obtain	From known	Use this formula
$r$ any radius to involute form, in	pressure angle ( $\phi$ ), radius of base circle $(R_b)$	$r = R_b / \cos \phi$
$\phi$ pressure angle at radius, r	any radius to involute form ( $r$ ), radius of base circle $(R_b)$	$\tan \phi = \sqrt{(\sqrt{r^2 - R_b^2})^2 / R_b}$
$\theta$ Vectorial angle	any radius to involute form ( $r$ ), radius of base circle $(R_b)$	$\theta = \sqrt{(\sqrt{r^2 - R_b^2})^2 / R_b} -$ $\tan^{-1} (\sqrt{r^2 - R_b^2} / R_b)$ <u>Or</u> $\theta = \tan \phi - \phi = \text{inv } \phi$

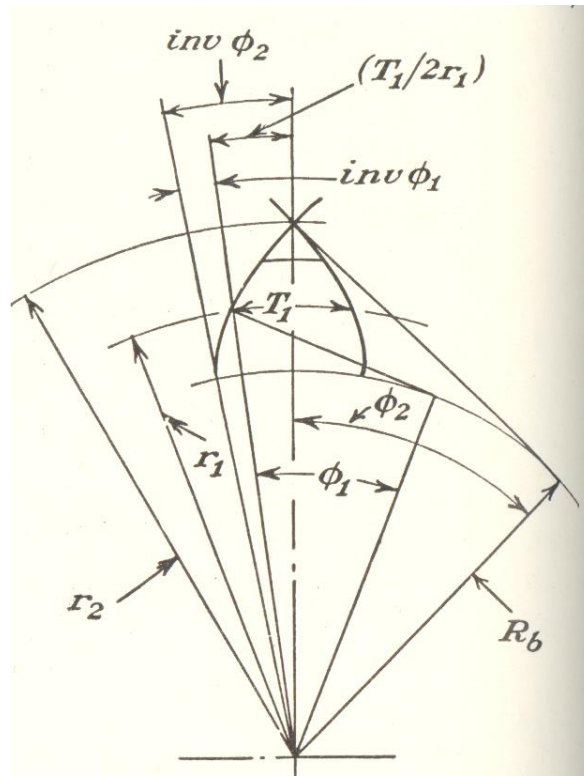


**Figure 4-26.** The gear tooth profile (Buckingham, 1949).

The following were previously decided:

**Arc tooth thickness ( $T_1$ )** = 0.628 mm, **Radius of base circle ( $R_b$ )** = 15.04 mm,

**Pitch Diameter ( $D_1$ )** = 32 mm and **Pressure Angle ( $\phi_1$ )** =  $20^\circ$

The worm wheel design tooth profile formulae, given in Table 4-2 were then used to calculate all the required dimensions:

$$\text{inv } \phi_2 = (T_1 / 2 r_1) + \text{inv } \phi_1$$

$$T_1 = 0.628 \text{ mm} = 0.628/25.4 = 0.025 \text{ in.}$$

$$r_1 = 32/2 \text{ mm} = 16/25.4 = 0.629 \text{ in.}$$

$$\text{inv } \varphi_1 = 0.014904 \text{ rad} = 0.8539^\circ$$

$$\text{inv } \varphi_2 = 0.025/(2 \times 0.629) + 0.014904 = 0.0347 \text{ rad} = 1.988^\circ$$

$$\varphi_2 = 26.168^\circ$$

$$\cos \varphi_2 = 0.898$$

$$R_b = r_1 \cos \varphi_1 = 16 \times \cos 20^\circ$$

$$= 15.035 \text{ mm} = 0.592 \text{ in}$$

$$r_2 = R_b / \cos \varphi_2 = 15.035 / 0.898 = 16.70 \text{ mm}$$

$$T_1 / 2r_1 = 0.628 / 2 \times 16 = 0.0196$$

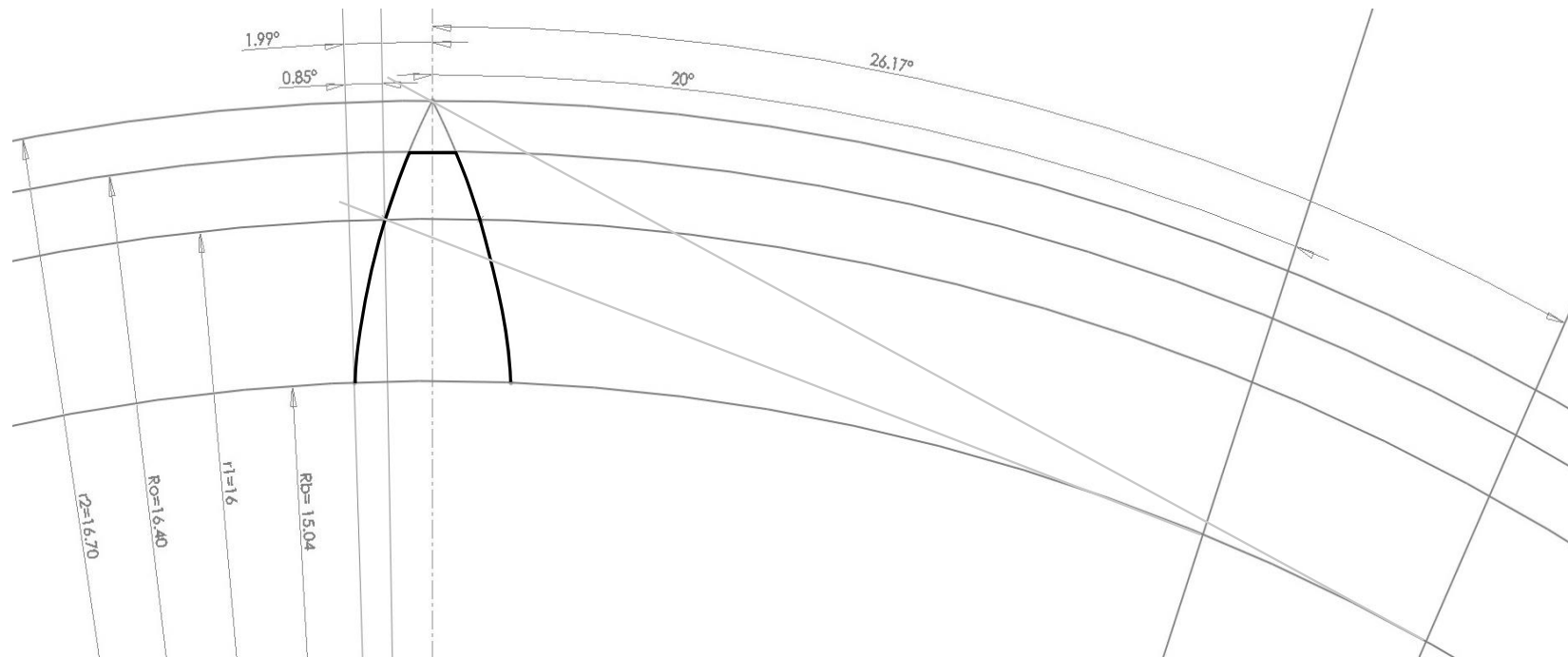


**Figure 4-27.** Engineering drawing of the worm wheel tooth profile.

The gear feature was improved where the bottom land was modified to be rounded with a radius  $R = 0.28$  mm aiming to decrease the generated stresses between the gear teeth as a result of application of the external load. It is designed to match the dimensions of the distal protractor hinge part top curvature slot. According to the engineering analysis of the failed Compass hinge device (see chapter 3) the worm wheel component material for this design has been selected to be metal. The worm wheel is the main component which is exposed to high stresses that are exerted during loading when its teeth are in a fixed position (see chapter 3 section 3.3.1). A surgical stainless steel 316LS material was selected for the worm wheel part (section 4.5.1). The 3D design of the worm wheel is shown in Figure 4-28, while the engineering drawing is shown in Figure 4-29.



**Figure 4-28.** 3D design of the worm wheel part.

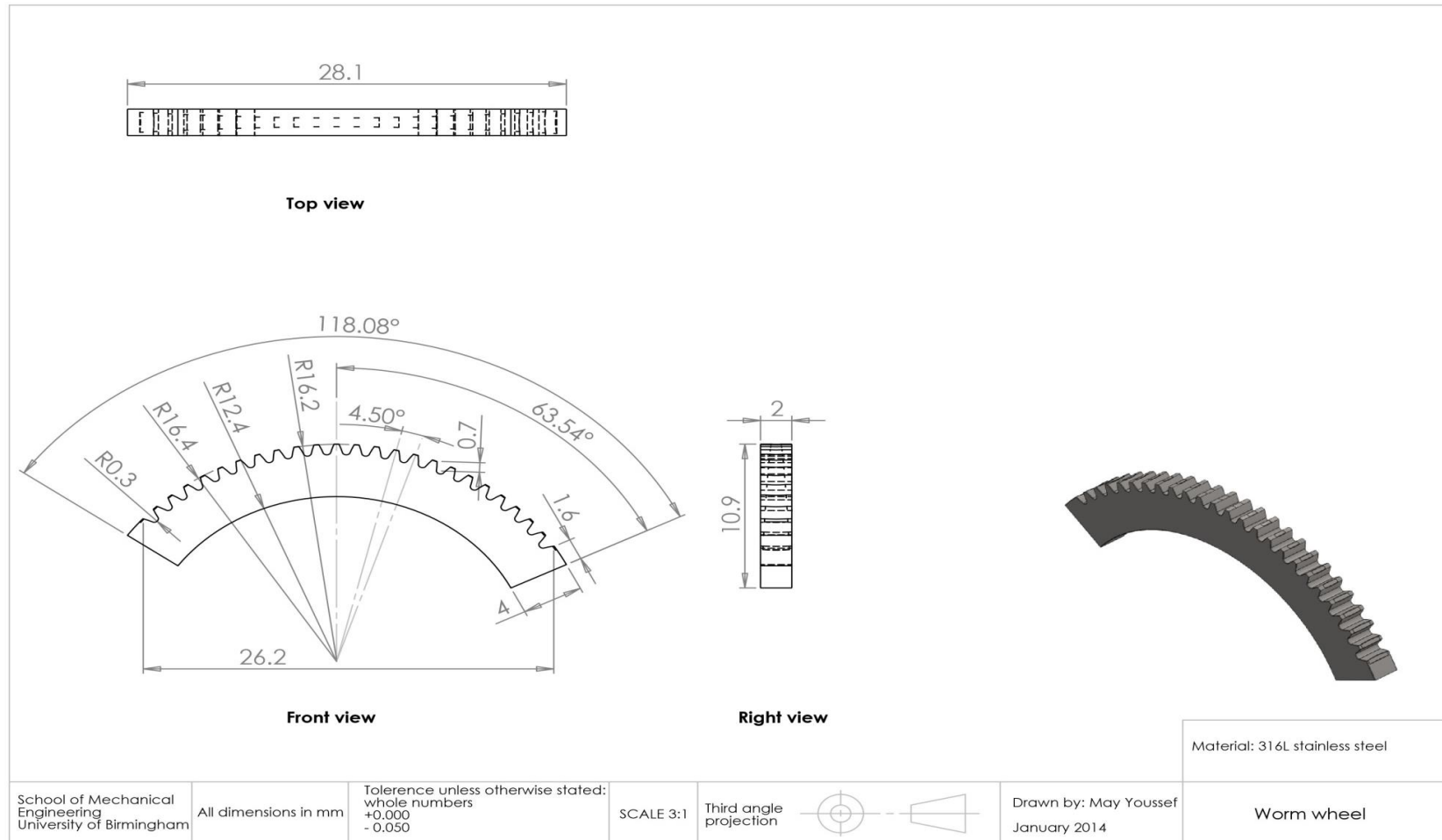


**Figure 4-29.** Drawing of the worm wheel part.

#### 4.5.2.4 Worm gear

A worm gear was included in the proximal protractor part. The specifications (0.4 module - 20° Pressure angle- 1.25 pitch) (Catalogue C14) were selected to mesh with the designed worm wheel and match with the size of the proximal protractor part. A worm is provided to move the proximal and distal protractor parts by mating with worm wheel teeth on the distal protractor part. The worm function is to translate rotational motion to the engaged gear teeth and thus it affects extension and flexion of the finger joint. The worm is adjustable within the worm housing in the proximal protractor hinge part to be either engaged or disengaged. A plastic material was suggested for that part as the engineering study of the Compass hinge device (chapter 3 section 3.3) confirmed that the worm gear was not subjected to high stresses and it was not the cause of a Compass hinge device failure. Towards keeping the new device with a low mass and compatible with the proximal protractor part which it will assemble to, the medical grade plastic VICTREX® PEEK 90G was selected for the worm gear (see section 4.5.1). The 3D design of the worm gear and its engineering drawing is shown in Figure 4-30 and Figure 4-31, respectively.

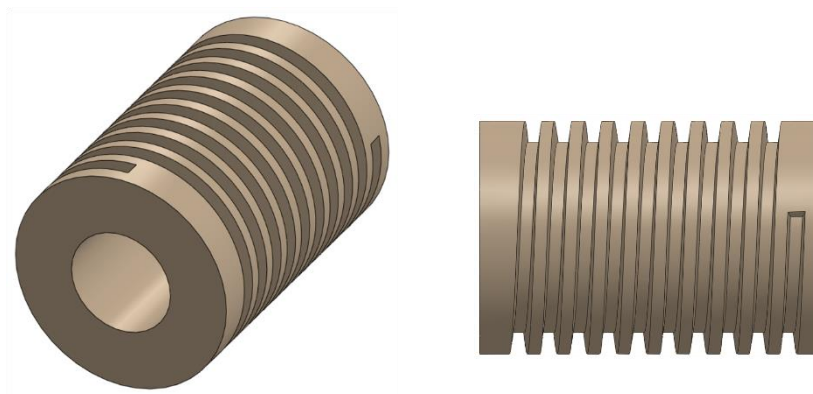


**Figure 4-30.** 3D design of the worm gear part.

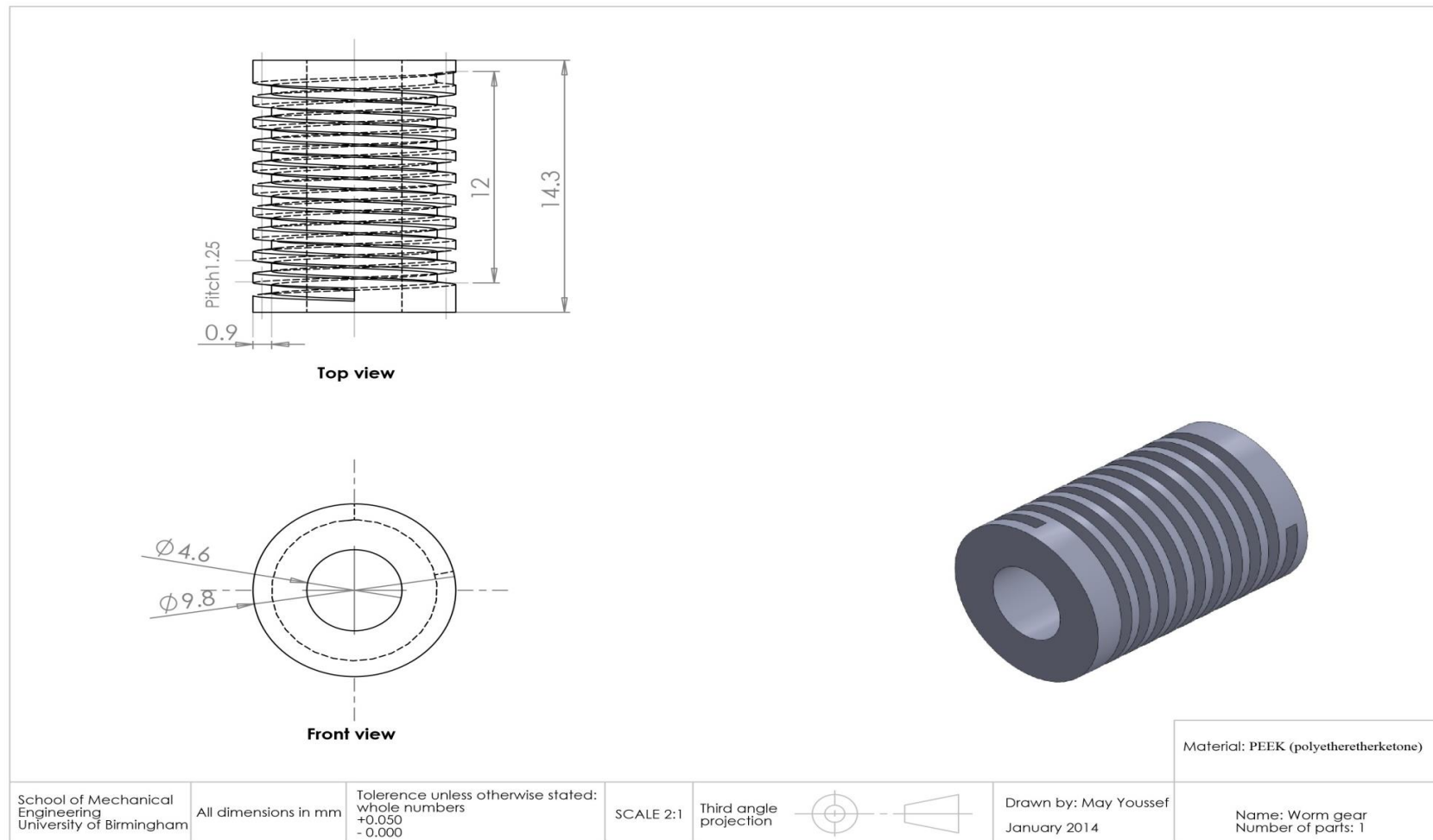


**Figure 4-31.** Engineering drawing of the worm part.

#### 4.5.2.5 Rod

The rod was designed as a shaft to include 2 small extra features at both ends of the rod to facilitate movement of the worm on the engaging surface of the worm housing at the proximal protractor part. This clutch permits the selected position of the engagement of the worm and the worm wheel teeth such that force is transferred between them. Also, it restricts free motion of the skeletal supported protractor parts and permits controlled motion of the joint. When the gear is disengaged the worm and worm wheel permit the proximal and distal protractor parts to move freely. Because the rod will be assembled with the worm gear, the material of manufacturing was chosen to be VICTREX® PEEK 90G (see section 4.5.1.). Figure 4-32 is the 3D design of the rod and Figure 4-33 is the engineering drawings of it.

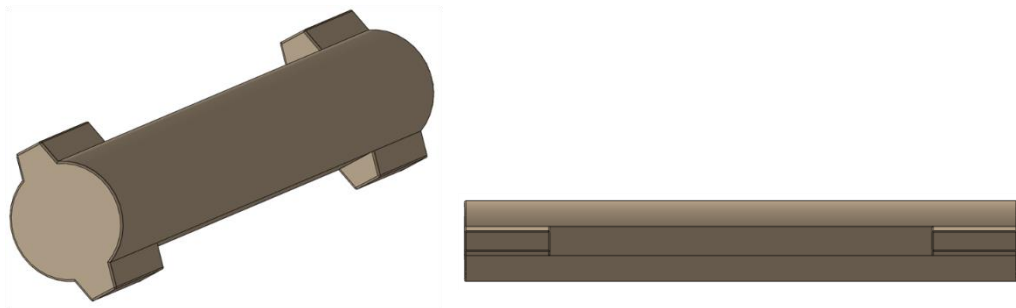


**Figure 4-32.** 3D design of the rod part.

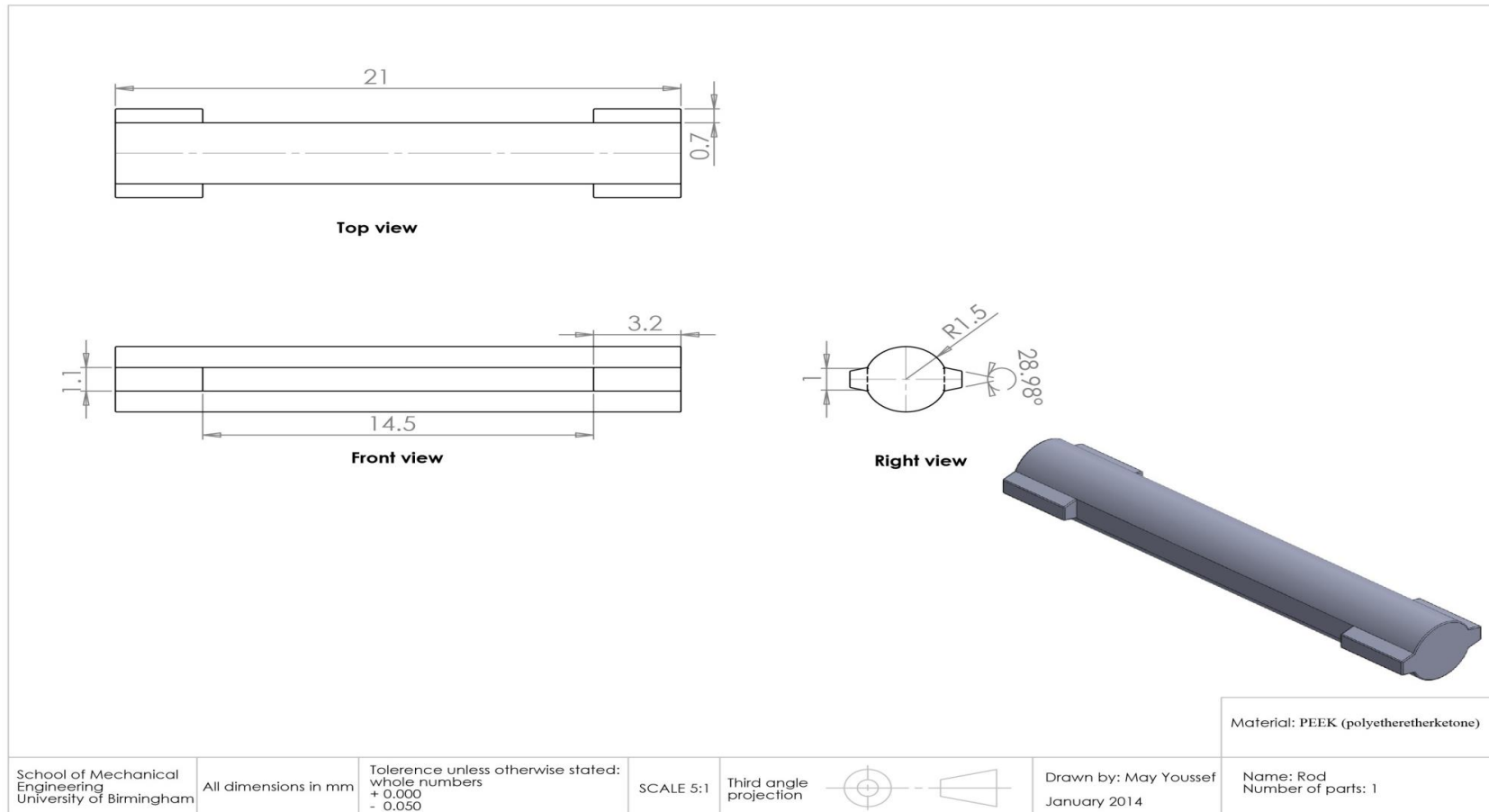
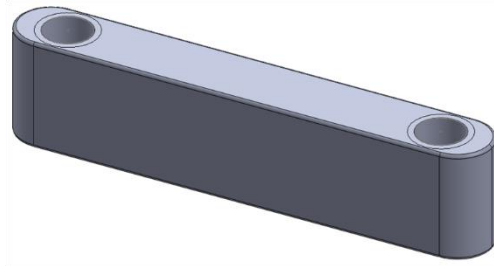


Figure 4-33. Drawing of the rod part.

#### **4.5.2.6 Slotted and solid clamping blocks**

The four solid clamping blocks and the two slotted clamping blocks were designed to be joined and tightened by vertical screws to engage the K-wires. Two of the solid blocks with the two slotted blocks were designed to be inserted inside each other. Therefore, the other two solid blocks will be assembled with the designed cavities where one is for the proximal part and another is for the distal part (see section 4.5.2.1 and 4.5.2.2). The solid blocks were chosen to be metal because these parts are directly in contact with the K-wires so the stress distribution from the load exerted will be minimized. The slotted blocks were selected to be polymer for that reason; these parts are the solid block houses so they will not affect directly with any exerting load which means a very high strength material (such as metal) was not required for these parts. The selected polymer material should be compatible with other plastic parts in this designed device so the medical grade plastic VICTREX® PEEK 90G was chosen for the slotted clamping blocks. A 316LS medical grade stainless steel was selected for the solid clamping blocks and for the main properties of these two materials refer to section 4.5.1 from this chapter. The 3D design of the slotted and solid clamping blocks can be seen in Figure 4-34 and Figure 4-35, followed by their engineering drawings in Figure 4-36 and Figure 4-37.



**Figure 4-34.** 3D design of the solid clamping blocks.

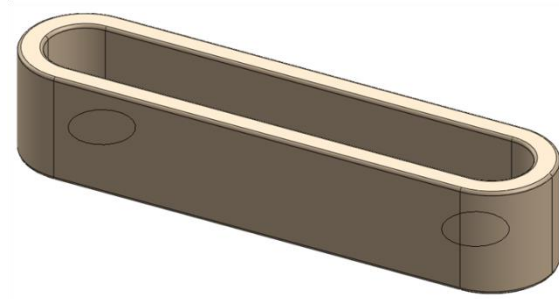


**Figure 4-35.** 3D design of the slotted clamping blocks.

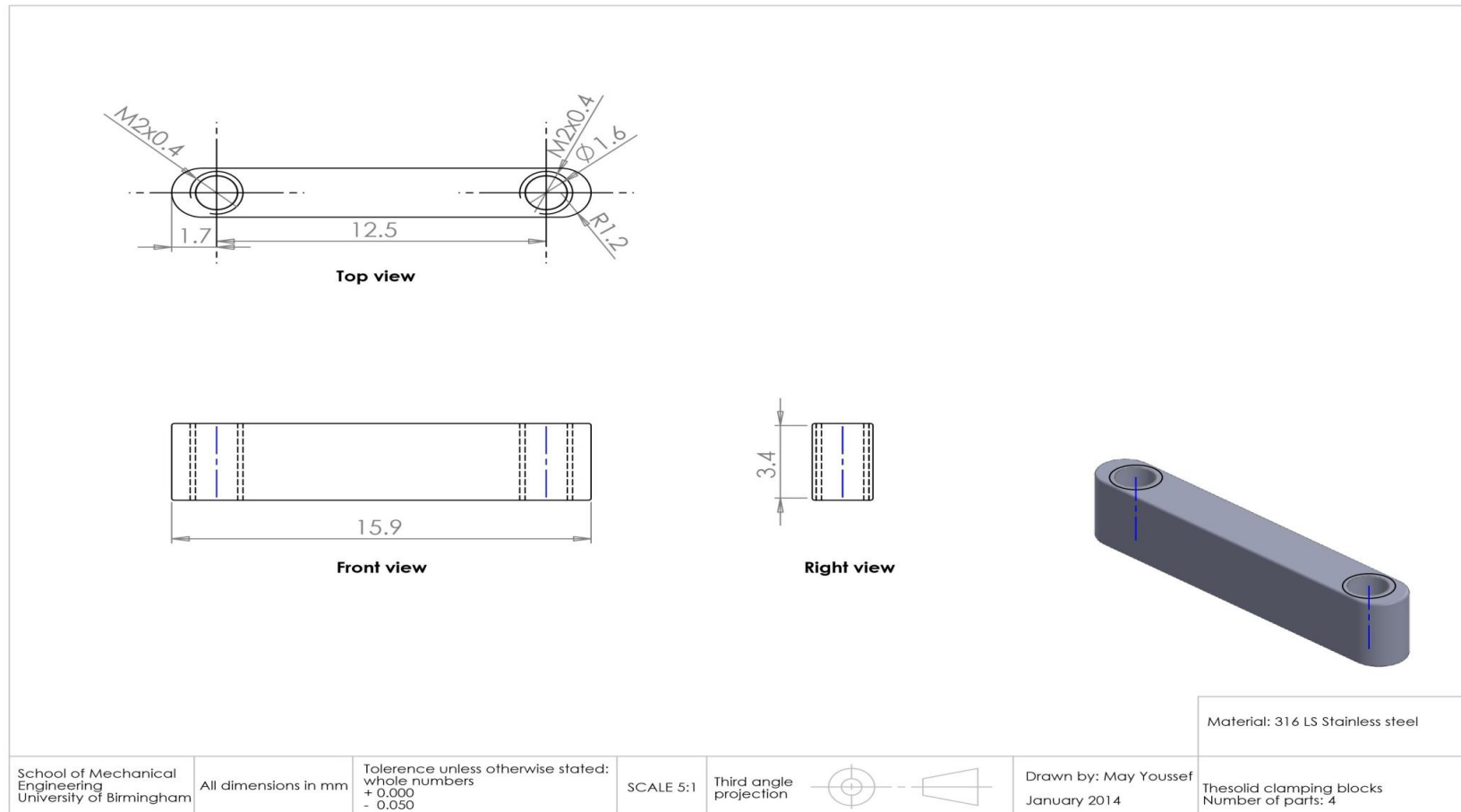


**Figure 4-36.** Drawing of the solid clamping block part.

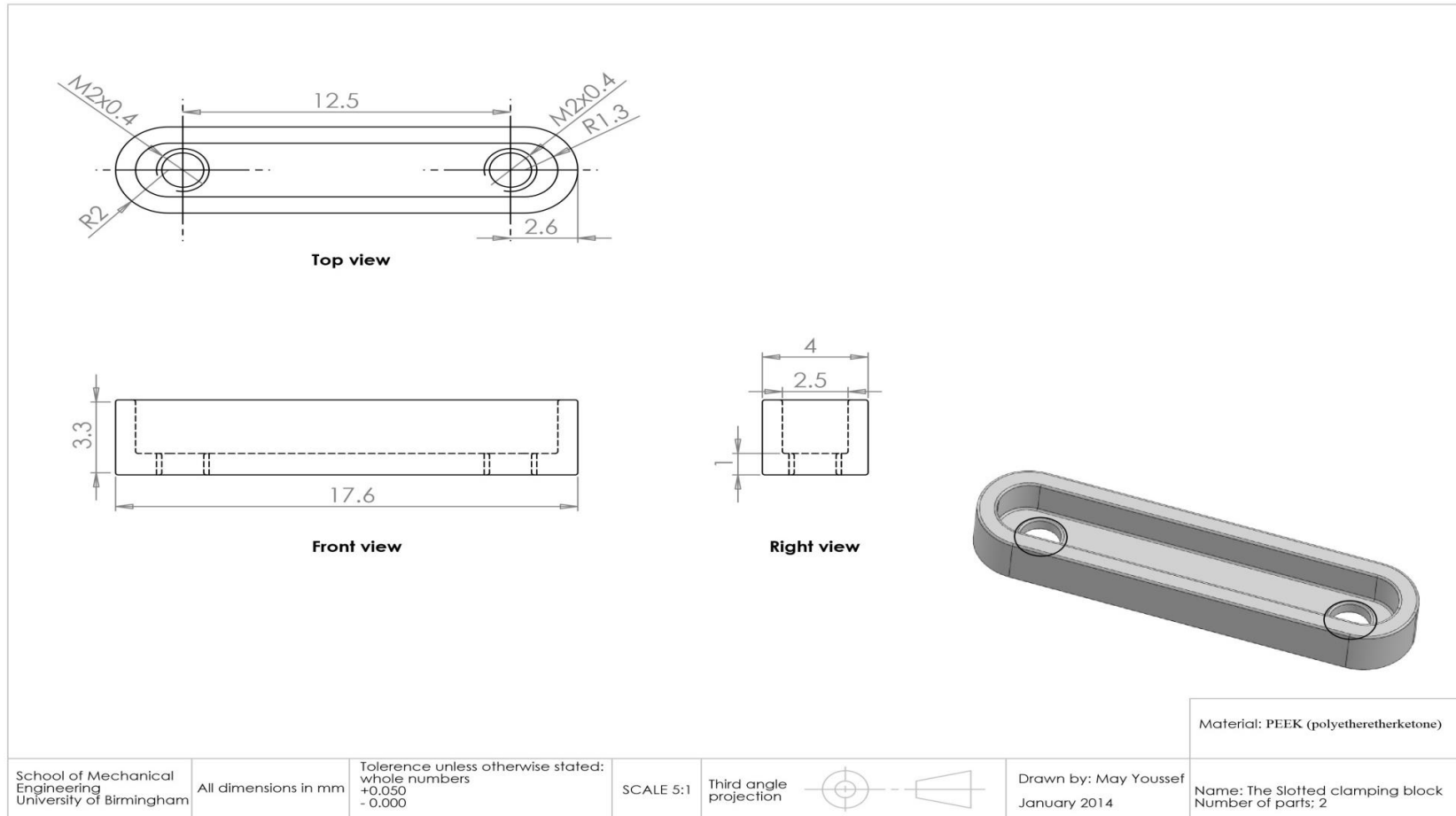


**Figure 4-37.** Drawing of the slotted clamping block part.

#### 4.5.2.7 Screw 1 and nut 2

The screw 1 and nut 2 connect together to attach to the proximal and distal protractor parts to each other. This screw axle with nut combination serve as the axis of rotation of the hinge and aligns the protractor parts with the natural axis of the PIP finger joint. The hole of 1.40 mm diameter along the screw and nut was designed with the diameter slight bigger than the diameter of the K-wires (1.15 mm diameter) to allow it to pass through the device. In the aim of overcoming the Compass hinge device complications, with one of them being the difficulty to see under x-ray the area around the radiopaque axle (see chapter 3 section 3.2.2) for surgeons to monitor the K-wire insertion process at the digit PIP joint center. A radiolucent material was selected to manufacture these two parts (screw and nut) and because the screw and nut will be assembled together the material selected had to be the same. Also the parts will be assembled with the proximal and distal protractor parts (see section 4.5.2.1 and 4.5.2.2) so the material of choice for both these parts was VICTREX® PEEK 90G medical grade polymer (section 4.5.1). PEEK 90G was not only chosen for the same reasons of previous selection of parts, but also to match all the device parts together. Figure 4-38 shows the 3D design of the two screw and nut and the engineering drawing of each one is shown in Figure 4-39 and Figure 4-40.



**Figure 4-38.** 3D design of the assembly of the screw 1 (left) and nut 2 (right).

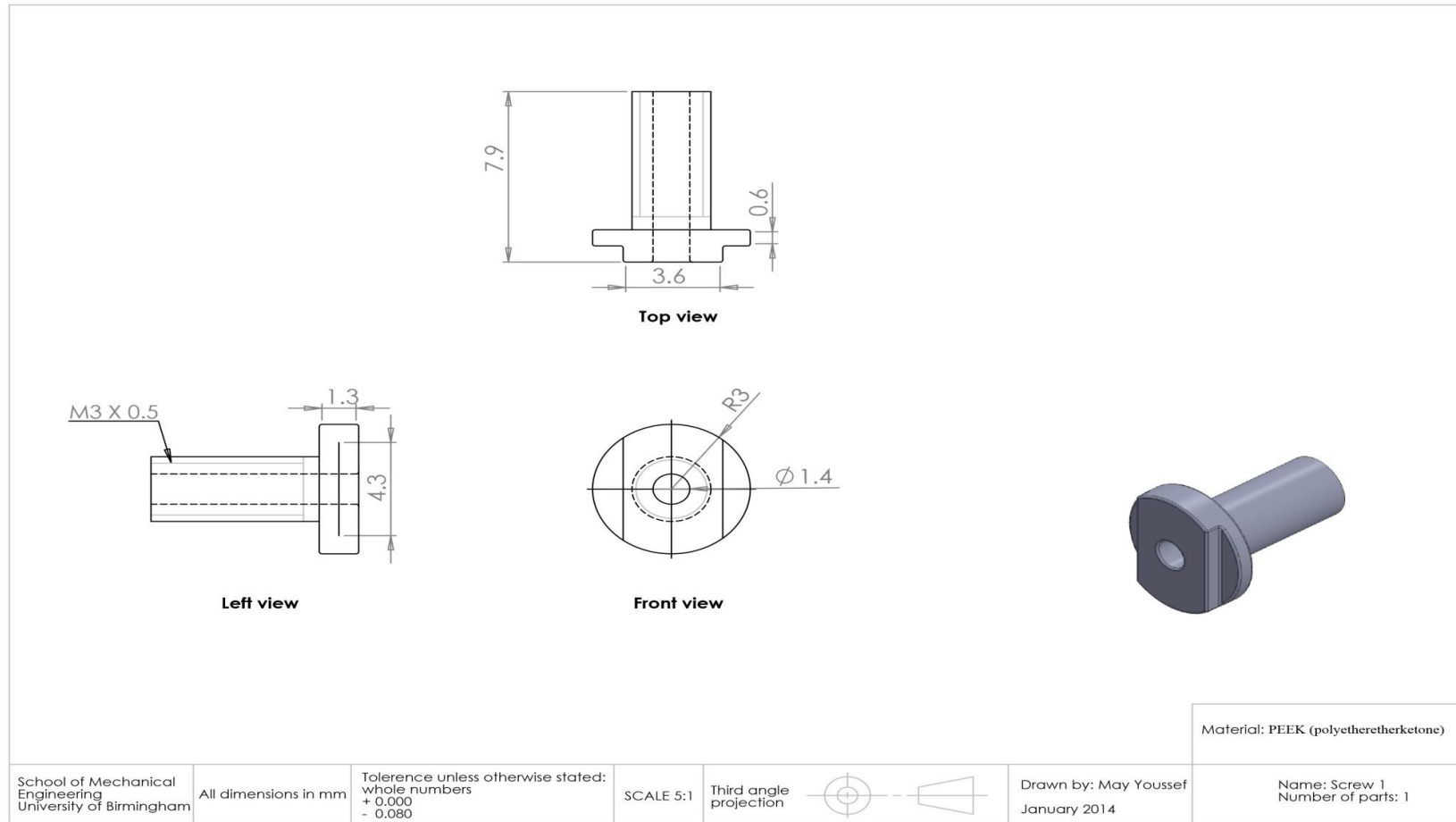


Figure 4-39. Drawing of the screw 1 part.

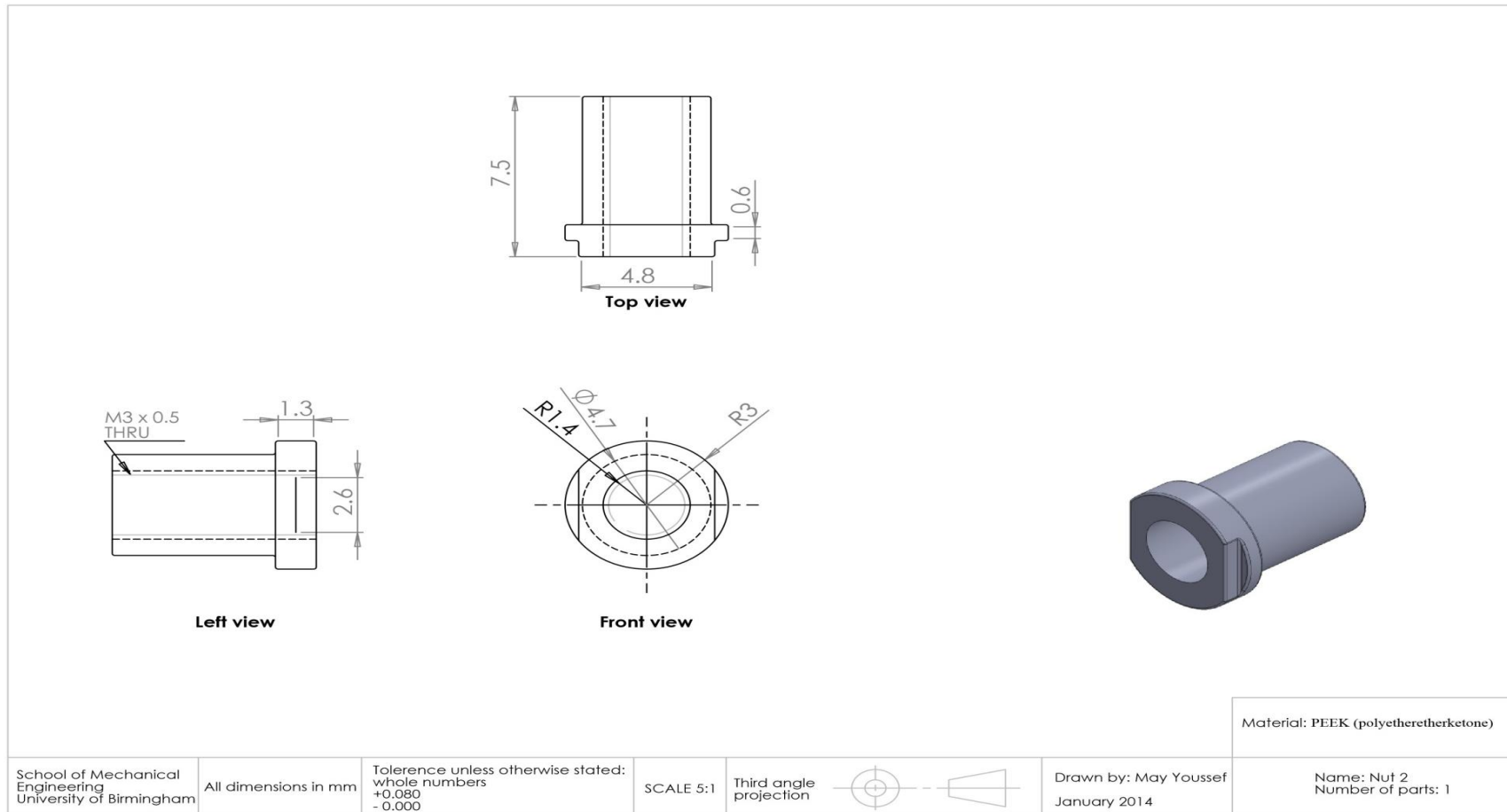


Figure 4-40. Drawing of the nut 2 part.

#### 4.5.2.8 Screws

Four  $M2 \times 0.4$  standard metric stainless steel screws were placed in either vertical or perpendicular positions on the slotted clamping blocks (Figure 4-16). To access the hexagonal heads of these screws that will be through the bottom of the device. These screws were selected to secure and keep the clamping blocks with the inserted K- wires in position by tightening them. The 3D and the engineering drawing of selected type screws are shown in Figure 4-41 and Figure 4-42, respectively.



**Figure 4-41.** The screw.

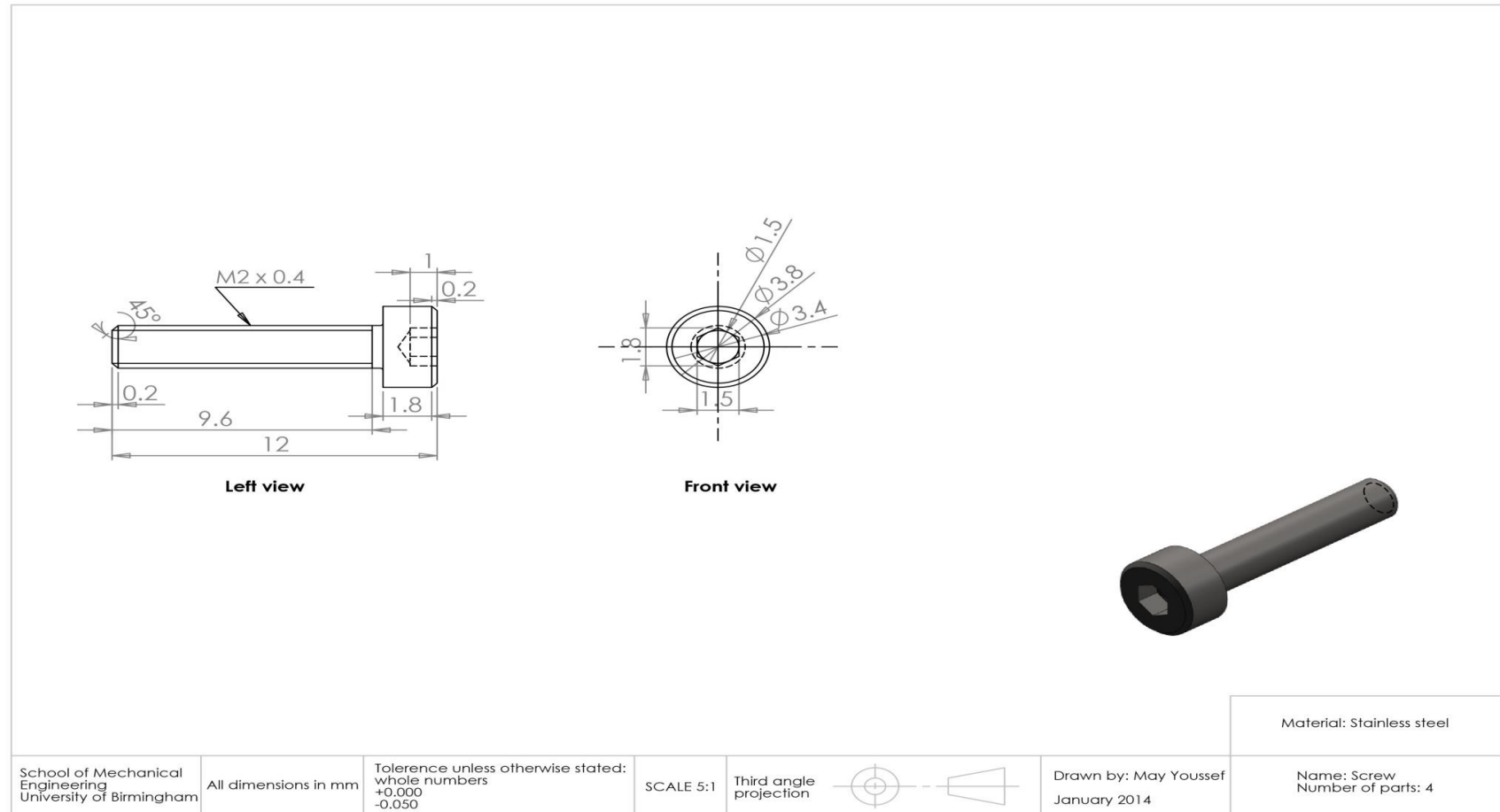
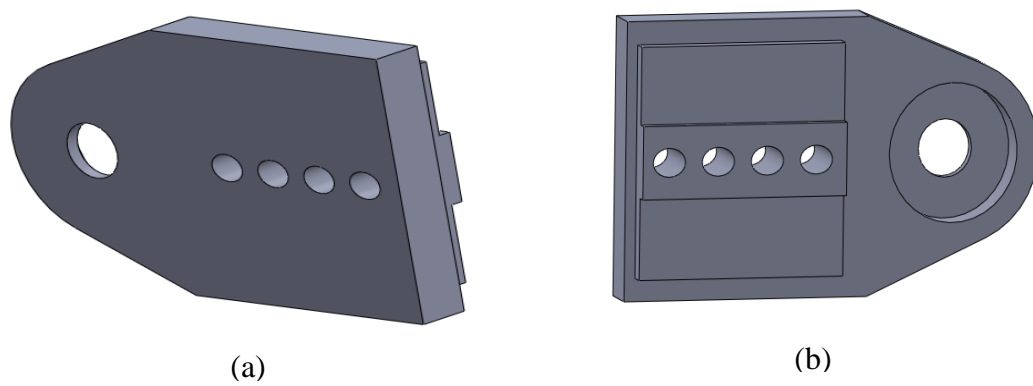
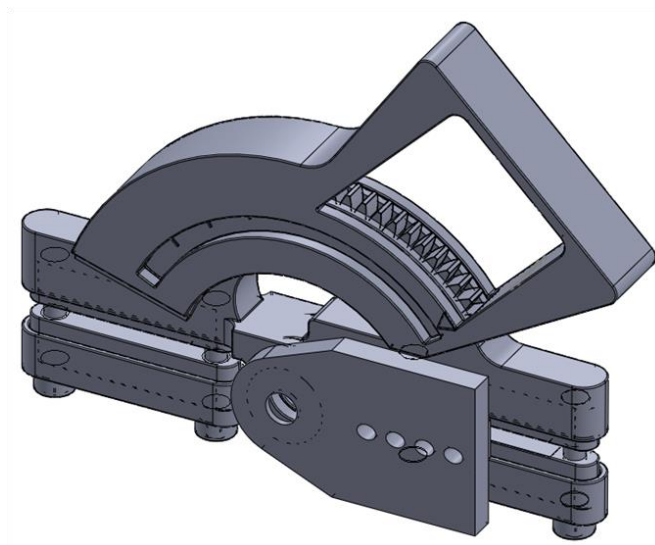


Figure 4-42. Drawing of the screw.

A guide jig for inserting the K-wires in the digit skeletal is also required to help surgeons during the surgical technique procedures to attach the fixator in the patient's finger. A simple jig was presented as a part from this project (as a concept design) and the 3D design, assembly 3D design of the jig with the PIP joint protractor hinge device and the engineering drawing are shown in Figure 4-43, Figure 4-44 and Figure 4-45, respectively. However, further engineering analysis is still required to finalise the design where more concept designs are needed to be generated. The concept designs would then be evaluated using methods such as the Pugh matrix. It was suggested to be manufactured from a radiolucent medical grade polymer material with a small ellipse holes to fit with inserted K –wires. The effect of the digit bone drilling technique to insert the K-wires on the jig geometry and material should be studied. The small material chips (abrasives from jig) can be generated and inserted inside the human body during the drilling process. That is harmful and not accepted so this is a key point of a risk analysis and should working on it very well. A hollow cavity was designed for the purpose of seating the jig in the head of the screw 1 part (see section 4.5.2.7). A step was provided in the jig to keep it in the correct position during the surgical procedure by supporting it on the slotted clamping block (section 4.5.2.6).



**Figure 4-43.** A guide Jig for inserting the K-Wires (a) Isometric view and (b) Rear view of the proposed design.



**Figure 4-44.** A 3D assembling design of the Jig with the PIP joint protractor hinge device.

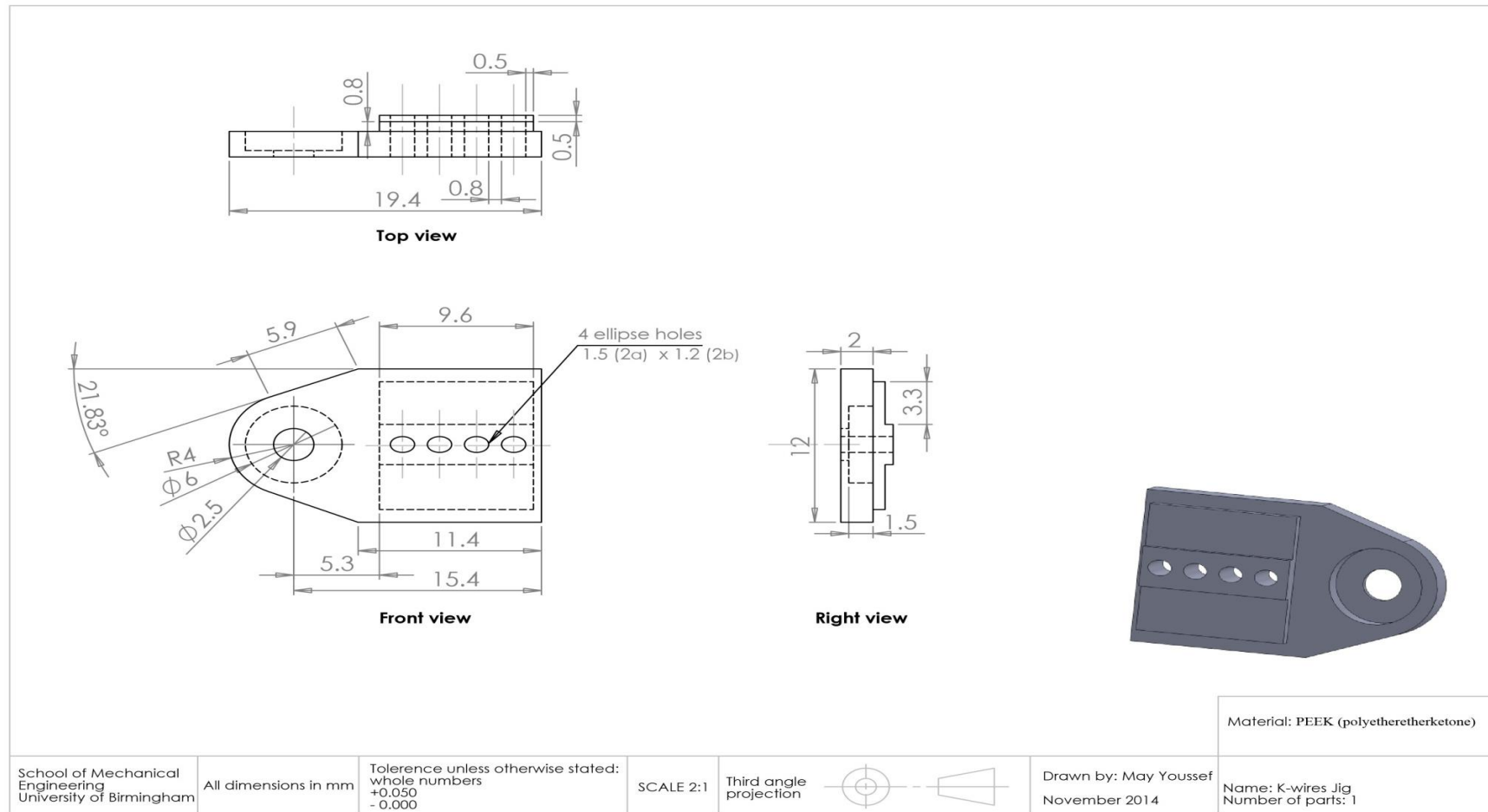


Figure 4-45. Drawing of the jig.

## 4.6 Discussion

A new external dynamic finger fixator based on development of the Compass hinge was designed. Areas that have been improved include replacing parts previously manufactured from a polymer with a metal so that the parts had greater strength. Further, PEEK (65 MPa at 5 Hz, 20°C and  $>10^7$  cycles) has been chosen for the remaining polymer parts rather than polyetherimide (PEI) (24 MPa at 5 Hz, 20°C and  $>10^7$  cycles) where the fatigue endurance limit for PEEK is approximately three times higher than PEI (Trotignon *et al.*, 1993).

Another aspect of the design that has been changed is reducing the dimensions of the device compared to the Compass hinge (see chapter 3 section 3.3.1). With the new design, the width has been reduced by 4 to 19 percent and the thickness by 26 percent where the design was based upon the medium (50% percentile) human hand size required. The dimensions for a medium size device are 47.5 mm width, 35.5 mm height and 8.5 mm thickness. The dimensions of the device are based on the anthropometry data of the human hand (Tilley and Associates, 2002; BS EN ISO 7250-1; Peebles and Norris, 1998; Alexander and Viktor, 2010). These dimensions were derived by calculating the overall average dimensions from the 50% percentile hand data for both men and women which were presented by the study of Tilley and Associates (2002). BS EN ISO 7250-1 is intended to serve as a guide for hand anthropometric terms definitions and basic measurements. The new device fixator would be required to be available in a range of sizes to take into account the different sizes of human fingers. The study which was presented by Alexander and Viktor (2010) about the human fingers phalanges lengths measurements was helped in specifying the different sizes of the new device. Three sizes that relate to different design criteria are suggested for the new

device as medium (M) designed for average, small (S) and large (L). In order to enable surgeons to determine which size of device to use, table 4-4 will guide them.

**Table 4-4.** The protractor hinge device size guide.

Device size	Middle phalanx length (mm) (Alexander and Viktor, 2010)
Small (S)	< 20
Medium (M)	From 20 to 26.5
Large (L)	$\geq 26.5$

The proposed guidance depends on the middle phalanx length of the patient. Anatomically the medial phalanx length for each digit is less than the proximal phalanx length (Alexander and Viktor, 2010) so the device size which fits the middle phalanx length will cover the proximal phalanx length as well. X-ray is suggested to help surgeons measure the patient's phalanx length to select the suitable size of device. The new device which is presented in this study was medium in size and for the other sizes, small and large, it was suggested that the only parts to have different dimensions are the slotted and solid clamping blocks (see section 4.5.2.6). For the small size (S) device, the length of the slotted part will be 14.6 mm and the solid part will be 12.9 mm. In the large (L) size, the length of the slotted part will be 20.6 mm and the solid part will be 18.9 mm.

The new device design also helps to overcome some of the disadvantages of the Compass hinge. The new design avoids slippage between the main device frame and blocks compared with the Compass hinge design. The part which the PIP Joint center pin is inserted is now

manufactured from a radio-lucent polymer which can be seen under x-ray rather than the radio-opaque metal used in the Compass hinge device.

The number of screws used was reduced to four and these are more accessible compared with those in the Compass hinge. To loosen and tighten the screws will be by the use of a standard dimension hexagonal head tool.

The worm gear has guide marks in the new finger device to aid the user in the amount of turns performed which is an advantage not found in the Compass hinge. As the new design has less parts the assembly during surgery is likely to be quicker.

The new device can be attached to both left and right hands on both the medial and lateral sides of the phalanx. With the compass hinge device this was not possible. The comparison between the 3D design of the Compass hinge device and the PIP joint protractor hinge device is shown in Figure 4-46.

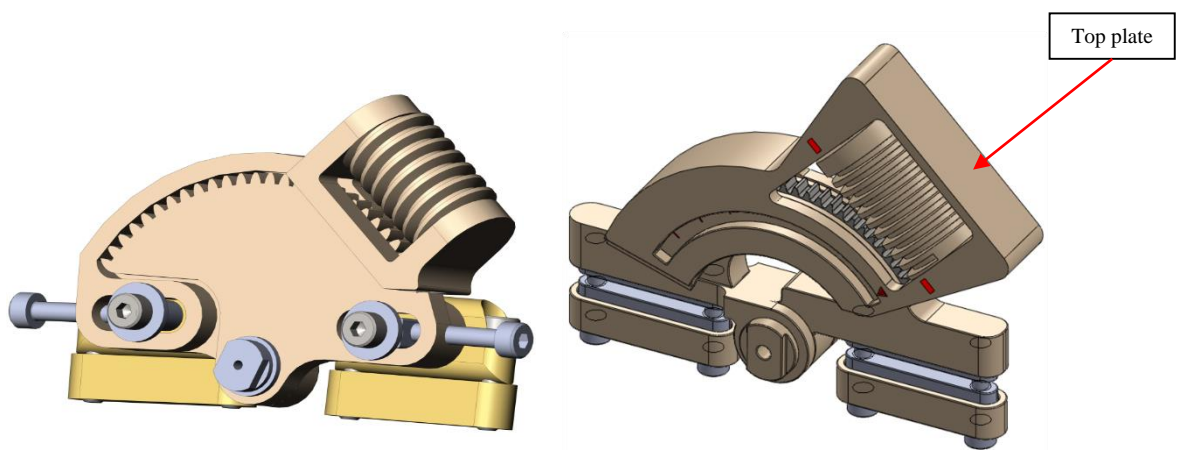


**Figure 4-46.** 3D design of the Compass hinge device (left) and the PIP joint protractor hinge device (right).

A top plate was designed to stop the worm gear from totally detaching from the device when the gear has been disengaged to enable the patient to undertake active motion.

## **4.7 Summary**

A new fixator based on development of the Compass hinge consists of 17 parts where 8 of them (proximal and distal protractor hinge parts, worm gear, screw 1 and nut 2, rod and 2 slotted clamping blocks) are to be made from a radiolucent medical grade plastic VICTREX® PEEK 90G. The stainless steel 316LS medical implant alloy, 90% cold worked was selected for the remaining components (worm wheel, four solid clamping blocks and four connection screws). A complete engineering analysis of the new designed device was required to determine its likely performance and this will be presented in the next chapt

# CHAPTER 5

## ENGINEERING ANALYSIS OF THE NEW DEVICE DESIGN

## **5 ENGINEERING ANALYSIS OF THE NEW DEVICE DESIGN**

### **5.1 Chapter overview**

In this chapter the engineering analysis of the new finger fixator is presented. In § 5.2 the finite element analysis for the new device components are presented. The risk assessment for the proposed design is presented in § 5.3 before the manufacturing method is explained in § 5.4. The mechanical testing is presented in § 5.5, followed by the discussion of the engineering analysis in § 5.6. Finally, a brief summary of the whole chapter is provided in § 5.7.

### **5.2 Finite element analysis**

Finite element analysis of the device was conducted to verify the proposed design. The finite element method allows the stress distribution and any deformation of a loaded structure to be assessed, before an expensive prototype is produced, which reduces the cost of development.

SolidWorks Simulation (SolidWorks 2011, Dassault Systèmes SolidWorks Corporation, Waltham, USA) was used to undertake the finite element analysis. The solid model consisted of the distal protractor hinge part assembled with the worm wheel, proximal protractor hinge part and both solid and slotted clamping blocks. The model was meshed with a total of 201,446 tetrahedral elements, which depended on the gear teeth fixation positions; this number was determined following mesh converge testing. Constraints were then applied to the model (Figure 5-1) as follows:

- The pivoting joint hole was constrained to allow rotation;
- Four gear teeth were fixed in all directions to simulate the gear teeth in engagement with the worm gear;
- The force was applied to the model either vertically downwards through the metal solid block part or perpendicular to the middle phalanx of the finger.

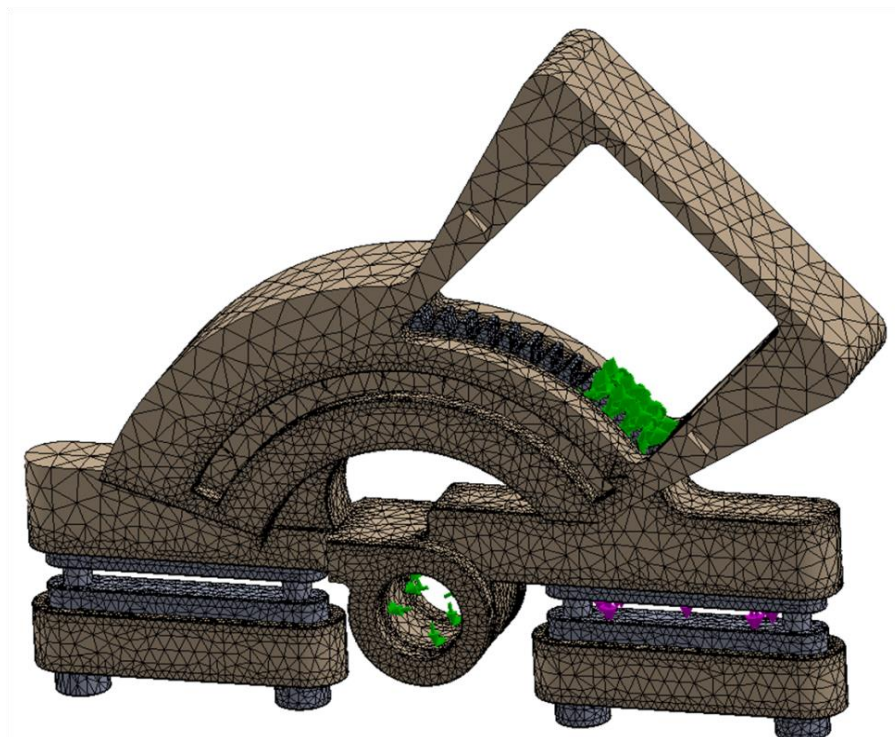
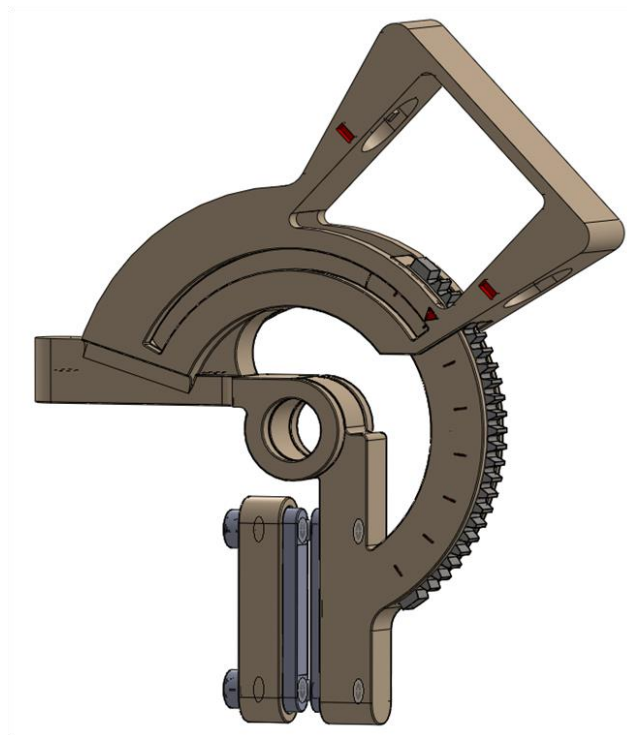
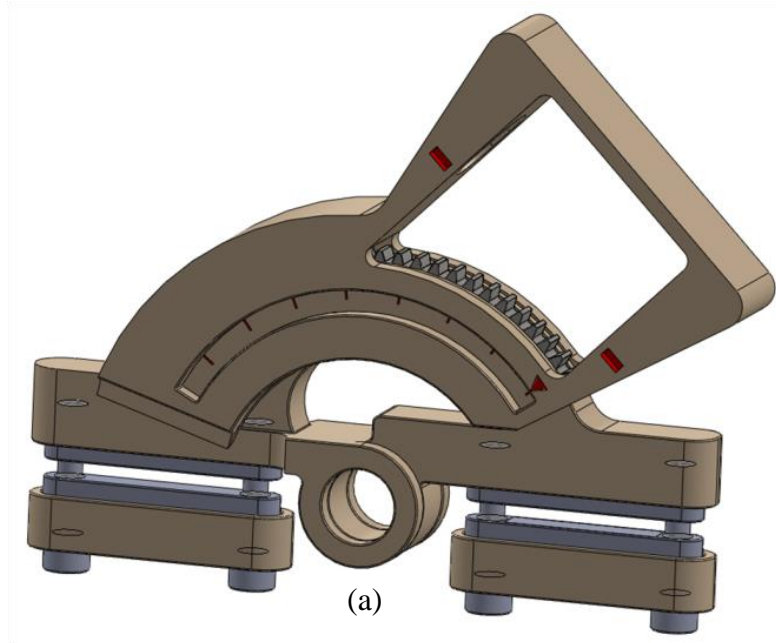


**Figure 5-1.** Meshed finite element model with the load of 210 N applied and constraints applied at position 1 with the gear teeth fixed at 15 - 30°.

Two different positions of engagement with the worm gear were investigated: position (1) teeth between  $15$  and  $30^\circ$ ; position (2)  $90$ - $105^\circ$  as two extreme gear teeth fixation positions (Figure 5-2).



(b)

**Figure 5-2.** Two different positions of engagement with the worm gear (a) position 1 gear teeth fixed at  $15 - 30^\circ$  (b) position 2 gear teeth fixed at  $90 - 105^\circ$ .

A force of 210 N was applied to the model to simulate the likely force a human could apply to the device, based on literature values for different finger activities (see chapter 2 section 2.3). Von Mises stress theory was selected for analysing the stresses in the model as the model materials were metal and PEEK (Semi-crystalline microstructure). Materials are classified as ductile materials for that reason von Mises failure criterion is appropriate theory and enables an accurate result (Collins, 1993). In the finite element analysis section for the Compass hinge device (see chapter 3 section 3.2.4) the maximum principle stress theory was selected for analysing the stresses in the Compass hinge device's models as the material was PEI.

### 5.2.1 Results

The results from the simulation analysis for the model showed that stress patterns were similar for the two positions of the fixed gear teeth. For the two cases the maximum value of the stress was 242.9 MPa and it was located along the screws which connect the blocks together with the distal protractor hinge part. The stresses in the models in the metal and polymer parts are less than the yield strength (946 MPa for 316LS stainless steel and 110 MPa for PEEK, respectively) (MatWeb, material property data; GE Plastics VICTREX®) and the fatigue strength of the selected materials for those parts ( $< 65$  MPa and 270 MPa at  $>10^7$ , 5 Hz for PEEK and stainless steel, respectively) (Trotignon *et al.*, 1993; BSSA, Fatigue resistance). Figure 5-3 and Figure 5-4 show the stress distribution patterns at position 1 with the gear teeth fixed at 15 - 30° and position 2 with the gear teeth fixed at 90 - 105° with a load of 210 N.

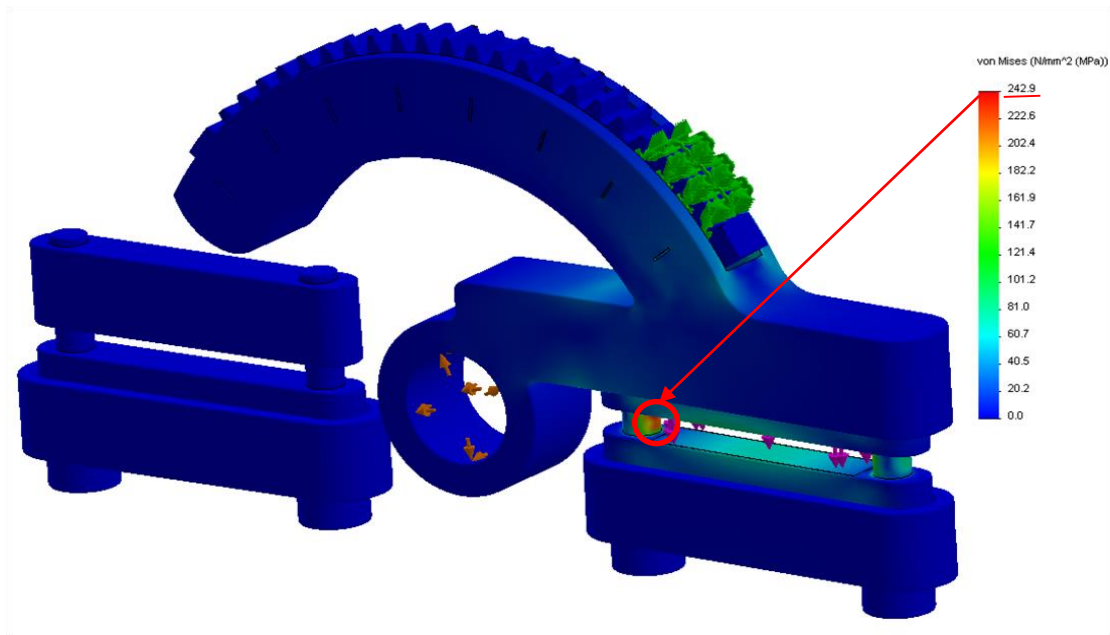


**Figure 5-3.** Distribution of stresses in the model for position 1 gear teeth fixed at 15 - 30°.

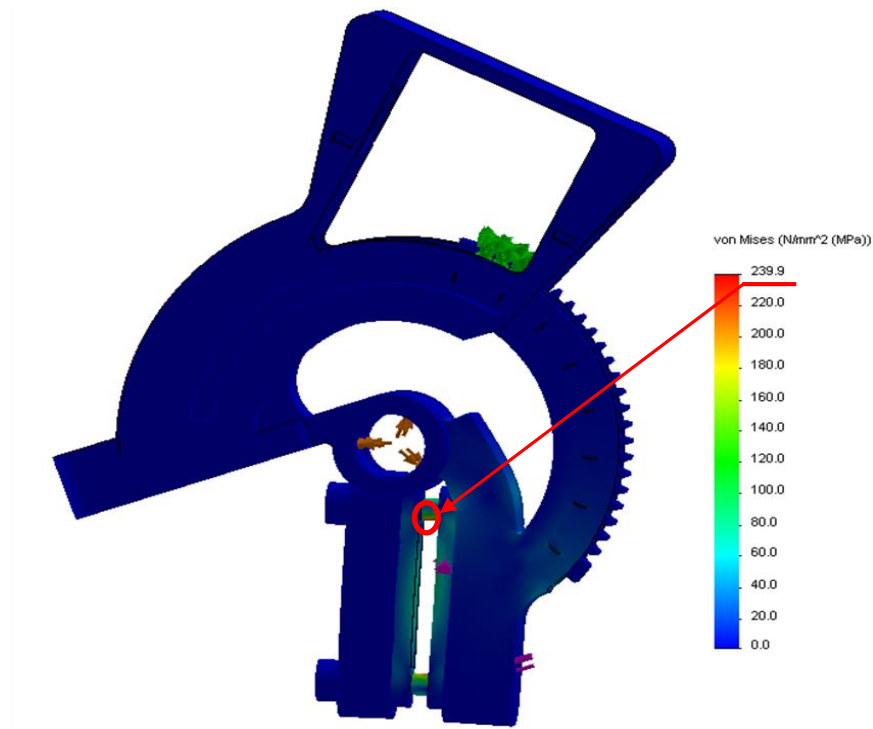


**Figure 5-4.** Distribution of stresses in the model for position 2 gear teeth fixed at 90 - 105°.

Further stress distribution patterns were studied by checking the Iso clipping analysis (the property manager in SolidWorks allows stresses of a specified value to be plotted) at different stress values with a load of 210 N:

- at the PEEK yield strength value of 110 MPa;
- at the PEEK fatigue stress endurance limit value of 65 MPa.

The high values of the stresses ( $> 110$  MPa) were located along the screws and metal solid blocks. Figure 5-5 shows the FEA Iso Clipping at 110 MPa with a load of 210 N. FEA Iso Clipping at 65 MPa at position 1 with the gear teeth fixed at  $15 - 30^\circ$  with a load of 210 N is shown in Figure 5-6. Figure 5-7 is the FEA Iso Clipping at 65 MPa in position 2 with the gear teeth fixed at  $90 - 105^\circ$  with a load of 210 N.

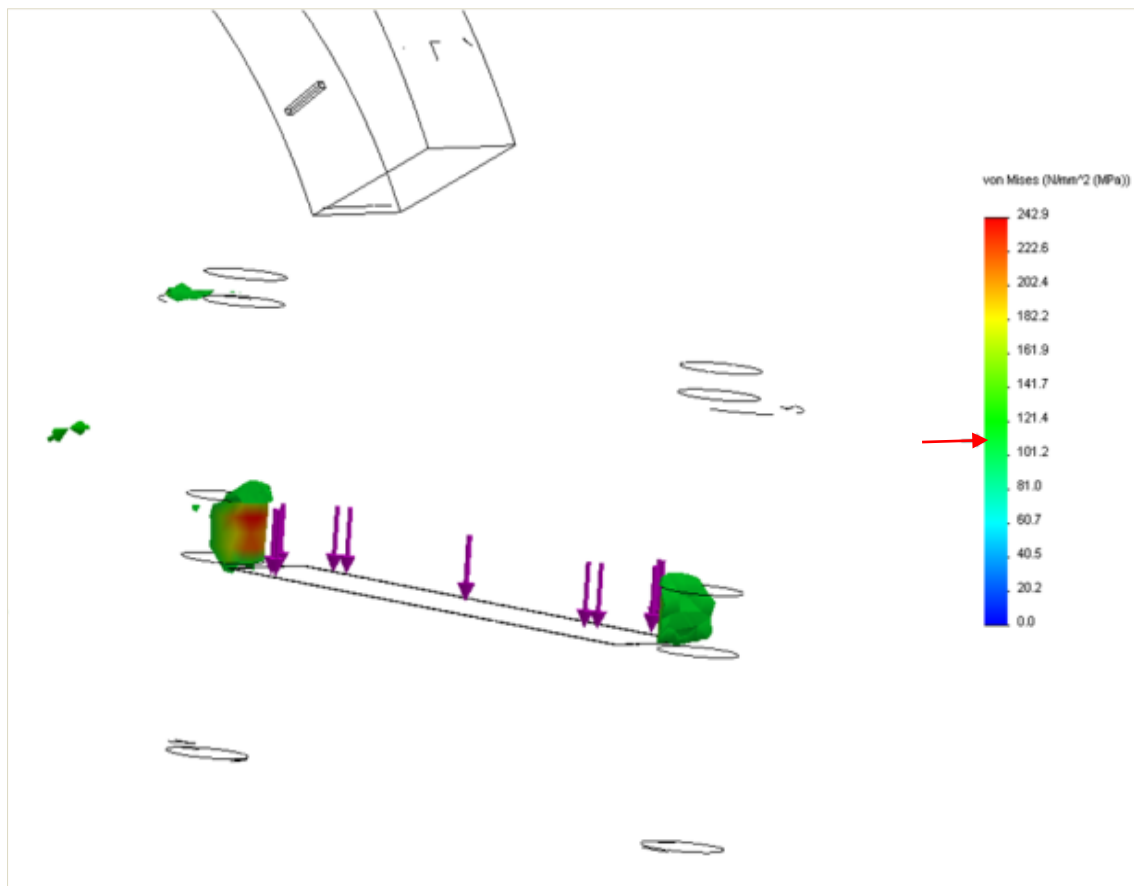


**Figure 5-5.** FEA Iso Clipping at 110 MPa with the gear teeth fixed at 15 - 30°.

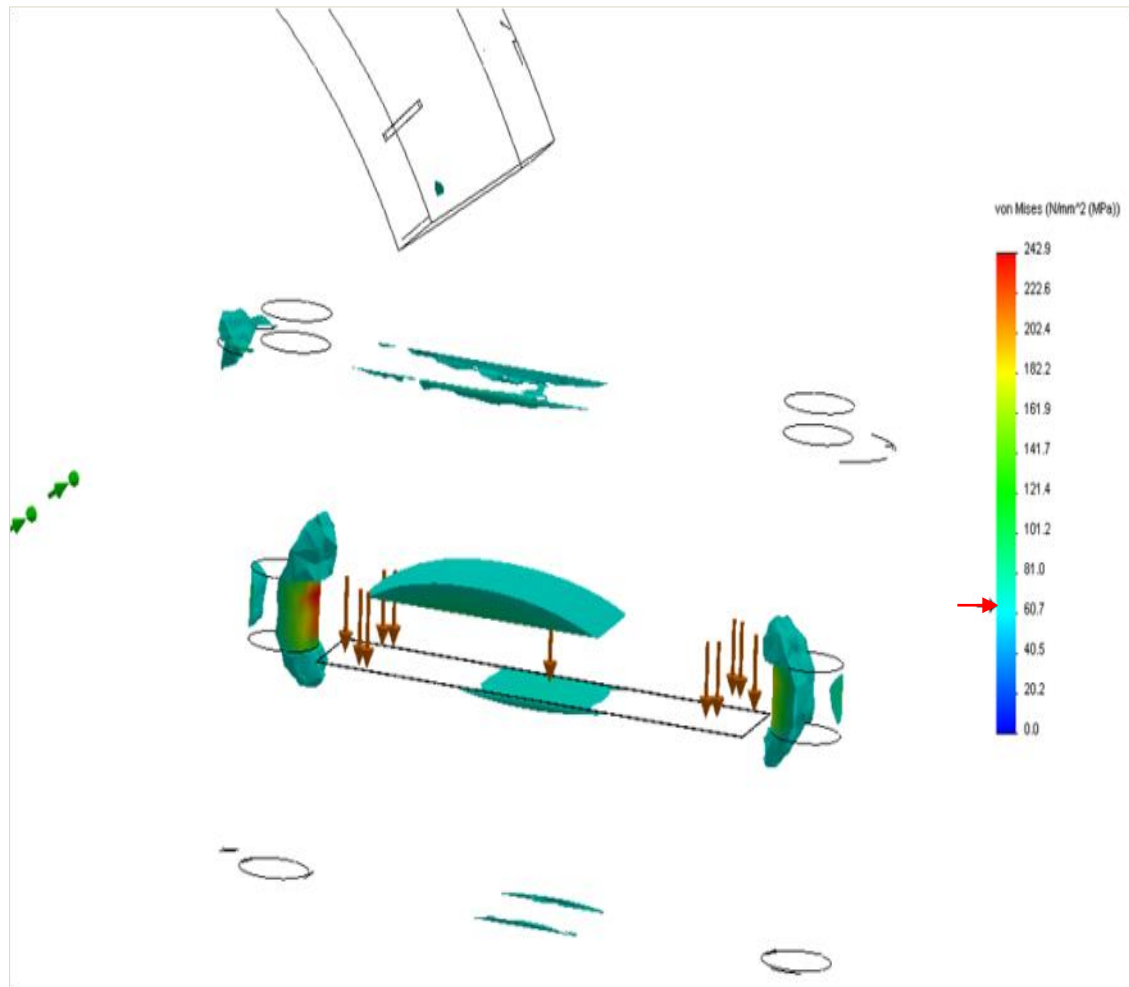


**Figure 5-6.** FEA Iso Clipping at 65 MPa with the gear teeth fixed at 15 - 30°.

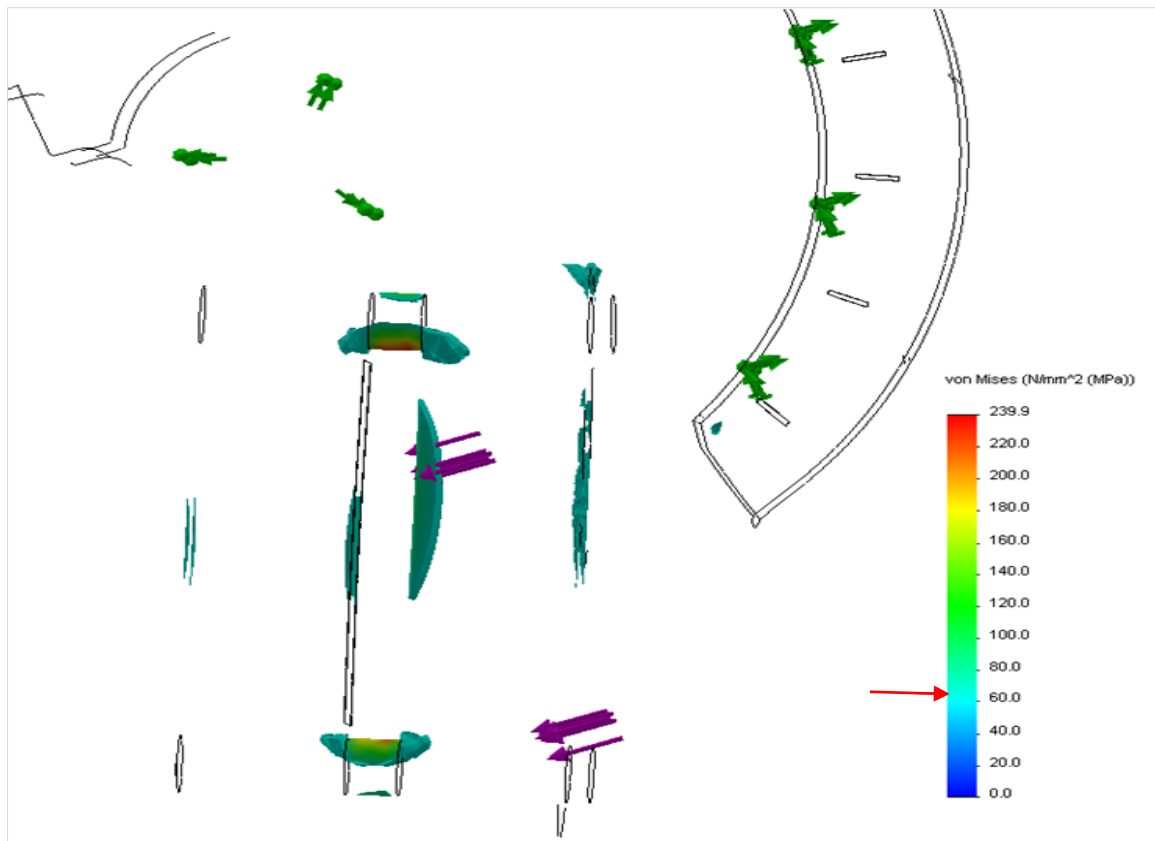


**Figure 5-7.** FEA Iso Clipping at 65 MPa with gear teeth fixed at 90 - 105°.

## 5.3 Risk analysis

### 5.3.1 Undertaking risk analysis

Once the characteristics of the medical device have been defined, it is necessary to identify all the possible hazards associated with the device such as hazards related to the use of the device (labelling, packaging and instructions for use), biological hazards (bio-incompatibility) and energy hazards (moving parts and mechanical force). It is important to

balance risk against benefit. High level risks must be identified to reduce them to an acceptable level that may include redesigning parts of the medical device, making the user instructions clearer or improving the device packaging.

A report on the risk analysis is produced so that a decision can be made towards the risks associated with the device are within the acceptable levels or are outweighed by the benefits to the patient. It is important to review the risk analysis at regular intervals during the development process.

Many techniques, such as Failure Mode Effect Analysis (FMEA) and Fault Tree Analysis (FTA) can be used in a risk analysis (Viceconti *et al.*, 2009). For each potential hazard associated with a medical device, there is a frequency of occurrence “O”, a severity of failure “S” and an ability to detect the failure “D”. Each of these elements was rated on a scale from 1 to 10 (Suresh *et al.*, 2014), for the hazards identified for the PIP joint protractor hinge device, as shown in table 5-1. A risk priority number was then calculated by multiplying the three ratings together.

**Table 5-1.** Rating of occurrence, severity and detection for potential hazards.

Rating	Occurrence “O”	Severity “S”	Detection “D”
1	Remote	No harm	Almost certain
2			
3	Low remote	Minor - unnoticed by customer	
4			
5	Moderate	Low - Customer notices	Easily spotted
6			
7	High	High - Customer complains	
8			
9	Very high	Device will not function at all	
10		Serious injury	Absolute uncertainty

### **5.3.2 Risk analysis of the PIP joint protractor hinge device**

The risk analysis should be considered for the individual parts of the assembly as well as the device as a whole. Sterilization, packaging and labelling are important, but are not being considered during this study, as only design was concerned. The results are presented in Table 5-2.

### **5.3.3 Design description and characteristics**

The characteristics of the new PIP joint protractor hinge device are:

- I. It is intended for external implantation for the diseased or damaged proximal interphalangeal joint. It is intended to extend the human digits and improve functionality of the joint.
- II. It is intended to be used by surgeons familiar with finger joint contractures.
- III. The selected design is a worm and worm wheel mechanism controlled design which consists of 13 assembled parts (see chapter 4 section 4.5.1).

### **5.3.4 Identification of hazards and estimation of risks**

The identification of the prospective hazards was carried out and the FMEA was used for the estimation of the risk of any hazards. The results of this procedure are presented in table 5-2. The estimation of the risk was made based on the risk priority number (RPN). As can be seen in table 5-2, the risk analysis identified that pin infection and the worm wheel part as a potential source of unacceptable hazards with a RPN of 560 and 300, respectively.

**Table 5-2.** Results of risk analysis.

Item	Function	Possible hazard or failure mode	Effect of hazard or failure	Causes of hazard or failure	O	S	D	RPN	Action to reduce or eliminate risk
Proximal protractor hinge	Main frame of the device	Wear	Loose connection between the proximal and distal parts	Sliding motion of the distal part to enable the required joint range of motion	2	3	2	12	Design tolerances to be considered
>>	>>	Breaks	Top plate part de-attached	Patient exerts a high force to disengage the gears	2	4	6	48	Clear instructions for patients
>>	>>	Wear	Loose connection between the proximal and the rod part	Repeated unnecessary engagement /disengagement of the worm gear	3	2	3	18	Redesign part geometry
Distal protractor hinge	Range of movement (ROM) guide	Breaks	Device non functional	Cyclic bending moment	1	3	1	3	Suitable material & geometry
>>	>>	Breaks	Inaccurate ROM	Assembly process with worm wheel fault	1	2	1	2	Assembly process steps should be provided
Worm wheel	Transfer the motion to the distal part via meshing with the worm part	Breaks	Device non functional	Cyclic bending moment between the gear teeth	5	10	6	300	Suitable material & geometry

Worm gear	Transmit the high torque to enable device motion	Wear	Device non functional	Excessive engagement and disengagement actions of worm with worm wheel	2	8	8	128	Suitable material & Clear instructions for patients
Rod	Connect the worm gear with the proximal part	Wear	Device non functional	High force exerted by patients to engage/disengage the worm gear	1	8	8	64	Suitable material & design
Solid clamping blocks	Clamp the K-wires	Wear	Loose K-wires	tightened /untightened actions of connecting screws	6	4	5	120	Suitable material
Slotted clamping blocks	Solid blocks housing & more support to clamp the K-wires	Breaks	Device non functional	Surgeons over torque the connecting screws	6	5	5	150	Adequate training and instructions for use to be supplied
>>	>>	Damage	>>	Manual assembly process fault with the solid blocks	3	2	3	18	Assembly process steps should be provided
Screw 1	Radiolucent device axle	Wear	Inaccurate device function	Tighten action to assemble screw1 with nut 2	4	2	2	16	Suitable material & instruction for use provided
Nut 2	Radiolucent device axle	Wear	Inaccurate device function	Distal part rotational motion	3	2	2	12	Suitable material selection
The PIP joint protractor hinge device	Treat the contracture of the PIP joint	Inadequate performance	Device non functional	Design problem	4	8	5	160	Re-evaluate the design process

>>	>>	Pin infection	Severe pain/ death	Insertion of K-wires	8	10	7	560	Suitable material selection & Surgeon advice (area around the wires should be clean / medicine)
>>	>>	Breaks	Device non functional	Stored and handled in the wrong way	2	2	2	8	Safety instructions should be followed
>>	>>	Deformations in device parts	>>	Apply wrong Sterilization Technique	2	2	2	8	Sterilization procedure should be followed for each part material

## **5.4 Manufacturing**

### **5.4.1 Techniques**

A three-dimensional (3D) printing technique, Computer numerical control (CNC) machining, injection molding process and electrical discharge machining (EDM) were considered to manufacture the prototypes of the new device parts. With regards to the fine detail dimensions of the designed components (see chapter 4 section 4.5) the 3D printing technique was selected rather than other traditional manufacturing techniques (e.g. CNC, EDM and injection molding). For the metal parts CNC and EDM should be advanced enough processes to offer the required part resolutions (minimum thickness is 0.7 mm) and complex geometry. Unfortunately, these machine tools were not available in the University of Birmingham's laboratories (technicians at the Mechanical Engineering School, University of Birmingham confirmed that). The injection molding forming process for polymer parts would be used in the case of mass production rather than rapid prototypes due to the high cost of this process where a die design and its manufacturing process were required to get a pattern to manufacture the parts. At this stage of the study, the communication was started with a number of manufacturing companies in the United Kingdom, Europe and United States to discuss with them the alternative techniques to manufacture both metal and polymer parts. Most of the companies such as Solid Concepts Inc. - A Stratasys Company, Los Angeles, USA and Proto Labs, Ltd., Shropshire, United Kingdom recommended 3D printing technology due to the complexity of the parts and the low mass production required.

3D printing is a methodology using 3D Computer Aided Design data to produce the 3D model. This process is also referred to as additive manufacturing (AM), rapid prototyping (RP), or solid free-form technology (SFF) (Ventola, 2014). The principle of rapid prototyping is to build a 3D physical model from the 3D computer models by the addition of material layers to check and validate product design (Ahmad *et al.*, 2015). The advantages presented by 3D printing are (Pîrjan and Petroșanu, 2013):

- The possibility of creating in a short timeframe the complex 3D objects with fine details from different materials;
- The material waste is almost zero;
- It is easy to print small movable parts.

The type of 3D printer chosen for an application often depends on the materials to be used and how the layers in the finished product are bonded. The technical type classification includes Stereolithography (SL), selective laser sintering (SLS), 3D printing (Binder-Jet), fused deposition modeling (FDM), direct metal laser sintering (DMLS), laminated object manufacturing (LOM) and electron beam melting (EBM) (Choi and Kim, 2015).

The 3D printers are currently limited to using only a handful of engineered materials, mostly plastics and a few metals. The plastic materials are generally of low quality and not suitable for most production products due to their limited strength, toughness, surface quality, and UV degradation properties. The 3D printing technique can produce visible layer lines on side walls and tool paths on the top and bottom surfaces. These can be eliminated, but that requires additional post-processing, such as an automated finishing station or some manual finishing Solid (Concepts Inc. - A Stratasys Company, Los Angeles, USA).

A major disadvantage of 3D printing is its high cost and sometimes, the build quality of 3D printed parts is lower than if it had been traditionally manufactured where the final product can have flaws that might affect not only the object's design, but also its functionality. (Pîrjan and Petroşanu, 2013).

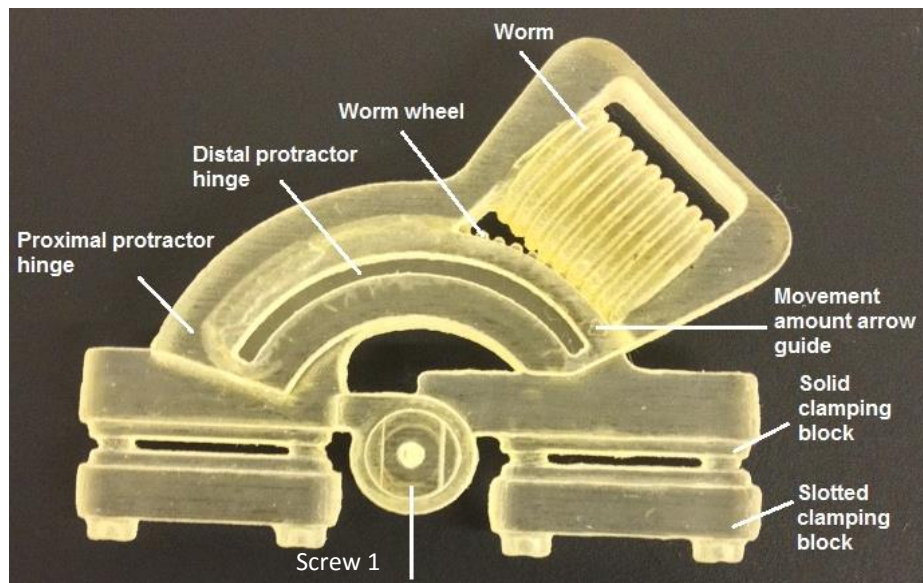
Wu *et al.* (2015) presented a recent study to investigate the effect of the layer thickness on mechanical properties of 3D-printed PEEK samples. The experiments confirmed that the layer thickness had a marked effect on tensile, compressive and three-point bending properties. The results showed that 3D-printed PEEK had high mechanical properties. They mentioned that the mechanical properties of 3D-printed PEEK parts may be improved by increasing the control accuracy and hardware precision of the 3D-printing system. Their experimental studies and comparative analyses were carried out to study the factors affecting PEEK 3D print forming quality, hoping to provide reference conditions under which to print PEEK. Pore formation during the printing process is still required, including further research to reduce it and to improve interlayer bonding. They believed that PEEK may be a significant and promising material for industrial applications of 3D-printed components.

## 5.4.2 Models

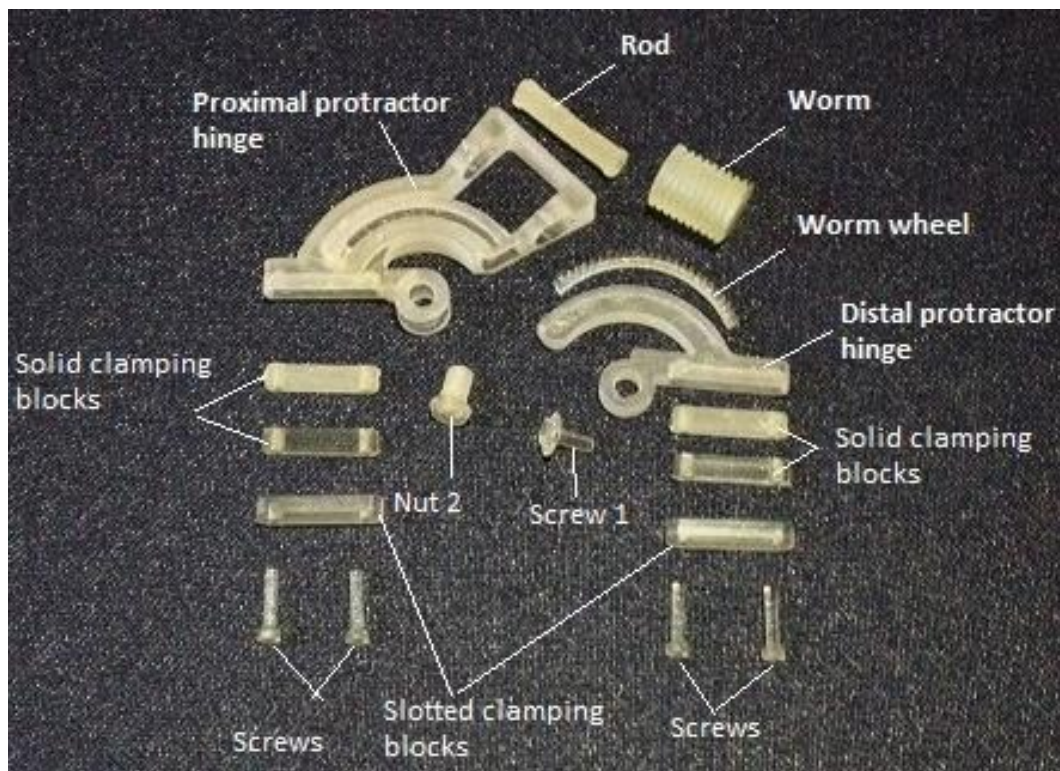
### 5.4.2.1 Rapid prototype model

Two solid rapid prototype models were manufactured using an Eden 250 3D Printer (Objet, Billerica, USA) and made out of an acrylic monomer based resin (brand name Fullcure 720) in the School of Mechanical Engineering, University of Birmingham (Birmingham, UK). One of these models was a 3D assembled solid model as a single part (Figure 5-8) and another was manufactured with separate parts which required assembly (Figure 5-9). These prototypes were manufactured for the purpose of:

- Checking the dimensions of each part;
- Confirming the working mechanism of the device;
- Checking the consistency and fitting together of the assembled parts of the device;
- Approving it from the medical point of view (shape, accessibility and functionality) according to the surgeon feedback.



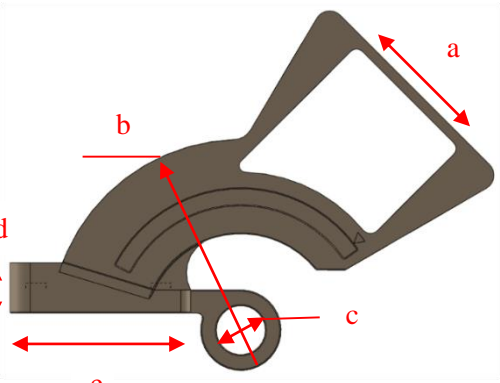
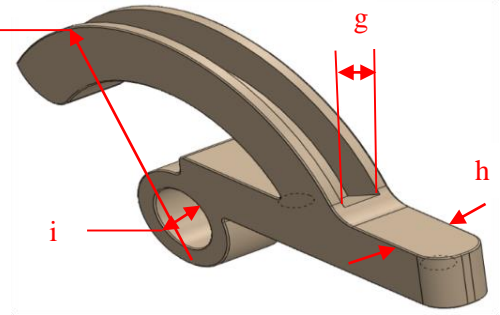
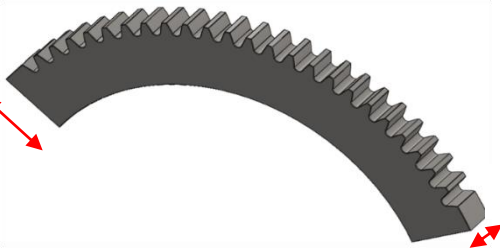
**Figure 5-8.** Rapid prototyping model of the PIP joint protractor hinge device.

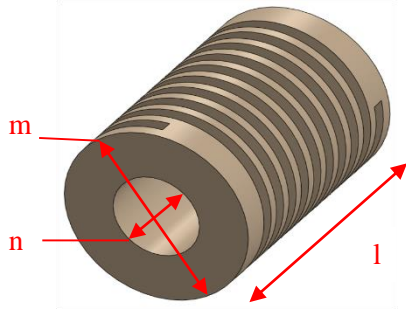
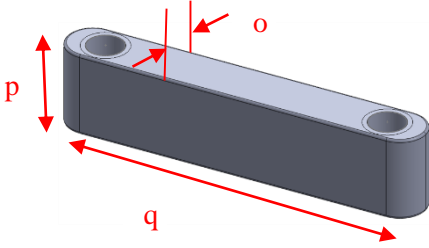
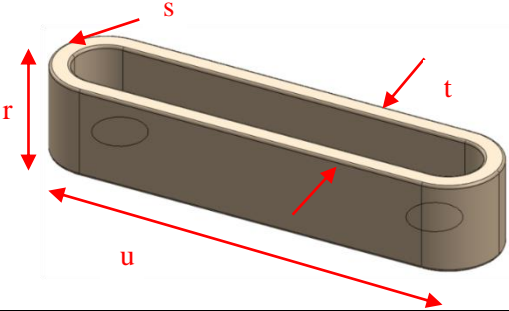
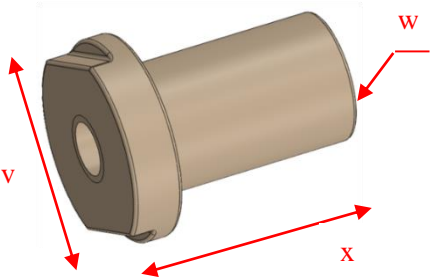


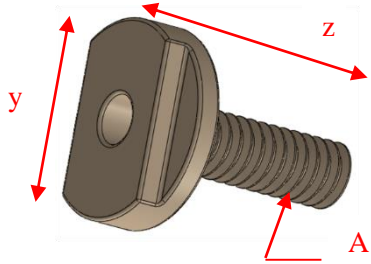
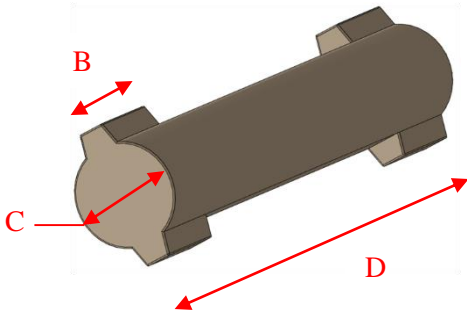
**Figure 5-9.** Disassembled rapid prototyping model of the PIP joint protractor hinge device.

The whole printed model (width, length and thickness) and all printed separate parts dimensions were measured using a digital vernier caliper (Hilka Tools (UK) Ltd, Surrey, UK) and the measurement results approved the design. An example of the comparison between the designed dimensions and average measured dimensions (refer to the prototyped parts in figure 5-9) for each part shown in table 5-3. The thread pitch for worm gear and screw 1 were checked by the thread gauge and the dimensions were confirmed. Some dimensions were slightly larger than designed and were adjusted manually using sand paper.

**Table 5-3.** Comparison between the designed and measured dimensions.

Part name	Symbol	Designed dimensions (mm)	Average measured dimensions (mm)
Proximal protractor hinge part 	<b>a</b>	14.5	14.49
	<b>b</b>	23	23.05
	<b>c</b>	4.9	4.87
	<b>d</b>	4.9	5.04
	<b>e</b>	18	18.03
Distal protractor hinge part 	<b>f</b>	19.6	19.56
	<b>g</b>	2.5	2.46
	<b>h</b>	4	4.17
	<b>i</b>	4.9	4.82
Worm wheel 	<b>j</b>	4	3.98
	<b>k</b>	1.9	1.97

<p>Worm</p> 	<b>l</b>	14.3	14.28
	<b>m</b>	9.8	9.77
	<b>n</b>	4.6	4.55
<p>Solid clamping block</p> 	<b>o</b>	2.4	2.37
	<b>p</b>	3.4	3.50
	<b>q</b>	15.9	15.86
<p>Slotted clamping block</p> 	<b>r</b>	3.3	3.70
	<b>s</b>	R 2	2.10
	<b>t</b>	4	4.13
	<b>u</b>	17.6	17.63
<p>Nut 2</p> 	<b>v</b>	6	5.93
	<b>w</b>	D 4.7	4.78
	<b>x</b>	7.5	7.54

 <p>Screw 1</p>	<b>y</b>	6	6.01
	<b>z</b>	7.9	7.92
	<b>A</b>	M3	3.04
 <p>Rod</p>	<b>B</b>	3.2	3.19
	<b>C</b>	3	3.01
	<b>D</b>	21	21.09

The teeth meshing between the worm and worm wheel was tested by assembling the two parts together and the worm was turned manually (Figure 5-10). The worm and worm gear working mechanism (active and passive movements) was found to be controlled and confirmed.

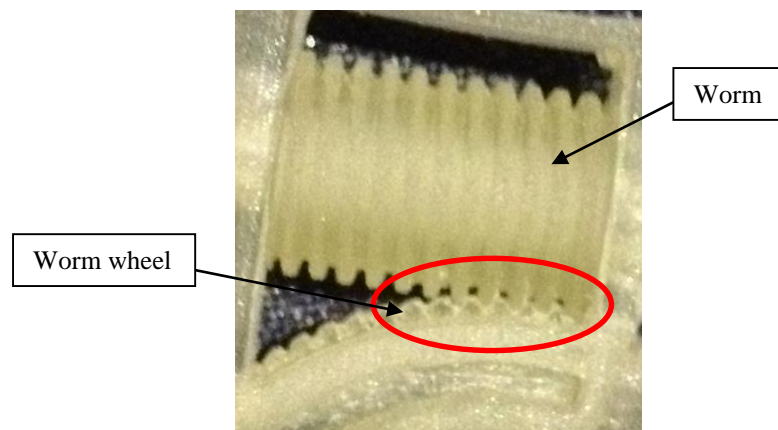


**Figure 5-10.** Worm and worm wheel teeth meshing.

The assembly process was done manually for the printed parts to check the tolerance fit for all parts which were assembled together.

A review meeting with Mr. Garth Titley (Consultant Plastics and Burns Surgeon at the Queen Elizabeth Hospital, Birmingham) about the prototype model was undertaken to gain his feedback; he approved the whole size of the new device and its thickness (8.5 mm) which allows the device to be implemented in the central digits easily. The worm and worm wheel mechanism achieves the continuous active and passive movements which is the main idea of the treatment process. The overall device feature with the marks used to guide to angle (see chapter 4 Figure 4-16) on the frame was strongly acceptable to be a digit fixator from the medical point of view.

#### 5.4.2.2 Working model

To assess the design, a working model of the finger fixator was manufactured (Figure 5-11). All parts were manufactured by Solid Concepts Inc. (A Stratasys Company, Los Angeles, USA). Selective Laser Sintering (SLS) was used to manufacture the polymer parts from NYTEK TM 1200 CF which is carbon filled nylon (Solid Concepts Inc.- A Stratasys Company, Los Angeles, USA). This material has similar mechanical properties to PEEK and was used as PEEK was not available for manufacture using SLS. For manufacturing the metal parts, Direct Metal Laser Sintering (DMLS) was used, and they were manufactured using stainless steel 17-4PH composition. The worm gear material was replaced from polymer to stainless steel 17-4PH composition as the Solid Concepts Inc. SLS machine did not allow to manufacture the dimensions of the worm. After manufacturing, it was found that the resolution of the DMLS technique was not sufficient to enable the worm gear to mesh with worm wheel part (Figure 5-12). Subsequently, the worm gear part was manufactured using an Eden 250 3D Printer (Objet, Billerica, USA) and made out of an acrylic monomer based resin (brand name Fullcure 720). Figure 5-13 shows the working model used in the mechanical test to evaluate the new device design.



**Figure 5-11.** External dynamic protractor hinge fixator working model.

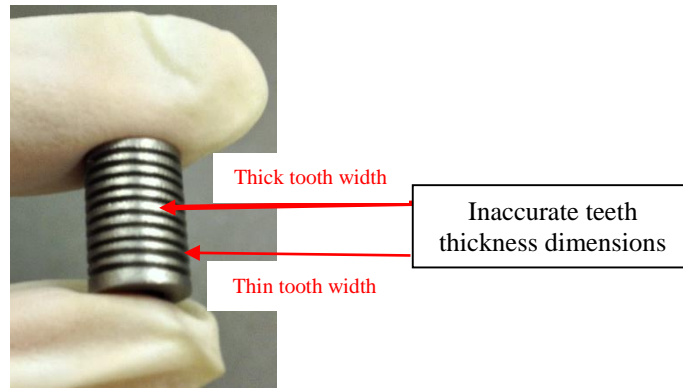


**Figure 5-12.** A manufactured worm gear by stainless steel 17-4PH composition, Solid Concepts Inc.

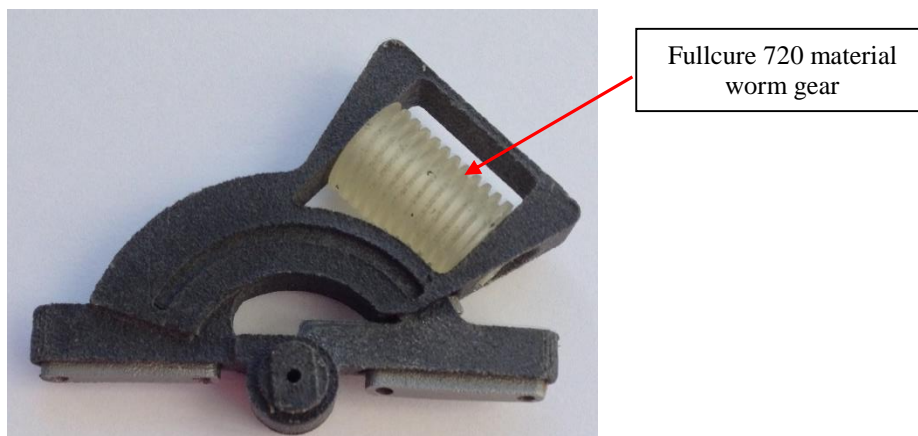


**Figure 5-13.** The mechanical test model

## 5.5 Mechanical testing

To validate the new device, the working model was subjected to the cyclic mechanical testing. The experimental test for the new device was guided by ASTM F1541-02. Section A4 of ASTM F1541-02, which describes the test procedure for external skeletal fixator joints was used in selecting the cyclic bend test.

### 5.5.1 Testing equipment

Mechanical testing of the working model was undertaken using a Bose ElectroForce® 3330 Series II Test Instrument (Bose Corporation, ElectroForce Systems Group, Eden Prairie, Minnesota, USA) run using Win Test software (Figure 5-14). The testing machine is designed with an electromagnetically controlled actuator which is able to move vertically up and down. The top and bottom plates can be manually moved up and down and be fixed at any desired position within this distance. The machine has a maximum range of motion of 25 mm and can be controlled in two ways: either statically between set displacements or cyclically with a number of alternating loading waveforms such as sine waves, square, triangles and ramp loading. Cyclically the machine can operate at a maximum frequency of 100 Hz. According to the manufacturer's specifications, this equipment has a peak dynamic force of  $\pm 3000$  N (Bose 1010CCH-1K-B) and a static force capacity of  $\pm 2100$  N.

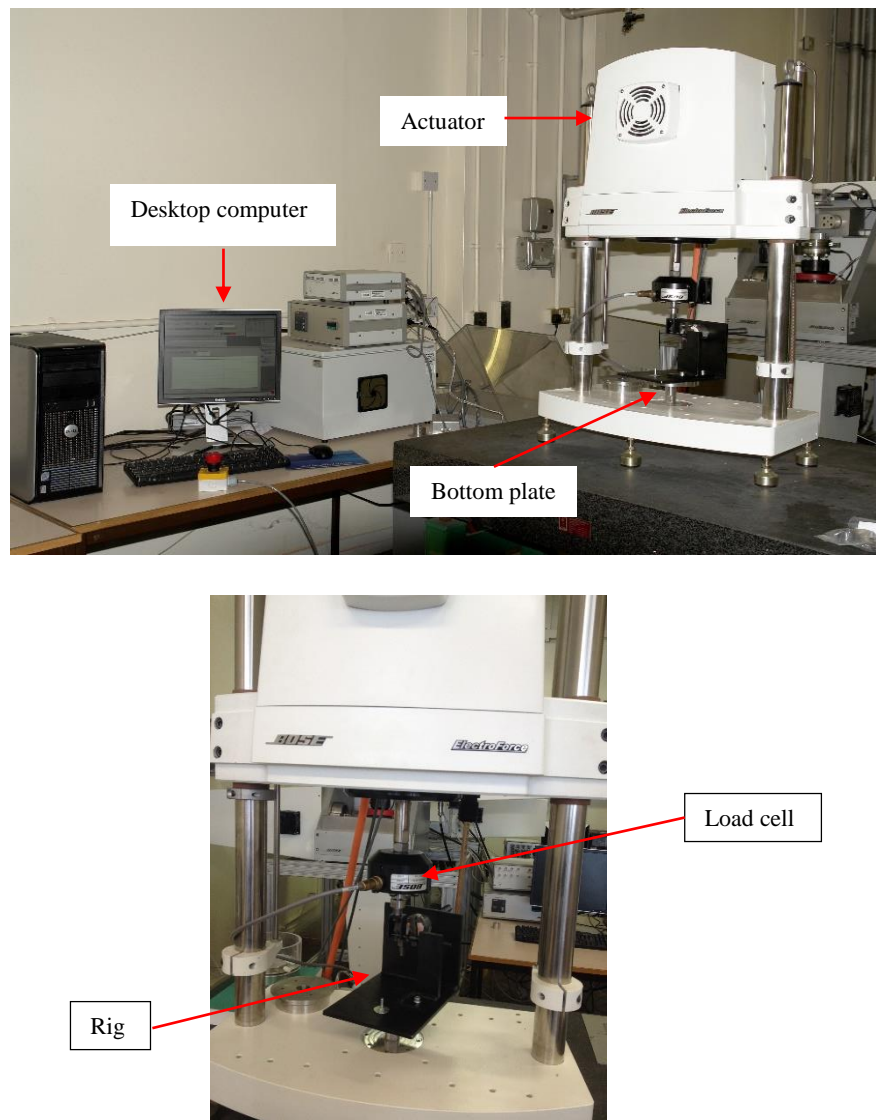


**Figure 5-14.** The Bose ElectroForce® 3330 Series II Test Instrument.

### 5.5.2 Testing setup

A rig was designed to enable the fixator to be held in position and subjected to mechanical loads. The rig consists of 5 parts: main frame, support frame, cup, load rod and wire. All these parts were manufactured by Proto Rig workshop (Birmingham, UK) (Figure 5-15). The rig main frame was designed to be attached to the base of the testing machine and works

as a bracket to carry other parts. On the main frame there was a cup into which an artificial bone (a section cut from a fourth-generation Sawbones (Pacific research laboratories Inc., Vashon, WA, USA) composite femur (item# 3406) was fixed in position using a fast cure acrylic denture base bone cement (WHW Plastics, East Yorkshire, UK). The device was then fixed to the artificial bone using a clamping bracket to keep the new device proximal protractor hinge part (the device left hand side) in position during the test. The device was fixed to the rig frame through the support frame. The support frame has a 1.5 mm diameter wire which acts as the PIP joint center wire for the new device. Loads were then applied to the fixator using the load rod which connected to the load cell of the Bose machine (Figure 5-14) by the screw thread part of the rod.

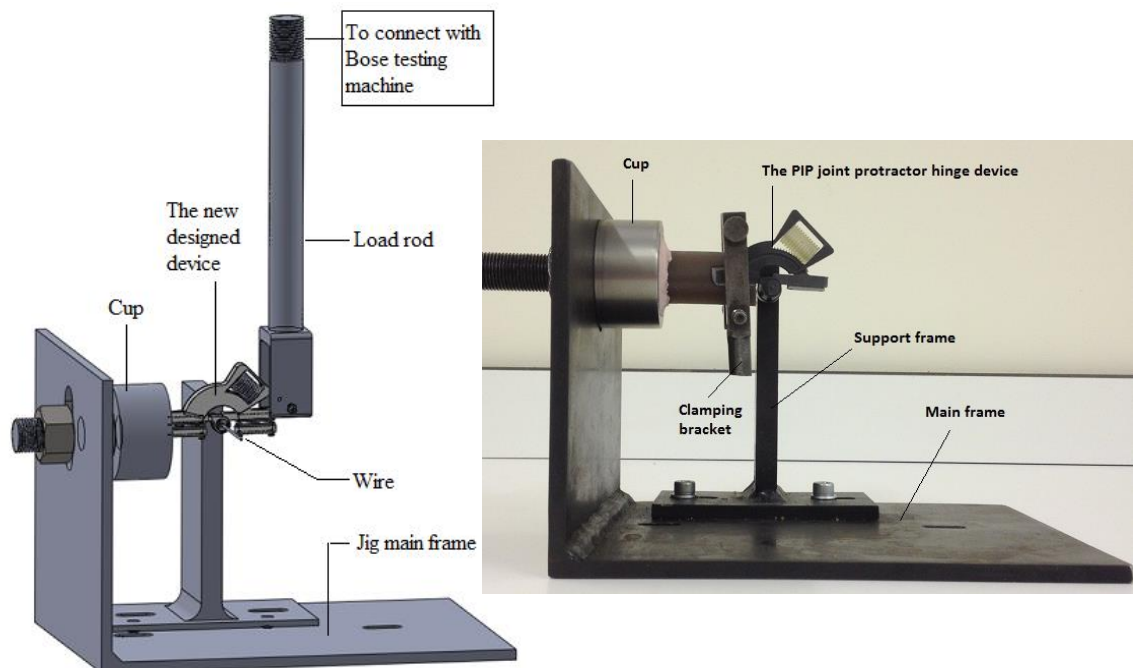


**Figure 5-15.** The designed mechanical test rig.

### 5.5.3 Methods

A compressive sinusoidally varying force of between 1.5 and 13 N was applied by the testing machine to the supported device at the protractor distal part. A preload of 1.5 N was used to ensure that there was contact between the device and the load cell. The loading was performed to a maximum of 13 N as this is that maximum force a prosthesis finger joint can exert (Joyce and Unsworth, 2000); there has been no force recorded for PIP joint contraction patients. The sine waveform was run at 2 Hz and testing continued until failure or run-out of 170,000 cycles was reached; this value was based on the assumption that around 1 million finger motions per year occur (Joyce and Unsworth, 2000) and the maximum period to support the device on an injured finger of a patient was reported as 64days (Bain *et al.*, 1998).

### 5.5.4 Results

Testing reached run-out of 170,000 cycles and was completed after 23 hours and 36 minutes with no cracks or damage was visible in the device parts. The maximum displacement under the maximum load applied of 13 N was 1.3 mm. Figure 5-16 shows the model after completing the test. Two areas were examined before and after running the test: the first one at the worm wheel teeth and spaces between them where they had been in contact together. The second area examined, the right side of the distal protractor hinge part, was the area assumed to have the maximum stresses from the finite element analysis (section 5.2.1).

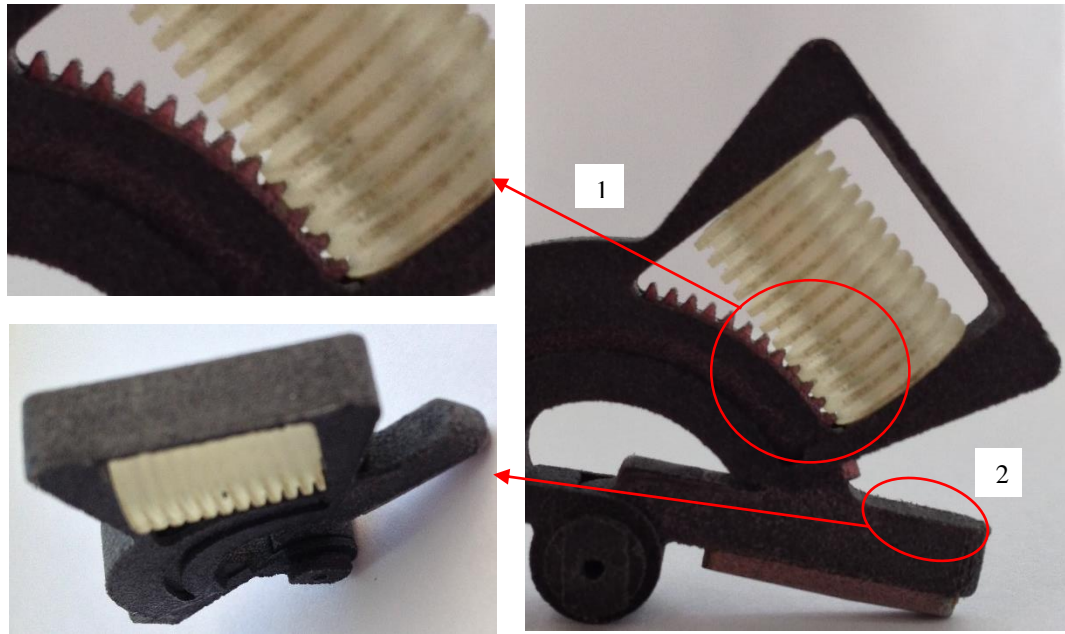


**Figure 5-16.** The device model after the cyclic bending mechanical test

For area 1 (Figure 5-16), no damage was seen at both the stainless steel worm wheel and the plastic worm gear. A magnification lens was used to check the worm and worm wheel manually and it was confirmed that no cracks were generated in either gear. On the other hand, unserious wear had happened at the worm gear; that result was predicted before running the test where the metal worm wheel material was harder than the polymer worm gear material (Kato and Adachi, 2001). The hardness of the stainless steel 17-4PH composition worm wheel in Rockwell scale “C” is 30 HRC (Solid Concepts Inc. - A Stratasys Company, Los Angeles, USA – DMLS material data sheet) and the hardness of the Fullcure 720 material in Rockwell scale “M” is 81 HRM (The FullCure® - Object geometries material data sheet). During the mechanical test, the applied cycling load caused the stainless steel teeth of the worm wheel to impinge on the polymer worm gear engagement teeth.

For the second tested area (Figure 5-16), it was predicted that the scratched line would appear on the surface of the distal protractor hinge part due to the effect of the applied load shaft (Figure 5-17). However, this line did not appear because of the rough surface finish of the new device plastic parts, as shown in Figure 5-16.

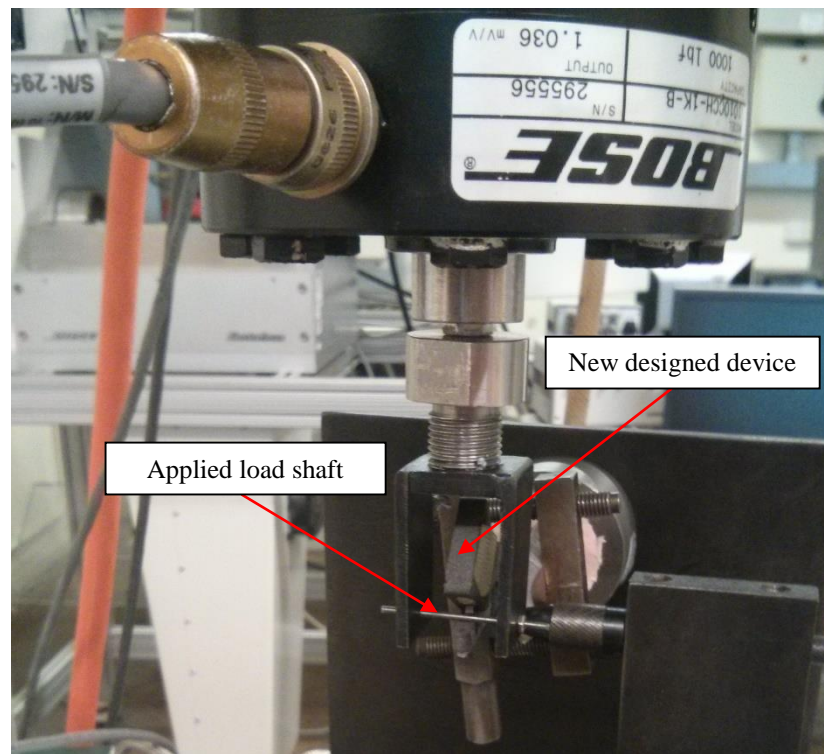


**Figure 5-17.** Applying cyclic load on the new designed device using a Bose ElectroForce® 3330 Series II Test Instrument

## 5.6 Discussion

The new design feature was generated, analysed and a working model manufactured. The new design was verified using the finite element analysis technique. That technique showed

that the Compass hinge had a maximum stress of 285.3 MPa (see chapter 3 section 3.3) and this occurred in a polymer part which was located between the gear teeth in the distal arcuate hinge member at a fixation position which engaged the gear teeth between 15 and 30°. In the new device the worm wheel part is now made from a metal and the maximum stress is now located along the connecting screws with a maximum value of 242.9 MPa (Figure 5-18).

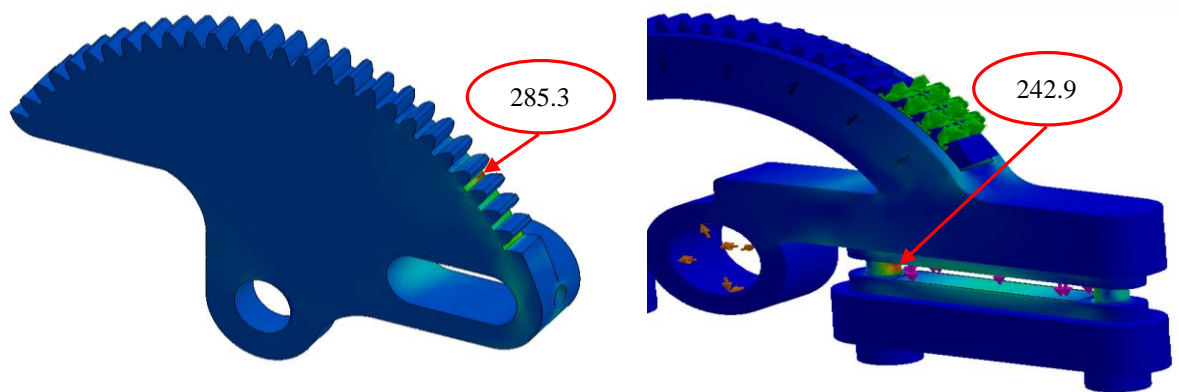


**Figure 5-18.** The maximum stress location for both models of the Compass hinge device (left) and the PIP joint protractor hinge device (right) at position 1 with the gear teeth fixed at 15 - 30° with a load of 210 N.

The gear tooth strength analysis was done by using Lewis bending stress equation (Schmid *et al.*, 2013) to get the maximum bending stress per worm wheel tooth (see chapter 4 section 4.5.2.3). The tooth bending stress was calculated at two different load values; firstly, at 210

N as the maximum applied load (see section 5.2). Secondly, at 13 N where the mechanical test was performed at the new device (see section 5.5.3). The results of the worm wheel tooth stress analysis were 0.22 MPa at 210 N and 0.014 MPa at 13 N. These stress analysis values were low compared with the fatigue strength of the stainless steel grade 316L worm wheel material (180 MPa to 520 MPa at 6 Hz and  $N > 10^7$  cycle (Huang *et al.*, 2006)).

A 0.7 mm minimum wall thickness dimension and the complex detailed features of the new designed components device meant that the 3D printing manufacturing technique was strongly recommended by Mechanical Engineering school technicians at the University of Birmingham and manufacturing companies (Solid Concepts Inc. - A Stratasys Company, Los Angeles, USA and Proto Labs, Ltd., Shropshire, United Kingdom) to manufacture them. On the other hand, the conventional manufacturing techniques such as CNC and EDM would not enable the required part dimensions since advanced machine tools were not available.

The stainless steel 316LS medical grade (90% cold worked) and PEEK 90G VICTREX® were selected to be the new materials for manufacturing the metal and polymer parts. These two materials were picked among other candidate materials for their mechanical properties which fulfil the new device requirements (chapter 4 section 4.3.2). Although the aluminum alloys ( $2.7 \text{ g/cm}^3$ ) are almost one third the density of stainless steel ( $8.0 \text{ g/cm}^3$ ) (Davis, 1994) they are typically not as strong as 316LS stainless steel, with a yield strength of 946 MPa (MatWeb, material property data). Despite PEEK and PEI polymer material being close in their mechanical properties where the yield strength and Young's modulus are 110 MPa, 3.6 GPa (Chou *et al.*, 2008; Hee and Kundnani, 2010) and 105 MPa, 3.3 GPa (Kirby, 1992), respectively, PEEK (65 MPa at 5Hz,  $>10^7$  cycles) exceeds the PEI (24 MPa at 5Hz,  $>10^7$

cycles) in the fatigue stress endurance limit by approximately three times (Trotignon *et al.*, 1993).

The new design and the 3D printed models were reviewed by Mr. Titley (Consultant Plastics and Burns Surgeon at the Queen Elizabeth Hospital, Birmingham) and it was concluded that this new fixator meets the needs of surgeons for a device that is, small, allowing active and passive motion, like the Compass hinge, but with a reduced chance of mechanical failure. It can be applied to the radial or ulnar side of any finger and is radiolucent to facilitate accurate placement.

## 5.7 Summary

The new fixator based on development of the Compass hinge consists of 17 parts where 8 of them (proximal and distal protractor hinge parts, worm gear, screw 1 and nut 2, rod, slotted clamping proximal and distal blocks) are to be made from a radiolucent medical grade plastic VICTREX® PEEK 90G. The stainless steel 316LS Medical Implant Alloy, 90% cold worked was selected for the remaining parts (worm wheel, four solid blocks and four connecting screws). The selected materials were not available for manufacturing using 3D printing so NYTEK TM 1200 CF which is carbon filled nylon and stainless steel 17-4PH composition were used to manufacture a working model. The new device would be attached to the patient fingers such that the distal protractor hinge part is attached to the middle phalanx of the patient's injured finger and the proximal protractor hinge part is attached to the proximal phalanx.

The new design was analysed using finite element analysis which showed that the maximum stress was 242.9 MPa and this was less than the yield strength and the fatigue endurance limits for the selected materials. A cyclic bending test was performed using a Bose ElectroForce® 3330 Series II Test Instrument which was guided by ASTM F1541-02. The results showed that testing reached run-out of 170,000 cycles with no cracks or damage visible in the device parts. The next chapter will present an overall discussion of the thesis and the conclusions which are drawn from the results.

# CHAPTER 6

## OVERALL DISCUSSION AND CONCLUSIONS

## **6 OVERALL DISCUSSION AND CONCLUSIONS**

### **6.1 Chapter overview**

This chapter provides an overall discussion of the thesis and brings together the various individual studies that have been undertaken. A reminder of the aims of the project is provided in section 6.2. The general discussion of this study is described in § 6.3. The surgical technique of the proposed device is presented in §6.4, followed by a comparison between the current and previous fixators together in §6.5. A number of areas worth exploring in developing this work is detailed in §6.6. A number of conclusions are drawn from the results and are listed at the end of the chapter.

### **6.2 Project objectives**

The overall aim of this project was to develop and test a prototype of an external PIP joint finger fixator. The specific objectives of this project were to:

- Analyse a failed Compass hinge device;
- Produce a new design of fixator device;
- Manufacture a prototype model of the new designed fixator;
- Analyse the new design using finite element modelling;
- Mechanically test the prototype of the new designed fixator.

### 6.3 Discussion

Following the development and completion of the new external finger fixator which was the ultimate aim of this research project, there are a number of important points of discussion.

Initially the study of the biomechanics and the different contracture of the PIP joint was presented. Then, as an example of these contractures, Dupuytren's disease was described in detail. A variety of fixators are offered for PIP extension mobilization. One designed distractor of the PIP for both extension and flexion mobilization is the Compass hinge device which was analysed and developed in this project.

The study and review of the current and past designs was vital as those can be the base for inspiration and a way to improve and develop a new design. This is especially important when complications from previous designs and failure analysis are published that could be an advantage in the design progress.

The design considerations and requirements take into account the available previous data on the biomechanics of the joint and the different designs that have been presented. The concept design procedure followed the design requirements procedure and a detailed design led to the final design.

Verification and validation methods have been used in this study. Finite element analysis has been performed for the optimal shape of the suggested design. The finite element modelling showed that the expected stresses experienced within the new design when the force of 210 N was applied would not exceed the fatigue strength of the new selected PEEK

and stainless steel 316LS manufacturing materials. The mechanical test has shown the device is strong enough and the worm and worm wheel mechanism system is stable enough to withstand the expected loading conditions in the human digit.

The proposed device, which has been designed and tested in this project, was a medium size, low mass, easy to use and natural color likely to be required for the attachment of the PIP joint fixator. It could be possible to design the skeletal external fixator in various sizes to fit into the different lengths of the human fingers. Small, medium and large are the three suggested sizes to manufacture the new device. These sizes were guided during the design stage by the different lengths of the middle phalanges of human digits (Alexander and Viktor, 2010).

### **6.3.1 Analysis of failed Compass hinge device**

The Compass hinge device engineering analysis study (chapter 3) was undertaken to investigate the different modes of failure. The finite element modelling and scanning electron microscopy techniques were used to determine the appropriate types and causes of the failure, since all the relevant information was not available in the literature. SolidWorks Simulation (SolidWorks 2011, Dassault Systèmes SolidWorks Corporation, Waltham, USA) was used for the finite element analysis. A Joel JSM-6060 scanning electron microscope (JEOL Ltd, Tokyo, Japan) was used to scan the fracture surfaces of the failed device.

The results of this study showed that the cyclic bending stresses are the main cause of the mechanical failure in the polyetherimide distal arcuate member in the Compass hinge device.

When the device was attached to the digit of a patient they try and move their PIP joint, thus causing high stresses to be generated in the weak resistant areas in the device which causes cracks to be initiated. As the patient carries on loading the device this means that cracks are likely to propagate rapidly. Lastly, the section of polyetherimide distal arcuate member will bend, fracture and detach from the device.

The results of the study of the distal arcuate member are given in section 3.3.2 and section 3.4.1 and from these results the features, dimensions and materials for manufacture (chapter 4 section 4.5.1) for the new design prototype were determined.

### **6.3.2 The PIP joint protractor hinge device design**

The PIP joint protractor hinge device design was presented in chapter 4 and the outer dimensions are 35.5 mm for height, 47.5 mm for width and the thickness is 8.5 mm. SolidWorks Computer Aided Design (SolidWorks 2011, Dassault Systèmes SolidWorks Corporation, Waltham, USA) software was used to model the new device design parts. Three device sizes were suggested to fit with a large range of patient finger sizes as medium (M) designed for average, small (S) and large (L). In this study, a medium (M) design was presented that was based upon the medium (50% percentile) human hand anthropometric data. The protractor hinge device will be attached to the finger bone by inserting 5 K-wires. One of these wires will be inserted in the center point of the PIP joint and will be removed later after the positioning surgical procedure has ended. The remaining four wires will be permanently fixed in the proximal and middle digit phalanges, with 2 wires for each phalanx.

The device depends on the worm and worm wheel mechanism which enables active and passive (flexion and extension) mobilization for the injured PIP joint.

### **6.3.3 Finite element modelling**

Finite element analysis was used to determine the stresses which would be experienced by the new device parts (chapter 5 section 5.2). A force of 210 N was applied to this model. This force magnitude was chosen from previous studies of the biomechanics for the human finger which predicted forces during daily activities (Chapter 2 section 2.3).

The results of the finite element analysis showed that the predicted stresses are not as high as the fatigue strength of the PEEK and stainless steel, the proposed materials for the prototype of the new designed device. The new designed components were modelled with the constraints at two different PIP joint flexion positions with the worm gear at: position (1) teeth between 15 and 30° and position (2) 90-105° as two extreme gear teeth fixation positions. The stress patterns were similar for the two positions, where the maximum value of the stress was located along the screws which connect the blocks together with the distal protractor hinge part, with the maximum stress being 242.9 MPa. For the Compass hinge the maximum stress was 285.3 MPa (see chapter 3 section 3.3) and this occurred in the main device part of the distal arcuate hinge member and was located between the gear teeth in the distal arcuate hinge member with the gear teeth fixed between 15 and 30°. It was concluded that the new design would be expected to withstand the likely forces which are exerted by the human fingers.

### 6.3.4 Prototyping

A 3D printing technique was used to manufacture both the metal and the polymer parts of the new device as high dimensional accuracy was required (0.7 mm minimum thickness). As there had been no recorded manufacturing techniques for other fixators, the 3D printing method was chosen among other possible conventional manufacturing techniques such as CNC and EDM for metal parts and injection molding for polymer parts for many reasons. These reasons are that firstly, traditional manufacturing techniques, such as CNC and EDM for metal materials in the School of Mechanical Engineering workshop at University of Birmingham would fail to get the required dimensional resolution. Although the CNC five axis machine may get the required dimensions, it will be expensive where a special design set up will be required to hold the tiny dimension work pieces. Also, an engineer or highly skilled technician would be required to monitor the cutting process which means a very high cost toward manufacture of the prototype models for the new device. For manufacturing the polymer parts by a traditional technique such as injection molding will be expensive where a die design will be required; this technique will be worth the money in the case of mass production of the new device, but not for prototype models.

A suggested strategy plan to manufacture mass production for a final device that was being implanted into patients was as follows. For all metal parts the wire EDM machining process was selected. That by reason of the advantage of this process as X, Y, and Z machine axes movements allow for the programming of complex profiles using simple electrode, complex sections can be produced accurately, fast and low cost to produce a large number of work

pieces (Dewangan, 2010). For the main polymer parts, proximal and distal protractor hinge parts and slotted clamping blocks (chapter 4 section 4.5.2.1, 4.5.2.2 and 4.5.2.6) the injection molding process was suggested to manufacture these parts. Prototype injection molds are most commonly produced by conventional machining, grinding or electrical discharge machining (EDM) techniques (Malloy, 1994). The advantages of the injection molding process are for complex geometries, high production output rates, close tolerances on small intricate parts and parts have a very finished look (Rosato and Rosato, 2012). The CNC machining process was suggested for the remaining polymer parts, rather than another alternative 3D printing technique, where the parts manufactured by CNC have high accuracy, is fast and it is the best solution when manufacturing a large number of complex objects. In addition, sometimes, the 3D printed build quality is lower than if it had been traditionally manufactured (Pirjan and Petroşanu, 2013).

In this study, three prototypes were manufactured; two of them were made out of an acrylic monomer based resin (brand name Fullcure 720) to check that the all of the features and the outer dimensions were acceptable. Since the designed materials were not available for manufacture by 3D printing another prototype was made from NYTEK TM 1200 CF which is carbon filled nylon for polymer parts and stainless steel 17-4PH composition for metal parts. This prototype was manufactured to be subjected to mechanical testing.

Another aspect that should be considered during the design process is the manufacturing cost. It is the sum of costs of all resources consumed in the process of making a device. The manufacturing cost is classified into three categories; direct materials cost (the cost of raw materials), direct labor cost (the cost of workers) and manufacturing overhead (the cost of

supervisors and material handling, the cost of associated with consumables and any expenses that keep the factory operating) (Ostwald and McLaren, 2004). The manufacturing cost of one of the PIP joint protractor hinge device should not exceed the range of 400-600 British Pound Sterling, which is the price range of other fixators in the current market, as confirmed by Mr. Titley.

### **6.3.5 Mechanical testing**

ISO and ASTM standards were checked carefully for testing procedures for external finger fixators, and very few standards were found. Therefore, the general requirements for non-active surgical implants (BS EN ISO 14630:2005), standard specification and test methods for external skeletal fixation devices (ASTM F1541-02 2001) were used as guides for the current study.

The mechanical testing of the prototype PIP joint protractor hinge device was carried out using a Bose 3330 materials testing machine (Bose Corporation, Minnesota, USA). The test set-up for the cyclic compression tests was modified so that the force was applied by the top load cell straight onto the distal protractor hinge part. In the cyclic compression test a sinusoidal load between 1.5 N and 13 N was applied at a frequency of 2 Hz. The mechanical testing showed that testing reached run-out of 170,000 cycles with no cracks or damage visible in the device parts. The prototype of the PIP joint protractor hinge device was strong enough to withstand the expected forces that it would be subjected to in the fingers. Further, the worm and worm wheel mechanism system was found to work well in the test.

The new designed device (13 components and 4 connecting screws) (see chapter 4 § 4.5.1) had a reduced number of parts compared with the Compass hinge device (16 components and 8 screws) (see chapter 3 § 3.2.4). The reduction by 7 parts would mean that the new device was more accessible and easier to manually assemble compared to the Compass hinge. An assessment method for assembling the new device parts was still required to confirm that. More solid models should be manufactured to apply this assessment method and volunteers to assemble the devices should be trained with the device assembly sequence plan to be sure all used the same sequence. Human factor aspects should be considered in choosing volunteers as gender and age where male and female with both right and left write hands should participate in the assessment.

## **6.4 The PIP joint protractor hinge surgical technique**

The axis of the protractor hinge is located at the axis of the PIP joint. To maintain motion during healing, the device is equipped with a worm gear that allows passive motion through the worm wheel in the device frame. The gear mechanism may be disengaged by the patient for active motion to maintain tendon excursion, particularly in the later phases of treatment. The protractor hinge device attaches with skeletal fixation to either side of the joint with stainless steel Kirschner (K)-wires, which are inserted along the lateral and mid-axial line of the finger phalanx. The new device is attached to the patient fingers such that the distal protractor hinge part is attached to the middle phalanx of the patient's injured finger and the proximal protractor hinge part is attached to the proximal phalanx. In order to enable surgeons to determine which size of device to use, table 4-4 was created (see chapter 4 section 4.6).

### 6.4.1 Further development

Further work supplementary to the current study could be done with the proposed PIP joint protractor hinge device design.

- Side walls were suggested to be added to the proximal protractor part to avoid any detachment of the assembled rod part (see section 4.5.2.5) so a rapid prototyping for the modified part is required to check the dimensions and the function to confirm it.

A 3D design of the modified proposed part is shown in Figure 6-1.

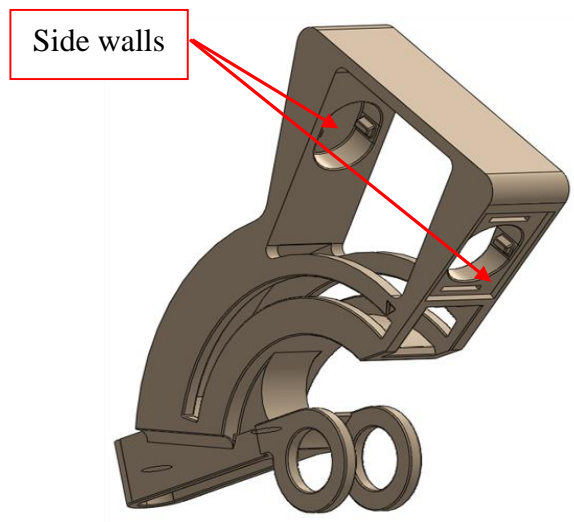


**Figure 6-1.** A new feature design for the proximal protractor hinge part.

- A prototype of the final design should be manufactured from the suggested materials (VICTREX® PEEK 90G, 316LS medical grade stainless steel, 90% cold worked condition) rather than manufacture with available materials.
- The accommodation of the design to cover the range of sizes that are needed to cover the different sizes of the human fingers.
- An *in vitro* clinical evaluation of the final design of a manufactured model is compulsory to be performed.

Approach In 1993, the European Committee for Standardization the international standard ISO 14155 first requirements for the clinical investigation plan was published. This International Standard addresses good clinical practice for the design, conduct, recording and reporting of clinical investigations carried out in human subjects to assess the safety or performance of medical devices for regulatory purposes. Clinical research studies can be categorized as either observational or analytical (hypothesis testing trials). Becker and Whyte (2007) described the clinical evaluation of medical devices and summarized the clinical investigation plan in 17 elements which should be considered at the validation stage of the medical design process (Aitchison *et al.*, 2009); device description, study objective, study design, study population, treatment regimen, control group, endpoints evaluated, trial success, study procedures and duration, sample size calculations, data analysis plan, risk analysis, case report forms, informed consent forms, investigational sites, data safety monitoring board, and monitoring plan.

ISO EN 14155-2 details that the individual who participates in a clinical investigation should be a patient. In addition to articulating the clinical condition of the subjects, investigators often include demographic criteria specifying patient, age, sex and race also educational level may be relevant *in vitro* diagnostics.

For the PIP joint protractor hinge device there are some aspects of the design process still required to accomplish to present the new device to the market as Aitchison et al. (2009) detail in their medical design process flow chart. The estimated timeline for the required design processes was summarized in Table 6-1 and the predictable time period is approximately 2 years.

**Table 6-1.** A predicted timeline of the design process required for the PIP joint protractor hinge device.

Medical design process (still required)	Process description	Approximate period of time (month)
Manufacture	Production	5
	Sterilization	1
Validation	Mechanical testing	1
	Clinical investigation	12
	Sterilization validation	2
Design transfer	Surgical technique	1
	Packaging & labelling	1
	Master device record	1

## **6.5 Comparison of the new proposed device with other external finger fixators**

The developed design presented in this thesis has some similar design features to the Verona and Compass hinge devices with the design dependent on the gear transmission mechanism system. A worm and worm wheel gear type were used according to its function which is the rotation motion which will allow higher torque to be transmitted by the patient due to turning the worm gear to device parts. Although the screw and nut mechanism in many finger fixators such as the TEC, JESS and Orthofix devices (Messina and Messina, 1993; Joshi, 1997; Houshian and Schröder, 2004) offered the same type of motion as the worm and worm wheel mechanism, but are difficult to implant and turn the nut to give movement in the patient's central digits. TEC is an example of the screw and nut mechanism in a working fixator (Figure 2-16), which is quite big which makes it not accepted by patients especially to be implemented in the central digits where they do not feel comfort since there is not enough space between the central digits (Citron and Messina, 1998). Furthermore, the screw and nut mechanism is not easy to be used by patients during the treatment period where the force was required to be exerted to turn a nut to move the fixator. The PIP joint protractor hinge device was designed to be based on development of the Compass hinge device. The new device idea not only works on overcoming the Compass hinge device complications (see chapter 3 section 3.2.3), but also the reported claims of other fixators (chapter 2 section 2.6). The new device advantages are mechanical failure of parts were reduced, there is no slippage between the device parts, it is small in size, it allows active and passive motion, some parts are manufactured from a radiolucent material and it has low thickness so it can be used in the central digits.

The new device was suggested to be manufactured from both metal and polymer medical grade materials (316LS stainless steel and VICTREX® PEEK 90G) to enable the advantages of both materials, namely low mass, radiolucent and natural color for the polymer material (VICTREX®) and high yield strength and fatigue stress endurance limit for the metal material (yield strength = 946 MPa) (MatWeb, material property data). The previous engineering analysis study (section 3.3 and section 3.4) for a failed Compass hinge device confirms that the bending cyclic stress was the main cause of the failure so a medical grade 316LS stainless steel material, which has a high fatigue strength, was selected to replace the Compass hinge device in areas of the parts with high stresses. Further, a medical grade plastic VICTREX® PEEK 90G material has been chosen for the remaining polymer parts rather than polyetherimide parts (used for the Compass hinge) where the fatigue endurance limit for the selected material (65 MPa at 5 Hz, 20°C and  $>10^7$  cycles) is higher by approximately three times that of the polyetherimide (24 MPa at 5 Hz, 20°C and  $>10^7$  cycles) (Trotignon *et al.*, 1993).

The PIP joint protractor device is unique where parts close to the PIP joint center are manufactured from a radio-lucent PEEK material polymer, which can be seen under x-ray rather than a radio-opaque metal used in the Compass hinge and Verona devices (Hotchkiss *et al.*, 1994; Citron and Messina, 1998). The new device has fine guide marks on the device frame and on the worm gear to aid the user with the amount of turns when using the worm gear.

The newly design device is small in size compared with the Compass hinge measured dimensions (the width has been reduced by 4 -19 percent and the thickness by 26 percent),

and the device has low thickness compared with other devices (TEC, JESS, Hoffmann II Micro External Fixation System and Compass hinge). Since the new device will attach in the lateral direction to the finger phalangeal, the attachment process to a patient's central digits is easy and will be accepted by patients, particularly with the advantages of the new device, namely small size and low thickness. This was concluded from Mr. Titley (Consultant Plastics and Burns Surgeon at the Queen Elizabeth Hospital, Birmingham) design meeting feedback. This enabled the new device advantage over other fixators which have used pins and elastic bands (White *et al.*, 2012) which were implemented in digits in the dorsal direction.

The new design device finite element analysis and the mechanical tested prototype analysis results confirmed that the occurrence of mechanical failure was vastly reduced compared with the results of the compass hinge device engineering analysis. The finite element simulation analysis (SolidWorks 2011, Dassault Systèmes SolidWorks Corporation, Waltham, USA) for the Compass hinge device showed that the high stress area was generated at the main polymer part of the device, which is the part which allows the device to move (Figure 3-14). The maximum stress value reached was 285.3 MPa. This value was more than the fatigue endurance limit of the Compass hinge distal part material which was PEI material (24 MPa at 5 Hz, 20°C and  $>10^7$  cycles) by eleven times and by 2.7 times of the yield strength (105 MPa). The conclusion of this analysis was confirmed that the Compass hinge device could not withstand the cyclic loads due to human daily activity motion and in the long run failure occurs. On the other hand, the finite element simulation analysis (SolidWorks 2011, Dassault Systèmes SolidWorks Corporation, Waltham, USA) for the new designed device showed that generated stresses were located in three areas (Figure 5-3). These areas were assumed to be high, medium and low stresses. The low stress

area were where the value of stresses were less than 60 MPa distributed at the right side of the PEEK distal protractor hinge part and these values were less than the PEEK fatigue endurance limit (65 MPa at 5 Hz, 20°C and  $>10^7$  cycles) and yield strength (110 MPa) by 2 times (Figure 5-6). That confirms that the polymer device parts can withstand the likely load conditions in the human hand during activities. For the medium and high stresses, values ranged from 60 MPa to 243 MPa and they were distributed along the distal solid blocks and the connecting screws (maximum stress 242.9 MPa). These parts were to be manufactured from a metal (316LS stainless steel) where the maximum generated stress was less than the 316LS yield strength (946 MPa) by 3.8 times. The new device analysis and its calculations verify theoretically the device from the engineering point of view.

More stages are still required according to the flow chart which was presented by Aitchison *et al.* (2009) for the design of new medical devices. The devices should be manufactured with the suggested manufacturing techniques. A required clinical investigation plan must be produced in accordance with BS EN ISO 14155-2 as the next required step. The Ethics Committee should approve the investigation and the manufacturer would be required to decide on the length of it, the number of patients to be involved and other type of data to be collected such as patient's digit flexion angle, PIP joint range of motion (ROM) after treatment and any complications should be recorded by both patients and surgeons. After that, the instructions for use of the new device should be prepared with the finalization of the surgical technique. Then, the design will be ready to transfer to production. The final stage for a new design is launch into the market and to have a post-market surveillance procedure in place. The manufacturer should work on the negative feedback and improve the design and this feedback must be fully documented. Repeating the design verification

process such as the finite element analysis and the validation process such as the mechanical testing may be required upon to the magnitude of the design changes. Also, a risk assessment should be updated to ensure that the full impact of the changes has been understood.

## 6.6 Conclusions

The conclusions from this thesis are as follows:

- The cyclic fatigue stresses are the main causes of the Compass PIP joint hinge distal arcuate hinge member part fracture that were investigated using finite element analysis and scanning electron microscope techniques.
- A new external fixator device has been designed that has an improved design compared with previous fixators, through smaller dimensions and the use of a radio-lucent polymer;
- Finite element analysis showed that the maximum stress was 242.9 MPa and this was less than the yield strength and the fatigue endurance limits for the selected materials;
- Mechanical testing showed that testing reached run-out of 170,000 cycles with no cracks or damage visible in the device parts;
- The verification and validation procedures for a new design fixator have shown that the device is strong and stable enough to withstand the likely loading conditions in the human digits.

# APPENDICES

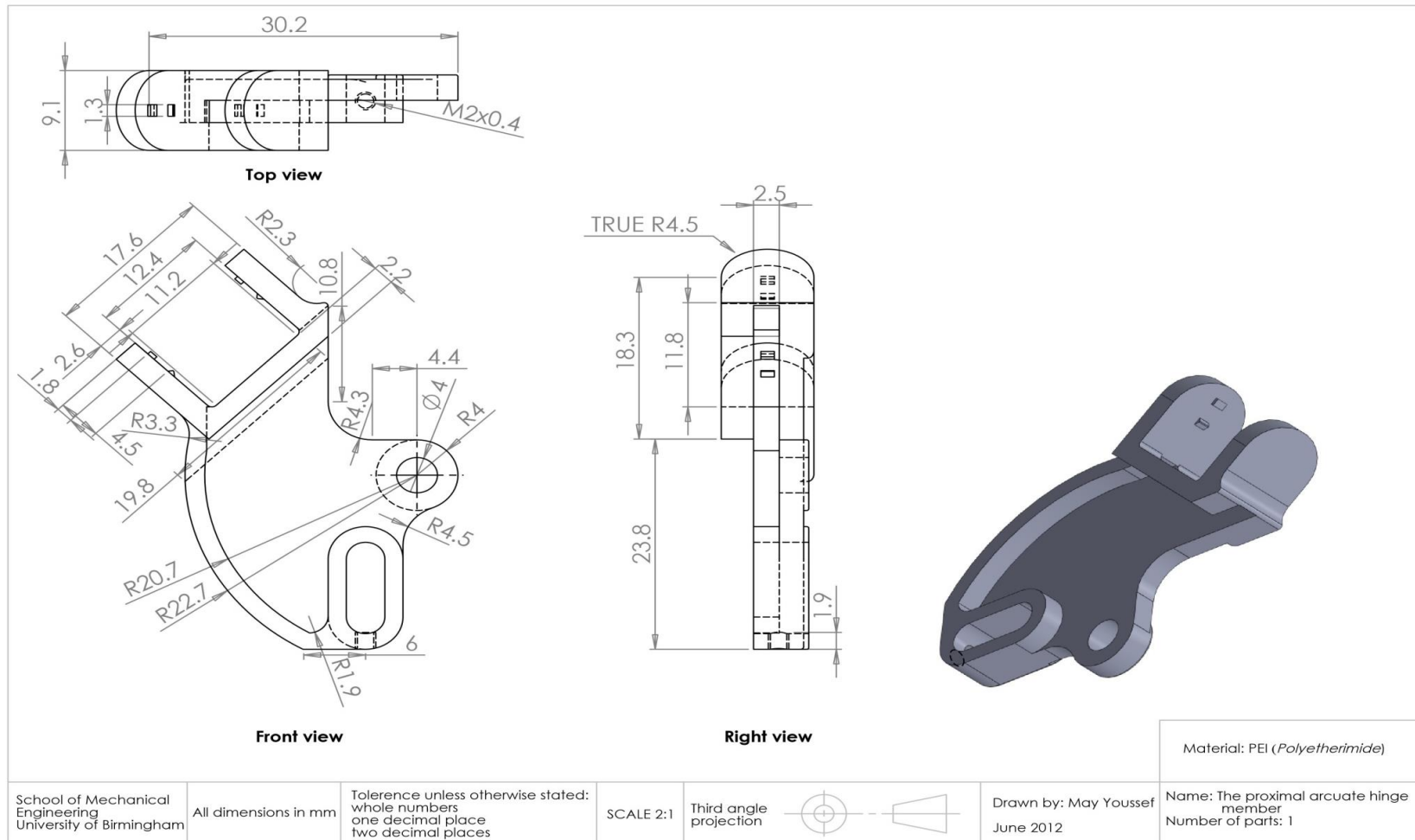
## **Appendix A**

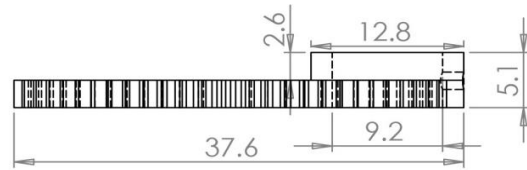
Free hand sketches drawing views of the Compass hinge device parts at measurement stage  
see (section 3.2.4).



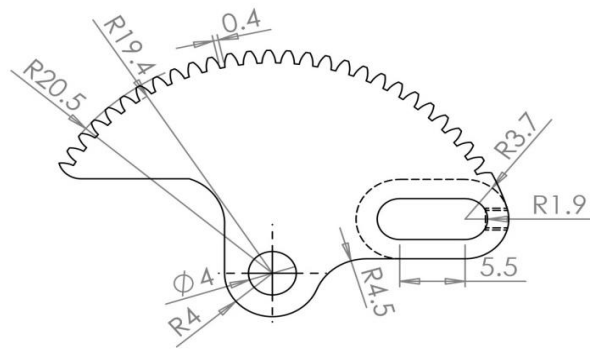
## **Appendix B**

The engineering drawings of the Compass hinge device parts (see section 3.2.4)

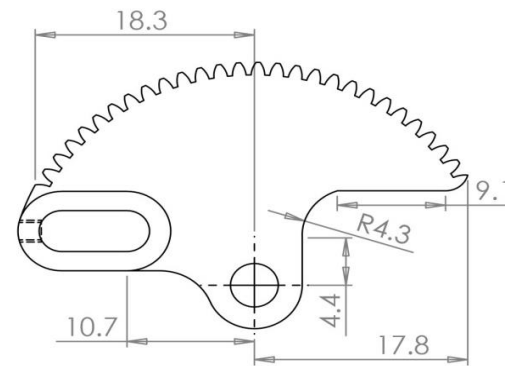




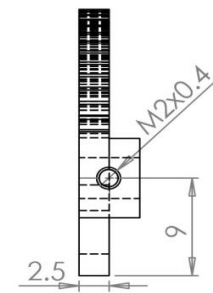
Top view



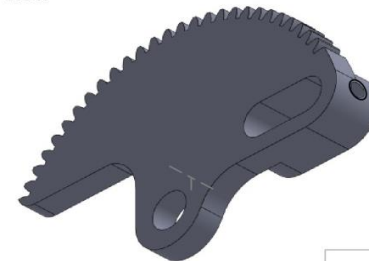
Front view



Rear view



Right view



Material: PEI (Polyetherimide)

School of Mechanical  
Engineering  
University of Birmingham

All dimensions in mm

Tolerance unless otherwise stated:  
whole numbers  
one decimal place  
two decimal places

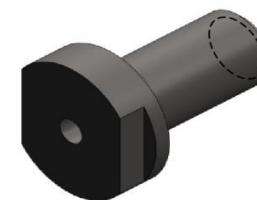
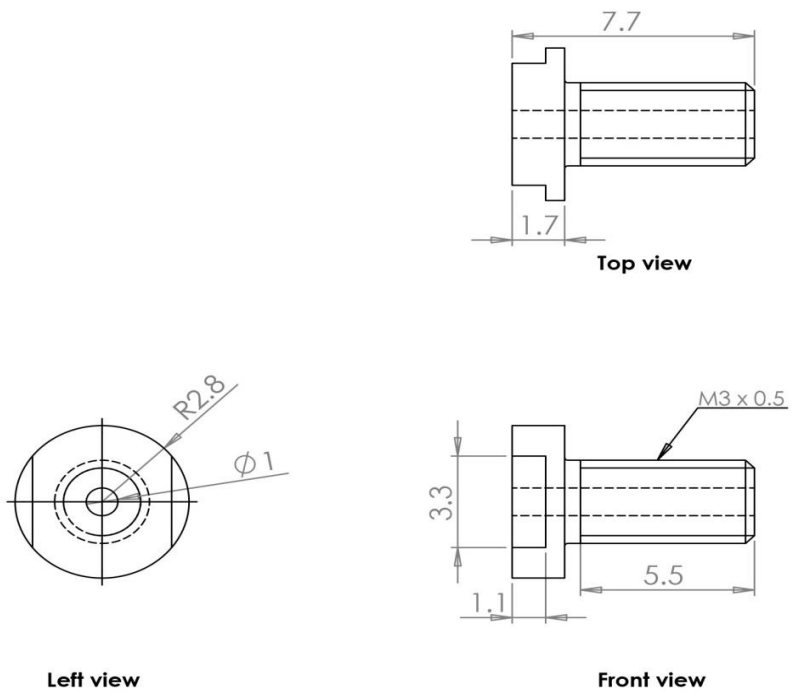
SCALE 2:1

Third angle  
projection



Drawn by: May Youssef  
July 2012

Name: The distal arcuate hinge  
member  
Number of parts: 1



Material: Stainless steel

School of Mechanical  
Engineering  
University of Birmingham

All dimensions in mm

Tolerance unless otherwise stated:  
whole numbers  
one decimal place  
two decimal places

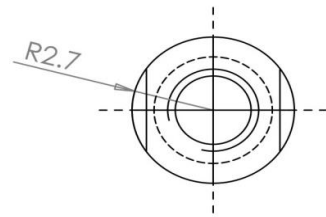
SCALE 5:1

Third angle  
projection

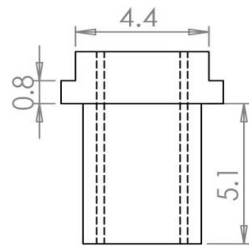


Drawn by: May Youssef  
June 2012

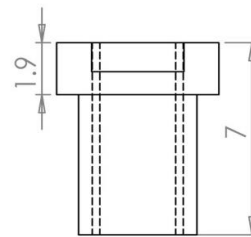
Name: The radiopaque axle 1  
Number of parts: 1



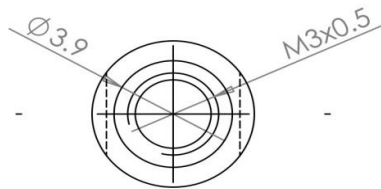
Top view



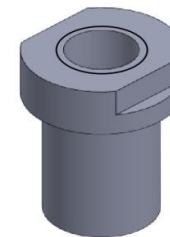
Front view



Right view



Bottom view



Material: Stainless steel

School of Mechanical  
Engineering  
University of Birmingham

All dimensions in mm

Tolerance unless otherwise stated:  
whole numbers  
one decimal place  
two decimal places

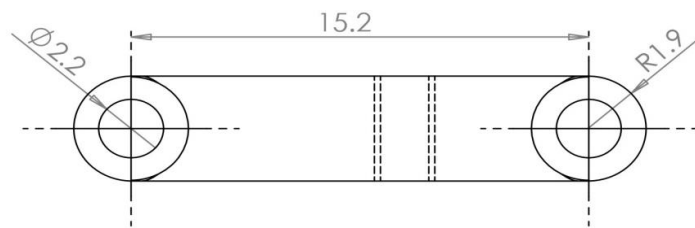
SCALE 5:1

Third angle  
projection

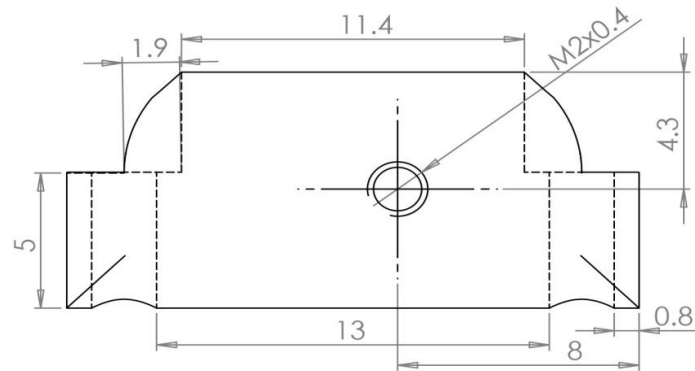


Drawn by: May Youssef  
June 2012

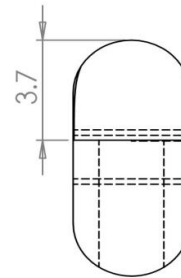
Name: A radiopaque axle 2  
Number of parts: 1



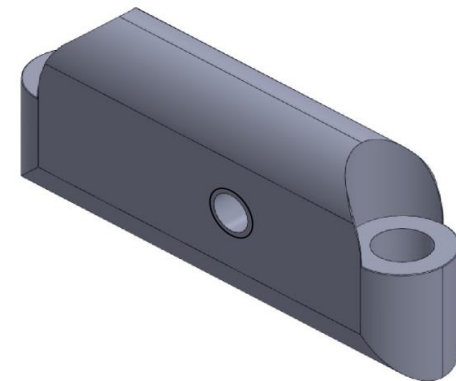
Top view



Front view



Right view



Material: Aluminum alloy

School of Mechanical  
Engineering  
University of Birmingham

All dimensions in mm

Tolerance unless otherwise stated:  
whole numbers  
one decimal place  
two decimal places

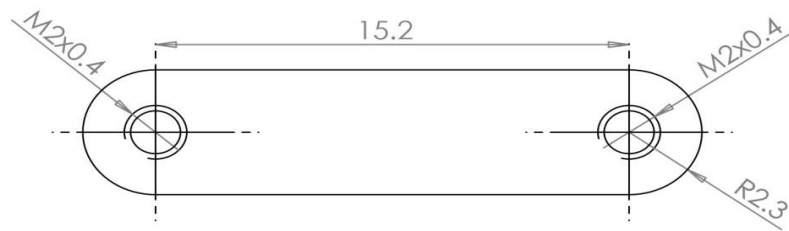
SCALE 5:1

Third angle  
projection



Drawn by: May Youssef  
June 2012

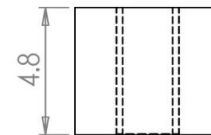
Name: Superior clamping blocks  
Number of parts: 2



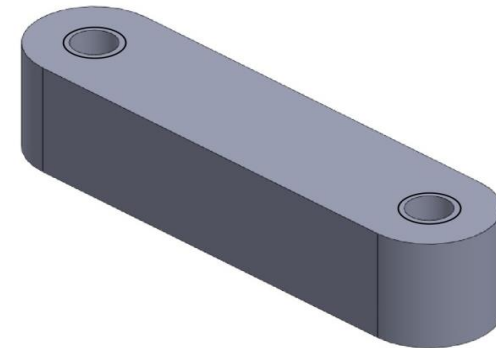
Top view



Front view



Right view



Material: Aluminum alloy

School of Mechanical  
Engineering  
University of Birmingham

All dimensions in mm

Tolerance unless otherwise stated:  
whole numbers  
one decimal place  
two decimal places

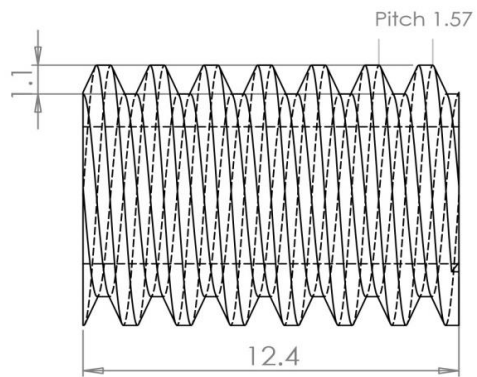
SCALE 5:1

Third angle  
projection

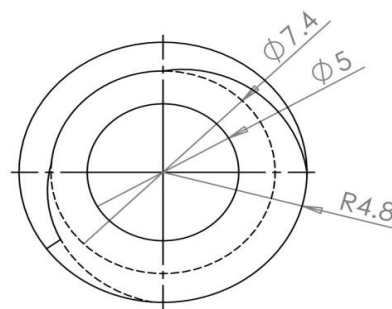


Drawn by: May Youssef  
June 2012

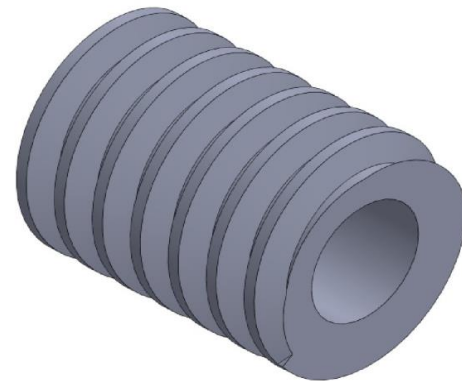
Name: Inferior clamping blocks  
Number of parts: 2



Front view



Right view



Material: PEI (*PolyetherimidE*)

School of Mechanical  
Engineering  
University of Birmingham

All dimensions in mm

Tolerance unless otherwise stated:  
whole numbers  
one decimal place  
two decimal places

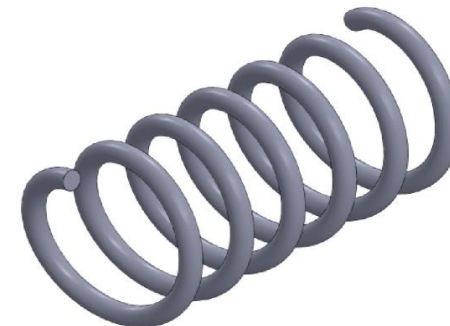
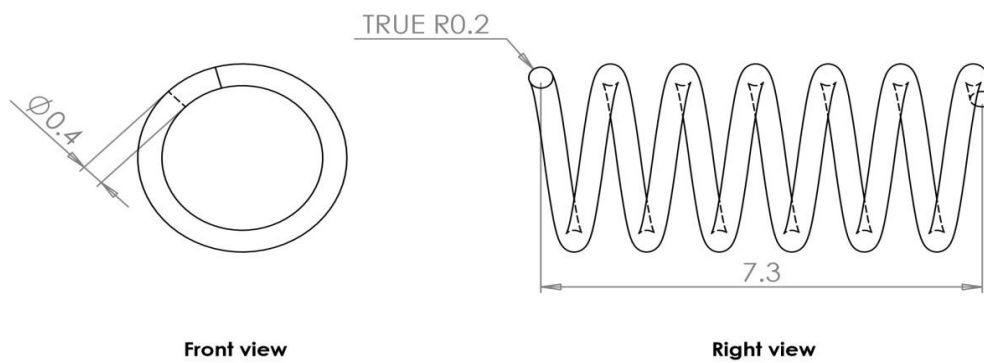
SCALE 5:1

Third angle  
projection



Drawn by: May Youssef  
July 2012

Name: Worm gear  
Number of parts: 1



Material: Stainless steel

School of Mechanical  
Engineering  
University of Birmingham

All dimensions in mm

Tolerance unless otherwise stated:  
whole numbers  
one decimal place  
two decimal places

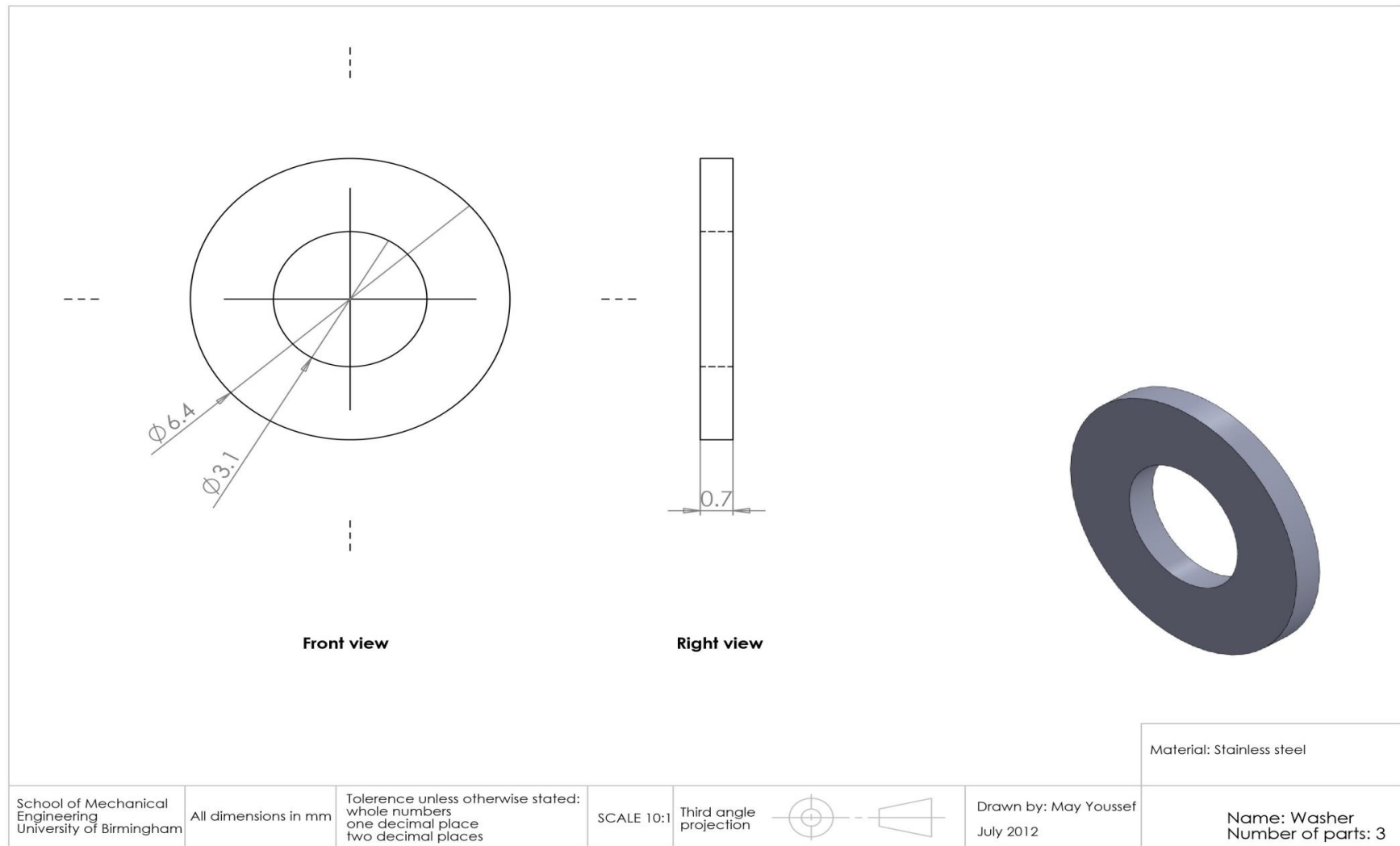
SCALE 10:1

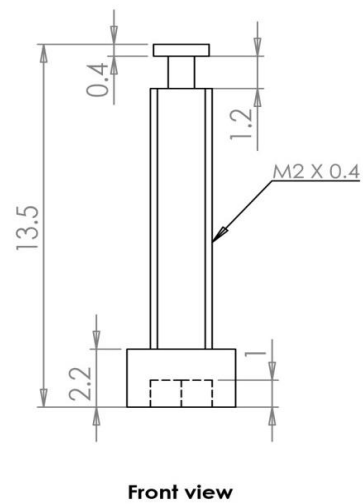
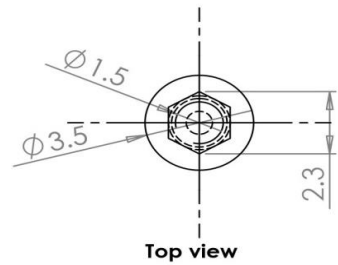
Third angle  
projection



Drawn by: May Youssef  
July 2012

Name: Spring  
Number of parts: 1





Material: Stainless steel

School of Mechanical  
Engineering  
University of Birmingham

All dimensions in mm

Tolerance unless otherwise stated:  
whole numbers  
one decimal place  
two decimal places

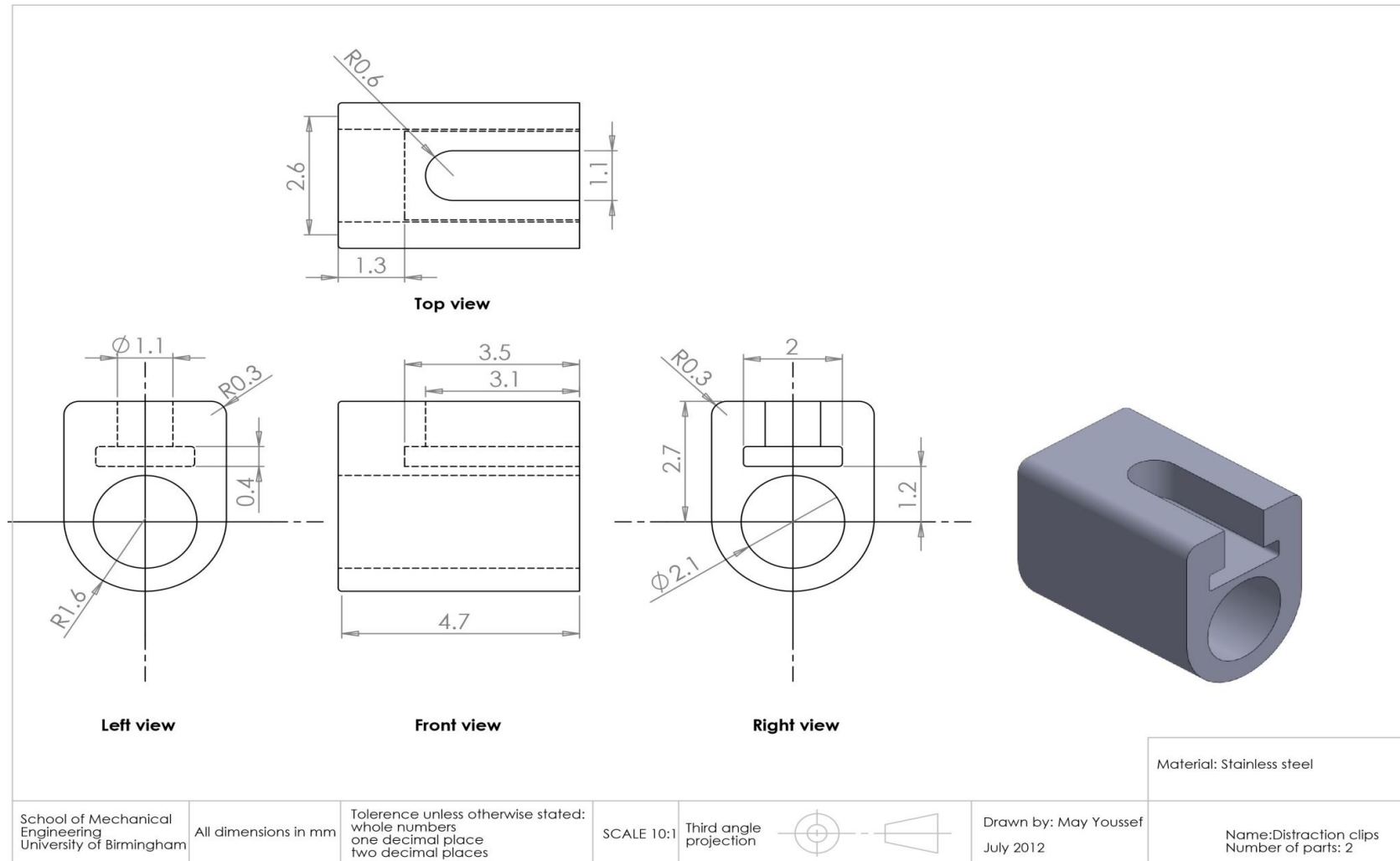
SCALE 5:1

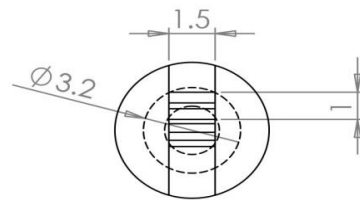
Third angle  
projection



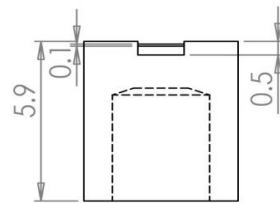
Drawn by: May Youssef  
July 2012

Name: Distraction screw  
Number of parts: 2

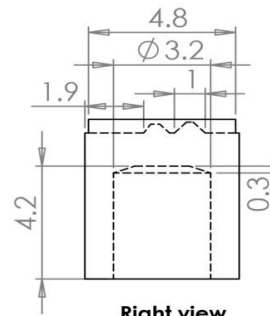




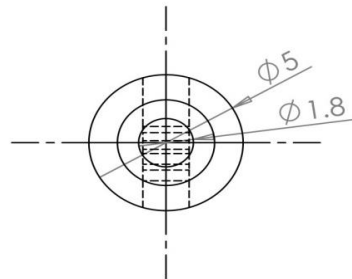
Top view



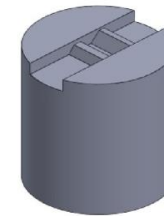
Front view



Right view



Bottom view



Material: PEI (*Polyetherimide*)

School of Mechanical  
Engineering  
University of Birmingham

All dimensions in mm

Tolerance unless otherwise stated:  
whole numbers  
one decimal place  
two decimal places

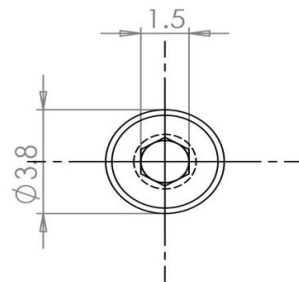
SCALE 5:1

Third angle  
projection

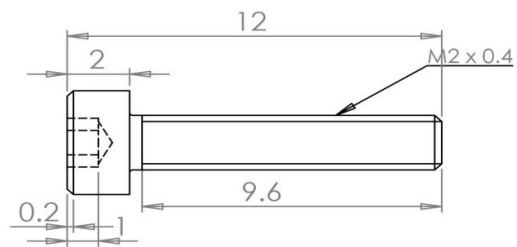


Drawn by: May Youssef  
July 2012

Name: Worm gear clips  
Number of parts: 2



Front view



Right view



Material: Stainless steel

School of Mechanical  
Engineering  
University of Birmingham

All dimensions in mm

Tolerance unless otherwise stated:  
whole numbers  
one decimal place  
two decimal places

SCALE 5:1

Third angle  
projection

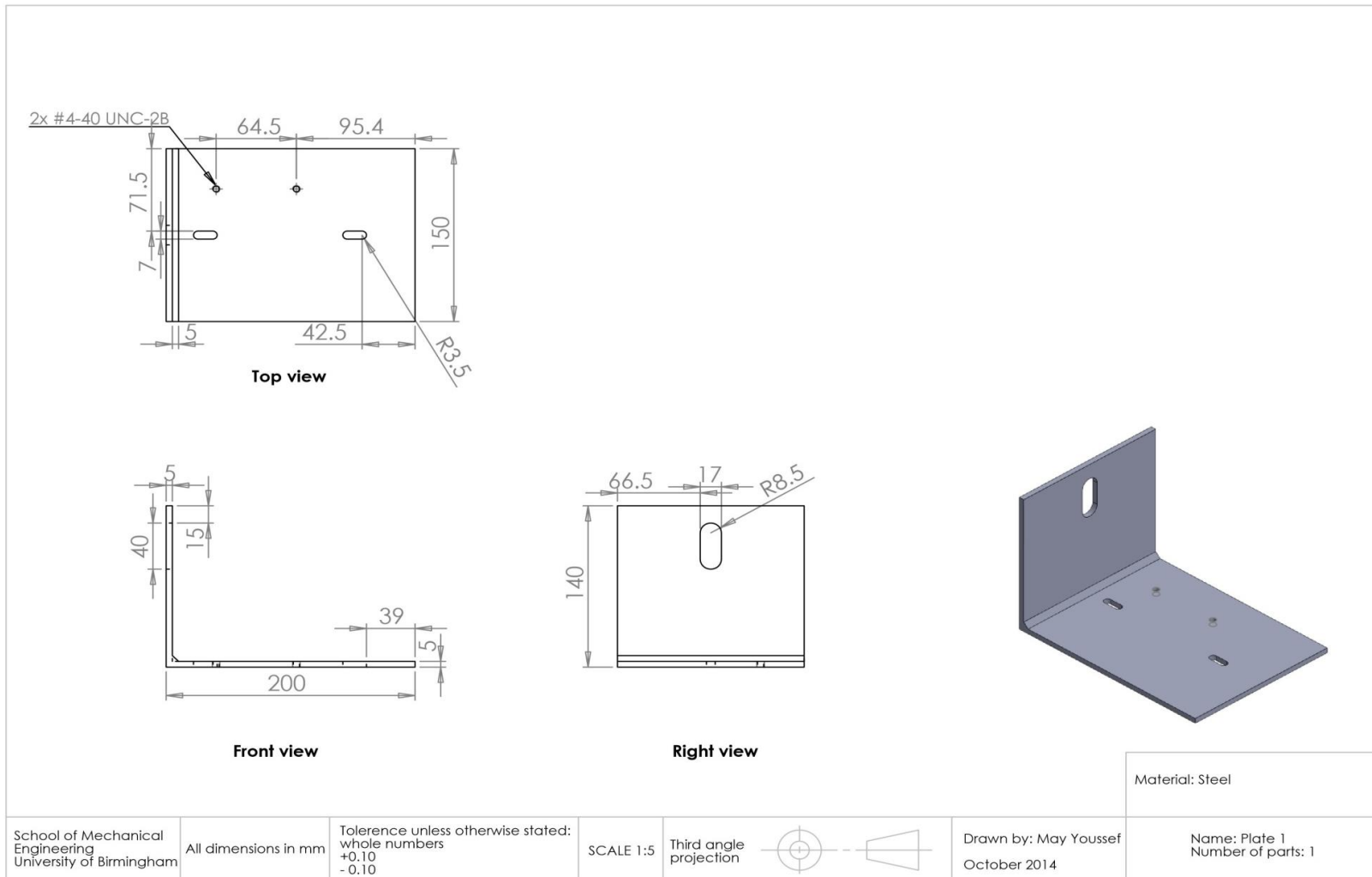


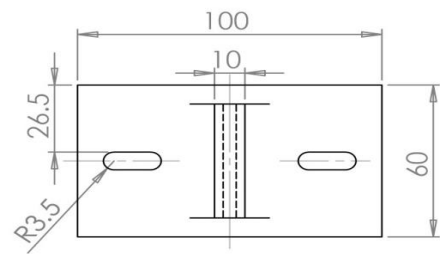
Drawn by: May Youssef  
July 2012

Name: Screw  
Number of parts: 6

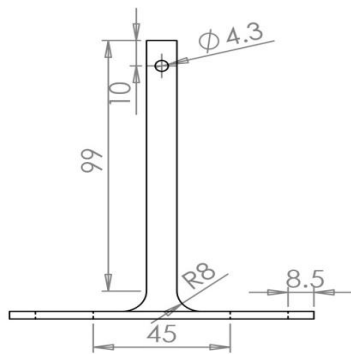
## **Appendix C**

The engineering drawings of the designed rig for the mechanical testing (see section 5.5.2)

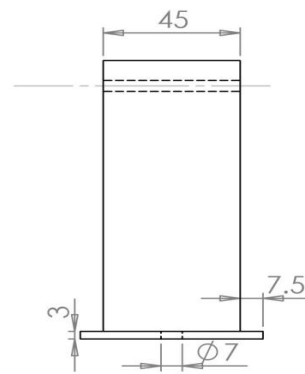




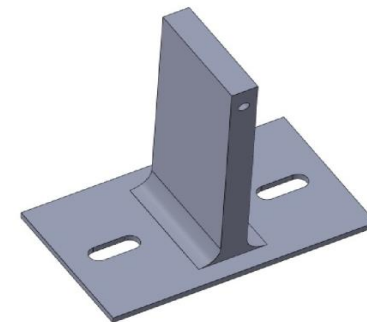
Top view



Front view



Right view



Material: Steel

School of Mechanical  
Engineering  
University of Birmingham

All dimensions in mm

Tolerance unless otherwise stated:  
whole numbers  
+0.10  
-0.10

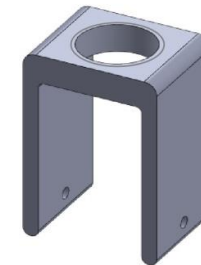
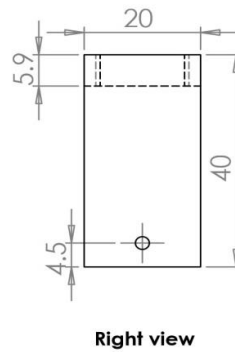
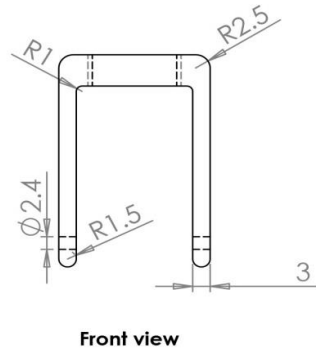
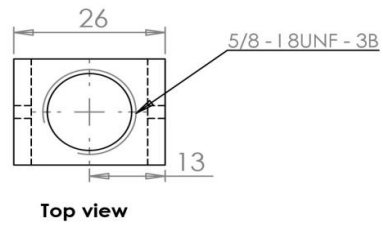
SCALE 1:2

Third angle  
projection



Drawn by: May Youssef  
October 2014

Name: plate 2  
Number of parts: 1



Material: Steel

School of Mechanical  
Engineering  
University of Birmingham

All dimensions in mm

Tolerance unless otherwise stated:  
whole numbers  
+0.10  
- 0.10

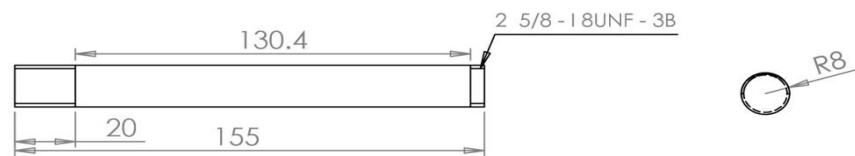
SCALE 1:1

Third angle  
projection



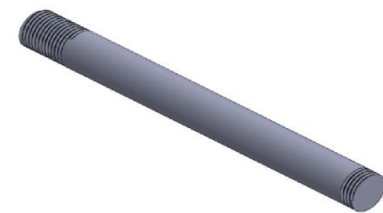
Drawn by: May Youssef  
October 2014

Name: main frame  
Number of parts: 1



Front view

Right view



Material: Steel

School of Mechanical  
Engineering  
University of Birmingham

All dimensions in mm

Tolerance unless otherwise stated:  
whole numbers  
+0.10  
-0.10

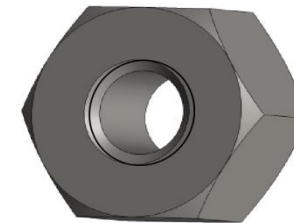
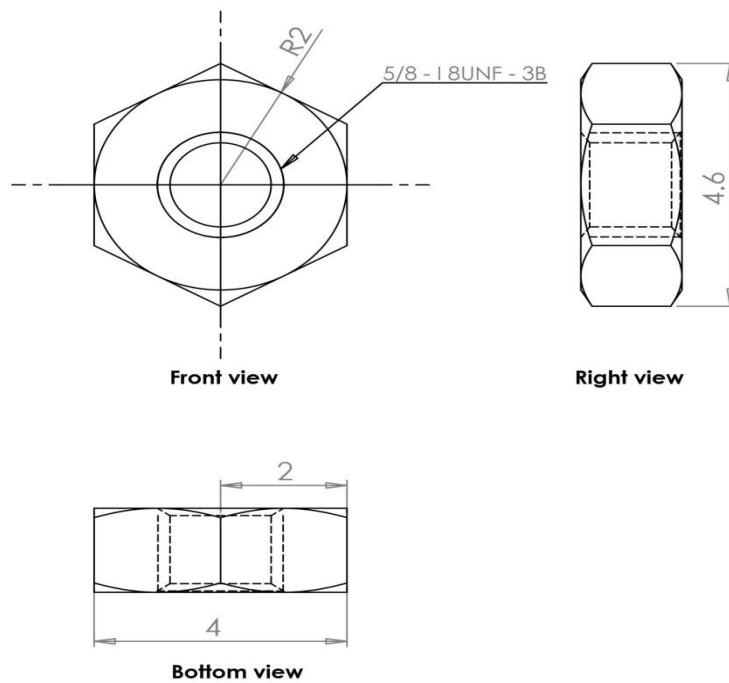
SCALE 1:2

Third angle  
projection



Drawn by: May Youssef  
October 2014

Name: Axial rod  
Number of parts: 1



Material: Steel

School of Mechanical  
Engineering  
University of Birmingham

All dimensions in mm

Tolerance unless otherwise stated:  
whole numbers  
+0.10  
-0.10

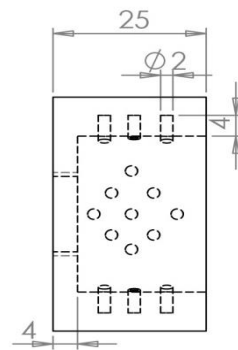
SCALE 10:1

Third angle  
projection

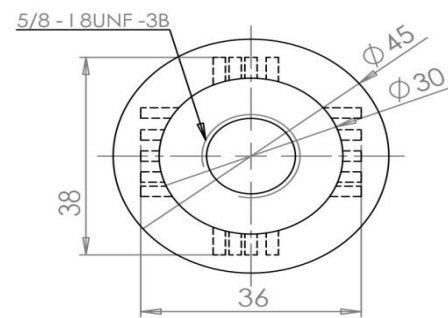


Drawn by: May Youssef  
October 2014

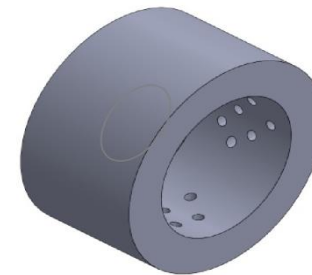
Name: nut  
Number of parts: 2



Front view



Right view



Material: Steel

School of Mechanical  
Engineering  
University of Birmingham

All dimensions in mm

Tolerance unless otherwise stated:  
whole numbers  
+0.10  
-0.10

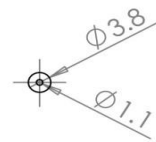
SCALE 1:1

Third angle  
projection

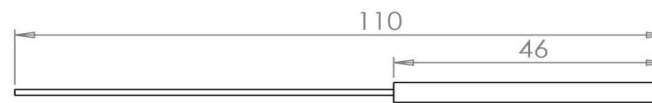


Drawn by: May Youssef  
October 2014

Name: cup  
Number of parts: 1



Front view



Right view



Material: Brass

School of Mechanical  
Engineering  
University of Birmingham

All dimensions in mm

Tolerance unless otherwise stated:  
whole numbers  
+0.10  
- 0.10

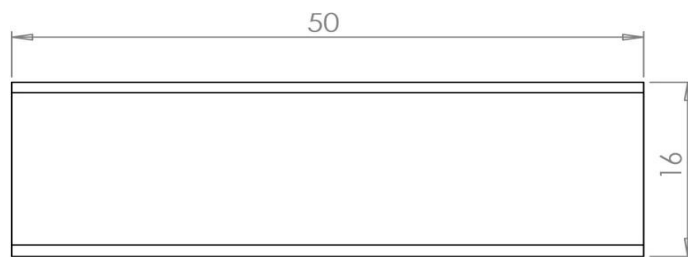
SCALE 1:1

Third angle  
projection

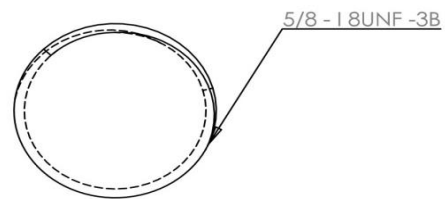


Drawn by: May Youssef  
October 2014

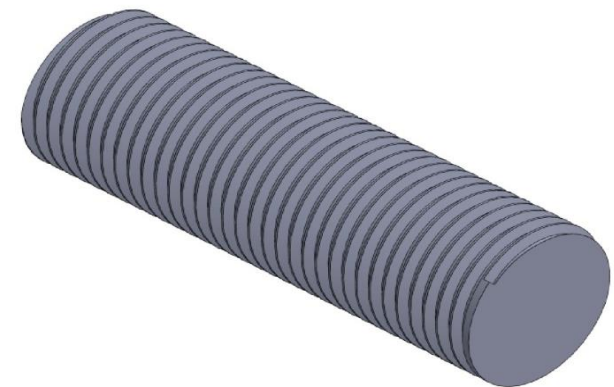
Name: pin  
Number of parts: 1



Front view



Right view



Material: Steel

School of Mechanical  
Engineering  
University of Birmingham

All dimensions in mm

Tolerance unless otherwise stated:  
whole numbers  
+0.10  
- 0.10

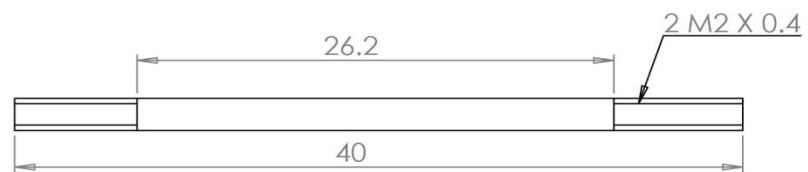
SCALE 2:1

Third angle  
projection



Drawn by: May Youssef  
October 2014

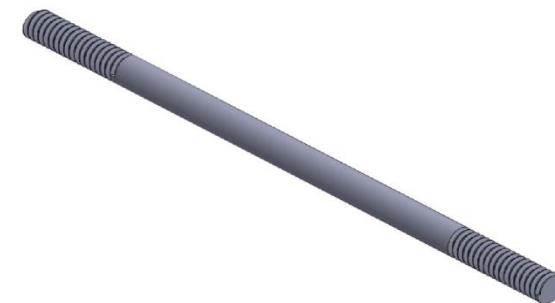
Name: Screw for plat 1  
Number of parts: 1



Front view



Right view



Material: Steel

School of Mechanical  
Engineering  
University of Birmingham

All dimensions in mm

Tolerance unless otherwise stated:  
whole numbers  
+0.10  
-0.10

SCALE 3:1

Third angle  
projection



Drawn by: May Youssef  
October 2014

Name: load rod  
Number of parts: 1

## Appendix D

The worm wheel teeth stress calculation (see section 5.6)

**Lewis Bending Stress** (Schmid *et al.*, 2013)

$$\sigma_t = \frac{W_t P_d}{FY}$$

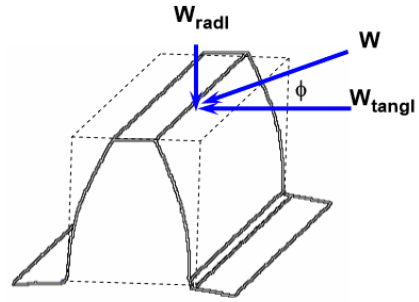
Where:

$W_t$  is the tangential load (lbs),

$P_d$  is the diametral pitch (in<sup>-1</sup>),

$F$  is the face width (in), and

$Y$  is the Lewis form factor (dimensionless)



Tooth bending stress at load  $W = 210\text{ N (47.21 lbs)}$

$$W_t = W \cos \phi_1$$

$$= 11.80 \cos 20^\circ = 11.088 \text{ lbs}$$

$$P_d = 1/m$$

$$= 2.5 \text{ mm} = 0.098 \text{ in}$$

$$F = 2 \text{ mm} = 0.079 \text{ in}$$

$$\sigma_t = (11.088 \times 0.098) / (0.079 \times 0.43) = 32 \text{ lbs/in}^2$$

$$\sigma_t = 0.22 \text{ MPa / tooth}$$

$$\sigma_t \text{ for four teeth is } 0.88 \text{ MPa}$$

Tooth bending stress at load  $W = 13\text{ N (2.92 lbs)}$

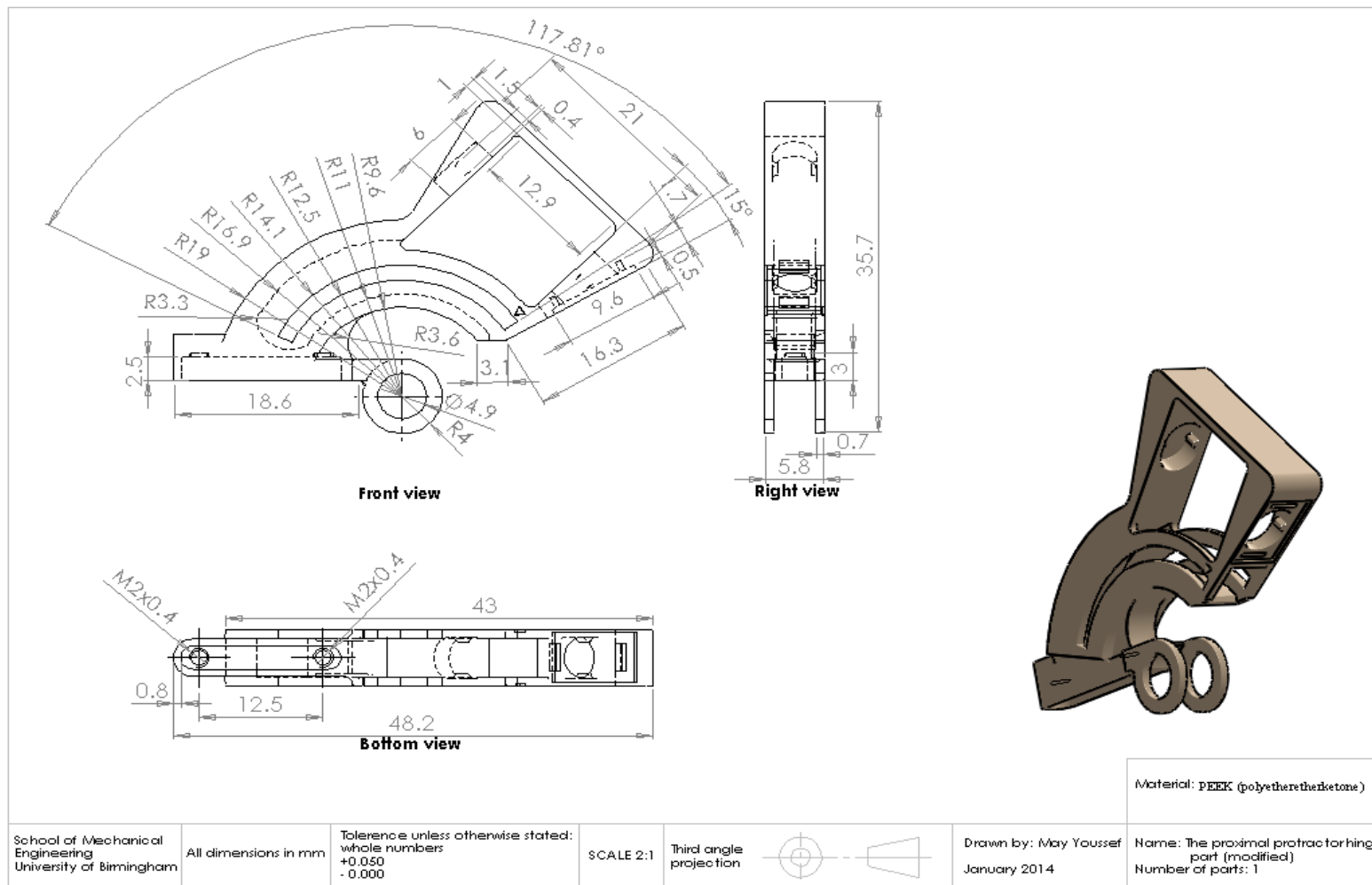
$$\sigma_t = (0.69 \cos 20^\circ \times 0.098) / (0.079 \times 0.43) = 1.99 \text{ lbs/in}^2$$

$$\sigma_t = 0.014 \text{ MPa / tooth}$$

$$\sigma_t \text{ for four teeth is } 0.056 \text{ MPa}$$

## **Appendix E**

The engineering drawings of a proposed future design of the proximal protractor hinge part (see section 6.4.1).



## Appendix F

List of publications for current work

- **Youssef, M.M., Shepherd, D.E.T., and Titley, O.G., 2015, “Engineering Analysis of A Failed Compass Proximal Interphalangeal (PIP) Joint Hinge,” *Biomedical Engineering: Applications, Basis and Communications*, 27 (2), 1550013.**
- **Youssef, M.M., Shepherd, D.E.T., and Titley, O.G., 2015, “Design of an Dynamic External Finger Fixator,” Under review by *Medical Devices Journal*.**

## REFERENCES

## LIST OF REFERENCES

- Abrahams, P.H., McMinn, R.M.H., Marks, S.C., and Hutchings, R.T. (2003), “McMinn’s color atlas of human anatomy,” Edinburgh, Mosby
- Ahmad, A., Darmoul, S., Ameen, W., Abidi, M., and Al-Ahmari, A. (2015), “Rapid prototyping for assembly training and validation,” **15<sup>th</sup> IFAC (International Federation of Automatic Control) Symposium on Information Control Problems in Manufacturing — INCOM 2015**, 48 (3), 412–417
- Aitchison, G.A., Hukins, D.W.L., Parry, J.J., Shepherd, D.E.T., and Trotman, S.G. (2009), “A review of the design process for implantable orthopedic medical devices,” **The Open Biomedical Engineering Journal**, 3, 21-27
- An, K.N., Cooney, W.P., Chao, E.Y. and Linscheid, R.L. (1978) “Functional strength measurement of normal fingers,” **ASME Advances in Bioengineering**, 89-90
- ANSI/AGMA 1012-G05 (2011), “Nomenclature, Definition of Terms with Symbols,” **American National Standards Institute /American Gear Manufacturers Association**, USA, 72
- Alexander, B., and Viktor, K. (2010), “Proportions of hand segments,” **International Journal of Morphology**, 28 (3), 755-758

Asche, G., Burgess A., Burny, F., Brown, C., Karaharju, E., Latta, L., Seligson D., and Zych, G. (2009), **Hoffmann II Micro External Fixation System**, Stryker Trauma AG, Bohnackerweg 1, CH-2545 Selzach, Switzerland.

Astin, A.D., and Nussbaum, M.A. (2003), “Measurement and prediction of single and multi-digit finger strength,” **Ergonomics**, 46 (15), 1531–1548

ASTM F138 (2013), “Standard Specification for Wrought 18Chromium-14Nickel-2.5Molybdenum Stainless Steel Bar and Wire for Surgical Implants (UNS S31673),” **American Society for Testing and Materials, West Conshohocken**

ASTM F1541-02 (2015), “Standard Specification and Test Methods for External Skeletal Fixation Devices,” **American Society for Testing and Materials, West Conshohocken**

Karen M. Becker, K.M., and Whyte, J.J. (2007), “Clinical evaluation of medical devices: principles and case studies,” Springer Science & Business Media, Humana Press, Totowa, New Jersey, USA. Chapter 1, 11-19

Bailie, S.D., Benson, L.S., and Marymont, J.V. (1996), “Proximal interphalangeal joint injuries of the hand. Part I: anatomy and diagnosis,” **The American Journal of Orthopedics**, 25, 474– 477

Bain, G.I., Mehta, J.A., Heptinstall, R.J., and Bria, M. (1998), “Dynamic external fixation for injuries of the proximal interphalangeal joint,” **The Journal of Bone and Joint Surgery [Br]**, 80-B (6), 1014-1019

Balakrishnan, C., Sugg, K.B., Huettner, W., and Jarrahejad, P. (2008), “Dupuytren’s contracture following burn injury of the hand: A case report and review of literature,” **Canadian Journal of Plastic Surgery**, 16 (1), 49-51

Bayat, A., and McGrouther D.A. (2006), “Management of Dupuytren’s disease – clear advice for an elusive condition,” **The Annals of The Royal College of Surgeons of England**, 88 (1), 3-8

Betts, J., DeSaix, P., Johnson, E., Johnson, J., Korol, O., Kruse, D., Poe, B., Wise, J., Womble, M., and Young, k. (2013), “Anatomy & Physiology,” Text book, OpenStax College, Rice University, Chapter 8 The appendicular skeleton, 301-303

Bhamra, J.S., Khan, W.S., and Pastides, P. (2012), “The use of the S-Quattro dynamic external fixator for the treatment of intra-articular phalangeal fractures: a review of the literature,” **The Open Orthopaedics Journal**, 6, 54-59

Bonasperti, G., Volpi, P., De Filippo, G., Damiani, L., and Pazzaglia, U.E. (1999), “L’utilizzo del Compass PIP joint hinge in pazienti affetti da morbo di dupuytren’ con retrazione in flessione dell’articolazione interfalangea prossimale,” **Minerva Ortopedica e Traumatologica**, 50 (3), 103-106

Bostock, S.H., Nee, P.A., and Fahmy, N.R. (1993<sup>a</sup>), “The S Quattro: a new system for the management of difficult intra articular fractures of the phalanges,” **Archives of Emergency Medicine**, 10 (1), 55-59

Bostock, S., Fahmy, N., and Nee, P. (1993<sup>b</sup>), “The S Quattro – results of treatment in 11 cases of sports injury,” **British Journal of Sports Medicine**, 27 (4), 628-670

BSSA, “Fatigue properties and endurance limits of stainless steels,” **British Stainless Steel Association**, Sheffield, UK.

Buckingham, E. (1949), “Analytical mechanics of gears,” McGraw-Hill Book Company, New York, 78-111

Budinski, K. (1991), “Tribological properties of titanium alloys,” **Wear**, 151 (2), 203-217

Bundhoo, V., and Park, E.J. (2005), “Design of an artificial muscle actuated finger towards biomimetic prosthetic hands,” **12<sup>th</sup> International Conference on Advanced Robotics-IEEE Journal**, 368-375

Byrne, A.M., Kearns, S.R., Morris, S., and Kelly, E.P. (2008), “S Quattro external fixator for complex intra-articular thumb fracture,” **Journal of Orthopaedic Surgery**, 16 (2), 170-174

Campbell, D., and White, J.R. (1989), “Polymer characterization, Physical techniques, London, Chapman and Hall Ltd.

Choi, J., and Kim, N. (2015), “Clinical application of three-dimensional printing technology in craniofacial plastic surgery,” **Journal of Archives of Plastic Surgery**, 42 (3), 267-277

Citron, N., and Messina, J.C. (1998), “The use of skeletal traction in the treatment of severe primary Dupuytren’s disease,” **The Journal of Bone and Joint Surgery [Br]**, 80-B (1), 126-129

Clavero, J.A., Alomar, X., Monill, J.M., Esplugas, M., Golano, P., Mendoza, M., and Salvador, A. (2002), “MR imaging of ligament and tendon injuries of the fingers,” **RadioGraphics**, 22 (2), 237–256

Collins, J. (1993), “Failure of materials in mechanical design: analysis, prediction, prevention,” John Wiley & Sons, New York, 140-177

Crisp, S. (1996), “The medical device directives and their impact on the development and manufacturing of medical implants,” **Journal of Engineering in Medicine**, 210 (4), 233-239

Davis, J. (1994), “ASM specialty handbook, Stainless Steels,” ASM International, William W. Scott, Jr., American Society of Metals, 7-8

Designatronics (1999), “Handbook of metric gears: product guide & technical data-catalog Q410,” Quality Transmission Components, USA.

Dewangan, S. (2010), “Experimental investigation of machining parameters for EDM using U-shaped electrode of AISI P20 tool steel,” Master thesis, Department of Mechanical Engineering, National Institute of Technology Rourkela, India.

Elshennawy, A., and Weheba, G. (2015), “Manufacturing processes & materials,” Society of Manufacturing Engineers (SME), 5th Edition, 85

Engel, L., Klingele, H., Ehrenstein, G.W., and Schaper, H. (1981), “An Atlas of polymer damage: surface examination by scanning electron microscope,” Munich; London, Wolfe science in association with Hanser.

EN14971, Medical Devices –Application of Risk Management to Medical Devices (2000), “ISO EN 14971,” **European Committee of Standardization**, London, UK.

EN14630, Non-active surgical implants – General Requirements (2005), “ISO EN14630,” **European Committee of Standardization**, London, UK.

EN7250-1, Basic Human Body Measurements for Technological Design. Body Measurement Definitions and Landmarks, (2010), “ISO EN 7250-1,” **European Committee of Standardization**, London, UK.

EN14155-2, Clinical Investigation of Medical Devices for Human Subjects. Clinical Investigation Plans, (2009), “ISO EN 14155-2,” **European Committee of Standardization**, London, UK.

Fahmy, N.R.M., and Harvey, R.A. (1992), “The S Quattro in the management of fractures in the hand,” **The Journal of Hand Surgery [Br]**, 17-B (3), 321-331

Fahmy, N.R (1990), “The stockport serpentine spring system for the treatment of displaced comminuted intra-articular phalangeal fractures,” **The Journal of Hand Surgery [Br]**, 15 (3), 303–311

Feldscher, S.B., and Blank, J.E. (2002), “Management of a proximal interphalangeal joint fracture dislocation with a Compass proximal interphalangeal joint hinge and therapy: A case report,” **Journal of Hand Therapy**, 15 (3), 266-273

Fowler N.K., and Nicol A.C. (2000), “Interphalangeal joint and tendon forces: normal model and biomechanical consequences of surgical reconstruction,” **Journal of Biomechanics**, 33 (9), 1055-1062

Freiberg, A. (2007), “Management of proximal interphalangeal joint injuries,” **Canadian Journal of Plastic Surgery**, 15 (4), 199-203

Ghosh, S., Ghosh, D., Datta, S., Chaudhuri, A., Roy, D., and Chowdhury, A. (2013), “External fixation by Joshi’s external stabilizing system in cases of proximal humerus fractures in elderly subjects,” **The Journal of the Scientific Society**, 40 (2), 99-102

Gudmundsson, K.G., Arngrímsson, R., Sigfússon, N., Björnsson, Á., and Jónsson, T. (1999), “Epidemiology of Dupuytren's disease clinical, serological, and social assessment. The Reykjavik Study,” **The Journal of Clinical Epidemiology**, 53 (3), 291-296

Halliwell, P.J. (1998), “The use of external fixators for finger injuries, pin placement and tethering of the extensor hood,” **The Journal of Bone and Joint Surgery [Br]**, 80-B (6), 1020-1023

Hamrock, B.J., Schmid, S.R., and Jacobson, B.O. (2007), “Fundamentals of Machine Element,” McGraw-Hill College, New York, 242-254

Hindocha, S., Stanley, J.K., Watson, J.S., and Bayat, A. (2008), “Revised Tubiana’s staging system for assessment of disease severity in Dupuytren’s disease—preliminary clinical findings,” **American Association for Hand Surgery**, 3 (2), 80–86

Hodgkinson, P.D. (1994), “Use of skeletal traction to correct the flexed PIP joint in Dupuytren’s disease,” **The Journal of Hand Surgery [Br]**, 19-B (4), 534–537

Hotchkiss, R.N. (1993), Surgical Technique Compass Proximal Interphalangeal (PIP) Joint Hinge, Smith & Nephew, Memphis, TN38116 USA.

Houshian, S., and Schrøder, H.A. (2004), “Distraction with external fixator contracture of proximal interphalangeal joint, good outcome in 10 cases,” **Journal of Acta Orthopaedica Scandinavica**, 75 (2), 225–228

Houshian, S., Chickamuniyappa, C., and Schrøder, H.A. (2007), “Gradual joint distraction of post-traumatic flexion contracture of the proximal interphalangeal joint by a mini-external fixator,” **The Journal of Bone and Joint Surgery [Br]**, 89-B (2), 206–209

Houshian, S., Gynning, B., and Schrøder, H. A. (2002), “Chronic flexion contracture of proximal interphalangeal joint treated with the Compass hinge external fixator. A consecutive series of 27 cases,” **The Journal of Hand Surgery [Br]**, 27-B (4), 356–358

Houshian, S., Jing, S.S., Chikkamuniyappa, C., Kazemian, G.H., and Tehrani, M.E. (2013), “Management of posttraumatic proximal interphalangeal joint contracture,” **The Journal of Hand Surgery [Am]**, 38-A (8), 1651–1658

Huang, J., Yeh, J., Jeng, S., Chen, C. and Kuo, R. (2006), “High-cycle fatigue behavior of type 316L stainless steel,” **The Journal of Materials Transactions**, 47 (2), 409- 417

HPC Gears Ltd., Catalogue C14 “Gear Transmission Products,” Chesterfield, England, UK, 98-99

Solid Concepts Inc. - A Stratasys Company, Los Angeles, USA

<https://www.solidconcepts.com/materials/sls-materials>

MatWeb, Material Property Data, Blacksburg, USA

<https://www.matweb.com/search/Datasheet.aspx>

Inanami, H., Ninomiya, S., Okutsu, I., Tarui, T. and Fujiwara, N. (1993), "Dynamic external finger fixator for fracture dislocation of the proximal interphalangeal joint," **The Journal of Hand Surgery [Am]**, 18-A (1), 160–164

John, V. (1992), "Introduction to Engineering Materials," London, Macmillan press Ltd.

Jose, R.M., and Bainbridge, L.C. (2010), "Current treatment of Dupuytren's disease and newer advances," **The Journal of Bone and Joint Surgery [Br]**, 1-3

Joshi, B.B. (1997), "Joshi's external stabilization system (JESS): a simple mini external fixator for the management of hand trauma and its sequels," **International Journal of the Care of the Injured**, 28 (3), 244

Joyce, J.T., and Unsworth, A. (2000), "The design of a finger wear simulator and preliminary results," **Proceedings of the Institution of Mechanical Engineers Part H Journal of Engineering in Medicine**, 214 (5), 519-526

Joyce, T.J. (2004), "Currently available metacarpophalangeal prostheses: their designs and prospective considerations," **Expert Review of Medical Devices**, 1 (2), 193-204

Kato, k., and Adachi, K. (2001), “Modern tribology handbook, Two Volume Set,” CRC Press, LLC, U.S.A, chapter 7, wear mechanisms, 1688-1715

Kasabian, A., McCarthy, J., and Karp, N. (1998), “Use of a multiplanar distracter for the correction of a proximal interphalangeal joint contracture,” **The Journal of Annals of Plastic Surgery**, 40 (4), 378–381

Khan, W., and Fahmy, N. (2006<sup>a</sup>), “The S-Quattro in the management of acute intra articular phalangeal fractures of the hand,” **The Journal of Hand Surgery [Br]**, 31 (1), 79–92

Khan, W., and Fahmy, N. (2006<sup>b</sup>), “The S-Quattro in the management of sports injuries of the fingers,” **Injury**, 37 (9), 860-868

Kim, G.S., Kim, H.M., Yoon, J.W., and Shin, H.S. (2010), “Development of cylindrical type finger-force measuring system for measuring grasping finger-force of human,” **Proceedings of the 2010 IEEE International Conference on Robotics and Biomimetics** December 14-18, Tianjin, China

Kirby, A.J. (1992), *Polyimides: Materials, Processing and Applications*, iSmithers Rapra Publishing, Oxford, UK, 5 (11), 33

Krakauer, J.D., and Stern, P.J. (1996), “Hinged device for fractures involving the proximal interphalangeal joint,” **Clinical Orthopaedics and Related Research**, 327, 29-37

Kurtz, S. (2011), "PEEK Biomaterials Handbook," William Andrew, USA, 281-287

Lahiri, A., Mahmoud, M.M., and Titley, O.G. (2007), "Management of proximal interphalangeal joint disorders with the Compass hinge dynamic external fixator," **The British Society for Surgery of the Hand Annual Scientific Meeting**, London, UK.

Lee, J.W., and Rim, K. (1990), "A new method for measurement of finger-phalangeal force," **Experimental Mechanics**, 30 (4), 392-397

Lee, J.W., and Rim, K., (1990), "Maximum finger force prediction using a planar simulation of the middle finger," **Journal of Engineering in Medicine**, 204 (3), 169-178

Long, P. (2008), "Medical devices in orthopedic applications," **The Journal Toxicologic Pathology**, 36 (1), 85-91

Mafi, R., Hindocha, S., and Khan, W. (2012), "Recent surgical and medical advances in the treatment of Dupuytren's disease - A systematic review of the literature," **The Open Orthopaedics Journal**, 6, 77-82

Malloy, R.A. (1994), "Plastic part design for injection molding: An Introduction," Hanser Publishers, Munich, Germany, Chapter 5, 285-339

Marco, R.W., Sharkey, N.A., Smith, T.S., Zissimos, A.g., Sacramento and California (1998), "Pathomechanics of closed rupture of the flexor tendon pulleys in rock climbers," **The Journal of Bone and Joint Surgery [Am]**, 81-A (3), 1012-1019

Mathiowetz, V., Kashman, N., Volland, G., Weber, k., Dowe, M., and Rogers, S. (1985), "Grip and pinch strength: normative data for adults," **Archives of Physical Medicine and Rehabilitation**, 66 (2), 69-72

McFarlane R.M. (1984), "The anatomy of Dupuytren's disease," **Bulletin of the Hospital for Joint Diseases Orthopaedic Institute**, 44 (2), 318-337

Messina, A., and Messina, J. (1993), "The continuous elongation treatment by the TEC device for severe Dupuytren's contracture of the fingers," **Plastic and Reconstructive Surgery Journal**, 92 (1), 84-90

Michou, L., Lermusiaux, J., Teyssedoub, J., Bardinb, T., Beaudreuilb, J., and Teixeira, E. (2012), "Genetics of Dupuytren's disease," **Joint Bone Spine Journal**, 79 (1), 7-12

Mullet J.H., Synnott, K., Noel, J., and Kelly, E.P. (1999), "Use of the S Quattro dynamic external fixator in the treatment of difficult hand fractures," **The Journal of Hand Surgery [Br]**, 24 (3), 350-354

Murphey, M.D., Ruble, C.M., Tyszko, S.M., Zbojniewicz, A.M., Potter, B.K., and Miettinen, M. (2009), “Musculoskeletal fibromatoses: radiologic-pathologic correlation,” **The Journal of Radio Graphics**, 29 (7), 2143–2176

Napier, J.R. (1956), “The prehensile movements of the human hand,” **The Journal of Bone and Joint Surgery [Br]**, 38 (4), 902-913

Neil, C.N., and Messina, J.C. (1998), “The use of skeletal traction in the treatment of severe primary Dupuytren’s disease,” **The Journal of Bone and Joint Surgery [Br]**, 80-B (1), 126–129

Ng, C.Y., and Oliver, C.W. (2009), “Fractures of the proximal interphalangeal joints of the fingers,” **The Journal of Bone and Joint Surgery [Br]**, 91-B (6), 705-712

Oberg, E. (2012), “Section 08. Fasteners – machinery’s handbook 29,” Industrial Press Inc., South Norwalk, Connecticut, USA, 1721

Olandersson, S., Lundqvist, H., Bengtsson, M., Lundahl, M., Baerveldt, A., and Hilliges, M. (2005), “Finger-force measurement-device for hand rehabilitation,” **Proceedings of the IEEE 9<sup>th</sup> International Conference on Rehabilitation Robotics**, Chicago, IL, USA

Peebles, L., and Norris, B. (1998), “Adult data: the handbook of adult anthropometric and strength measurements: data for design safety,” Department of Trade and Industry, Great Britain, 134-142

Pîrjan, A., and Petroșanu, D. (2013), “The impact of 3D printing technology on the society and economy,” **Journal of Information Systems and Operations Management**, 7 (2), 360-370

Pugh, S. (1991), “Total design: integrated methods for successful product engineering,” Addison-Wesley, Boston, USA, 44-65

Radwin, R.G., Oh, S., Jensen, T.R., and Webster, J.G. (1992), “External finger forces in submaximal five- finger static pinch prehension,” **Ergonomics**, 35 (3), 275-288.

Radzevich, S. (2012), “Dudley's Handbook of Practical Gear Design and Manufacture,” CRC (Chemical Rubber Company) Press, USA, 1-3

Rayan, G.M. (2007), “Dupuytren disease: anatomy, pathology, presentation, and treatment,” **The Journal of Bone Joint and Surgery [Am]**, 89 (1), 189 -198

Reese, N.B., and Bandy, W.D. (2013), “Joint range of motion and muscle length testing,” **Elsevier Health Sciences** “Appendix B”, 472

Riester, S., Wijnen, A., Rizzo, M., and Kakar, S. (2014), “Pathogenesis and treatment of Dupuytren disease,” **The Journal of Bone and Joint Surgery**, 2 (4), 1-10

Rosato, D.V., and Rosato, M.G. (2012), “Injection molding handbook,” Springer Science and Business Media, Germany, chapter 1, 1-26

Ruland, R.T., Hogan, C.J., Cannon, D.L., and Slade, J.F. (2008), “Use of dynamic distraction external fixation for unstable fracture-dislocations of the proximal interphalangeal joint,” **The Journal of Hand Surgery [Am]**, 33 (1), 19-25

Salafia, A., and Chauhan, G. (1997), “Joshi external stabilising system (JESS) in proximal interphalangeal joint (PIP) contractures in leprosy,” **Indian Journal of Leprosy**, 69 (4), 331-340

Sathishchandra, B.K., Ashok Shah, and Bindiya, R.S. (2011), “Efficacy of Joshi’s external stabilizing system in fractures and mangled hand-a prospective study,” **International Journal of Biomedical and Advance Research**, 2 (9), 329-343

Schmid, S., Hamrock, B., and Jacobson, B. (2013), “Fundamentals of machine elements,” CRC Press, LLC, USA, 3<sup>rd</sup> edition, chapter 14, 400-405

Schweizer, A. (2001), “Biomechanical properties of the crimp grip position in rock climbers,” **Journal of Biomechanics**, 34 (2), 217-223

Shaw, R.B., Chong, A.S., Zhang, A., Hentz, V.R., and Chang, J. (2007), “Dupuytren’s disease: history, diagnosis, and treatment,” **Plastic and Reconstructive Surgery**, 120 (3), 44-54

Shih, B., and Bayat, A. (2010), “Scientific understanding and clinical management of Dupuytren disease,” **The journal of Nature Reviews Rheumatology**, 6 (12), 715-726

Slater, R.R., Agee, J.M., and Goss, B.C. (2003), “Dynamic extension torque for the reversal of PIP contractures,” **The Journal of Operative Techniques in Plastic and Reconstructive Surgery**, 9 (4), 161-168

Suresh, R., Sathyanathan, M., Visagavel, K., and Kumar, M. (2014), “Risk assessment for blast furnace using FMEA,” **The International Journal of Research in Engineering and Technology**, 3 (11), 27-31

Swanson, A.B., Matev, L.B., and de Groot, G. (1974), “The strength of the hand,” New York University, Medical School, Inter-Clinic Bulletin, 13 (1), 1-8

Tate, P. (2011), “Seeley's principles of anatomy and physiology,” McGraw-Hill Education, New York, 2 edition, chapter 7, 171

Taylor, C.L., and Schwarz, R.J. (1955), “The anatomy and mechanics of the human hand,” **The Journal of Artificial Limbs**, 2 (2), 22–35

Tilley, A.R., and Associates, H.D. (2002), “The measure of man and woman: human factors in design,” John Wiley & Sons, New York, USA, 22-25

Townley, W.A., Baker, R., Sheppard, N., and Grobbelaar, A.O. (2006), “Dupuytren’s contracture unfolded,” **British Medical Journal**, 332 (7538), 397–400

Trojian, T.H., and Chu, S.M. (2007), “Dupuytren’s disease: diagnosis and treatment,” **American Academy of Family Physicians**, 76 (1), 86-89

Trotignon, J.P., Verdu, J., Martin, C., and Morel, E. (1993), “Fatigue behavior of some temperature-resistant polymers,” **Journal of Materials Science**, 28 (8), 2207-2213

ULTEM ® PEI Resin Product Guide, General Electric Ltd. UK

US Patent 0097944 A1, Hotchkiss, R., Hotchkiss, K., and Woodward, A. (2004), “Fixation device and method for treating contractures and other orthopedic indications,” 05-20

US Patent 4604997, De Bastiani, G., Brivio, L., Aldegheri, R., and Faccioli, G. (1986), “Articulated mini external fixation device,” 08-12

US Patent 5100403, Hotchkiss, R., Hotchkiss, K., and Woodward, A. (1992), “Dynamic elbow support,” 06-8

US Patent 5376091, Hotchkiss, R., Hotchkiss, K., and Woodward, A. (1994), “Dynamic finger support,” 12-27

Ventola, C. (2014), “Medical applications for 3D printing: current and projected uses,”  
**Journal of Pharmacy and Therapeutics**, 39 (10), 704–711

Viceconti, M., Affatato, S., Baleani, M., Bordini, B., Cristofolini, L., and Taddei, F. (2009),  
“Pre-clinical validation of joint prostheses: A systematic approach,” **Journal of The  
Mechanical Behavior of Biomedical Materials**, 2 (1), 120-127

Vigouroux, L., Quainea, F., Labarre-Vilab, N., and Moutet, F. (2006), “Estimation of finger  
muscle tendon tensions and pulley forces during specific sport-climbing grip techniques,”  
**Journal of Biomechanics**, 39 (14), 2583–2592

Walker, P.S., Davidson, W., and Erkman, M.J. (1978), “An apparatus to assess function of  
the hand,” **The Journal of Hand Surgery [Am]**, 3 (2), 189-193

Weightman, B., and Amis, A.A. (1982), “Finger joint force predictions related to design of  
joint replacements,” **Journal of Biomedical Engineering**, 4 (3), 197-205

White, J., Kang, S., Nanchoo, T., Floyd, D., Kambhampati, S., and McGrouther, D. (2012),  
“Management of severe Dupuytren’s contracture of the proximal interphalangeal joint with  
use of a central slip facilitation device,” **The Journal of Hand Surgery [Br]**, 37-E (8),  
728-732

Woods, J.T., and Nimmer, R.P. (2001), “Plastics failure analysis and prevention,” William  
Andrew, Schenectady, USA. Chapter 8, Failure Prevention, 267-268

Xin, H., Shepherd, D.E.T., and Dearn, K.D. (2013), “A tribological assessment of a PEEK based self-mating total cervical disc replacement,” **Wear**, 303 (1-2), 473-479

Youssef, M.M., Shepherd, D.E.T., and Titley, O.G. (2015), “Engineering analysis of a failed compass proximal interphalangeal (PIP) joint hinge,” **Biomedical Engineering: Applications, Basis and Communications**, 27 (2), 1550013

Zimmerman, D.L., and Jones, R.W. (1994), “SEM analysis of polymeric mechanical failures in polyetherimide,” **International Journal Polymeric Materials**, 23 (3-4), 151-165